DEVELOPMENT OF FLUOROUS SOLID-PHASE EXTRACTION (FSPE)

ON A MICROCHIP AND ITS APPLICATION TO PROTEOMICS

by

ZHENPO XU

A thesis submitted to Department of Chemistry in conformity with the requirements for

the degree of Doctor of Philosophy

Queen's University

Kingston, Ontario, Canada

November, 2013

Abstract

The origin of fluorous interaction was explored and experimentally examined based on both HPLC and CEC data in this project. It was found that the selective fluorous interaction is a kind of reduced instantaneous or induced dipole interaction compared to the hydrophobic interaction.

A series of FPPM preparation parameters were optimized. The optimized FPPM column can resolve the components in a manner that was otherwise not possible with its non-fluorous (hydrocarbon) counterpart.

Following, the CEC separation of fluorous analytes on FPPM stationary phase based upon fluorous-fluorous interaction was realized for the first time. It was also found that, quantitatively, hydrophobic stationary phases have better methylene selectivity (α_{-CH_2-}), while fluorous stationary phases have better perfluoromethylene selectivity (α_{-CF_2-}). Thermodynamically, $\Delta G^{\circ}_{-CF_2-\to-CF_2-} : \Delta G^{\circ}_{-CH_2-\to-CH_2-}$ (Gibbs free energy change of transferring a $-CF_2-$ unit to pure fluorous stationary phase *versus* Gibbs free energy change of transferring a $-CH_2-$ unit to pure hydrophobic stationary phase) is approximately equal to 8:1.

A new concept, hypothetical water percentage (HWP) based on the comparison of α_{-CH_2-} and α_{-CF_2-} was proposed for the first time to quantitatively evaluate the hydrophobicity/fluorophilicity of a stationary phase. A stationary phase can be classified as

fluorous stationary phase when the HWP is less than 0 (more negative indicates more fluorous), or as a hydrophobic stationary phase when the HWP is larger than 100. For the range between 0 and 100, the stationary phase can be treated as either fluorous or hydrophobic due to the similar values of α_{-CH_2-} and α_{-CF_2-}.

Fluorous tagged peptides and proteins (up to 5800 Da) were effectively separated from their non-fluorous counterparts on the FPPM stationary phase in capillary-based columns and detected both on-line with ESI-MS and off-line with MALDI-MS. Finally, the FPPM solid-phase extraction (SPE) stationary phase was transplanted from the capillary to a microchip format. This microchip exhibits the merits of both selective fluorous interaction and micro total analysis system (μTAS).

Co-Authorship

This Ph.D project was completed under the supervision of Dr. Richard D. Oleschuk. Part of the work presented in Chapter 3 was co-authored by Dr. Adam B. Daley. Part of the work presented in Chapter 4 was co-authored by Dr. Graham. T. T. Gibson. Some results of the project have been published in the following three papers:

Daley, A.B.; Xu, Z.; Oleschuk, R.D. *Anal. Chem.* **2011,** *83,* 1688-1695

Xu, Z.; Gibson, G. T. T.; Oleschuk, R.D. *Analyst*. **2013**, *138*, 611-619

Xu, Z.; Oleschuk, R.D. *Electrophoresis*. **2013**, DOI: 10.1002/elps.201300365

Acknowledgements

I would like to acknowledge my supervisor, Dr. Richard D. Oleschuk, for the guidance during my entire Ph.D project research as well as the comfortable and aspirant environment of "O" group originating from his knowledge, patience, sense of humor, and the contributions from all group past and present members.

I would like to thank my supervisory committee members Dr. Philip Jessop and Dr. David Zechel, Dr. Igor Kozin, and Dr. Jiaxi Wang. Thanks for their valuable suggestions and discussions.

I would also like to thank my beloved family members: my mother Jinxia Liu, my father Xueli Xu,   my mother-in-law Shuzhen Cao, my father-in-law Zhenron Shao, my wife Bing Shao, my son Weiran Xu, my younger sisters Xin Xu, and Ling Xu. Thanks for their love, support, and encouragement. I could not have accomplished this project without their contributions.

Finally, I would like to thank Queen's University and the Natural Sciences and Engineering Research Council for financial support of this project, Micralyne for the donation of the microfluidic chips, and CMC for the help on microfluidic chip design/fabrication.

Statement of Originality

I affirm that the work presented within this thesis originates from my own. Any published and

unpublished ideas, methods, techniques, and data from others are fully acknowledged in

accordance with the standard referencing.

Table of Contents

List of Tables

List of Figures

List of Schemes

List of Abbreviations

Abbreviations	Full Name
μTAS	micro total analysis system
ACN	acetonitrile
AIBN	azobisisobutyronitrile
AMPS	2-acrylamido-2-methylpropane sulfonic acid
BA	butyl acrylate
BDDA	1, 3-butanediol diacrylate
BME	benzoin methyl ether
CE	capillary electrophoresis
CEC	capillary electrochromatography
CHCA	*alpha*-cyano-4-hydroxycinnamic acid
COC	cyclic olefin copolymer
CTMS	chlorotrimethylsilane
DIDP	diisodecyl phthalate
DTT	dithiothreitol
DVB	divinylbenzene
EDMA	ethylene dimethacrylate
EOF	electroosmotic flow
ESI	electrospray ionization
FBA	1H,1H-heptafluorobutyl acrylate
FBS	fluorous biphasic systems

Abbreviations	Full Name
FSPE	fluorous solid-phase extraction
FPPM	fluorous porous polymer monolith
GC	gas chromatography
GMA	glycidyl methacrylate
GN	graphene nanosheets
GO	graphene oxide
HETP	height equivalent to a theoretical plate
HFUA	heptadecafluoroundecylamine
HILIC	hydrophilic interaction chromatography
HMDS	hexamethyldisilizane
HPLC	high performance liquid chromatography
HWP	hypothetical water percentage
I.D.	inner diameter
LC	liquid chromatography
LLE	liquid-liquid extraction
Log P	logarithm of octanol-water partition coefficient
MALDI	matrix-assisted laser desorption/ionization
METAM	[2-(methacryloyloxy)ethyl] trimethylammonium methylsulfate
MS	mass spectrometry
N Series	N-f-CbZ-4-nitro-benzylamine mixture
N1, N2, N3, N4	fluorous-tagged carbamate mixture with an N-substituted 4-nitrobenzyl group ($C_{17+x}H_{17}F_{2x+1}N_2O_4$; x=3, 4, 6 and 8; named N1, N2, N3, N4, respectively, according to increasing fluorous tag length)
NMR	nuclear magnetic resonance

List of Abbreviations

Abbreviations	Full Name
NP	normal phase
O.D.	outer diameter
ODS	octadecylsilane
P Series	N-f-CbZ-4-phenyl-benzylamine mixture
P1, P2, P3, P4	fluorous-tagged carbamate mixture with an N-substituted 4-phenylbenzyl group ($C_{23+x}H_{22}F_{2x+1}NO_2$; x=3, 4, 6 and 8; named P1, P2, P3, P4, respectively, according to increasing fluorous tag length)
PAH	polyaromatic hydrocarbon
PDMS	polydimethylsiloxane
PET	poly(ethylene terephthalate)
PFDA	1H,1H,2H,2H-perfluorodecyl acrylate
PMMA	poly(methyl methacrylate)
PMME	polymer monolith microextraction
PPM	porous polymer monolith
PTM	post-translational modification
R-FSPE	reverse fluorous solid-phase extraction
RP	reversed phase
SD	standard deviation
SEM	scanning electron microscopy
SPE	solid-phase extraction
TFBDA	2,2,3,3-tetrafluoro-1,4-butyl diacrylate
TFEM	2,2,2-trifluoroethyl methacrylate
THF	tetrahydrofuran
TMSPMA	3-(trimethoxysilyl)propyl methacrylate

Abbreviations	Full Name
UPLC	ultra-performance liquid chromatography
UV	ultraviolet
XIC	extracted ion current
γ-MAPS	3-(trimethoxysilyl)propyl methacrylate

Chapter 1 – Introduction

1.1 – Fluorous Chemistry Terminology

Initially the term "fluorous" phase did not exist. Instead it was termed "super hydrophobic" reversed-phase. The term "fluorous" was introduced by Horvath and Rabai in 1994 [1] as an analog to the term aqueous. The fluorous phase was originally defined as the perfluoroalkane, perfluorodialkyl ether or perfluorodialkyl amine rich phase of a biphasic system. Furthermore, it did not receive much attention until it was explored as an alternative for liquid-liquid extraction (LLE) phase in fluorous biphasic separations (FBS). [2,3]

Eight years following the first use of the term fluorous, a formal definition of fluorous was offered by Gladysz and Curran. [4]

"Of, relating to, or having the characteristics of highly fluorinated saturated organic materials, molecules or molecular fragments. Or, more simply (but less precisely), 'highly fluorinated' or 'rich in fluorines' and based upon sp^3 –hybridized carbon." Similar to the definitions of "hydrophilic" and "hydrophobic," it was proposed that "fluorophilic molecules, materials or fragments show an affinity for fluorous media under a given set of conditions, while fluorophobic ones do not."

This definition refers in particular to sp^3 – hybridized carbon. The aromatic C-F bond featuring sp^2 – hybridized carbon does not have a strong fluorous feature which will undergo

1

dipole-dipole interactions, making aryl- and perfluoroaryl-containing ligands much more soluble in organic solvents.[5]

A series of concepts concerning fluorous interaction were also introduced, for example, fluorous medium, fluorous separation technique, fluorous tag, fluorous reaction component, and fluorous chemistry. Similar to the definition of hydrophilic and hydrophobic, it was proposed that "fluorophilic molecules, materials or fragments show an affinity for fluorous media under a given set of conditions, while fluorophobic ones do not".

Through the definition, the authors wanted to prompt many readers to "take a dive in the fluorous pool". The flourishing fluorous chemistry community that followed had proven the validity of their forecasts.[6-8] However, the researchers interested in fluorous chemistry continue to be confused by the classic question: what exactly is the fluorous interaction?

1.2 – Fluorous Interaction Theory

What exactly is the fluorous interaction? Where is the fluorous interaction coming from? A clue might be found from the atomic properties of fluorine and the properties of molecules containing significant amounts of fluorine.

Figure 1.1 illustrates the interaction types, in which Israelachvili et al. attempted to survey the common types of forces that exist between atoms and molecules in the classic article, "*The Nature of van der Waals Forces*".[9] Depending upon the reference quoted,[9,10] van Der Waals interactions, named after Dutch scientist Johannes Diderik van der Waals, are defined

"narrowly" as "dispersion forces" derived from instantaneous or induced dipoles.[11] It has been more "widely" defined as the total attractive interactions, other than covalent bonds, hydrogen bonds, or the electrostatic interactions of ions with one another or with neutral molecules. Alternatively it has been defined as the sum of both attractive and repulsive interactions.

The van der Waals interaction is composed of three interactions: permanent dipoles interaction (also called the Keesom force, named after Willem Hendrik Keesom), permanent dipole-induced dipole interaction (also called the Debye force, named after Peter J.W. Debye), and instantaneous or induced dipoles interaction (also called the London dispersion force, named after Fritz London). No matter which definition of a van der Waals interaction is used, the dipole moment is always a primary factor in the interaction.

Dipole moment is a measure of how far a negative (electrons rich) center and positive center are away from each other when either produced initiatively (permanent dipole and instantaneous dipole) or passively (induced dipole). Furthermore, for a single bond, the dipole moment can be approximated by the electronegativity difference between the two atoms that form the bond.
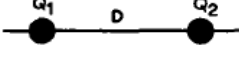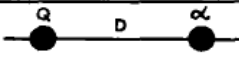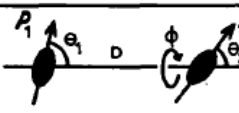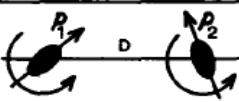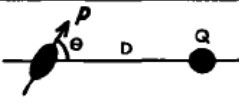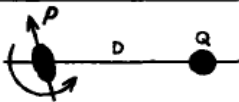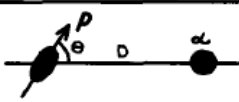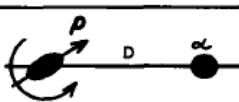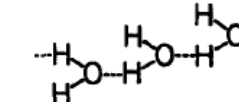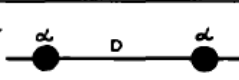
TYPE OF INTERACTION		INTERACTION ENERGY
COVALENT	(H H) H_2 (HH/O) H_2O	COMPLICATED, SHORT RANGE
CHARGE—CHARGE	Q_1 — D — Q_2	$U = + Q_1 Q_2 / (4\pi \varepsilon_0 D)$
CHARGE—NEUTRAL	Q — D — α	$U = - q^2 \alpha / (8\pi \varepsilon_0 D^4)$
DIPOLE— DIPOLE	P_1 θ_1 — D — ϕ P_2 θ_2 FIXED DIPOLES (LOW T)	$U = \dfrac{-P_1 P_2}{4\pi \varepsilon_0 D^3} (2\cos\theta_1 \cos\theta_2 - \sin\theta_1 \sin\theta_2 \cos\phi)$
	P_1 — D — P_2 FREELY ROTATING DIPOLES (HIGH T)	$U \approx \dfrac{-p_1^2 p_2^2}{6\pi \varepsilon_0 kT D^6}$
CHARGE— DIPOLE	P θ — D — Q FIXED	$U = -Qp\cos\theta / (4\pi \varepsilon_0 D^2)$
	P — D — Q ROTATING	$U = -q^2 p^2 / (12\pi \varepsilon_0 kT D^4)$
DIPOLE— NEUTRAL	P θ — D — α FIXED	$U = -p^2 \alpha (1+3\cos^2\theta) / (8\pi \varepsilon_0 D^6)$
	P — D — α ROTATING	$U = -p^2 \alpha / (4\pi \varepsilon_0 D^6)$
HYDROGEN BONDING	H O··· –H O–H O–H O– H O	$U \approx -$ CONSTANT$/D^2$ SHORT RANGE
NEUTRAL—NEUTRAL (VAN DER WAALS OR DISPERSION)	α — D — α	$U = -(3/4) h\nu \alpha^2 / [(4\pi \varepsilon_0)^2 D^6]$

Figure 1.1: Common types of interactions between atoms and molecules. U = interaction energy (in Joules), Q = electric charge (Coulomb), p = electric dipole moment (C m), k = Boltzmann constant (1.38×10^{-23} J/K), T = absolute temperature (K), D = distance between interacting atoms or molecules (m), θ = angle, a = electric polarizability (F m), h Planck constant (6.626×10^{-34} J s), ν = electron orbiting frequency (s^{-1}), ε = permittivity of free space (8.854×10^{-12} F/m). The force is obtained by differentiating the energy U with respect to distance D. This figure is reproduced from reference.[9]

4

Fluorine ($1s^2$, $2s^2$, $2p^5$) has the smallest atomic radius among the Period 2 elements except for the noble gas neon.[12,13] Its most striking feature is the power to "pull" and hold electrons. For example, the electronegativities for C, H and F are 2.55, 2.20, and 3.98 respectively.[12,14] The electronegativity difference between C and F is 1.43,[13,15] while the difference for C and H is 0.35.[14,16] In fact, the large difference in electronegativity between C and F renders the C-F bond highly polarized which affords additional stabilization (C-F bond is one of the strongest in organic chemistry, bond dissociation energies of up to 105.4 kcal/mol have been reported while, for C-H bond, dissociation energies are typically 98.8 kcal/mole[16]). Furthermore the C-F bond length is quite short (typically 0.135 nm), which is believed to result from strong Coulombic interactions between the partially negatively charged fluorine and the partially positively charged carbon ($\overset{\delta+}{C}\!\!-\!\!\overset{\delta-}{F}$) rather than the traditional covalent bond.[17-19]

A highly polarized C-F bond should show stronger molecular interactions due to a strong permanent dipole-dipole interaction. As a result, fluorous species are expected to possess high boiling points and good miscibility with common solvents (*e.g.* water and ACN). Nevertheless, the experimental data gives the totally opposite results. Perfluorinated liquid phases have been shown to be some of the least polar compounds that exist.[20] For example, the n-perfluoroalkanes with more than four carbon atoms are always more volatile (lower boiling point) than their hydrocarbon analogues (Figure 1.2).[6] The relatively low boiling point reflects weaker inter-molecular interactions.[21] In addition, they are neither miscible with water nor most organic solvents (*e.g.* ethanol, acetone, benzene, and chloroform).[22]

Oxygen solubility in fluorous compounds is substantially higher than other solvents and might result from very weak interactions between fluorous solvent molecules.[7]
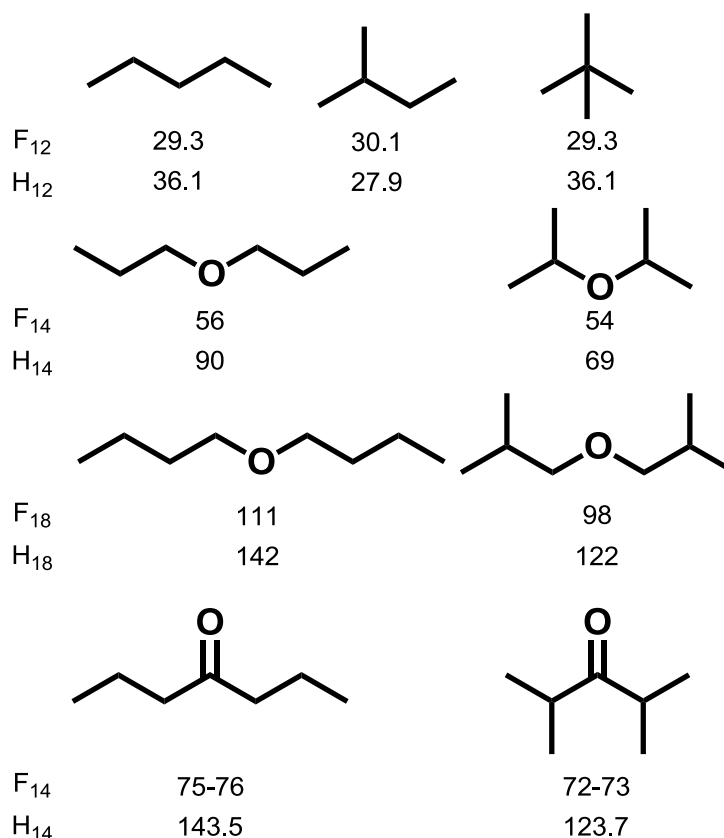
Figure 1.2: Boiling point (℃) comparison between fluorous reagents and corresponding hydrocarbon analogues. This figure is reproduced from reference.[6]

What is the reason behind this seemingly opposite character? Figure 1.3 offers one speculation. A polarized C-F bond does not imply higher molecular dipole moment or moiety dipole moment. Since C-F bonds usually appear in a group in a given fluorous molecule, the strong individual C-F dipoles, then organize in a dendriform arrangement, where partially negatively charged fluorine atoms act as leaves, and partially positively charged carbon atoms act as the trunk. All partial negative charges float in the outer crown forming a single

integrated C-F dipole shell. The process is akin to the pi bond formation in a benzene ring. This dipole shell is very "hard" due to the large electronegativity difference between C and F and consequently a large C-F permanent dipole results.[23] All partial negative charges are held firmly in the outer shell, while all partial positive charges remain within the core. Consequently, an individual dipole shell interacts with another dipole shell through a reduced instantaneous – instantaneous dipole interaction. Instantaneous or induced dipoles interactions are proportional to electric polarizability (Figure 1.1). The large electronegativity difference between C and F results in a much weaker induced dipole interaction compared to the C-H counterpart (Figure 1.3), *i.e.* the polarizability of this hard integrated C-F dipole shell is decreased to give a reduced instantaneous or induced dipole interaction. This is also the reason why fluorinated organic species show ultra high hydrophobic properties, and why fluorous phases were initially treated as a type of less polar reversed-phase or as an organic modifier.[24,25] However, fluorous phase (fluorous interactions) deserves an independent position rather than being an accessory (sub category) to reversed-phase (hydrophobic) interactions, especially in chromatographic applications.[26]

A similar idea has been developed in biochemistry where the term "polar hydrophobicity" is used to describe specific fluorous interactions.[16,27] At first thought, it seems as though polar contradicts hydrophobicity. However, polar in this case refers to the individual C-F bond; while hydrophobicity is the overall reduced inter-molecular interaction through the formation of a single integrated "hard" C-F dipole shell (Figure 1.3).
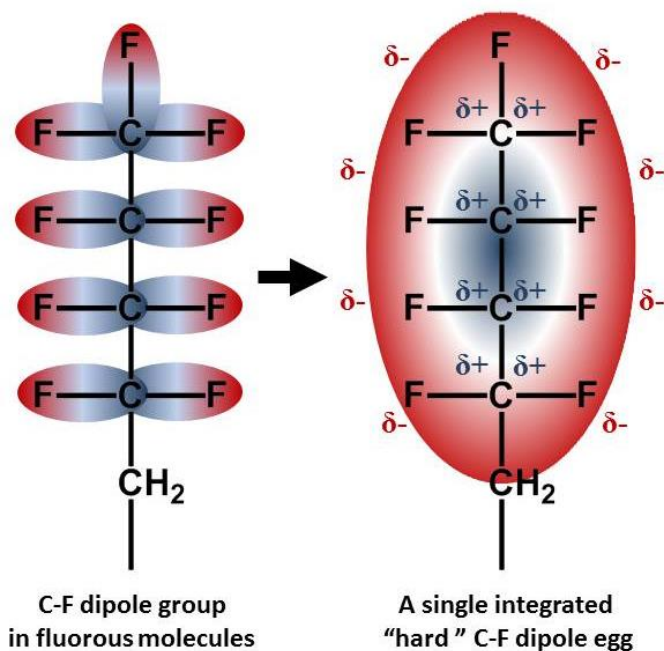
Figure 1.3: A single integrated "hard" C-F dipole shell in fluorous species derived from a group of C-F dipoles.

When referring to hydrophilic-, hydrophobic-, fluorophilic-, and fluorophobic interactions, two comparable phases are usually employed to discuss whether they attract (-philic) or repel (-phobic) each other. Figure 1.4 is a model with two phases or molecules. A boundary between them is set along the horizontal axis, while the vertical axis is the imaginary boundaries within the same phases. There are always several interactions occurring at the boundary interfaces. These interactions are listed in Figure 1.1, and follow the general strength sequence, ion-ion (charge-charge) interaction > covalent bonds > >hydrogen bonding > >dipole-dipole interaction > instantaneously induced dipoles interaction.[10]

In Figure 1.4, the different types of interactions are arranged along the axis with the scale increasing in the direction of the arrow. Both the size of double sided arrow, and dashed rectangle area, represent the scale of inter-phasic or inner-phasic interactions. Fluorous

interaction mainly results from the reduced instantaneous/ induced dipoles interaction, located at the innermost of all dashed rectangles with the smallest area (*i.e.* smallest amount (magnitude) of interaction, red rectangle 5, Figure 1.4). If a fluorous phase and another organic solvent (*e.g.* ACN) are represented in the system of Figure 1.4, the inner-phasic interactions for ACN include permanent dipoles interactions, permanent dipole-induced dipole interactions, and instantaneous or induced dipoles interactions. Half of the area of dashed rectangle 2 represents the amount of total interaction (area not necessarily proportional). While the inner-phasic interactions for fluorous phase includes only the reduced instantaneous or induced dipoles interaction, half of the area of red rectangle 5 represents the amount of total interaction.
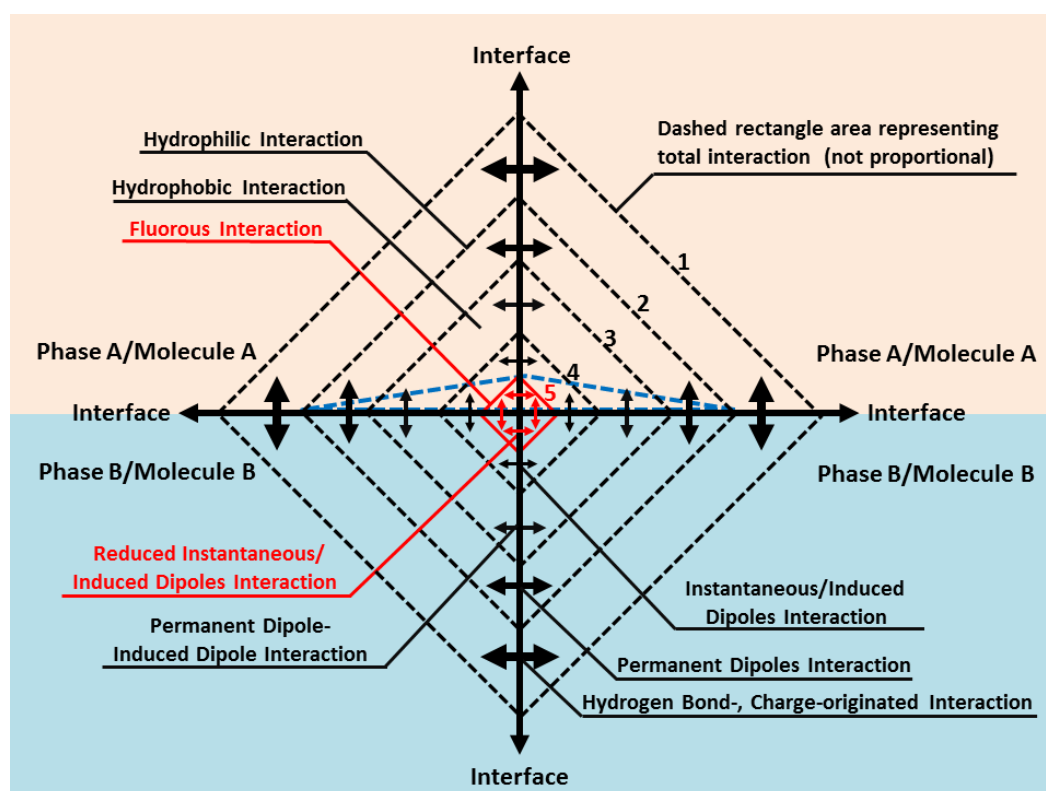
Figure 1.4: An illustration showing the molecular/phasic interaction scale and the origin of the fluorous interaction.

There are also inter-phasic interactions between the fluorous phase and organic phase, which mainly consist of the interaction between permanent dipoles (from organic molecules) and reduced instantaneous or induced dipole interactions (from fluorous molecules), as well as the interaction between instantaneous or induced dipoles (from organic molecules) and reduced instantaneous or induced dipoles (from fluorous molecules). The area of the blue triangle can approximately represent the amount of total interaction, which is significantly smaller than the inner-phasic interactions for the organic phase (hydrophobic interaction).

The inter-phasic interaction between the fluorous phase and organic phase is akin to a divisive force trying to overcome the inner-phasic interactions for the organic phase. However, the desolvation strength of the fluorous phase is not high enough to make it miscible with the organic phase without the addition of heat. Similarly this also happens in the interface between a fluorous phase and an aqueous phase, in which miscibility becomes much more unfavorable due to extensive hydrogen bonding.

To sum up, the fluorous interaction is a kind of reduced instantaneous or induced dipole interaction. The specific interactions of fluorinated molecule - fluorinated molecule and fluorinated molecule - non-fluorinated molecule are weaker than interactions between non-fluorinated molecules, which prevent miscibility of fluorinated/non-fluorinated and fluorinated/aqueous solvent mixtures.

A similar idea is shown in the data within Table 1.1, which summarizes the relationship between solubility and the polarities for both solute A and solvent B. The ambiguous term

"like dissolves like" also suggests the inter-molecular interaction for two phases should be comparable to enhance miscibility.

Table 1.1: Solubility and polarity

Solute A	Solvent B	Interaction			Solubility of A in B
		$A \cdots A$	$B \cdots B$	$A \cdots B$	
Nonpolar	nonpolar	weak	weak	weak	can be high[a]
Nonpolar	polar	weak	strong	weak	probably low[b]
Polar	nonpolar	strong	weak	weak	probably low[c]
Polar	polar	strong	strong	strong	can be high[a]

[a] Not much change for solute or solvent.
[b] Difficult to break up $B \cdots B$.
[c] Difficult to break up $A \cdots A$.
This table is reproduced from reference.[28]

Several parameters have been employed to quantitatively evaluate how similar two phases are (*e.g.* Hildebrand solubility parameter (δ), Hansen solubility parameters (R_a), gas-liquid partition coefficient K, and Snyder solvent scale P`).

(1) Hildebrand solubility parameter (δ),[29-31] which is equal to the square root of the cohesive energy density (energy needed to move a molecule from its neighboring molecules to an infinite distance, which is equal to the heat of vaporization divided by molar volume, Equation 1.1), can be used to estimate the inter-molecular interactions and to indicate solubility. In a specific solute and solvent system, a comparable amount of interactions needs to be applied to solute molecules to separate them from each other and to be surrounded by the solvent. Species with similar values of Hildebrand solubility parameter are more likely to mix.

$$\delta = \sqrt{\frac{\Delta H_v - RT}{V_m}}$$
<div align="right">Equation 1.1</div>

ΔH_v: Vaporization enthalpy

R: Ideal gas constant

T: Temperature

V_m: Molar volume, equal to the molar mass (M) divided by the mass density (ρ)

(2) Hansen solubility parameters (R_a) were developed by Charles Hansen.[32]

$$(R_a)^2 = 4(\delta_{d2} - \delta_{d1})^2 + (\delta_{p2} - \delta_{p1})^2 + (\delta_{h2} - \delta_{h1})^2$$
<div align="right">Equation 1.2</div>

δ_d: The energy from dispersion forces between molecules

δ_p: The energy from dipolar inter-molecular force between molecules

δh: The energy from hydrogen bonds between molecules

These three parameters can be used as co-ordinate values in a known Hansen three dimensional space. The closer two species are in this space; the more likely they are to dissolve with/into each other.

(3) Gas-liquid partition coefficients of selected solutes, K, developed by Rohrschneider through gas chromatography.[33]

$$K = \frac{c_l}{c_g}$$
<div align="right">Equation 1.3</div>

c_l: Concentration of a solute in the solvent

c_g: Concentration of a solute in the gas phase

(4) Snyder solvent scale, P' for the solvent properties of common liquids, developed by

Snyder based on Rohrschneider Gas-Liquid Partition Coefficients of selected solutes, K.[34]

$$P' = \log(K_g'')_{ethanol} + \log(K_g'')_{dioxane} + \log(K_g'')_{nitromethane} \qquad \text{Equation 1.4}$$

$$K_g'' = \frac{K_g'}{K_v} = K_g \cdot V_s \qquad \text{Equation 1.5}$$

V_s: Molar volume of solvent (mL/mole)

K_g: Gas-liquid partition coefficients of selected solutes

K_v: Estimated K_g' value for an n-alkane whose molar volume is the same as the

solute

Both the gas-liquid partition coefficient, K, and the Snyder solvent scale, P' attempt to

evaluate a liquid affinity scale to one or several reference solvents to classify their

inner-molecular interactions.

There are many other models to evaluate the inter-molecular interaction and species (phase,

molecules, and solvents) properties. Regardless of the model chosen, fluorinated species

show the least inter-molecular interaction when compared with their hydrocarbon analogues

due to reduced instantaneous or induced dipoles interactions.[35]

Different molecular interactions are employed depending upon the chromatographic mode utilized. The molecular characteristics of the target analytes are key factors to consider when choosing which type of interaction should be used. For example, in normal-phase chromatography, the stationary phase is hydrophilic. Therefore it has a strong affinity for hydrophilic analytes. Conversely, reversed-phase chromatography employs a non-polar stationary phase where the mobile phase is significantly more polar. Hydrophobic analytes in the polar mobile phase are prone to adsorb to the hydrophobic stationary phase, and hydrophilic analytes in the mobile phase will pass through the column and are eluted. Ion exchange chromatography employs a charged stationary phase to separate ionic melecules. Chromatography based on fluorous interaction takes advantage of fluorous interactions between target analytes and the stationary phase to produce a separation, and is typically employed for molecules containing significant amounts of sp^3 hybridized C-F or those that have been tagged with perfluoroalkyl substituents. Like normal-phase and reversed-phase chromatography, fluorous phases provide another powerful class of stationary phase for chemists.[36,37] In fluorous solid-phase extraction (FSPE) or fluorous chromatography, the specific fluorous interaction is used to separate analytes with a fluorous moiety from ones without a fluorous moiety, or to separate analytes according to their different fluorous content. A brief survey on fluorous chemistry focusing upon the analytical branch will be conducted in the next section.

1.3 – Fluorous Chemistry Evolution

Fluorous chemistry is a long existing but initially-slowly-evolving discipline. In 1940, a liquid fluorocarbon was first used as a solvent to separate uranium isotopes for the Atomic Energy Project (Manhattan project).[21] Even though fluorous liquids possess some remarkable chemical/physical features including chemical inertness, thermal stability, non-flammability, etc., they did not attract much initial academic or commercial interest. Furthermore, fluorous species were not initially considered as an independent class of chemicals. For example, the first report of their use as a fluorous stationary phase treated them as an alternative reversed-phase material for extraction in 1980s.[24,25,38,39]

At the time when the term "fluorous chemistry" was coined, "heavy" fluorous reagents were quite popular. Increasing the fluorine atom ratio is the simplest and most effective way to increase the solubility of fluorous solvents towards fluorous solutes. Heavy fluorous reagents were particularly welcome in fluorous biphasic systems (FBS) [2,3,40,41] derived from the traditional biphasic liquid-liquid extraction (LLE),[42] and quite suitable for large-scale processes.

The FBS concept was first introduced by Horvath and co-workers in 1994.[1,43] It arose from the search for suitable solvent for the reaction where methane in natural gas is catalytically oxidized to produce methanol. Similar to other liquid-liquid biphasic systems, a FBS consists of a fluorous phase containing reagents or catalysts that are preferentially fluorous soluble,

and another phase that could be either an organic or inorganic solvent, with poor solubility in the fluorous phase.

The solubility of fluorous reagents or catalysts in a fluorous phase can be adjusted through the length of the fluorous tag. Higher fluorine density leads to higher solubility in the fluorous phase and poorer solubility (positive by-product) in the other phase (organic or aqueous).

For a specific catalytic system, attaching a fluorous tag containing significant amounts of the highly electronegative element fluorine inevitably leads to a rearrangement of the electronic distribution of the molecule and can change reactivity. Insulating methylene group(s) can be inserted between the active center and fluorous tag of the molecule to eliminate or weaken the electron-withdrawing impact of the fluorous tag. Computational simulation results suggest that a two-methylene-group-insulating spacer is large enough to weaken the electron-withdrawing effect of the fluorous tag.[2,3]

The FBS can be applied to both the synthesis and separation processes. For the fluorous/organic biphasic system, there is a bonus. Elevated temperatures can switch the mixture of fluorous and organic solvent from heterogeneous to homogeneous. This is quite effective for the facile control of both the synthesis and consequent separation.[44] A typical application that enables a fluorous-tagged catalyst to be recycled is shown in Figure 1.5.
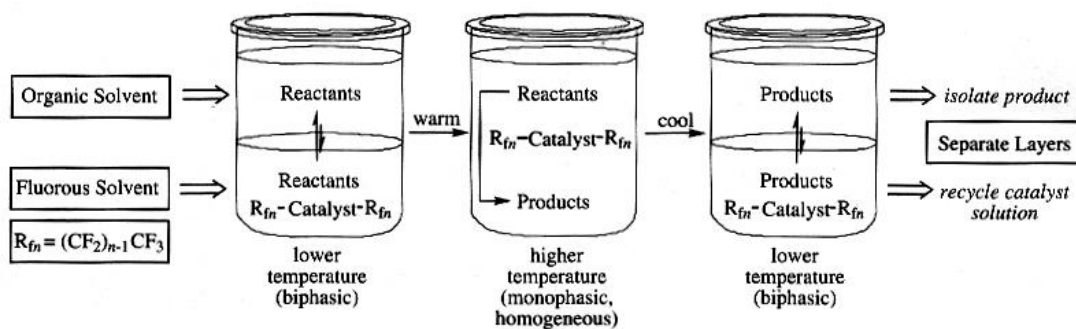
Figure 1.5: First reaction and recovery sequence applied to a fluorous catalyst. This figure is reproduced from reference.[7]

With the temperature-dependent heterogeneous/homogeneous switchable properties, FBS can combine the advantages of one-phase (homogeneous) reaction with biphasic (heterogeneous) product separation. This can be realized thorough careful control of reaction temperature, *i.e.* conducting the reaction at higher temperatures and separating the products at lower temperatures. Fluorous triphasic LLE resembles fluorous biphasic LLE but takes advantage of the poor miscibility with both organic phase and/or aqueous phase as well.[45]

Typically, a structure that contains more than 60% fluorine molecules (by molecular weight), or more than 39 total fluorine atoms is considered to be in the "heavy" classification, while those that are less than 40% fluorine by molecular weight, or contain less than 21 total fluorine atoms fall into the "light" group.[46] Structures in the intermediate range of percentages (41-59% fluorine) are difficult to classify. Instead, classification will depend on the presence or absence of other functional groups to dictate the physical characteristics (*e.g.* polar functional groups would increase organic character at the expense of fluorous).

The drawback of heavily fluorinated molecules is that they have very poor solubility in either aqueous or organic solvents, limiting their broader applicability. The increasing concerns over the persistence of fluorinated substances in the environment and their potential effect therein are another impediment to broader application. As a result, chemists sought alternatives to heavy fluorous groups and light fluorous chemistry was introduced in 1999.[2] Fluorous moiety sizes were decreased drastically, which made fluorous compounds more miscible with organic media, thus greatly expanding their applicability. One negative tradeoff however is reduced solubility in fluorous media, which inevitably decreases the FBS fluorous specificity. The limitations associated with both heavy and light fluorous chemistry led to the use of fluorous stationary phases in fluorous solid-phase extraction (FSPE). The first report of FSPE (called a special type of reversed-phase at that time) was in 1980,[43] 22 years earlier than the creation of the formal "fluorous" definition. FSPE was first described by Curran and coworker in 1997.[3]

1.4 – Fluorous Solid-Phase Extraction (FSPE)

1.4.1 – Overview of Solid-Phase Extraction (SPE)

Before discussing FSPE in detail, it is necessary to have a brief review of the more general solid-phase extraction (SPE) technique. SPE is a fast, cost-effective extraction technique to purify and/or pre-concentrate target components and/or to remove the undesirable interferences from sample matrix prior to conducting chromatography or other processes.

The principle of SPE, which is similar to that of liquid chromatography (LC), takes advantage of stationary phases that have different selectivity for target components or interferences from the sample matrix. By adjusting the mobile phase composition, undesired interferences and components of interest may be eluted sequentially in accordance with their different affinities for the stationary phase.

SPE is an ideal alternative for LLE.[37] It features lower solvent consumption, enhanced sample throughput, more tunable selectivity by appropriate choice of stationary phase, cleaner extracts as well as higher and more reproducible recoveries. It has replaced many of the classical LLE techniques, which are labor-intensive and more difficult to automate.[37] A typical SPE procedure includes four steps as shown in Figure 1.6:

Step 1. Conditioning: the stationary phase in the SPE column is solvated to readily accept liquid sample, typically, with a low elutropic strength solvent.
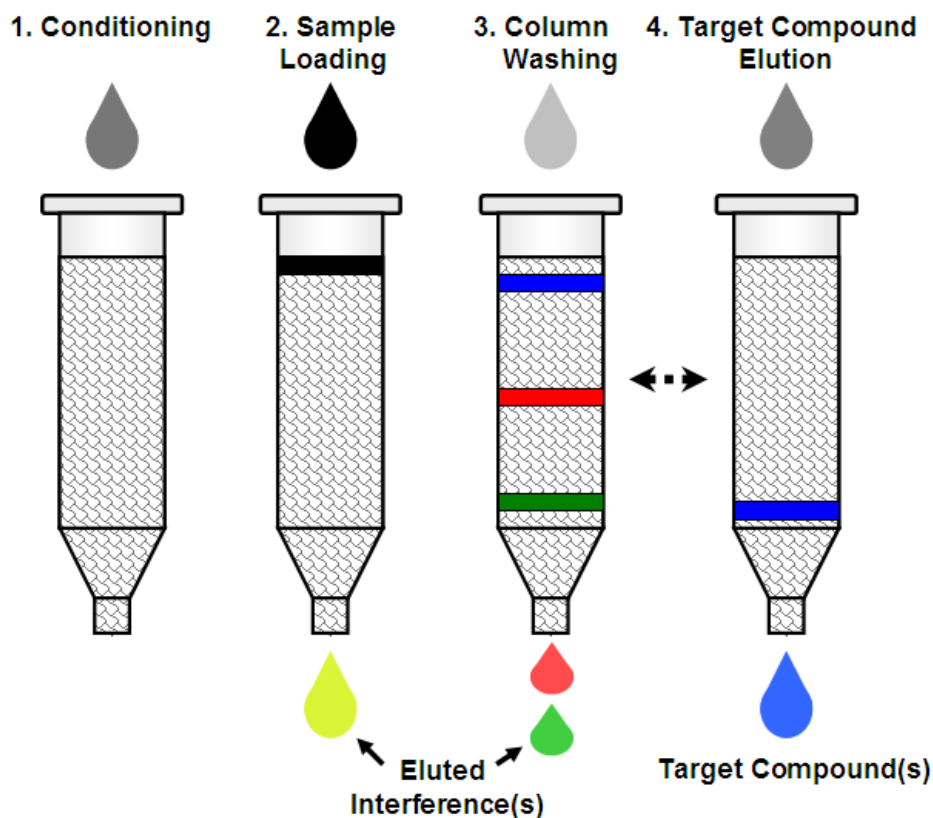
Figure 1.6: Diagram of solid-phase extraction (SPE).

Step 2. Sample Loading: the analyte is loaded onto the column in a low elutropic strength

solvent. The least retained components in sample can sometimes be eluted in this step.

Step 3. Column Washing: the washing step removes undesired interferences.

Step 4. Target Component Elution: this step involves the use of a stronger elutropic strength

solvent (strong elution ability to target component, relatively weak to undesired interferences)

to elute the target component.

Steps 3 and 4 can be reversed through reversing the corresponding mobile phase elution. The

FSPE procedure is identical to SPE, with one critical difference. That is the fluorophobic

mobile phase component and fluorophilic mobile phase components applied in steps 3 and 4, respectively.

1.4.2 – Stationary Phase Material and Morphology for SPE

There is a variety of support choices for preparing SPE stationary phases,[47] for instance, inorganic oxides (silica, alumina, titania, zirconia, and etc.), chemically bonded inorganic oxide, polymer coated inorganic oxides, porous polymer, porous graphitic carbon, nonporous particles, or monoliths. Due to the similar mechanisms, SPE utilizes similar stationary phase chemistries as HPLC. A great number of research groups have worked in the SPE area, and numerous articles including several excellent reviews can be found elsewhere.[37,48-50] This section will be restricted to two types of stationary phase materials rather than an exhaustive discussion: one is silica microsphere-based stationary phases (most widely and deeply studied in the past). The other is porous polymeric monolith (PPM)-based stationary phase (actively studied recently and holds promising future).

1.4.2.1 – Silica Microsphere-Based Stationary Phase

Silica-based stationary phases have dominated SPE for years. It is by far the most important adsorbent for both SPE and HPLC. Silica microspheres with narrower particle diameter distribution have almost completely replaced porous inorganic oxides. Porous inorganic oxides are not able to provide both high efficiency and fast separation time as a result of broad size distributions, large particle sizes, and the slow diffusion of sample molecules through their deep pores. Silica microspheres are mechanically strong and easily prepared in a wide

range of particle size (1.8-25 μm) and pore diameters (6-100 nm) to meet variable requirements.[51] For analytical SPE of small molecules, silica microspheres of 3-10 μm are most widely used, as these sizes provide a reasonable compromise between column performance, stability, operating pressure and separation time. Larger diameter beads, generally between 10 to 25 μm, are used in preparative-scale liquid chromatography. The functional groups on the unfunctionalized silica surface include siloxane, isolated silanol, geminal silanols, and associated silanols (Figure 1.7).[47]

Siloxane   Isolated silanol   Geminal silanols   Associated silanols
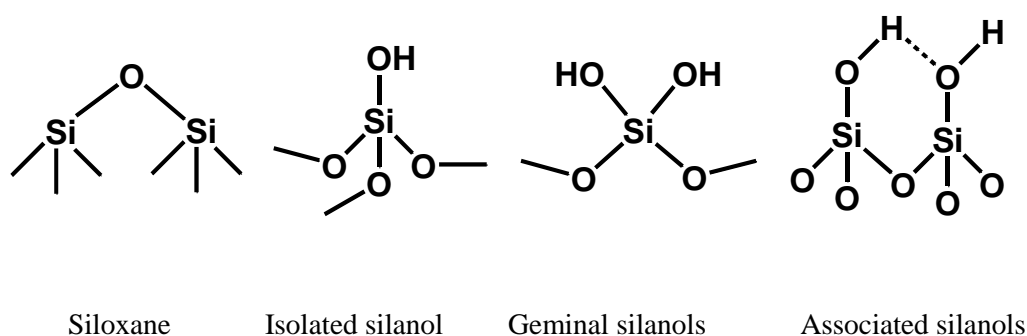
Figure 1.7: The functional groups on the silica surface. This figure is reproduced from reference.[47]

For general applications in SPE and chromatography, the main problems associated with silica are its poor stability in alkaline solution (pH>8), the limited hydrolytic stability of siloxane-bonded phases in acidic solution (pH<2) and strong interactions with basic compounds resulting in distorted peak shape for both native silica and chemically bonded silica surfaces. For example, above their pK_a values (around 4.5-4.7), these silanol groups become ionized and are negatively charged. Positively charged compounds such as protonated amines can interact electrostatically with the ionized silanols. Such strong ionic

interactions might be difficult to overcome with organic solvent elution, and analyte recovery for these polar compounds is affected. To improve the silica microsphere selectivity, modification of the silica surface with chemically bonded organic groups can be done to meet a wide range of separation requirements. For example, C_8 or C_{18} hydrophobic units can be bonded on the silica surface to produce a reversed-phase material. Cyano or amino hydrophilic units bonded to silica or bare silica could be used as a normal-phase material; and in ion-exchange resins, strong anionic sulphonic acid or cationic quaternary amine are bonded. Briefly, three steps are involved in the modification process.

Step 1. Pre-heating: the silica is generally heated over 200 ℃ under vacuum for a few hours to remove physically adsorbed water without dehydrating the surface.

Step 2. Bonding reaction: various organosilanes are used as bonding reagents. The silica will reflux in an inert solvent with organosilanes. The major reaction is shown in Figure 1.8.[52,53] In the monomeric case, mono-functional silanes react with the silanols at the silica surface. Due to the steric limitation, only about half of surface silanol groups are covalently bonded (a, Figure 1.8). A higher ratio of bonded silica surface could be obtained through the reactions of di- or tri-functional silanes with silica. With the addition of water, polymerization of organosilanes could happen in the solution (b, Figure 1.8) or on the surface of the silica (c, Figure 1.8).[54] Bonded silanol concentration could be as high as 2-6 $\mu mol/m^2$, compared with 2-3.5 $\mu mol/m^2$ in the monomeric case.[52,55] Figure 1.9 shows a way to enhance the resistance towards extreme pH. Through introducing bulkier branches, like replacing the methyl groups in alkyldimethylsilane

reagents with a bulky isopropyl or isobutyl group to provide better steric protection of the siloxane (Si-O-Si) bond to hydrolysis at low pH.[56]

Step 3. Endcapping: undesired non-bonded silanols in step 2 can be minimized by reaction with an endcapping reagent, like chlorotrimethylsilane (CTMS) or hexamethyldisilizane (HMDS)[57-59] at higher temperature, *e.g.* above 300 °C for octadecylsilane (ODS)-modified silica.[59] There is no need to perform endcapping for normal-phases that utilize silanols on the silica surface.

After proper surface modification, the silica microsphere is suspended in a solvent, and loaded into a tube with a frit to fabricate a SPE or chromatography column. The next section will discuss another type of stationary phase, PPM. The pros and cons of these two stationary phases are also compared.

Monomeric Synthesis

Solution Polymerization

Surface Polymerization
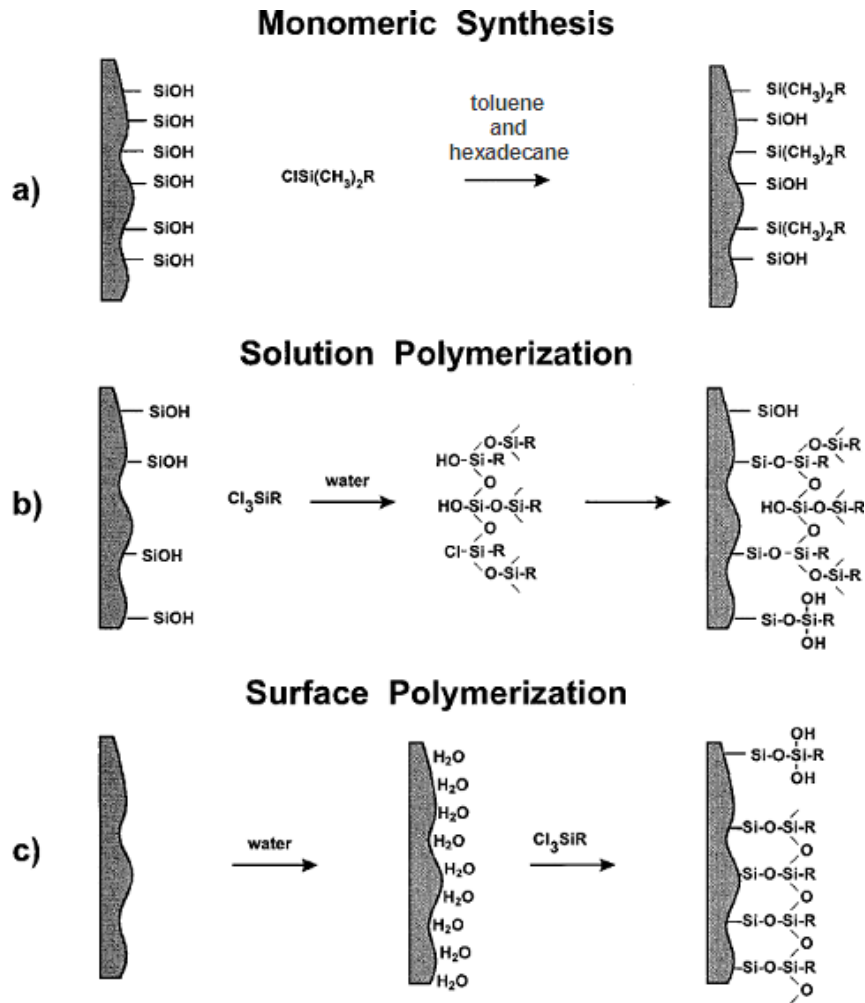
Figure 1.8: Bonding schemes for silica-based stationary phases: (a) monomeric synthesis (b) solution polymerization synthesis, (c) surface polymerization synthesis. This figure is reproduced from references.[52,53]
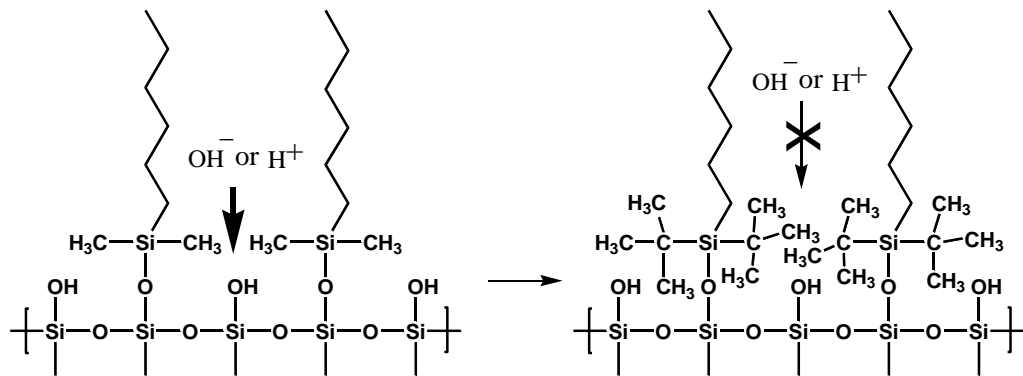
Figure 1.9: Protection from hydrolysis of siloxane (Si-O-Si) bond

1.4.2.2 – Porous Polymeric Monolith (PPM)-Based Stationary Phases

PPM (Figure 1.10) is a newer concept in SPE and chromatography,[60] which unlike packed columns; do not depend on particle technology for their operation.[59] This section will focus upon the positive and negative attributes of PPM's as well as their synthesis and characterization.
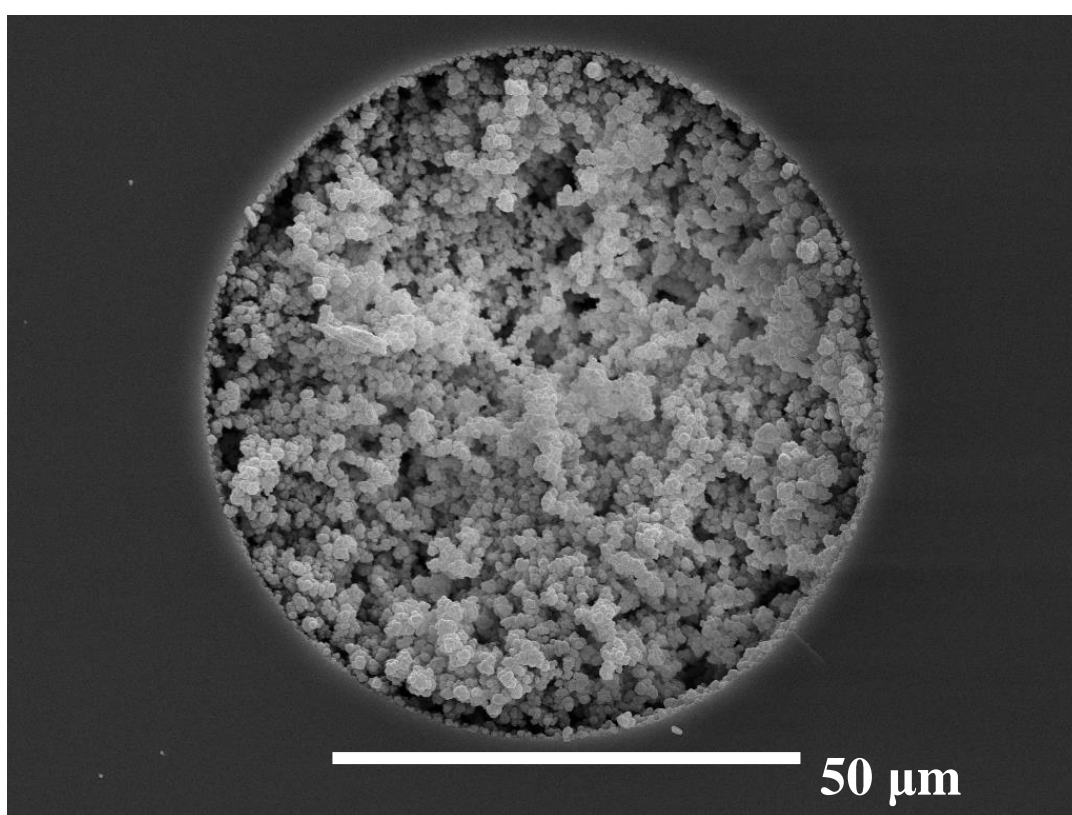
Figure 1.10: Fluorous PPM synthesized in our group

The first PPM preparations can be traced back to 1970s in the works of Ross, Schnecko, Lynn, and others.[61-63] Compared to the silica microsphere-based stationary phases, PPM-based materials possess a number of positive attributes making them attractive as stationary phase materials.[64-66]

(1) PPM-based stationary phase fabrication is a time- and labor-saving facile technique. No frit is required to retain the microspheres in a desired position. In fact, this process is similar to the frit fabrication step for silica microsphere-based columns. The rate of success of PPM preparation is close to 100%. The hydrodynamic backpressure that drives solvent through the bead slurry increases proportionally with the length of packed column. For a column with diameter of 75 μm, 1 cm of mechanically stable silica microsphere (3 μm) packing will produce resisting pressure drops of over 5600 psi (38.6 MPa).[67] Whereas a PPM column with the same diameter and same length only produce < 200 psi resisting pressure drops. Besides, the sedimentation of microspheres in the slurry source is also problematic. Clogging is a common occurrence, especially when packing the columns for analytical applications where diameters can be as low as 50 μm. It is more difficult to apply microsphere-based column packing protocols onto microchips that have thinner microchannel dimensions below (*e.g.* 20 μm × 50 μm rectangular cross-section). The corners in microchip designs also impede the packing of microspheres. When using PPM based materials to form chromatographic columns in microchip applications, the challenges associated with drastic increases in back pressure during the packing process and clogging in narrow channels or columns are minimized. Since the pre-polymerization liquid is a homogenous solution (*vide infra*), it can be pumped through a much smaller diameter microchannel (down to 0.2 μm)[68] and consequently be synthesized *in situ.*

(2) PPM is more resistant in drastic changes in pH.[48] It is totally organic with a homogeneous surface devoid of strong bonding sites (*e.g.* Si-OH), and can be frequently used

with mobile phases of extreme pH where silica-based materials are degraded due to the formation of soluble silicates or hydrolysis of siloxane bonds.

(3) Polymer-based columns have higher capacity under comparable column volume. Higher capacity means that smaller sorbent bed volumes and less sample and solvent are needed. A comparison was made between a commercial ethylvinylbenzene- divinylbenzene (DVB) copolymer SPE packing with a surface area of 1200 m^2/g and conventional silica-based SPE packings, a non-endcapped C_{18} and an endcapped C_{18}.[37] Using caffeine and diisodecyl phthalate (DIDP) as target analytes, it was found that the polymeric column averaged an order of magnitude increase in capacity for the more polar compound, caffeine. For the non-polar DIDP, the increase in capacity was slightly lower.

(4) There is no potential movement in the stationary phase which occurs in silica microsphere-based column. The movement will lead to degraded column performance and irreproducible results.[69]

(5) Variable morphology control, which will be discussed in the preparation section.[70]

There is one argument against PPMs on their relatively smaller surface area due to the lack of mesopores compared to silica microspheres, which impacts the binding capacity.[71-74] However, this shortcoming of PPMs can dramatically turn into another advantage when high flow rates and/or large analytes, like proteins are applied. It is believed that the mass transport at PPM stationary phases is dominated by convection, while the mass transport into mesopores on silica microspheres is dominated by diffusion.[75-77] There is not enough time for large molecules to diffuse into mesopores under high flow rates on silica microsphere stationary phase. Therefore,

an increase in height equivalent theoretical plate (HETP) will be observed (*i.e.* efficiency decrease).

A typical procedure for fabricating a PPM-based column may involve three steps:

Step 1. Pre-treating the surface of the inner wall of a silica tube to attach a vinyl-containing monomer, so that the later synthesized polymer in the column is covalently linked to the inner wall. The attachment of polymer to the column inner wall helps prevent the mobile phase from flowing between the monolith and wall, bypassing the PPM and anchors the PPM in place preventing its extrusion from the column or chip. The most frequently used procedure is through a classic silanization reaction (similar to the silica modification discussed above, Figure 1.8) For example, 3-(trimethoxysilyl)propyl methacrylate (γ-MAPS) could be dissolved in methanol or a mixture of purified water and glacial acetic acid to place a vinyl group on the silica surface.[78]

Step 2. Monolith Polymerization; Reagents including a monomer with one vinyl functional group (*e.g.* butyl acrylate (BA) or 2,2,2-trifluoroethyl methacrylate (TFEM)), a cross-linker with multiple vinyl functional groups (*e.g.* 1,3-butanediol diacrylate (BDDA)), a porogen (*e.g.* 60:20:20 (ACN : ethanol : water), a polymerization initiator (thermal initiator, such as azobisisobutyronitrile (AIBN),[79] or photo initiator, for example benzoin methyl ether (BME)[80-82]). This reaction is a free radical polymerization process, which had been studied systematically as early as the 1970s.[83-86] When ultraviolet (UV) light promotes BME to its excited state, radicals will form through α bond cleavage. Following initiation, propagation

29

and termination, PPM is fabricated *in situ*. The PPM characteristics can be customized by adjusting the ratio of polymerization monomers to porogen, initiator usage, UV wavelength, power, and initiation length. Typically intensities in tens of milliwatts per square centimeter produce polymerization times in the tens of seconds for capillaries and microfluidic channels that are approximately 200 μm in diameter.[87]

Step 3. Modification of the polymeric bed (if necessary),[88-91] for example, as shown in Figure 1.11, graphene oxide (GO) /graphene nanosheets (GN) can be coated onto the poly(glycidyl methacrylate ethylene dimethacrylate, GMA-EDMA) monolith to prepare a polymer monolith microextraction (PMME) material for better recovery of sarcosine and reproducibility.[92]
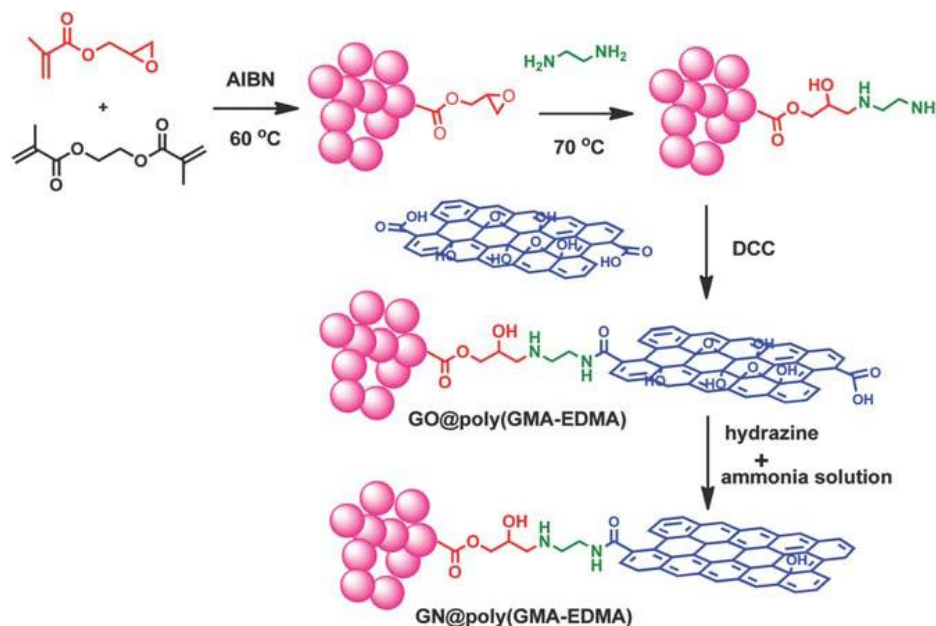
Figure 1.11: Illustration of the procedure for preparing GO@poly(GMA-EDMA) and GN@poly(GMA-EDMA) monoliths. This figure is reproduced from reference.[92]

Over the past two decades,[50,60,93] PPM has won more respect in the SPE and chromatography fields. A variety of PPM-based SPE columns have been reported that have used a number of different chromatographic modes, *e.g.* reversed-phase, ion exchange, size exclusion, and more recently fluorous. There are many commercially available fluorous packing materials and almost all of them are fabricated from fluorous modified silica gel, (*e.g.* FluoroFlash[TM] by Fluorous Technologies Inc., Figure 1.12). An analogous PPM based column can be prepared using a fluorous monomer or fluorous cross-linker. The details on fluorous PPM column fabrication protocol developed by our group will be discussed in detail in Chapter 2 and 3.
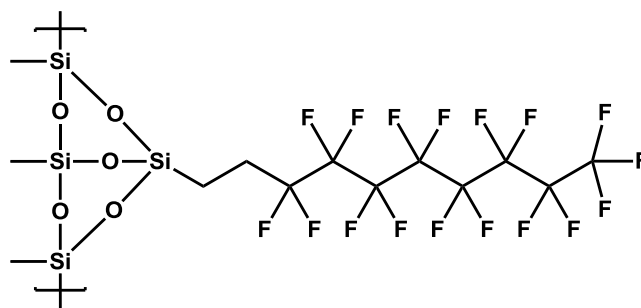
Figure 1.12: Fluorous modified silica gel, featuring $Si(CH_2CH_2C_8F_{17})$.

FSPE and chromatography separate compounds based upon their fluorophilicity and fluorophobicity. Fluorophobic components will spend more time in the mobile phase than the fluorophilic components (*i.e.* the fluorophilic component will spend more time in FSPE stationary phase than the fluorophobic component). A comparison of conventional-FSPE and reverse-FSPE is shown in Table 1. 2.[3,94]

Table 1.2: Comparison of conventional-FSPE and reverse-FSPE

SPE Type	Stationary Phase	Mobile Phase	
		First Elution	Second Elution
Conventional-FSPE introduced in 1997	Fluorous solid-phase Bare silica bonded fluorocarbon SiMe$_2$(CH$_2$)$_2$C$_8$F$_{17}$ FluoroFlash[a]	Fluorophobic solvent 70-80% Methanol/H$_2$O to elute non-fluorous compounds	Fluorophilic solvent (100% Methanol)
Reverse-FSPE introduced in 2004	Bare silica	Fluorophilic solvent perfluorobutyl methyl ether + ethyl acetate to elute fluorous compounds	Fluorophobic solvent

1.4.3 – FSPE and Fluorous Chromatography

SPE and chromatography operate on very similar principals. Both employ a stationary phase with different selectivity towards analytes to realize the separation goal. SPE is usually used for simple/easy tasks or pre-concentration of a specific analyte or a group of analogues where there are large differences in the partitioning ability of the compounds in question. Contrastingly, chromatography is more qualified to cope with tougher tasks (*e.g.* the separation of isomers, chiral mixtures, homologs, etc.) There is a grey area where either SPE or chromatography could be a suitable medium.[60] A group of fluorinated analytes will be separated from their non-fluorinated counterparts in the columns patterned with a fluorous stationary phase. FSPE is the suitable term to describe this process. However, when fluorous analytes are separated in the same column according to fluorous content, fluorous chromatography will be used to describe the process.

1.5 – Microfluidics Technology

1.5.1 – Overview of Micro Total Analysis Systems (µTAS)

A microchip is the core unit for micro total analysis systems (µTAS), which integrates one or several laboratory functions, *e.g.* sampling, sample transport, extraction, dilution, chemical reactions, purification, separation and detection on a single chip, only millimeters to a few square centimeters in size.[95-97]

More than three decades ago, the first microchip fabricated on silicon, a miniaturized gas chromatographic analyzer, was presented.[98] The remarkable gas chromatograph (GC) was

able to separate a simple mixture of compounds on the order of seconds. It included an injection valve, a 1.5 m separation column, and thermal conductivity detector. Unfortunately, its rapid separation capabilities and minute size did not evoke a fierce response in the scientific community. The first attempt to do LC on a chip was one decade later.[96] A 5 mm × 5 mm chip containing an open-tubular column of 6 μm × 2 μm × 15 cm was fabricated.

1.5.2 – Materials for Microchip Fabrication

1.5.2.1 – Glass-Based Microchip

Glass is particularly beneficial for the fabrication of microchips,[95,99-105] since it features well-defined surface properties: uniform surface charge that is critical for electro-osmotic flow (EOF) as a driving force; established micro-fabrication techniques; optical transparency for optical-based detection schemes like UV detection; good compatibility with a range of reagents and negligible swelling after long contact with solvent; good thermal conductivity, which is important for the efficient dissipation of Joule heating in electro-kinetically driven systems.

The main drawback to fabricating microfluidic chips in glass or fused silica is the unit cost for large production runs and their fragility, which can make them difficult to produce at relatively low cost. Furthermore, processing steps such as wet etching using corrosive agents, *e.g.* hydrofluoric acid, require special safety precautions and clean room conditions.

1.5.2.2 – Polymer-Based Microchip

Polymer-based microchip devices are an alternative to glass-based ones. The major advantages of polymers include: easy to fabricate large quantities of devices at low cost; allow simple and fast prototyping methods; easy to fabricate high aspect ratio, mixed-scale structures with multiple levels. The most widely used polymers for microfluidic devices are polydimethylsiloxane (PDMS), poly(ethylene terephthalate) (PET), poly(methyl methacrylate) (PMMA), cyclic olefin copolymer (COC), as well as others.[106]

Unfortunately, unlike glass, there are no ionizable groups (*e.g.* silanol groups) on the surface of most polymers, which hinders their application in electro-kinetically driven applications. Some intrinsic properties of polymers prevent them from being utilized directly in some specific cases. For example, the surface properties of PDMS could lead to sample adsorption (*e.g.* proteins), which contributes to enhanced material losses.[107] Polymers also suffer from more significant joule heating because polymeric systems have low thermal conductivities. Internally generated heat is more difficult to dissipate, which is a problem in electro-kinetically driven microfluidic chips. Furthermore, adequate heat dissipation is critical for temperature-sensitive chemical reactions and thermally labile analytes. Polymer-based chips can also be more sensitive to organic solvents and may not be sufficiently transparent at wavelengths required for monitoring optical responses.

1.5.3 – Advantages

Compared to the traditional analytical processes that utilize a fully equipped chemical laboratory and a qualified technician, microchip-based µTAS provides the following advantages:

(1) Faster analysis and response times due to short diffusion distances, fast heating, high surface-to-volume ratios, small heat capacities and high-throughput analysis.[95,108,109]

(2) Lower fabrication costs, allowing cost-effective disposable single use chips, which make it possible to eliminate contamination issues between samples. Disposability is an important consideration for clinical applications where sample carryover artifacts cannot be tolerated.[110]

(3) Compactness of the systems due to the integration of multiple device functionalities and consequent portability. Compactness is extremely critical when the equipment weight and volume become essentially as important as it performance (*e.g.* equipment mounted on spacecraft)[111] or for *in-situ* clinical diagnosis in remote areas.[112-115]

(4) Low sample consumption (less waste, lower reagent costs and lower required sample volumes).[116] Microchips can handle extremely small volumes of sample, typically picolitres (10^{-12}).

(5) Better process control because of faster system response (*e.g.* thermal control for exothermic chemical reactions).

(6) Safer platform for chemical, radioactive or biological studies because of the integration of functionality, smaller fluid volumes (*e.g.* fuel cells, radioactive tracer synthesis).

These attractive advantages make microfluidic chips useful in many application areas, such as cell culturing and handling,[117-119] clinical diagnostics,[120-123] DNA separation and analysis,[124,125] proteomics,[126] etc.[101-105,112,126-131]

1.6 – Integration of SPE within a Microchip

The primary function of SPE is to pre-concentrate samples. Microchips with solid phase extraction allow one to both purify and pre-concentrate samples prior to detection.

Transplanting SPE from traditional columns to micro-channels within chips triggers a series of new challenges,[67,132] the most troublesome challenge being how to load and retain the chromatographic material into only specific positions with complex channel geometries Furthermore, the chip real world interface can be problematic. In particular, the interface between fluid delivery device and microfluidic chip has pressure limitations for packing chromatographic material. In addition, the microsphere-based stationary phase requires a retaining element/ physical barrier to retain the particles, which has necessitated the use of frits, membranes, or weirs, further complicating microchip designs.[133-137] PPM offers an attractive solution since they can be formed *in situ* (*i.e.* no packing required) and do not need a retaining frit (covalently attached to channel wall).

1.7 – Overview of Proteomics

Proteomics,[138,139] the large-scale study of proteins, particularly their structures and functions, is attracting more and more attention. Biochemists have found that challenges with proteomics far

outweigh its previous analogue, genomics. DNA can be readily amplified using polymerase chain reaction (PCR) to facilitate detection. To date, no similar amplification strategy is available for protein and peptide samples.[140] To complicate matters further, even a single cell could include many proteins and those proteins could also be further altered by hundreds of post-translational modifications (PTM),[141] such as disulfide bonds, alkylation, hydroxylation, phosphorylation, etc. If the number of human genes is about 30,000-50,000, and each gene gives 5-10 different proteins through differential splicing and post-translational modifications, the analytical biochemist may have to handle up to 500,000 proteins, which is beyond current analytical capabilities. Moreover, there is a large protein concentration dynamic range in living organisms. For example, in standard human cells, the most abundant protein is often actin, which is present at about 10^8 molecules per cell. On the other hand, some cellular receptors or transcription factors are probably present at 100-1000 molecules per cell. This makes a 1×10^6 dynamic range. Furthermore, protein size can range from a few tens of amino acids (*e.g.* toxins) to several MDa (*e.g.* human titin, ~27,000 to ~33,000 amino acids depending on the splice isoform). The chemical properties of the proteins vary significantly. In particular their hydrophobicities can make them difficult to handle/recover from aqueous solutions or in gels.[142]

Microchip techniques have been seen as a powerful weapon for researchers and a variety of proteomics operations have been realized using a microchip format,[143] for example protein separation,[128,144] isoelectric focusing,[145] protein digestion,[100] etc.

1.8 – Combination of Fluorous Solid-Phase Extraction and Proteomics

Combining FSPE and proteomics provides a new weapon in the arsenal of chemists and biochemists.[146-149] In fluorous proteomics, specific types of amino acid residues in proteins or peptides can be tagged with a fluorinated tag.[150] The mixture of tagged and non-tagged protein/peptide samples can then be loaded onto columns packed with FSPE stationary phase to undergo concentration, enrichment, and separation.[151,152] Fluorous tags can be versatile and used di-functionally. Firstly, it can serve as a protecting moiety during the peptide synthesis process, and following this step, the tag can be used to enhance separation and purification based upon the fluorous interaction. Fluorous proteomics is extremely selective, and can be readily tailored to separate diverse protein and peptide samples using a single purification method, while other affinity methods require the discovery and development of an individual protocol for each specific functionality, such as antigen-antibody or biotin-streptavidin techniques.

1.9 – Project Objectives

A FPPM-based solid-phase extraction microchip for proteomics application will be fabricated. This microchip will integrate the merits of both fluorous interaction and μTAS technology, and enable target proteins or peptides with fluorous tags to be isolated from non-fluorous tagged proteins based on fluorous-fluorous interaction with a PPM FSPE stationary phase. Then, the tagged species will be detected using ESI-MS, UV, fluorescence, and MALDI-MS.

This project will be disassembled into a series of sections. These include fluorous porous polymer monolith (FPPM) stationary phase development and optimization (Chapter 3), capillary electrochromatography (CEC) on FPPM stationary phase (Chapter 4), qualitative and thermodynamically quantitative study of the fluorous and hydrophobic interaction with PPM stationary phases (Chapter 5), FPPM column liquid chromatography – mass spectrometry (Chapter 6), and Peptide separation using FPPM photo-patterned within microchip channels combined with laser induced fluorescence (Chapter 7).

Chapter 2 – Experimental Section

2.1 – Materials

Butyl acrylate (BA), 1,3-butanediol diacrylate (BDDA), benzoin methyl ether (BME), 3-(trimethoxysilyl)propyl methacrylate (γ-MAPS), DL-dithiothreitol (DTT, 99%), 2-acrylamido-2-methyl-1-propanesulfonic acid (99%) (AMPS), thiourea, sodium phosphate, nitrobenzene, *alpha*-cyano-4-hydroxycinnamic acid (CHCA), insulin, benzene, toluene, ethyl benzene, n-propyl benzene, n-butyl benzene, n-hexyl benzene, and n-octyl benzene were obtained from Aldrich (Oakville, ON, Canada). 1H,1H-heptafluorobutyl acrylate (FBA) and 2,2,3,3-tetrafluoro-1,4-butyl diacrylate (TFBDA, fluorous cross linker) were purchased from Oakwood Products (West Columbia, SC). Glacial acetic acid, acetonitrile (ACN, HPLC grade), and tetrahydrofuran (THF) were obtained from Fisher Scientific (Nepean, ON, Canada). Formic acid (98%) was purchased from BDH Chemicals (Toronto, ON, Canada). Ethanol (95%) was acquired from Commercial Alcohols (Brampton, ON, Canada). Water for aqueous solutions was purchased from Fisher Scientific (Ottawa, ON, Canada).

Custom peptide I (acetylated leucine-leucine-cystine-leucine-leucine) with purity greater than 90% was synthesized by JPT Peptide Technologies GmbH (Berlin, Germany). Custom peptide II (Alanine-Serine-Lysine-Serine-Cystaine, >90% purity) was synthesized by Biomatik (Cambridge, ON, Canada). The HPLC and MS characterization data provided by Biomatik are shown in Appendix Figure 1 and Appendix Figure 2 respectively. Cy5-NHS mono-functional

ester (purity is 93.9% determined by HPLC) was bought from GE Healthcare UK limited (Little Chalfont Buckinghamshire, UK).

N-f-Cbz-4-nitrobenzylamine mixture (N Series, $C_{17+x}H_{17}F_{2x+1}N_2O_4$; x = 3, 4, 6, and 8; named N1, N2, N3, N4, respectively, according to the fluorous moiety length) and *N*-f-Cbz-4-phenylbenzylamine mixture (P Series, $C_{23+x}H_{22}F_{2x+1}NO_2$; x = 3, 4, 6, and 8; named P1, P2, P3, and P4, respectively, according to the fluorous moiety length), were custom analytes synthesized by Fluorous Technologies (Pittsburgh, PA, USA), who also provided N-[(3-perfluorohexyl)propyl]iodoacetamide. N Series and P Series nuclear magnetic resonance (NMR) characterization spectra provided by Fluorous Technologies are shown in Appendix Figure 3 and Appendix Figure 4 respectively. The synthesis protocol is shown in Appendix Scheme 1.

Some materials structures are shown in Figure 2.1.
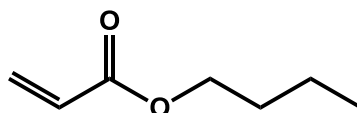
Butyl acrylate (BA)
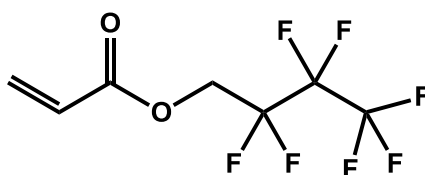
1H,1H-heptafluorobutyl acrylate (FBA)
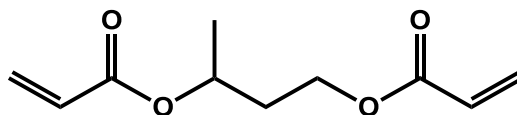
1,3-butanediol diacrylate (BDDA)
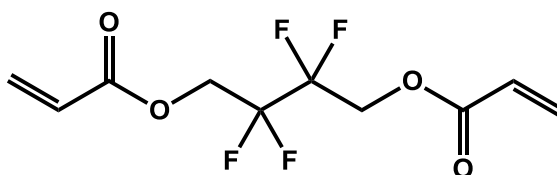
2,2,3,3-tetrafluoro-1,4-butyl diacrylate (TFBDA, fluorous cross linker)
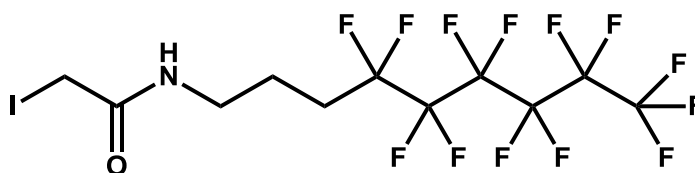
N-[(3-perfluorohexyl)propyl]iodoacetamide
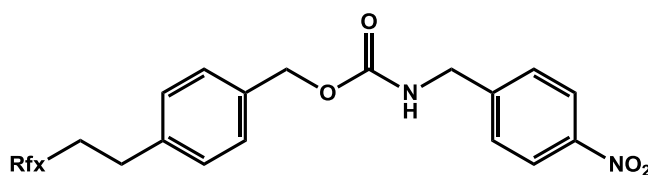
N Series, Rfx = C_3F_7; C_4F_9; C_6F_{13}; or C_8F_{17}
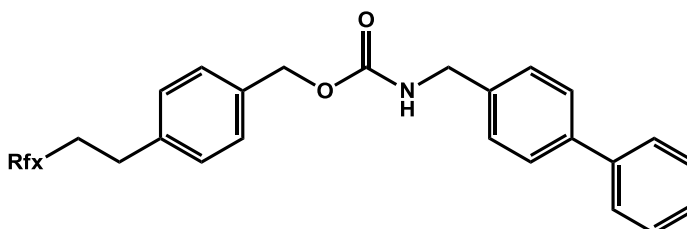
P Series, Rfx = C_3F_7; C_4F_9; C_6F_{13}; or C_8F_{17}
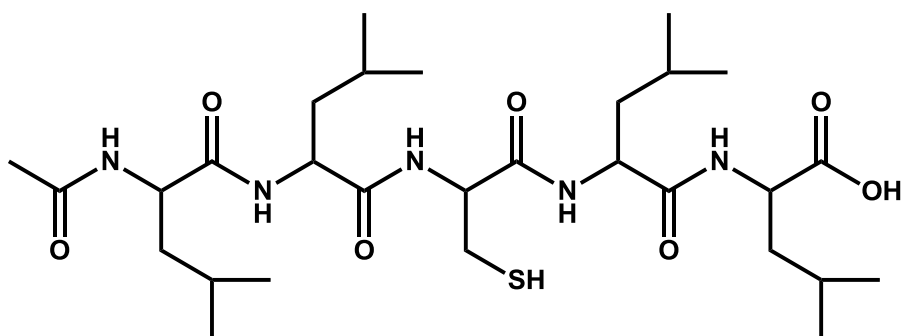
Custom peptide I (acetylated leucine-leucine-cystine-leucine-leucine)
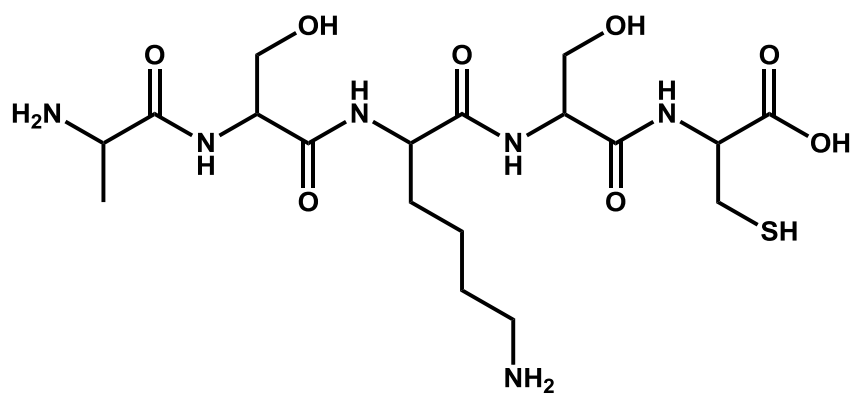
Custom peptide II (Alanine-Serine-Lysine-Serine-Cystaine, >90% purity)
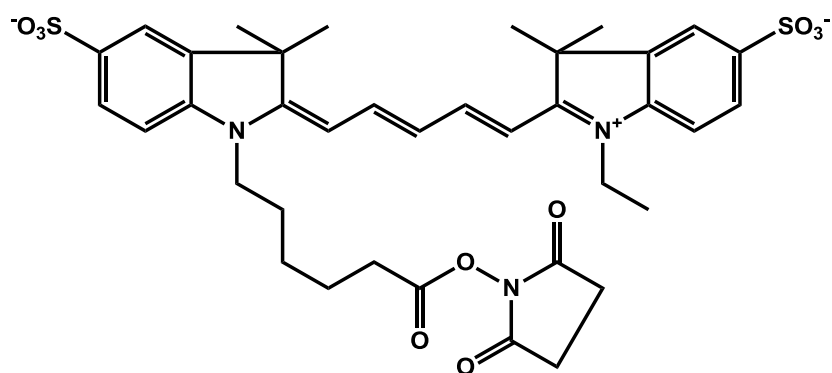
Cy5-NHS mono-functional ester
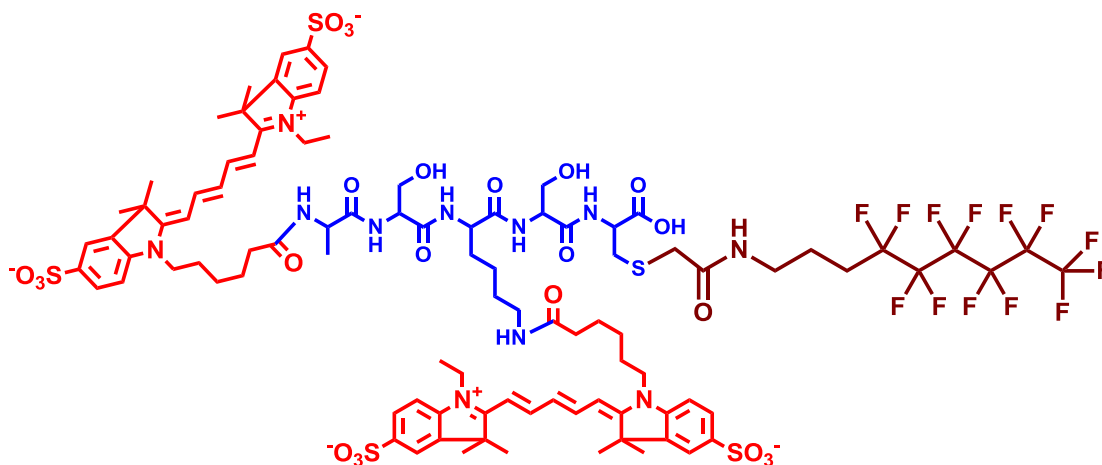
Fluorous and fluorescently tagged custom peptide II with Cy5-NHS mono-functional ester

and N-[(3-perfluorohexyl)propyl]iodoacetamide

Figure 2.1: Materials structures

2.2 – Capillary-Based HPLC PPM Column Fabrication

Capillary-based HPLC PPM column fabrication process is shown in Figure 2.2. Firstly, fused

silica capillary (75 μm I.D., 363 μm O.D. with a UV-transparent coating; Polymicro

Technologies; Phoenix, AZ, US) was employed as a vessel for the monoliths. Prior to

polymerization, the inner walls of the capillary were pre-treated with a solution of γ-MAPS,

water, and glacial acetic acid (20:50:30; all values in volume percent unless otherwise stated) to

functionalize them with vinyl groups (facilitating monolith attachment). The reaction is shown

in Scheme 2.1. Capillaries filled with this pre-treatment solution were left to react for 24 hours.

Next, a mixture consisting of polymerizable material (70:30, (BA or/and FBA) : (BDDA or/and

TFBDA)), porogenic solvent (60:20:20, (ACN : water : ethanol)), γ-MAPS (4 μL for every mL

of polymerizable materials; improves polymer attachment to capillary walls), and BME

(serving as free-radical initiator) was manually injected into the pre-treated capillary by syringe. Polymerization was initiated using UV light (254 nm (Model Spectroline EBF-280C), 312 nm (Model Spectroline EBF-280C), or 365 nm (Model Spectroline EN-180) UV lamp; 115 V, 60 Hz, 0.2 A; Spectronics Corporation, Westbury, New York, USA) and carried out for 4 minutes. The polymerization is a typical free radical initiated one as shown in Scheme 2.2. Finally, the capillaries were connected to a HPLC pump (model 590; Waters; Milford, MA; 95:5 (ACN : water) solvent) for 2 hours at a flow rate of 10 μL/min to flush away any unreacted monomer and cross-linker prior to testing the resultant monoliths.

With the use of UV-initiated polymerization, monoliths can be selectively patterned in the capillaries by masking any regions where polymer is not desired. Unfortunately, small amounts of heterogeneous polymer still tend to form at the boundaries between the masked and exposed regions, presumably due to leaching under the mask. In these areas, the monolith density and morphology are uncontrollable and unpredictable, meaning that they need to be eliminated prior to testing. This can be accomplished by forming a monolith that is slightly longer than the desired length and subsequently cutting off the two boundary regions to leave a material of the proper scale and without any structural concerns. More details about the unwanted polymerization will be discussed in Chapter 7.
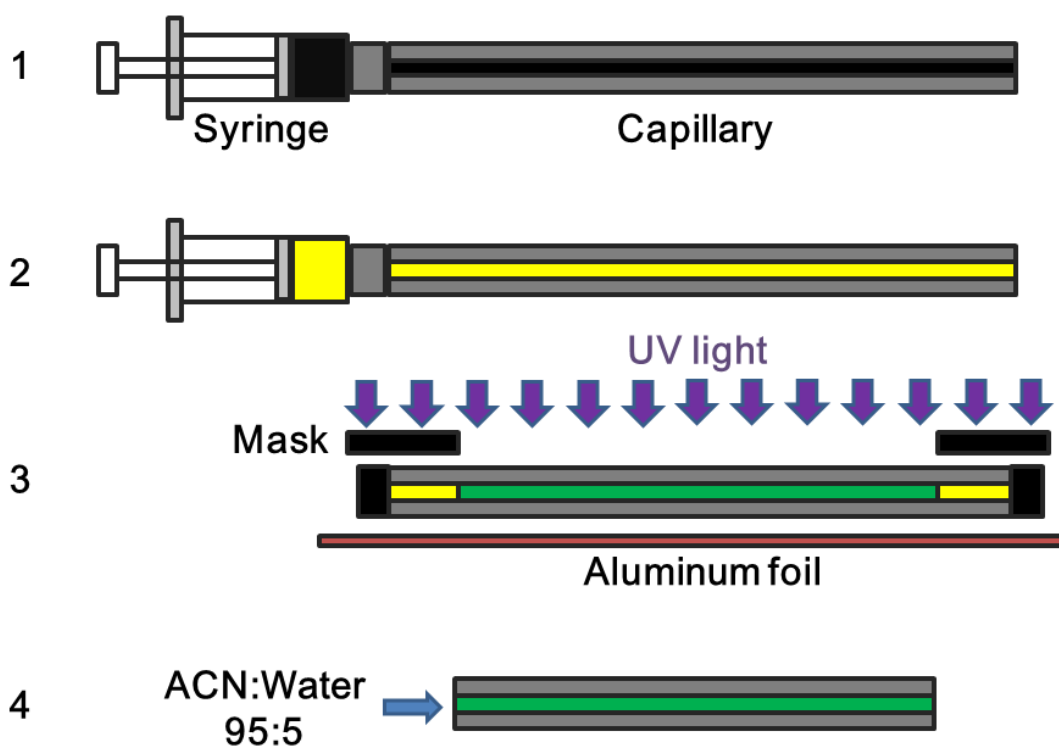
Figure 2.2: Capillary based HPLC PPM column fabrication process. Step 1. Functionalization of the capillary wall with γ-MAPS; Step 2. Loading of the PPM pre-polymerization solution; Step 3. UV-initiated polymerization; Step 4. Flushing the unreacted monomer and the cross-linker.
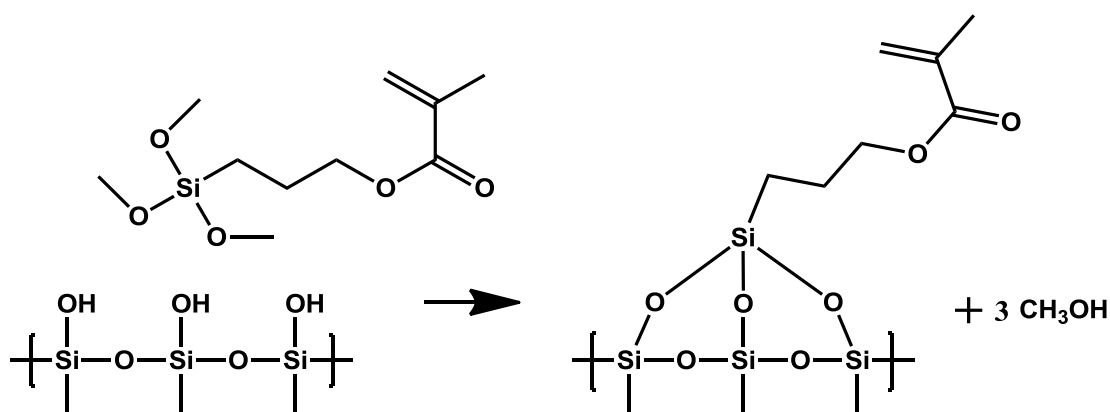
Scheme 2.1: Column pre-treatment with γ-MAPS
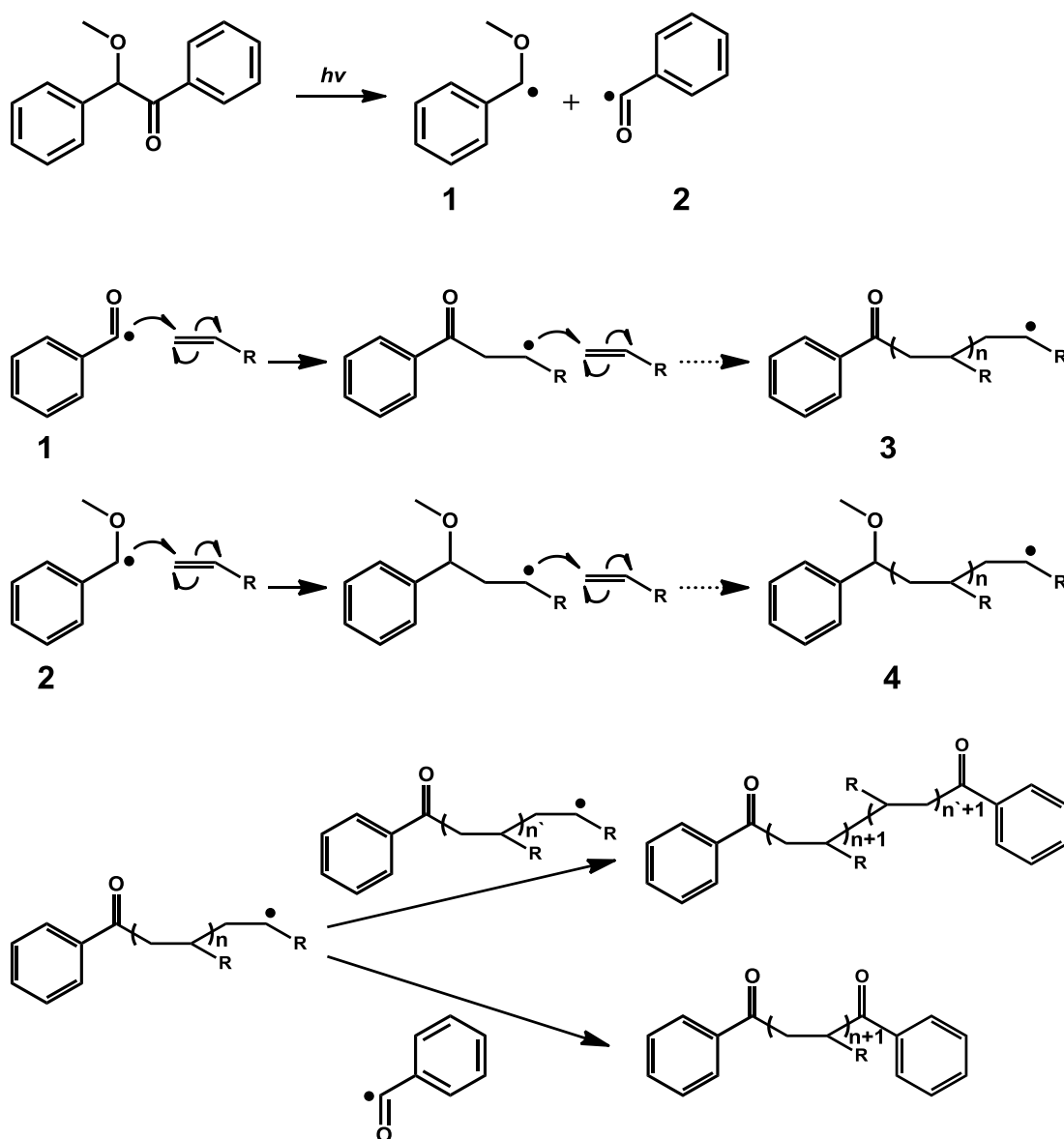
Scheme 2.2: UV initiated polymerization to prepare PPM. The reaction includes three steps free radical initiating (top), chain transfer (2 middle reactions), and chain termination (bottom)

2.3 – Capillary-Based CEC PPM Column Fabrication

Transferring the PPM technology from LC to CEC experiments requires some necessary adjustments to the fabrication process, which is briefly described in Figure 2.3.

First, the inner wall of fused silica capillary (40 cm long, 75 μm I.D., 363 μm O.D. with a UV-transparent coating; Polymicro Technologies, Phoenix, AZ, USA) was pre-treated for 24 hours. A solution of γ-MAPS, glacial acetic acid, and water (20:30:50) was used to functionalize the capillary inner wall with vinyl groups to facilitate monolith attachment during subsequent polymerization. Next, a PPM polymerization mixture comprising 25% polymerizable material (70:30, (BA or/and FBA) : (BDDA or/and TFBDA)), 75% porogenic solvent (60:20:20 (ACN : water : ethanol)), free-radical initiator BME (2.1 mg/mL), and AMPS (charge-bearing monomer to promote EOF,[153,154] 1.75 mg/mL), was manually injected into the pre-treated capillary by syringe. This concentration of AMPS was chosen because the resulting EOF velocity in the column was in a good range for CEC,[154,155] and the chromatographic performance of this AMPS-modified PPM column was not significantly different from one without AMPS as judged by the LC separation of the N series of analytes.

Due to the size limitation of the UV lamp (20 cm effective exposure length), a two-step polymerization was employed. In step 3, both ends of the capillary containing PPM polymerization mixture were sealed with LB-1 rubber septa (Supelco Analytical, Bellefonte, PA, USA). The capillary was masked with black tape for 14 cm from one end to prevent polymerization there. Polymerization of the other end was then initiated using 312 nm light for 5 minutes. The second polymerization step (step 4, Figure 2.3) was initiated after removing the mask from step 3 and masking 26.5 cm of the capillary from other end. This leaves 0.5 cm of the capillary that was masked in both polymerization steps, resulting in a window containing no polymer that allows subsequent absorbance detection by the diode array detector in a Beckman

Coulter P/ACE MDQ capillary electrophoresis system (Fullerton, CA, USA). Both polymerization steps included aluminum foil underneath to more evenly illuminate the capillary during polymerization.

Finally, the resulting PPM was flushed with 95:5 (ACN : water) using a HPLC pump (model 590, Waters, Milford, MA,) for 2 hours at a pressure of 9.6 MPa to remove any unreacted monomer and cross-linker (step 5). Step 6 in Figure 2.3 and Figure 2.4 show the schematic diagram of the setup employed for the CEC separation experiments.
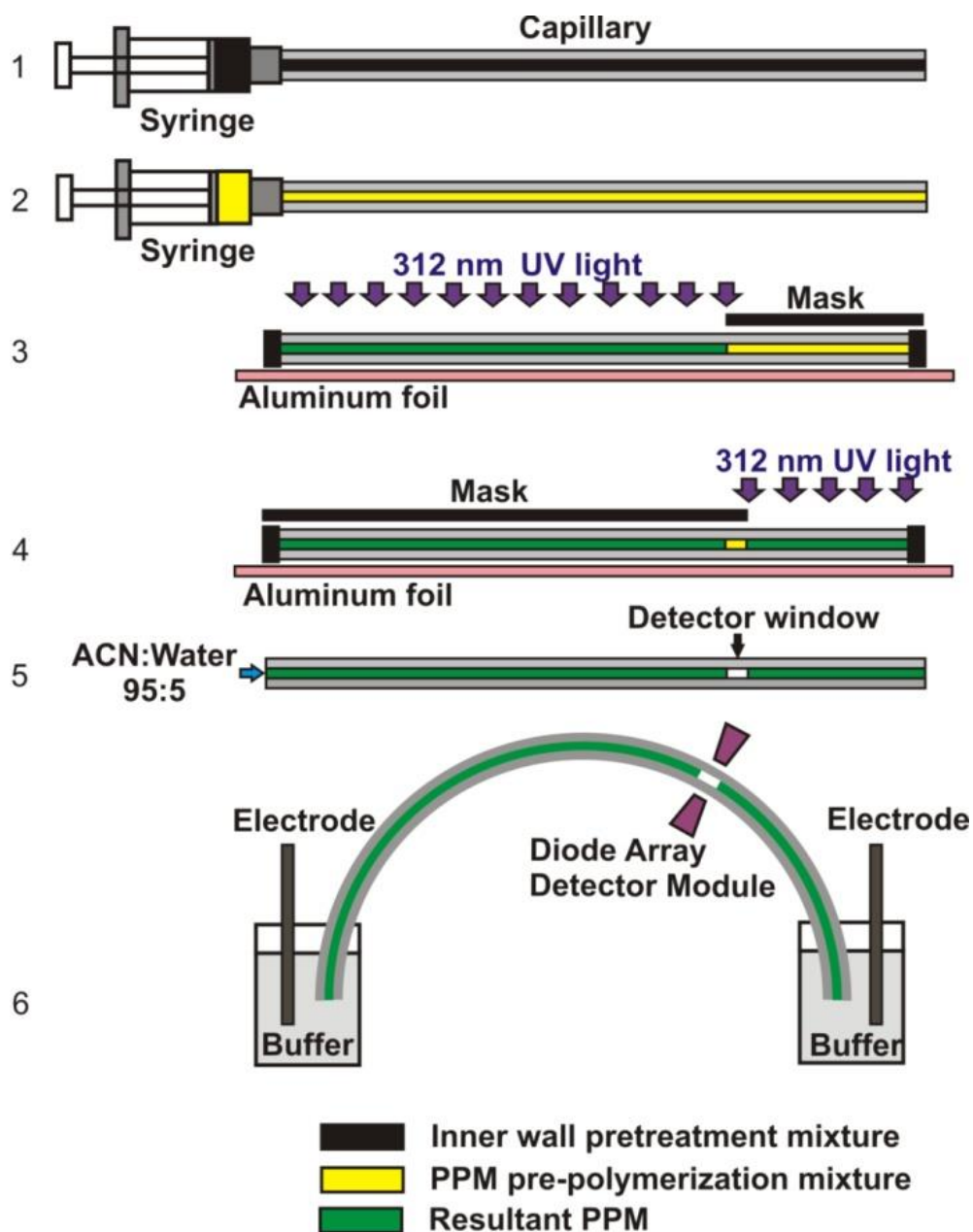
Figure 2.3: Fabrication process of a PPM column by UV photo-initiated polymerization. Step 1. Functionalization of the capillary wall with γ-MAPS; Step 2. Loading of the PPM pre-polymerization solution; Step 3. First UV-initiated polymerization (front part of column); Step 4. Second UV-initiated polymerization (column downstream of detector); Step 5. Flushing the unreacted monomer and the cross-linker; Step 6. General setup of the PPM column in a CEC experiment.
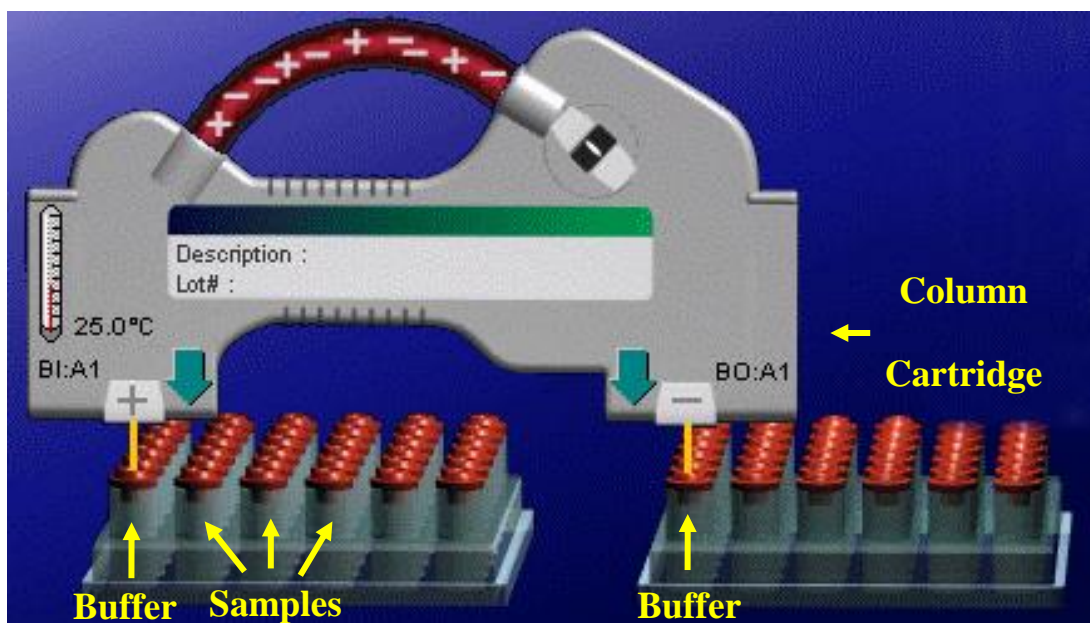
Figure 2.4: The CE cartridge containing the PPM column uses coolant cycling to maintain the capillary temperature of the Beckman Coulter CE system.

2.4 – Microchip Channel-Based FPPM Column Fabrication

The fabrication process of the FPPM column based on UV photo-initiated polymerization on capillary-based column had been described in Section 2.2 – Capillary-Based HPLC PPM Column Fabrication, Section 2.3 – Capillary-Based CEC PPM Column Fabrication, and in some of our previous work. Transferring the FPPM synthesis from capillary to microchip requires some necessary adjustments.

A custom clamp was fabricated to hold the NanoPort™ (Upchurch Scientific®, IDEX Corporation, Oak Harbor, WA, US, Panel A, B, Figure 2.5) to the chip to introduce reagent and sample solutions.[156] The custom clamp had holes that matched the size and pattern of the chip (chip dimensions shown in Panel C, Figure 2.5, Micralyne Inc, Edmonton, AB, Canada).

Once the clamp was affixed, the pre-treatment solution, flushing liquid, pre-polymerization mixture, and CEC buffer could be introduced using a LC pump (Panel A and B, Figure 2.5).

First, a solution of γ-MAPS, glacial acetic acid, and water (20:30:50) was used to functionalize the microchip channel inner wall with vinyl groups to help monolith attachment during subsequent polymerization. The inner wall of microchip channel was pre-treated for 24 hours. Next, a FPPM pre-polymerization mixture comprising 25% polymerizable material (70:30, FBA : BDDA), 75% porogenic solvent (60:20:20, (ACN : water : ethanol)), free-radical initiator BME, AMPS (charge-bearing monomer to promote EOF, 1.75 mg/mL), and nitrobenzene (free radical quencher) was introduced into the pre-treated channel by syringe through the home-made clamp with NanoPort^{TM}. Polymerization was initialized by the UV lamp using 312 nm light for 5 minutes (ENF-280C, Spectronics Corporation, Westbury, NY, USA). 312 nm initiating UV wavelength was chosen based on the discussion in Section 3.2.4 – Initiating UV Wavelength Impact on PPM Morphology and Chromatographic Performance and Figure 2.6. The short UV Wavelength (e.g. 254 nm) cannot penetrate the upper layer of microchip. On the other hand, the long UV Wavelength (e.g. 365 nm) will produce finer PPM skeleton and consequent clogging as discussed in Section 7.2.1 – Unwanted Polymerization Initiated by UV Light Migrating under Photo-Masked Area.

Areas where polymer was not required were masked with black tape. Aluminum foil was employed underneath the microchip to more evenly illuminate the channel during polymerization. Finally, the resulting FPPM was flushed with 95:5 (ACN : water) using a

HPLC pump (model 590, Waters, Milford, MA,) for 2 hours at a pressure of 5.0 MPa to remove any unreacted monomer and cross-linker.

Four sample containers were prepared from 101-1000 µL Redi-Tip™ General Purpose Pipet Tip (Fisher Scientific, US) and cap for Target® Vial C4010-1BC (National Scientific Company, Thermo Fisher Scientific, Rockwood, TN, US). The pipet tip was cut into three parts (3 mm, 38 mm, and 29 mm respectively from tip end, Panel D, Figure 2.5). The middle part (38 mm in length) was chosen as the container. Since its thin end O.D. fits the reservoir diameter whereas its thick end I.D. fits Target® Vial cap O.D. A complete custom microchip with sample containers is shown in Panel E, Figure 2.5. The edges of the caps were cut off to enable them to be placed in close proximity. These caps have a self-closing slot which allows the Pt electrodes to pass through to minimize evaporation of the samples.

In Panel F, Figure 2.5, an integrated microchip was mounted on a Microfluidic Tool Kit. An elevating arm over the microchip was set to hold the Pt electrodes and LED lights. Pt electrodes were arranged according to the pattern of microchip reservoir design. A slot under the microchip enables the detector (integrating excitation laser, fluorescence inlet, and optical microscope objective) lens to be positioned through an x-y-z stage. In our trial, the detector was set immediately downstream of the FPPM along the channel to minimize the post-column dead volume.

Sample was driven from R2 to R3 in the sample loading step that lasts 30 seconds. Then the sample portion located in the joint cross area of channel from R2 to R3 and channel from R1

to R4 was carried by the buffer from R1 downstream (to R4). Fractions in the sample were separated on the FPPM based on fluorous stationary phase selectivity towards fluorous moieties. Fluorescent detection was conducted immediately after the FPPM stationary phase.
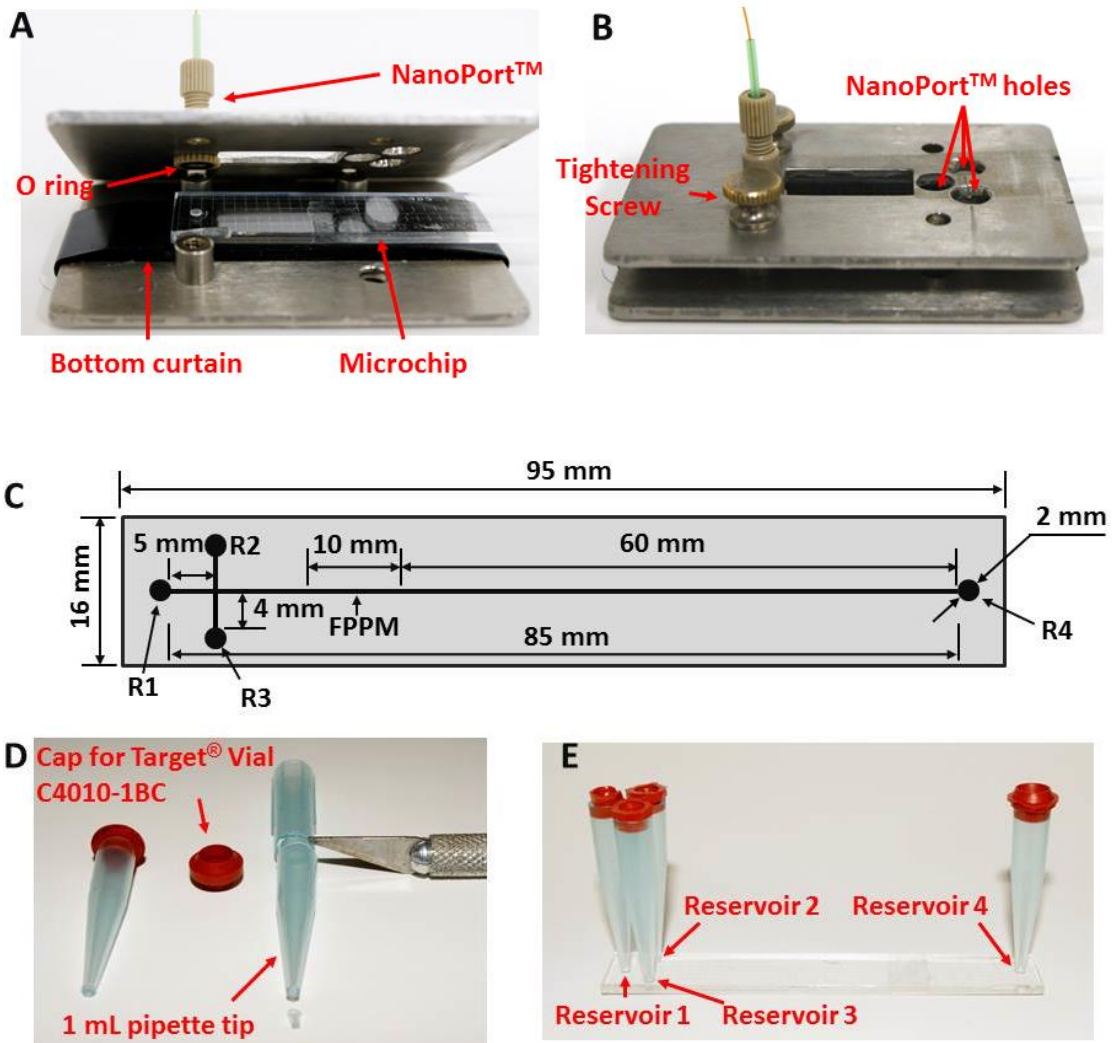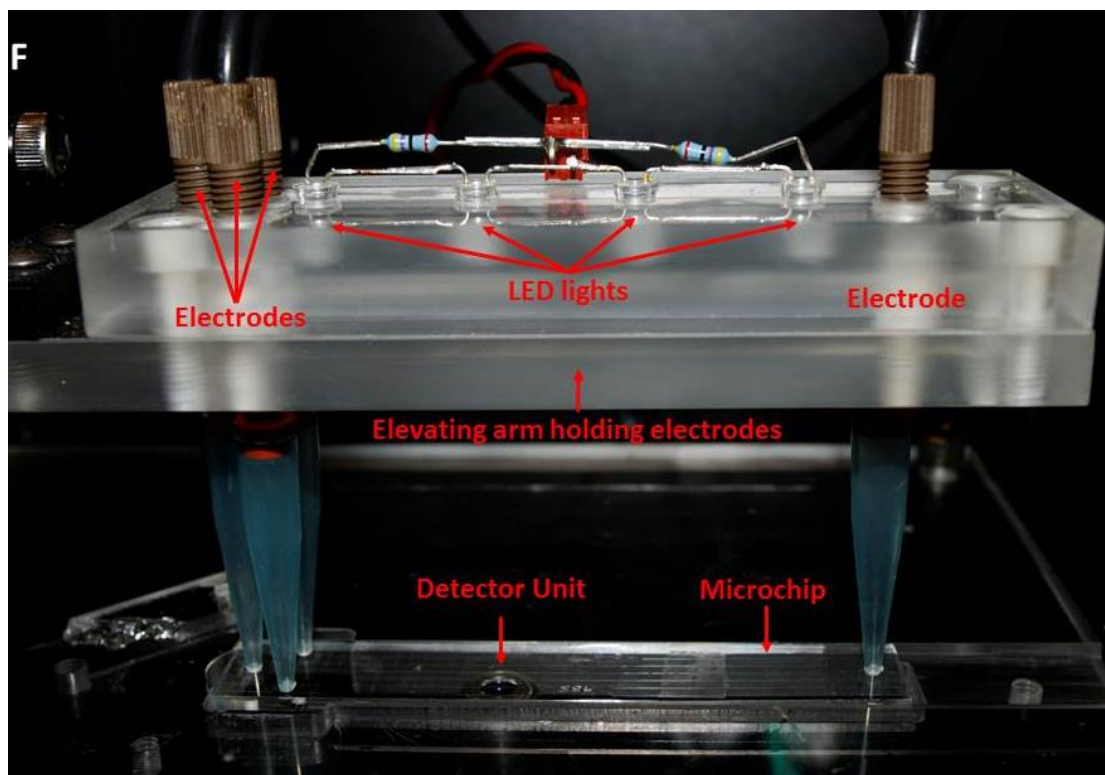
Figure 2.5: Fabrication process of the FPPM column based on UV photo-initiated polymerization on microchip channel. Panel A, Panel B, custom clamp with holes matching the size and position of NanoPort^{TM} fittings (Upchurch Scientific$^®$, IDEX Corporation, Oak Harbor, WA, US); Panel C. Design and dimensions of microchip obtained from Micralyne Inc, Edmonton, AB, Canada. Reservoir 1, 2, 3, and 4 are identified as R1, R2, R3, and R4 respectively; Panel D. Samples containers made from 101-1000 μL Redi-Tip^{TM} General Purpose Pipet Tip (Fisher Scientific, US) and cap for Target$^®$ Vial C4010-1BC (National Scientific Company, Thermo Fisher Scientific, Rockwood, TN, US); Panel E. A complete microchip with sample containers; Panel F. Microchip mounted on a Microfluidic Tool Kit (Micralyne Inc, Edmonton, AB, Canada).
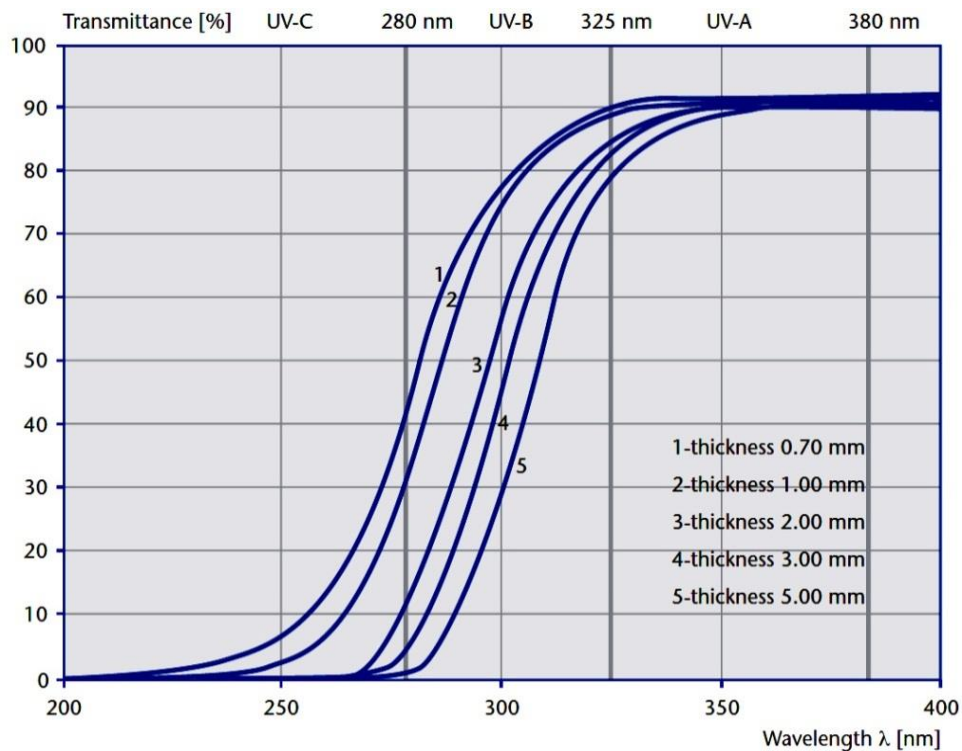
Figure 2.6: Low fluorescence Schott Borofloat[TM] (SCHOTT North America, Inc., Elmsford, NY, USA) glass, transmittance in the UV range. This figure is reproduced from reference.[157]

2.5 – CEC Mobile Phase Preparation

Four sodium phosphate buffer solutions were all prepared at pH 7.0 to ensure all analytes are neutral. The mobile phase compositions prepared were ACN : water (80:20), (75:25), (70:30) and (65:35), with total buffer concentrations of 1.6 mM, 2.0 mM, 4.0 mM and 4.0 mM, respectively. In each case, the required amount of sodium phosphate was dissolved in the aqueous component of the mobile phase, the pH was adjusted to 7 with 1 M HCl using a pH meter (accumet® BASIC AB15, Fisher Scientific, USA), then the ACN component was added. Then, the buffer was degassed for 15 minutes in an ultrasonic cleaner (AQUASONIC[TM] Model 75T, VWR, West Chester, PA, USA).

2.6 – HPLC Operation

HPLC experiments were conducted on a nanoAcquity UPLC system (Waters Corporation, Milford, MA, US). UV detection wavelength was 228 nm. Auto-sampler temperature was maintained at 25 °C. Aqueous phase (A, 99.9% water with 0.1% formic acid) and organic phase (B, 99.9% ACN with 0.1% formic acid) were combined to make the total mobile phase. Total flow rate was 400 nL/minute. Sample injection volume was 2 μL. Column length was 10 cm. A gradient method was employed and shown in Figure 2.7: 99% to 10% A over 15 minutes, then to 1% A over 5 minutes, and finally back to 99% A in 1 minute to give a total time of 21 minutes.
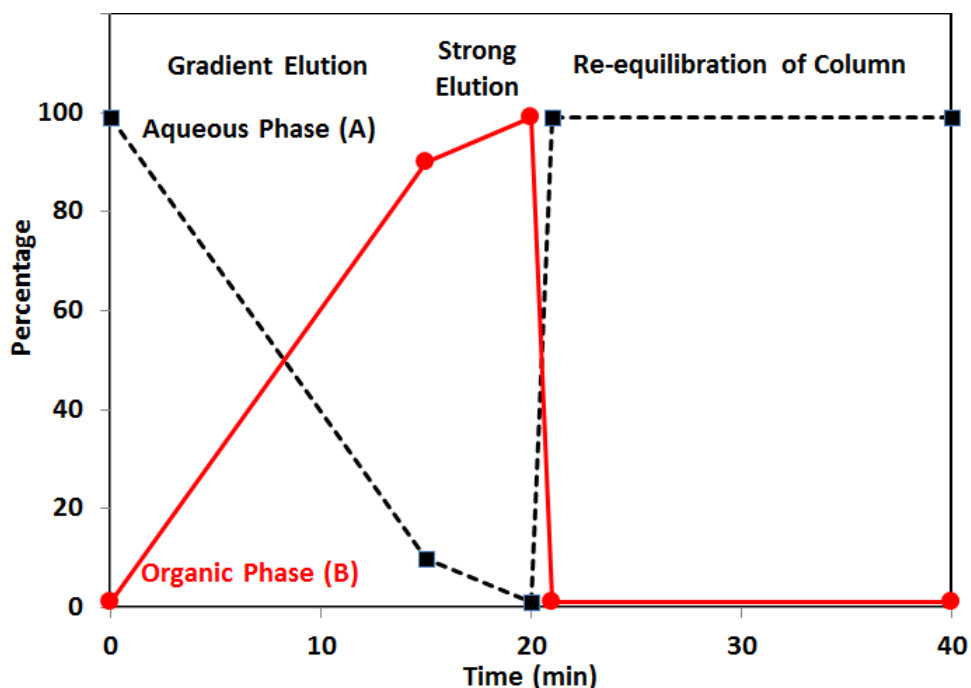
Figure 2.7: Gradient elution steps in nanoAcquity UPLC system.

2.7 – CEC Operation

CEC operation was conducted on a Beckman Coulter CE system. The CE cartridge containing the PPM column uses coolant cycling to maintain the capillary temperature at 25 °C. The detector window is 20 cm to the left end of the capillary and 10 cm to the right end (Step 6, Figure 2.3). N Series and P Series analyte solutions were prepared at 0.280 mg/mL in 80:20 (ACN : water) mobile phase with a thiourea (EOF Marker) concentration of 0.020 mg/mL. Phenyl Alkane Series containing n-propyl benzene, n-butyl benzene, n-hexyl benzene, and n-octyl benzene analyte solution was prepared at 2.5 mM for all fractions with a thiourea concentration of 0.100 mg/mL. All analytes were loaded from the injection end (*i.e.* 20 cm effective column length). The samples were loaded by electro-kinetic injection using 10.0 kV for 3 seconds for all trials.

A photodiode array detector was used to determine an optimal wavelength for detection. Figure 2.8 shows a separation of the N Series of fluorous compounds over time in the absorption range 190-300 nm. Despite much stronger analyte absorption at shorter wavelengths, 214 nm was chosen for detection as each of the fluorous analogues exhibited some absorption at this wavelength and background noise from absorption by the mobile phase was limited, resulting in a smooth baseline.

A 635 nm Laser Module (excitation wavelength is 635 nm, emission wavelength is 675 nm) (Fullerton, CA, USA) was employed for the laser induced fluorescence detection.
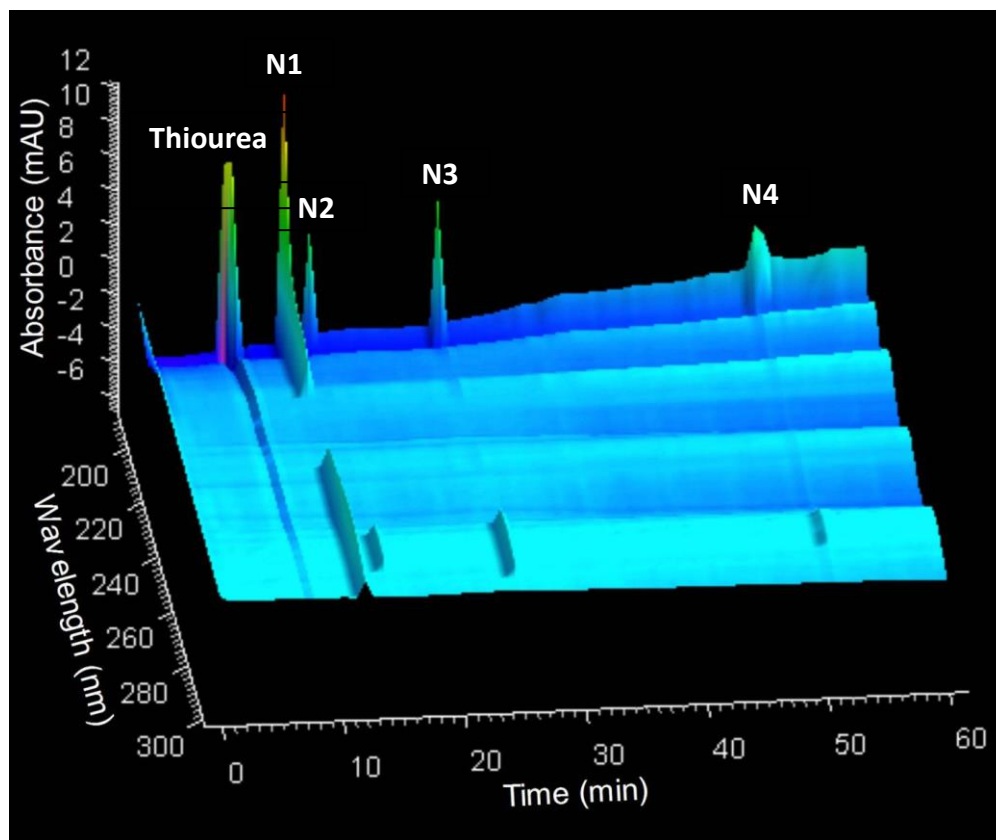
Figure 2.8: 3D electrochromatogram showing the separation of thiourea and the N series of fluorous analytes over the wavelength range of 190-300 nm using a diode array detector. Applied voltage is 7.5 kV, mobile phase is 70:30 (ACN : water).

2.8 – Backpressure Measurement

Backpressures for PPM columns were obtained using a Waters nanoAcquity UPLC system. Columns were cut to an accurate length of 10 cm for backpressure measurements. Flow rate was kept constant at 400 nL/minute. And a solvent of 50:50 (ACN : water) with 0.1% formic acid was used.

2.9 – Scanning Electron Microscopy (SEM)

Scanning electron microscopy was performed on a Jeol JSM-840 scanning microscope (Tokyo, Japan). Columns with monolith were cut into small pieces (around 5 mm), which were subsequently mounted perpendicularly to the surface of an aluminum stub to allow an unobstructed view of the cross section. Prior to SEM analysis, a Hummer 6.2 Sputtering System (Anatech; Hayward, CA) was employed to coat a thin layer of gold on the small pieces of column.

2.10 – Custom Peptide I Fluorous Tagging

The custom peptide I was initially dissolved in ACN to achieve a concentration of 125 μM and then combined with 4 μL of 45 mM DTT (in water, reaction as shown in Scheme 2.3) and 10 μL of 10 mM N-[(3-perfluorohexyl)propyl]-iodoacetamide (in tetrahydrofuran). This mixture was shielded from light and allowed to react for 90 minutes at 37 °C (reaction as shown in Scheme 2.4), after which point it was diluted with 581 μL of water and subsequently analyzed.
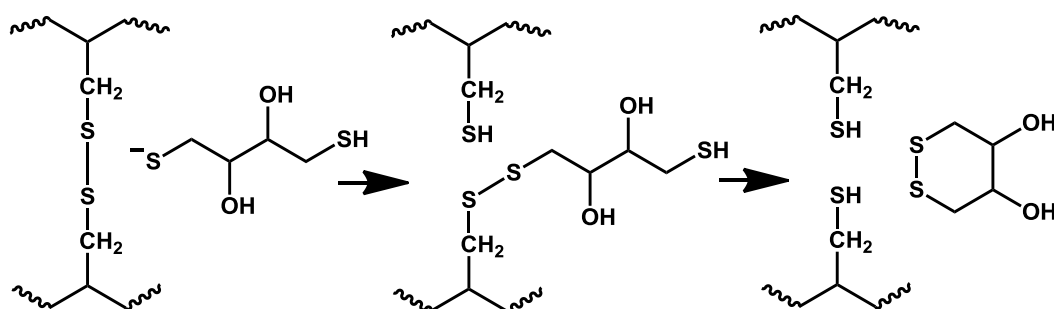
Scheme 2.3: Reaction between disulfide bond and DTT to break disulfide bond. This figure is reproduced from references.[158,159]
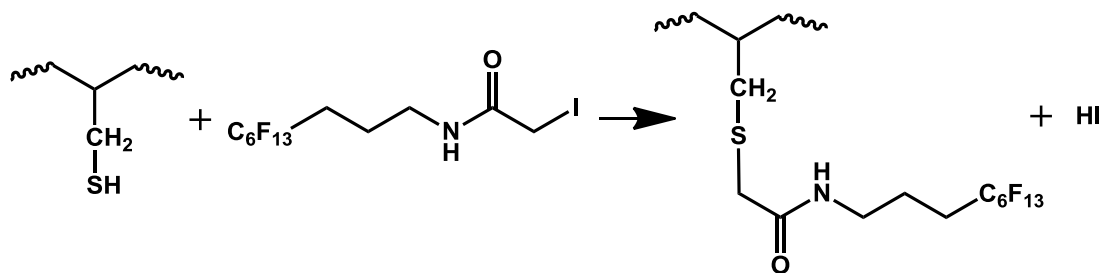
Scheme 2.4: Independent cystene residue reacts with fluorous reagent (N-[(3-perfluorohexyl)propyl]iodoacetamide).

2.11 – Custom Peptide II Fluorous & Fluorescently Tagging

The custom peptide II was initially dissolved in a 80:20 (ACN : water) sodium phosphate buffer. Concentration was set at 2.0 mM. 30 μL of custom peptide II solution was then mixed with 10 μL of 10 mM N-[(3-perfluorohexyl)propyl]-iodoacetamide THF solution. This mixture was shielded with aluminum foil from light and reacted for 90 min at 37 ℃ (reaction as shown in Scheme 2.4). 30 μL of Cy5-*N*-Hydroxysuccinimide mono-functional ester aqueous solution (2.0 mg/mL) was added to conduct fluorous tagging. After 2.0 hours reaction at room temperature, the resulting fluorous and fluorescently tagged mixture (structure of fluorous/doubly fluorescently tagged custom peptide shown in Figure 2.1) was diluted with 500 μL of sodium phosphate buffer and subsequently analyzed.

2.12 – Insulin Fluorous Tagging

The insulin was initially dissolved in water to achieve a concentration of 1 μg/μL solution. 35 μL 20 mM Tris buffer in water was then added to 5 μL insulin solution. 5 μL of 45 mM DTT (in water) was added and incubated for 50 minutes at 37 ℃ (reaction as shown in Scheme

2.3). Then, 10 µL of 10 mM N-[(3-perfluorohexyl)propyl]-iodoacetamide (in tetrahydrofuran) was added. This mixture was shielded with aluminum foil from light and allowed to react for 90 minutes at 37 ℃ (reaction as shown in Scheme 2.4), after which it was diluted with 581 µL of water and subsequently analyzed.

2.13 – ESI-MS Operation

HPLC in tandem with nanoESI interface and MS detection was performed on an API 3000 triple-quadrupole mass spectrometer (MDS Sciex; Streetsville, Ontario, Canada) and shown in Figure 2.9. A fluorous monolith (10 cm; 30% PPM density) was first mounted between the pump (NLC-1DV-500; Eksigent; Dublin, CA) and a 54 hole, photonic fiber-based emitter of the type previously reported by our group using a MicroTee union (Upchurch Scientific; Oak Harbor, WA).[160-164] Spray voltage was applied after the fluorous column (through the union) and maintained at 3.55 kV during gradient elution. The distance between the outlet of the fiber-based emitter and the orifice of the mass spectrometer was 8 mm. For the gradient, aqueous phase (A, 99% water, 1% ACN, with 0.1% formic acid relative to the volume of water plus ACN) and organic phase (B, 99% ACN, 1% water, with 0.1% formic acid relative to the volume of ACN plus water) were combined in differing ratios to comprise the mobile phase. The gradient employed was 90% to 10% A over 15 min, 10% A to 1% A over 10 min, back to 90% A in 1 min, and finally 90% A maintained for 10 min to give a total run time of 36 min. The flow rate was constant at 400 nL/min for all steps, with a sample loading time of 1 min.

Figure 2.9: Illustration of HPLC - PPM column – ESI – MS setup

2.14 – MALDI-MS Operation

A voyager DE STR matrix-assisted laser desorption/ionization time of flight mass spectrometer (MALDI-TOF-MS, Applied Biosystems, Foster City, CA, USA) was used to analyze all peptides/proteins samples. A two layer sample preparation method that uses CHCA as matrix was employed for analysis of all peptide samples.[165] First layer was 6 mg/mL CHCA solution in 70:30 (acetone: methanol); Second layer was the acidified mixture which was prepared by adding an acidified peptide/protein sample (1 % TFA), and 8 mg/mL CHCA saturated solution in 40:60 (methanol : water) in 1:1 ratio. To make saturated CHCA solution, CHCA powder was dissolved completely in methanol. Then, water was added to make a portion of the CHCA precipitate. The 1.0 μL aliquot of the solution was spotted on the MALDI 100-spot target plate. The second layer was applied after the first layer had dried completely.

Chapter 3 – Fluorous Porous Polymer Monolith (FPPM) Stationary Phase Development and Optimization

3.1 – Introduction

3.1.1 – Monolith Materials as Supports for Fluorous Chromatography

There are two main branches of monoliths in separation science, polymer-based (*i.e.* PPM) and silica-based monoliths. In terms of LC performance, it is well known that PPM stationary phases are more suitable for larger molecules (peptides and proteins) while silica-based monoliths are more preferred for the separation of small molecules. The SEM images in Figure 3.1 and pore diameter distribution chart in Figure 3.2 provide the rationale for this division of labour. The silica-based monoliths have been found to have more permanent meso-pores (Panel A, Figure 3.1, top dashed line, Figure 3.2). Within the monolithic structure, it is believed that both convection and diffusion can occur in the larger pores while only diffusion occurs in the smaller pores.[93,166,167] The relatively slow and time-consuming diffusion of large molecules minimizes access to the meso-pores, precluding their use.[93,166]
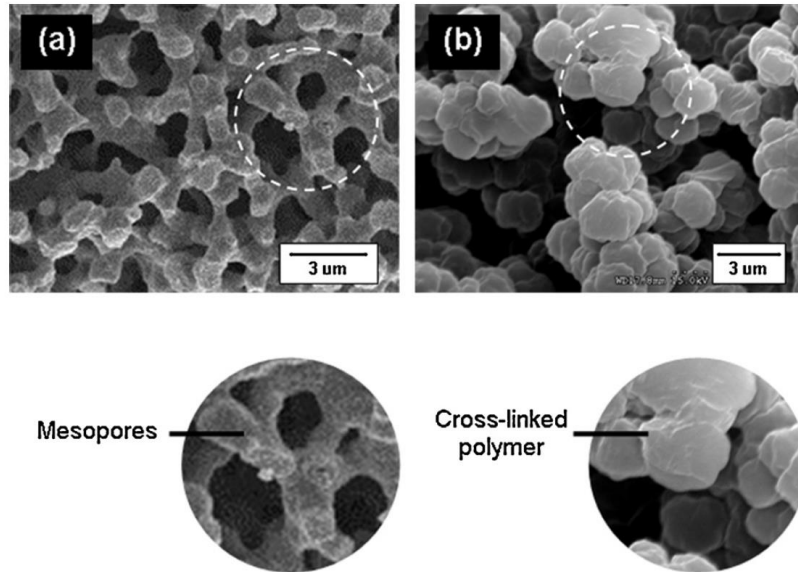
Figure 3.1: SEM images of (a) hierarchically-structured silica-based monolithic materials with macro-pores and a relatively thin skeleton containing permanent mesopores, and (b) typical polymer-based monolithic materials with globular structures composed of cross-linked polymer. This figure is reproduced from references.[93,166,167]
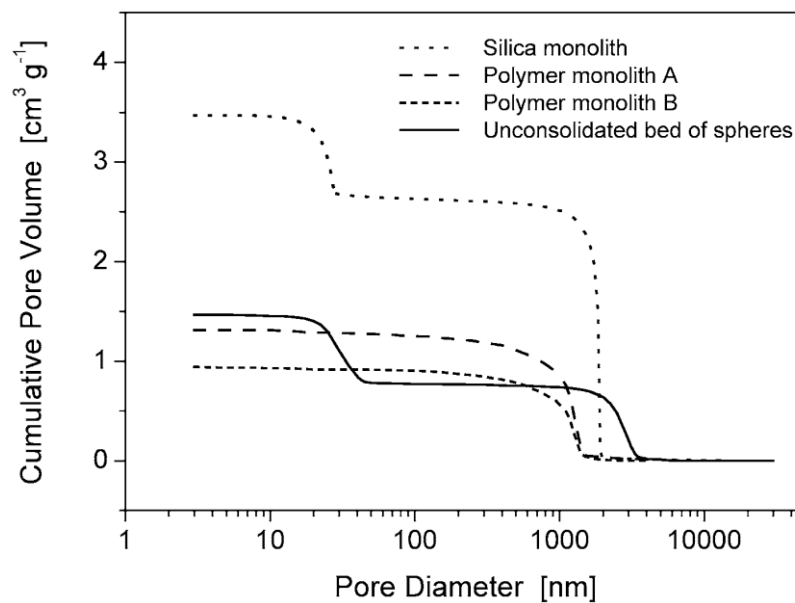
Figure 3.2: Cumulative pore volume data for the monolithic and particulate fixed beds indicating monomodal pore size distributions in the case of the polymer monoliths and bimodal pore size distributions for both the silica-based monolith and the bed of porous silica beads. This figure is reproduced from reference.[166]

My project aims to provide an optimal stationary phase for fluorous-proteomic samples. Therefore, the PPM rather than silica-based monolith was chosen based upon the above discussion.

3.1.2 – PPM Polymerization Parameters

In theory, all parameters involved in the pre-treatment of the column, PPM synthesis, post-polymerization treatment, and separation will affect the PPM morphology and chromatographic performance. A good PPM morphology requires a comprehensive consideration of all materials synthesis factors. For example, the diameter of the capillary must be carefully considered as it has an effect on the PPM morphology and consequently the chromatographic performance may be altered. Nischang and co-workers found that smaller PPM column diameters can reduce the chromatographic peak width and improve the sensitivity for mass spectrometric detection.[167]

Several key experimental factors are optimized in this chapter, including: the photo initiating wavelength, monomeric composition, and porogenic solvent. Additional adjustments to PPM stationary phase composition/development are explored in the subsequent chapters including the addition of AMPS as a charge bearer (electro-kinetic flow) and the nitrobenzene as free radical quencher to eliminate the clogging. Part of the work in this chapter was published in Daley, A. B.; Xu, Z.; Oleschuk, R. D. *Anal. Chem.* **2011**, *83*, 1688.

3.2 – Results and Discussion

3.2.1 – Monolith Density

It has previously been established that flow-induced backpressure is a useful indicator of monolith porosity in the native state,[67,80,168] avoiding alterations to the substrate such as extrusion and drying that are needed for more conventional techniques. Additionally, this analysis of porosity can be coupled with a simple visual assessment of the monoliths using SEM to ascertain the effects of changing the amounts of reactive component (monomer and cross-linker) relative to porogenic solvent. The combination of these factors provides a thorough picture of the density that arises in each monolithic column, an understanding that is vital to the characterization of the fluorous substrates.
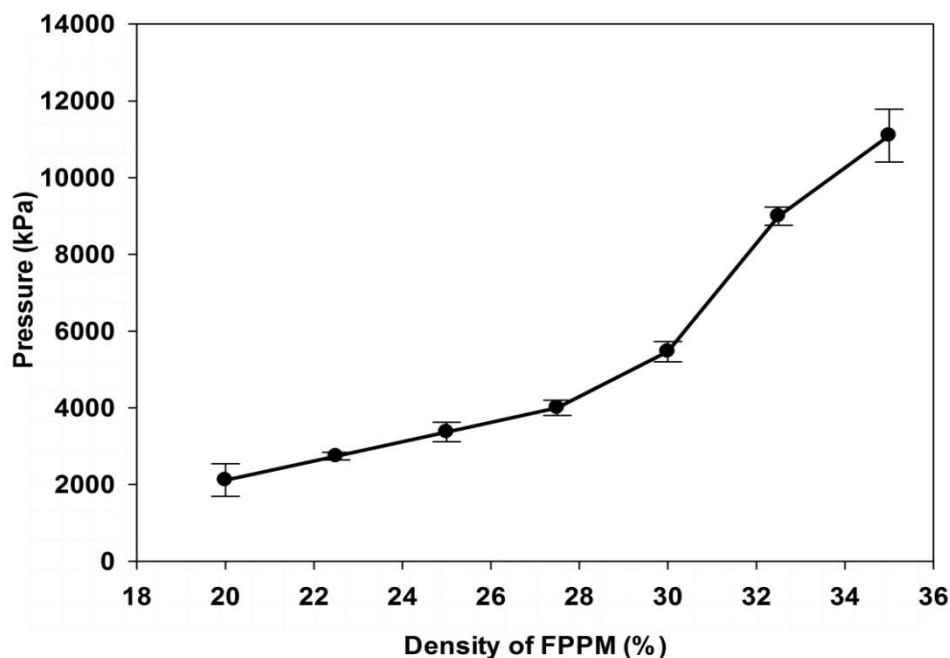
Figure 3.3: Backpressure of FPPM with different densities. Column length is 10 cm. Each data point is the average of the results for three replicate columns, along with their associated standard deviation.

Looking first at a plot of backpressure *versus* monolith density (Figure 3.3), there is an obvious trend toward higher pressures as the amounts of polymer-forming components are increased. It should be noted that the errors for both the 20% and 35% formulations are relatively high (approximately 427 and 689 kPa, respectively) as compared to the other mixtures (which are all less than 276 kPa), although for entirely different reasons in each case. For the column with 20% total polymerizable material, the small amount relative to a large porogenic solvent content results in significant, inhomogeneous macro-pores and poor PPM robustness.[169] Conversely, for the column with 35% polymerizable material, the solubility of the fluorous monomer in the porogen becomes sufficiently poor such that heterogeneous polymerization and inconsistent porosity are the result (regions of both dense polymer and large, heterogeneous macro-pores coexist). If these results are compared to those obtained using SEM (Figure 3.4), the same basic trends can be observed. The reproducibility of the fluorous monoliths appears to be optimal at a composition of around 30%, with mixtures on either side of this point showing a greater propensity for void formation and irregularity. It was previously noted that no significant change in structure occurs in a PPM when switching between fluorous and non-fluorous components, although these results did not have two exactly analogous mixtures to completely verify the point. Here this previous assertion can indeed be confirmed, as looking at the physical structures of the 30% fluorous monolith and its non-fluorous analogue (replacing FBA with BA), there was no discernible visual difference between the polymeric networks that resulted (panels E and H, Figure 3.4).
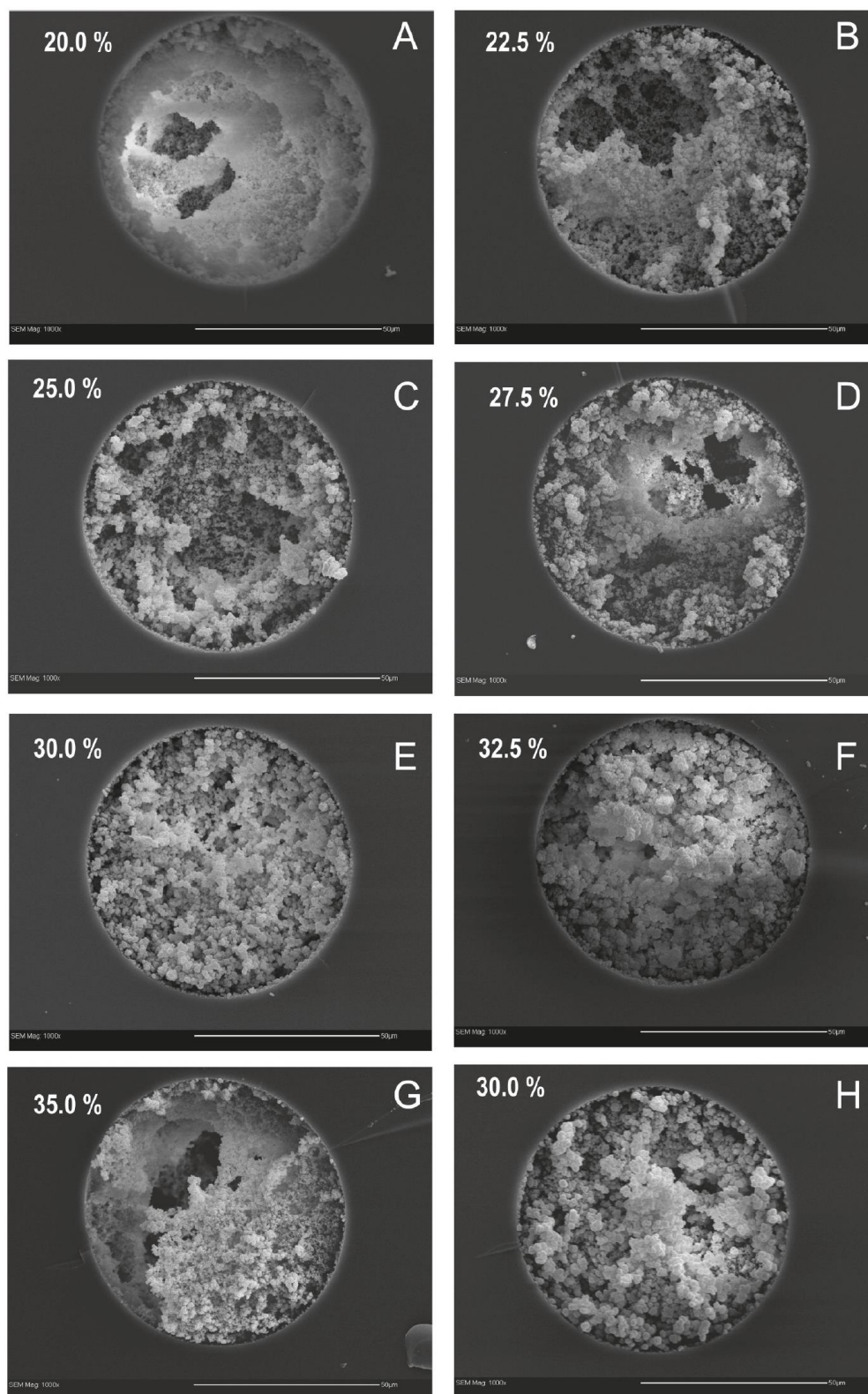
Figure 3.4: SEM images of PPM in the capillary. The first seven images (A-G) are for FPPM with different total concentrations of polymerizable material, while the last (H) is for a non-fluorous PPM (the direct analogue of column E).

One of the most useful conclusions drawn from our previous work with fluorous monoliths was that fluorous separations were not hindered by switching from fluorous to non-fluorous cross-linkers but rather showed noticeable improvements in performance.[80] At the time, it was hypothesized that the solubility gain incurred by eliminating the fluorous component yielded a more uniform polymerization, offsetting the loss in specificity that would accompany the removal of fluorine from some of the monolithic substrate. Concurrently, it was also believed that the improved solubility should mean that even denser fluorous monoliths than the 20% solutions tested previously should be a possibility.[80]   Here we have shown both of these prior hypotheses to be in fact true, forming a series of FPPM from solutions that would have been impossible to create while limited by the solubility of a fluorous cross-linker. These more saturated polymerization solutions subsequently allow the benefits of greater densities to be realized in a fluorous monolith,[170] meaning that truly optimized regimes (such as those seemingly around the 30% solution discussed here) can be further explored.

3.2.2 – Density Optimization of FPPM Based on HPLC Results

Testing column performance for the various PPM formulations under chromatographic conditions is another important characterization step. Here, we chose two series of analytes based on a benzylamine backbone (N Series and P Series, Figure 2.1): one with a non-polar phenyl side chain and the other with a more polar nitro group. These compounds were ideal for our purposes as they both possessed a chromophore to make UV detection accessible (enabling online testing). Additionally, introducing identical fluorous groups in both the N Series and P Series allowed selectivity and the impact of secondary effects to be assessed for

the FPPM, as separation differences between identically tagged compounds with different inherent polarities could be noted.

Prior to these more complex analyses of monolith selectivity and specificity, the first test that had to be undertaken was a comparison of the resolution for the fluorous analyte series that could be attained using a variety of monolithic densities. With the use of SEM and backpressure results (*vide supra*), it was previously suggested that a composition of 30% showed the best porosity characteristics. Comparing those initial results to what is observed during chromatography (Figure 3.5 and Table 3.1), an excellent correlation between the data sets can be found. Fluorous resolution for both the N and P series reaches a maximum at a monolith density of 30%, a result that is consistent with what the structural characteristics predicted to be the most consistent material. These results also serve to reinforce the benefit of the fluorous interaction relative to a purely reversed-phase separation, as monoliths made with FBA significantly outperform their BA counterpart in terms of fluorous analyte resolution (a factor of 2-3 greater under identical conditions). Similar to resolution, peak shape for the fluorous series can also be noticed to follow this same overall trend in quality (Table 3.1). Looking at the peaks for the most strongly retained tagged species (N4 and P4, the compounds that should best exhibit fluorous interactions), the signals are narrowest when the monolithic composition is at 30% (which makes sense given that resolution is partially dependent on peak width). Finally, it is worth noting that the distribution and relative intensities of the observed peaks on the fluorous monoliths were consistent with the data obtained by the custom synthesis provider during their characterization of the analytes, reinforcing the identity of the peaks as they are

currently tagged here. Looking more closely at interaction specificity, it can be seen in the separate plots for the N and P Series (Figure 3.5) that compounds with identical fluorous tags (*e.g.*, N1 and P1) do not exhibit identical retention times on the fluorous monoliths. Similar to earlier discussions, this suggests that secondary effects causing deviation from a purely fluorous interaction must be present (separation based solely on fluorine content would show no difference between fluorous tagged benzylamines that differed only by a nitro or phenyl substituent). While it was expected that these types of secondary effects might occur in the compounds with smaller (C_3F_7 and C_4F_9) fluorous tags (where the amount of fluorine is less significant relative to the total molecular size), for them to also appear for the larger tags suggests that the secondary effects must be as much of a contributor here as they are in the commercial, silica particle-packed fluorous columns that have already been discussed.[171-174]
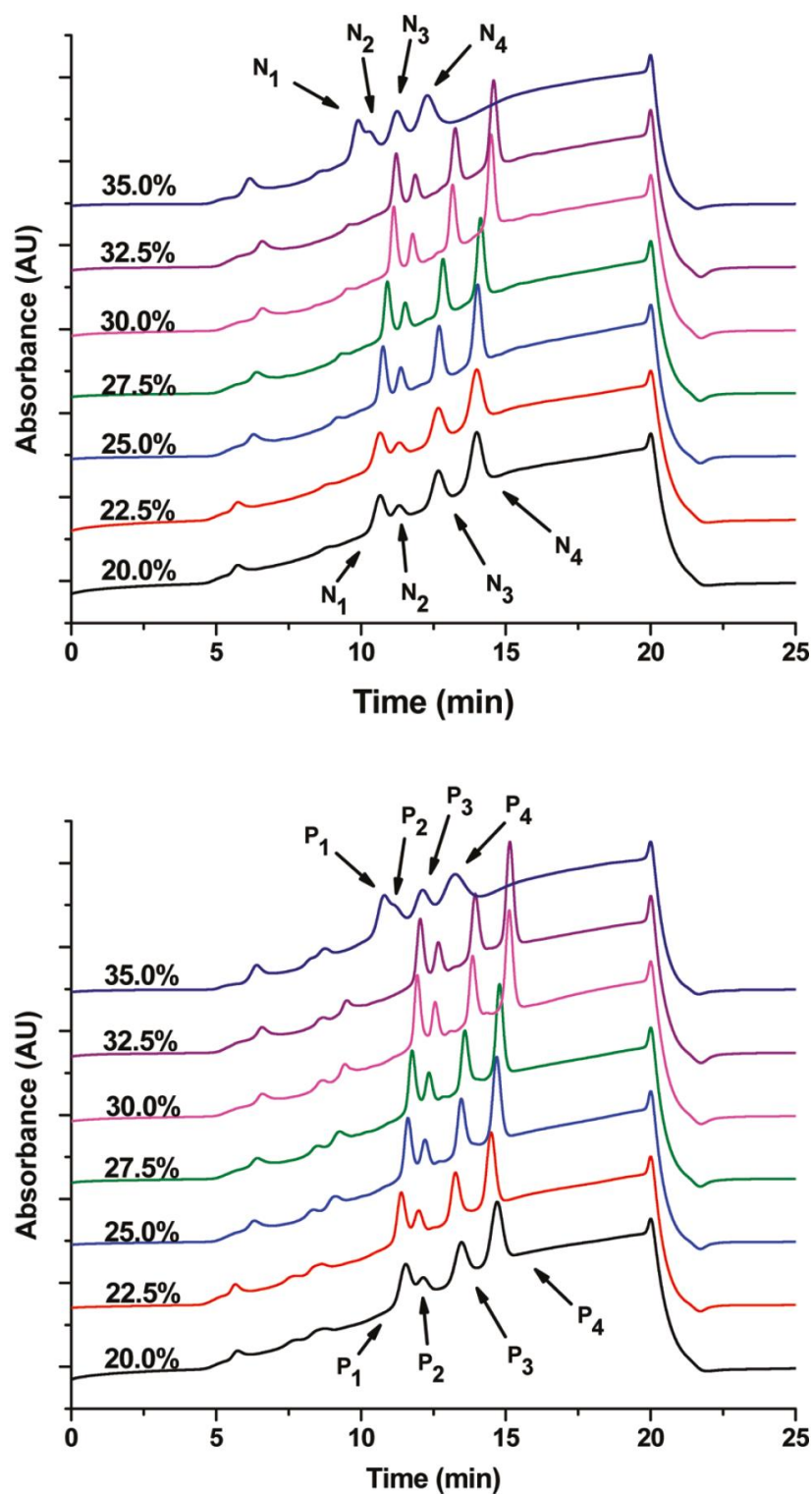
Figure 3.5: Chromatograms for N (top) and P Series (bottom) using columns with different fluorous PPM densities. The results are consistent for trials with two replicate columns of each monolith composition. Traces are offset for clarity.

Table 3.1: Resolution of fluorous analytes or columns with different PPM densities

Column	Density (%)	Resolution				Peak Width (min)	
		R(N1/N2)	R(N3/N4)	R(P1/P2)	R(P3/P4)	N4	P4
Fluorous Column	20.0	0.86±0.00	1.70±0.02	1.02±0.42	1.55±0.02	0.81±0.01	0.81±0.03
	22.5	1.26±0.09	2.29±0.04	1.05±0.02	2.16±0.08	0.60±0.02	0.54±0.05
	25.0	1.39±0.04	2.59±0.05	1.16±0.07	2.22±0.04	0.54±0.03	0.56±0.02
	27.5	1.52±0.03	2.81±0.01	1.26±0.03	2.43±0.05	0.50±0.04	0.50±0.03
	30.0	1.68±0.01	3.12±0.05	1.46±0.03	2.58±0.01	0.44±0.04	0.50±0.01
	32.5	1.50±0.02	2.84±0.04	1.34±0.00	2.39±0.01	0.48±0.00	0.50±0.01
	35.0	0.54±0.02	1.22±0.02		0.96±0.03	0.97±0.00	1.34±0.08
Non-Fluorous Column	30.0	0.74±0.01	1.14±0.01	0.48±0.05	0.89±0.00		

Each value is reported as the average from two separate columns for each PPM composition.

3.2.3 – Secondary Effects as Separation Utility

While it might initially be thought that the presence of secondary effects indicates a drawback of the monolithic materials, we do not believe this to be the case. As was seen with the commercial, microsphere-based fluorous columns, the inherent reversed-phase character of fluorous stationary phases coupled with only a partial fluorous character for analytes that have their fluorine introduced through tagging reactions allows other interactions and effects to provide a significant contribution to the retention that is observed. In the assessment of the quality of fluorous monoliths then, it is necessary to evaluate their performance in terms of the benefits that their fluorous character confers relative to equivalent phases that lack fluorination. Similarly, with secondary effects seemingly unavoidable, if it were possible to find a way to use these deviations from purely fluorous separations as a tool for further analysis it would be highly beneficial.

In this vein, one way to highlight the power of our fluorous monoliths is to perform more complex separations (initially modeled here by combining the mixtures of both N and P Series). By comparison of the performance of our fluorous column with an equivalent monolith that replaces the fluorinated monomer with its hydrocarbon analogue (Figure 3.6), the resultant chromatograms demonstrate the benefits arising from monolith fluorination. For the mixture separation on the fluorous substrate, all eight components can be identified, with only N2 and P1 showing a significant amount of overlap. Compare this to the non-fluorous column where N4, P1, and P2 essentially co-elute, and it is evident that the introduction of stationary phase fluorination has a positive impact on analysis. When separation is based solely on polarity (as it

is in the reversed-phase column), there is not enough of a difference imparted by the fluorous tags to help differentiate the species outside of their nitro- or phenyl-composition. All of the N Series therefore elute before any of the phenyl-compounds, a result of the additional fluorine content in longer tags not appreciably altering the polarity of the compounds. This is contrasted by the fluorous case, where the small additional amounts of fluorine in each subsequent tag produce a measurable difference in the overall fluorous character. Consequently, this results in a grouping of analytes based predominantly on tag choice rather than substrate polarity (N2 does still elute marginally before P1 in a polarity based fashion due to a combination of the small fluorous tags and secondary effects), which is a different paradigm than for the reversed-phase column. Providing this different selectivity with no changes to the LC method or system other than the introduction of column fluorination demonstrates the power of the fluorous interaction for complex analyses, since it allows analyte grouping and detection that would otherwise be difficult on more conventional chromatographic substrates.
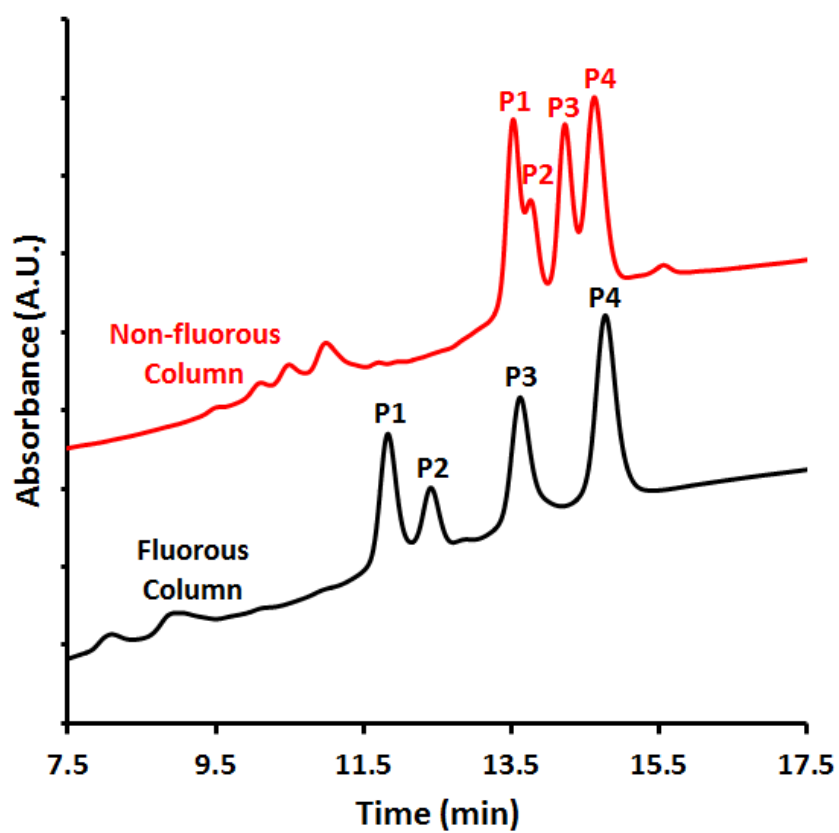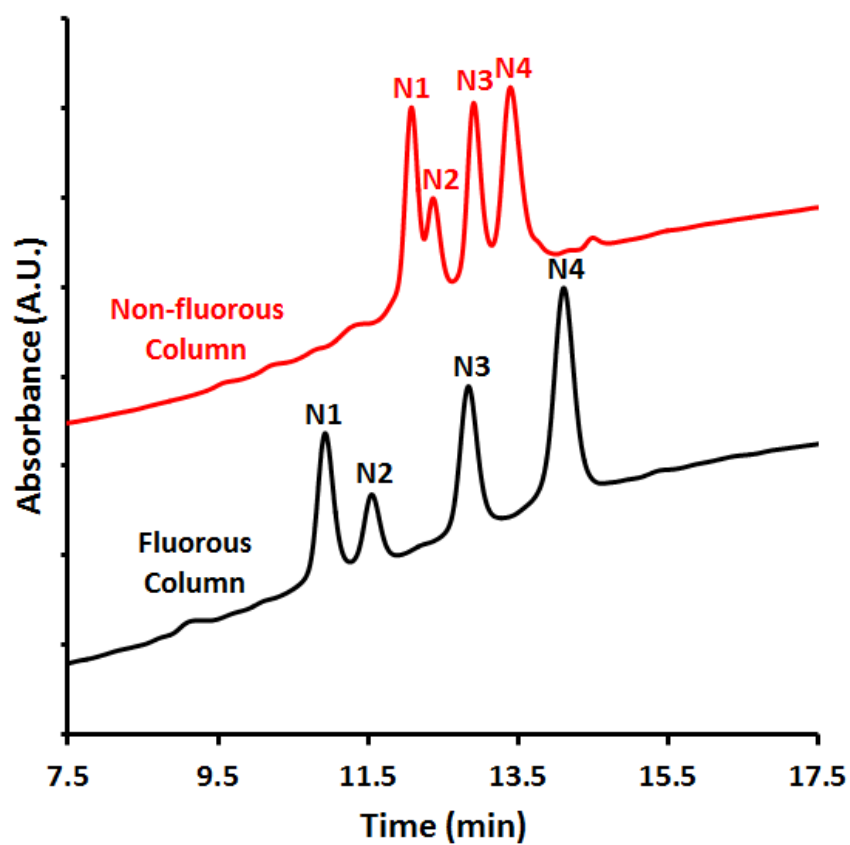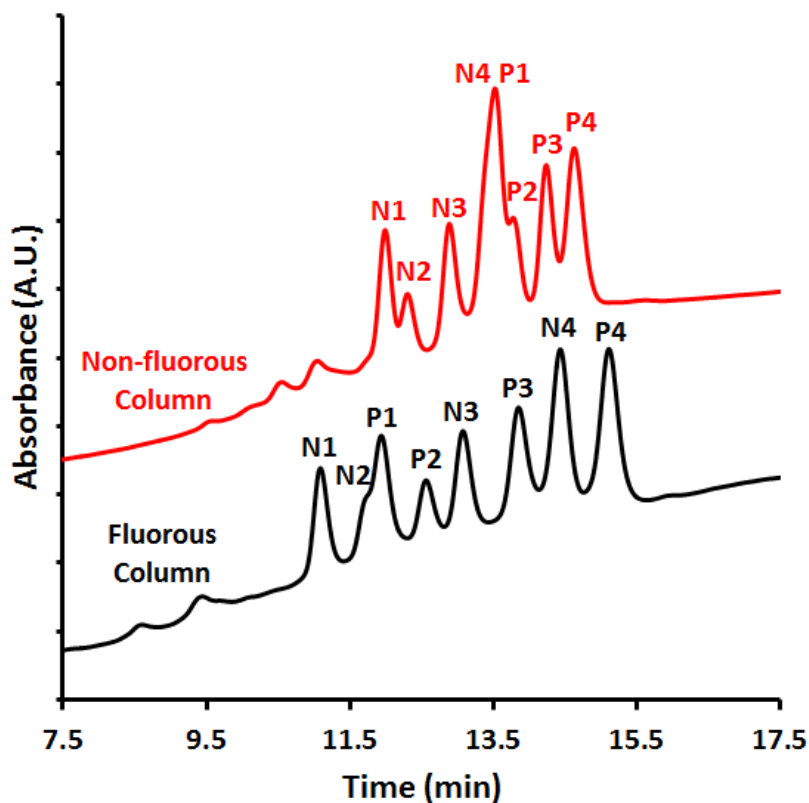
Figure 3.6: Chromatograms for individual N (top) and P (middle) Series as well as a combined sample with both N and P Series mixed together (bottom). Each panel shows separations using a fluorous column (upper trace) and its non-fluorous analogue (lower trace). The PPM density is 30% in each case, with only the monomer choice being varied (FBA or BA). Traces are offset from each other for clarity.

Looking more closely at the secondary effects, they can be noticed to manifest in a predictable manner for the fluorous monoliths. The less-polar P Series have uniformly longer retentions than their more polar nitro- counterparts, which is the expected result given the hydrocarbonaceous nature of the monolithic substrate. This in turn leads to slight differences in retention between identically tagged species based on their inherent substrate polarity, although the vast majority of the retention character is still dictated by the choice of fluorous tag (*vide supra*). Interestingly, these differences in retention times for species with the same tag but

different analyte character may actually be used as a benefit in fluorous analyses, serving as a second dimension for separation. This ability to differentiate between compounds of different polarity but identical tagging could become particularly useful in complex analyses such as those often found in proteomics. Here, it is possible to imagine a situation where there would be multiple peptides with similar post-translational modifications or other targets that could be tagged with fluorous groups to simplify the analysis of a digest. If it were further possible to identify these fragments based on their polarity after tagging (differences that would result from specific amino acid residues), that would be a large benefit for further characterization. We believe that the secondary effects exhibited by fluorous monoliths coupled with their demonstrated tag specificity represent one such manner to achieve these proteomic separations.

3.2.4 – Initiating UV Wavelength Impact on PPM Morphology and Chromatographic Performance

For photo initiating polymerization, the wavelength at which polymerization is carried out at is another key factor impacting the PPM morphology and consequent chromatographic performance. Three UV wavelength choices (254 nm (Model Spectroline EBF-280C), 312 nm (Model Spectroline EBF-280C), or 365 nm (Model Spectroline EN-180) UV lamp; 115 V, 60 Hz, 0.2 A; Spectronics Corporation, Westbury, New York, USA) were employed to explore the effects of the initiating UV wavelength. As shown in Figure 3.7, changing the initiating UV wavelength from 254 nm to 365 nm (keeping the rest of parameters identical) produces a finer PPM skeleton. The flow-induced backpressure data in Table 3.2 agree with SEM image information. The finer PPM skeleton exhibits higher flow-induced backpressure,

i.e. for cases of 254 nm, 312 nm and 365 nm, the flow-induced backpressure are 6495 kPa, 7212 kPa, and 7908 kPa respectively. The mechanism behind this trend is still unknown. We speculate that the longer UV initiating wavelength is less attenuated by the growing PPM skeleton and consequently penetrates deeper into the polymerizing mixture. Therefore, more free radicals are produced. Larger numbers of free radicals will produce more individual growing polymer chains, but with shorter chain lengths (*i.e.* smaller and finer PPM skeleton), since there is more competition for the limited monomers and cross-linkers, and a greater chance for chain termination (i.e. quenching due to interaction with another free radical). More experimental data is required to further understand the mechanism. Regardless of the wavelength employed, functional chromatographic columns resulted. Both N and P Series were separated on the columns fabricated using the three UV initiating wavelengths (Figure 3.8). The resolutions for N1/N2, N3/N4, P1/P2, and P3/P4 were calculated and are shown in Table 3.2. As we predicted through the SEM morphology information and flow-induced backpressure data, the column fabricated using an initiating wavelength of 365 nm exhibits the best performance for both N Series and P Series. R(N1/N2) was enhanced from 1.37 using 254 nm to 2.38 using 365 nm, while R(P1/P2) was enhanced from 1.20 using 254 nm to 2.12 using 365 nm. These resolution improvements are much more meaningful, especially for compounds where resolution lower than 1.5 (*i.e.* baseline resolution) was achieved previously.
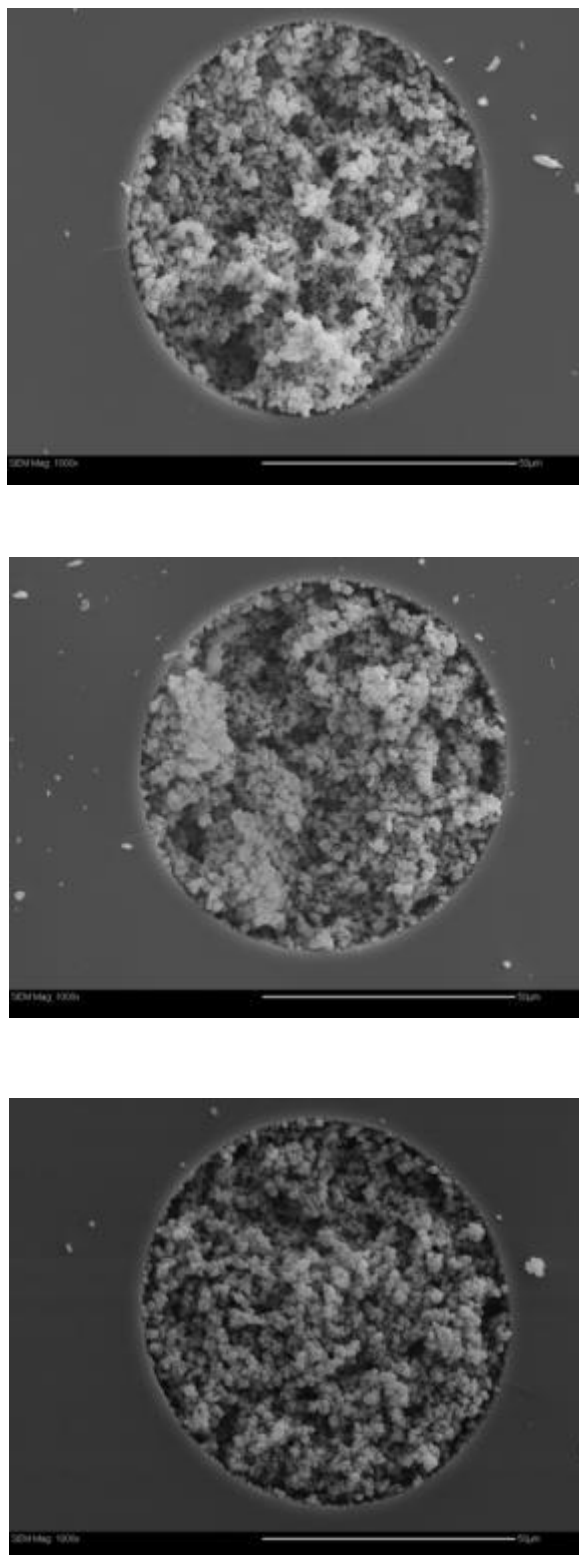
Figure 3.7: SEM images of FPPM in the capillary under initiating UV wavelength 254 nm (top), 312 nm (middle), and 365 nm (bottom).
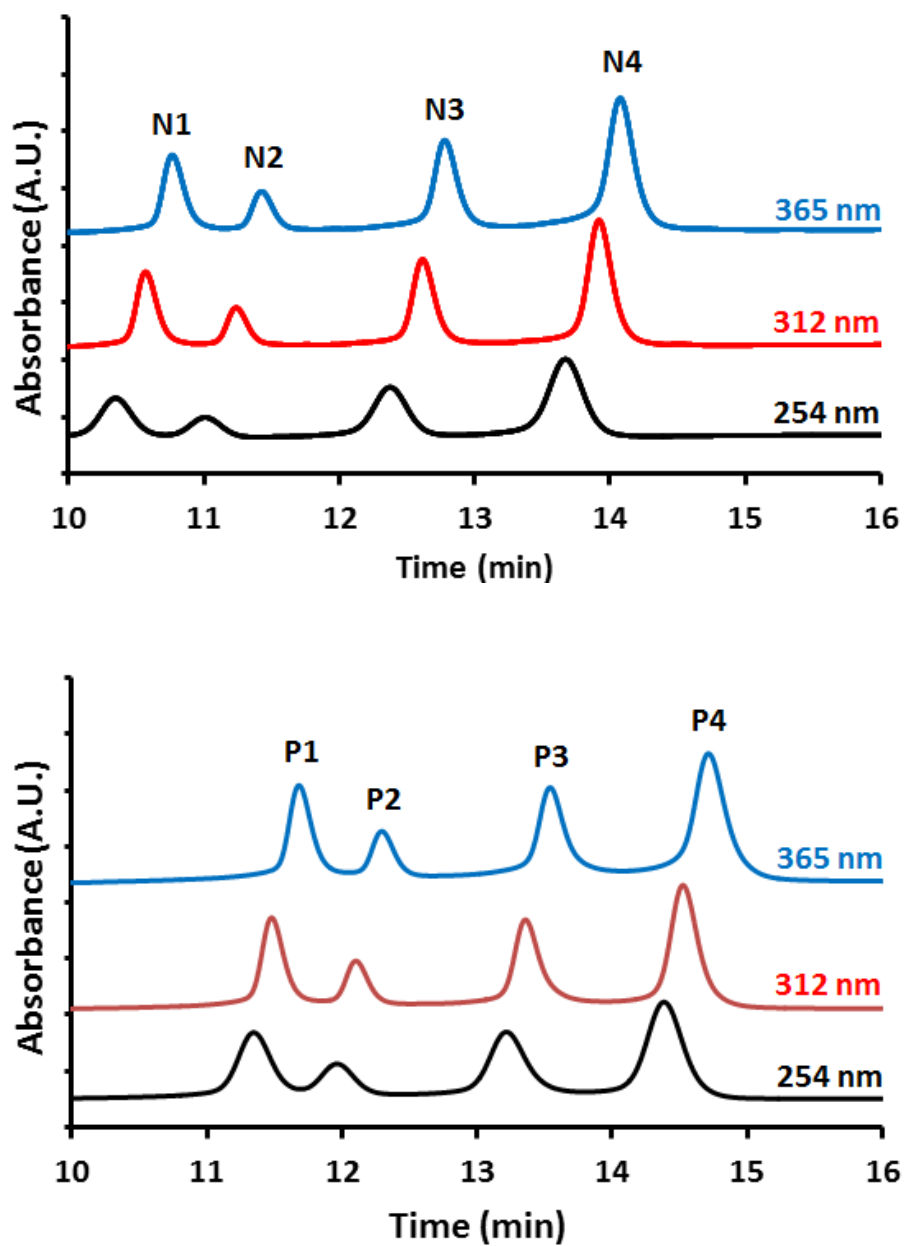
Figure 3.8: Chromatograms for N (top) and P Series (bottom) using columns prepared under different initiating UV wavelength, 10 cm length, 30% FPPM density.

Table 3.2: Flow-induced backpressure and resolution of N and P Series on 10 cm 30% FPPM columns fabricated using different initiating UV wavelength

UV Initiating Wavelength	Flow-induced Backpressure (kPa)	R(N1/N2)	R(N3/N4)	R(P1/P2)	R(P3/P4)
254 nm	6495 $\pm$48	1.37 $\pm$0.02	2.51 $\pm$0.02	1.20 $\pm$0.02	2.22 $\pm$0.09
312 nm	7212 $\pm$69	2.13 $\pm$0.06	3.79 $\pm$0.10	2.08 $\pm$0.03	3.27 $\pm$0.13
365 nm	7908 $\pm$55	2.38 $\pm$0.03	4.03 $\pm$0.13	2.12 $\pm$0.03	3.34 $\pm$0.01

Each value is reported as the average from three replicate trials.

3.2.5 – Photo Initiator BME Usage Impact on Chromatographic Performance

BME has been used as a photo initiator for more than a half century. A typical UV initiated polymerization used to prepare PPM with BME is shown in Scheme 2.2. The conditions used were based on previous work.[82] The benchmark solution concentration of BME was 3.7×10^{-5} mol/L. A range of BME concentrations ($0.10\times$ to $1.00\times$) of the benchmark were used with different initiating UV wavelengths. In the first group of trials, the optimal resolution of the N Series (Table 3.3) and P Series (Table 3.4) frequently appeared in the $0.10\times$ to $0.50\times$ range. For longer initiating UV wavelengths, optimal resolution results more consistently appeared in the range of $0.25\times$ to $0.50\times$. For the second group of optimization trials (BME use from $1.00\times$ to $5.00\times$ benchmark), at shorter initiating UV wavelength, *e.g.* 254 nm, the resolution results of both N Series (Table 3.3) and P Series (Table 3.4) were significantly lower as the BME concentration was increased from $1.00\times$ to $5.00\times$. Conversely,

upon changing the initiating UV to a longer wavelength *e.g.* 312 nm and 365 nm, no significant changes resolution changes were noted.

When transferring the FPPM from capillary-based columns to microchip-based columns, the lower transmittance of initiating UV light due to the chip substrate in the shorter wavelength region, *e.g.* 254 nm (discussed in detail in Chapter 7), resulted in an optimum BME concentration of $0.375\times$ benchmark, *i.e.* 1.4×10^{-5} mol/L, compared to the volume of polymerizable reagents (monomers and cross-linkers).

Table 3.3: Resolutions of N Series on 10 cm 30% FPPM columns fabricated with different BME (initiator) concentrations

BME Usage*		R(N1/N2)			R(N2/N3)			R(N3/N4)		
		254 nm	312 nm	365 nm	254 nm	312 nm	365 nm	254 nm	312 nm	365 nm
	0.10×	1.75	2.15	2.03	3.56	4.36	4.15	2.91	3.83	3.23
	0.25×	1.74	2.06	2.52	3.53	4.15	4.91	3.08	3.38	4.06
First Group	0.50×	1.59	2.10	2.49	3.29	4.35	4.92	3.03	3.44	4.06
	0.75×	1.33	2.00	2.13	2.79	4.25	4.29	2.58	3.83	3.51
	1.00×	1.25	2.06	1.55	2.48	4.18	3.91	2.29	3.44	3.41
	1.00×	1.39	2.27	2.13	2.80	4.49	4.03	2.57	3.77	3.51
Second Group	2.00×	0.92	2.23	2.10	1.88	4.31	4.12	1.82	3.75	3.69
	5.00×	0.71	2.03	2.16	1.43	4.06	4.34	1.51	3.55	3.72

* BME Use is compared with the original benchmark amount. For example 0.10× means reducing the use of BME to 10% of the original amount; 5.00× means increasing the usage of BME to 500% of the original amount; 1.00× Benchmark BME concentration is 3.7×10^{-5} mol/L, compared to the volume of polymerizable reagent (monomers and cross-linkers).

86

Table 3.4: Resolutions of P Series on 10 cm 30% FPPM columns fabricated with different BME (initiator) concentrations

BME Usage		R(P1/P2)			R(P2/P3)			R(P3/P4)		
		254 nm	312 nm	365 nm	254 nm	312 nm	365 nm	254 nm	312 nm	365 nm
First Group	0.10x	1.41	2.06	1.66	3.00	4.16	3.27	2.44	3.20	2.75
	0.25x	1.54	1.72	2.09	3.00	3.53	4.26	2.44	2.67	3.25
	0.50x	1.34	1.67	2.20	2.72	3.41	4.31	2.18	2.77	3.32
	0.75x	1.15	1.75	1.82	2.42	3.64	3.60	1.92	2.94	2.38
	1.00x	1.10	1.73	1.60	2.20	3.49	3.16	1.91	2.73	2.67
Second Group	1.00x	1.24	1.94	1.82	2.47	3.73	3.68	2.19	2.88	2.85
	2.00x	0.82	1.80	1.85	1.71	3.69	3.60	1.59	2.93	2.75
	5.00x	0.55	1.73	1.85	1.15	3.35	3.66	1.28	2.85	2.95

3.3 – Conclusion

After a thorough analysis of fluorous monolith density, initiating UV wavelength, and initiator (BME) use, we have shown that a 30% mixture of polymerizable material (mixture of FBA and BDDA) relative to the porogenic solvent produces the best results for fluorous separations. It was found that these materials have the greatest degree of reproducibility, while also exhibiting superior resolving power as compared to their non-fluorous counterparts (mixture of BA and BDDA). Analysis of a mixture of benzylamines (both N Series and P Series) that were tagged with fluorous groups further expanded upon these results, as the optimal monolith could resolve the components in a manner that was otherwise not possible with a non-fluorous column. We also found that longer initiating UV wavelength (365 nm) produces a finer PPM skeleton which exhibits better separation performance for fluorous analytes.

The presence of secondary effects in addition to the fluorous interaction was also observed for these optimized columns (identical to those noted for fluorous silica gels). Despite this, there was no adverse effect on the performance of the monoliths. Analyte specificity was noted to primarily be a function of the choice of fluorous tag, with the secondary effects causing slight (predictable) deviations from ideal fluorous behavior (less polar analytes retained slightly longer than their more polar counterparts). These effects are suggested to have positive implications for the analysis of complex mixtures though, with the differentiation of components with different polarities but identical tagging potentially providing useful information in more complex separations with multiple dimensions.

Chapter 4 – Capillary Electrochromatography (CEC) on FPPM Stationary Phase

4.1 – Introduction

CEC is a hybrid of two types of analytical techniques, HPLC and capillary electrophoresis (CE), in which the mobile phase is driven through the chromatographic stationary phase by electro-osmotic flow (EOF) rather than by hydrodynamic driving force (HPLC).[175-178] Typically, EOF results from the ionization of acidic silanol groups on the inside wall of the capillary (Figure 4.1). The analytes can be resolved based on their charges, hydrodynamic radius and mobility similar to CE as well as interaction with a stationary phase.[179] CEC benefits from the high efficiency afforded by the plug flow (Figure 4.1).
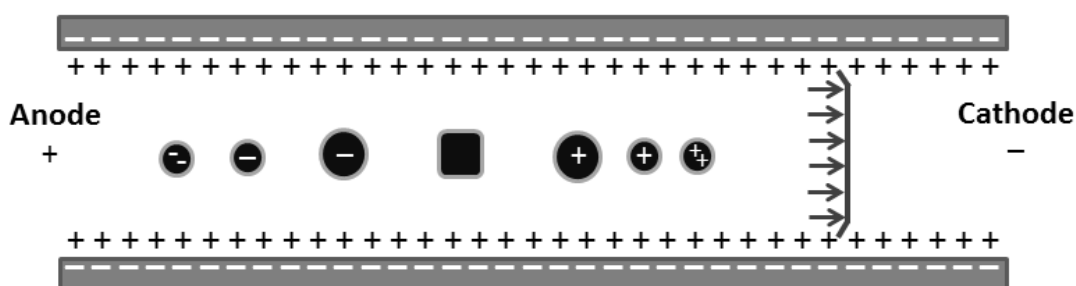
Figure 4.1: Schematic illustration of capillary electrophoresis

Fluorous PPM stationary phases are an alternative to the traditional particulate-based CEC stationary phase materials.[180] However, there are few reports on the use of fluorous stationary phases for CEC to date. Yurtsever *et al.*[79], thermally synthesized FPPM from the monomer 2,2,2-trifluoroethyl methacrylate (TFEM) and cross-linker ethylene dimethacrylate (EDMA).

Alkylbenzenes and phenols as well as aniline and benzoic acid derivatives, were separated on the FPPM stationary phase by CEC. However no fluorous analytes were examined. Choodum *et al.*[180] produced a fluorous monolith using thermal initiation from 1H,1H,2H,2H-perfluorodecyl acrylate (PFDA), EDMA, and [2-(methacryloyloxy)ethyl] trimethylammonium methylsulfate (METAM), the latter being a positively charged component to generate EOF for CEC. Polar phenolic compounds (hydroquinone, phenol, and catechol), non-polar aromatic hydrocarbons (benzene, toluene, and xylene) and only one fluorine-containing compound, *tau*-fluvalinate, were separated by the FPPM column. The fluorous phases in these reports were exploited for their reversed-phase character without more discussion on any fluorous selectivity.

This chapter presents an enhanced separation of fluorous analytes. Specifically, FPPM is photo-patterned within a capillary using UV initiation. The resulting columns are used to separate two sets of fluorous tagged analytes (N Series and P Series) by CEC, with analysis of the electrochromatograms convincingly demonstrating the FPPM stationary phase to be more selective/efficient for fluorous analytes than the non-FPPM stationary phases. Part of the work in this chapter was published in Xu, Z.; Gibson, G. T. T.; Oleschuk., R. D. *Analyst* **2013**, *138*, 611.

4.2 – Results and Discussion

4.2.1 – Optimization of Separation Voltage

Applied potentials from 5 to 30 kV were investigated to determine the most suitable separation voltage for the N Series of fluorous analytes. The mobile phase composition was set at 70:30 (ACN : water) phosphate buffer. Over this voltage range, Joule heating was not significant as judged by the linearity of the plot of mobile phase velocity (calculated from the migration of the unretained EOF marker thiourea) *versus* voltage shown in Figure 4.2 (R^2>0.999). Joule heating-related mobile phase viscosity variation, diffusion, and consequent separation efficiency reduction, therefore, can be ignored.[181,182]
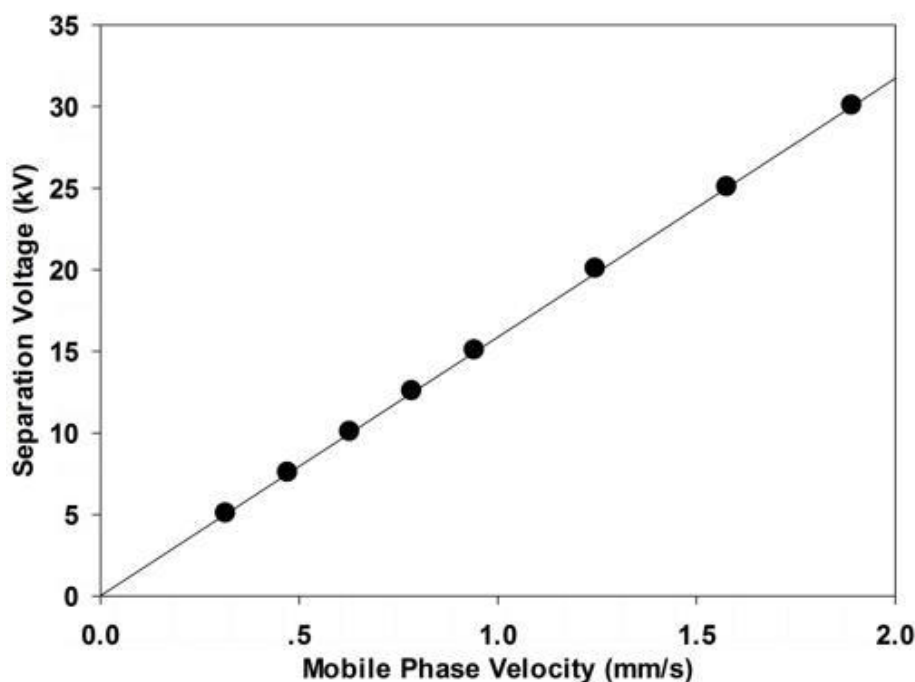
Figure 4.2: Mobile phase velocity over the separation voltage range 5-30 kV.   Mobile phase is 70:30 (ACN : water). R^2>0.999

The retention times of all fractions, including EOF marker, N1, N2, N3, and N4, decreased with increased separation voltage, as expected (Figure 4.3, Table 4.1). The resolutions R(N1/N2), R(N2/N3), and R(N3/N4) are presented in Table 4.2. All resolutions were much higher than 1.5, which is highly desirable in quantitative analysis.[183] The highest resolution was always obtained at applied potentials of 7.5 kV, 10 kV or 12.5 kV, while increasing the voltage to 30 kV resulted in a gradual decline in resolution, *e.g.* from 10.22 ±0.20 at 7.5 kV to 6.87 ±0.42 at 30 kV for R(N1/N2).
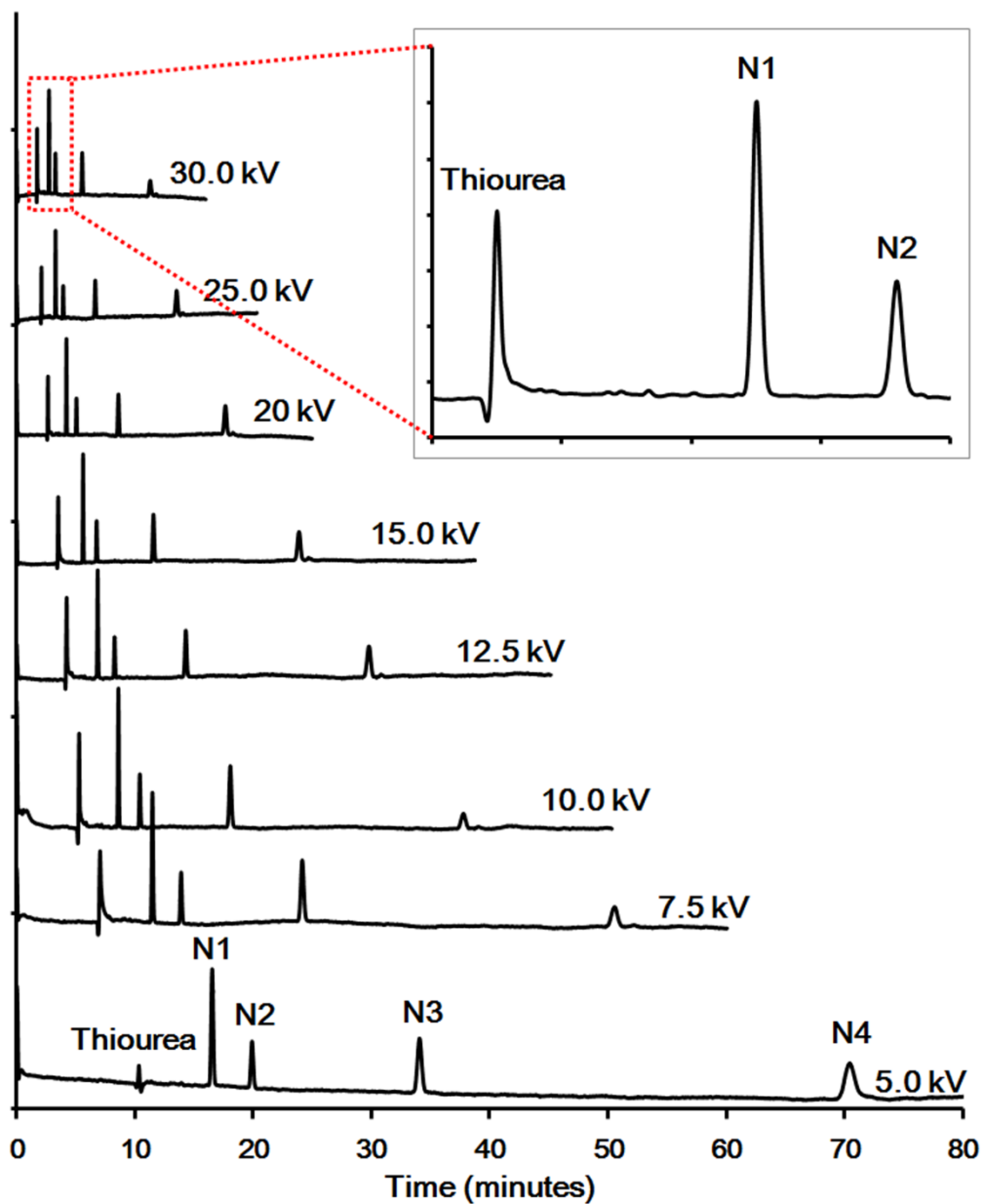
Figure 4.3: Electrochromatograms for the CEC separation of thiourea and the N Series using separation voltages from 5 to 30 kV and a mobile phase of 70:30 (ACN : water).

Table 4.1: Retention times for the CEC separation of the N Series on the FPPM column under different conditions

Mobile phase composition (ACN : water)	Separation Voltage (kV)	Thiourea (EOF marker)	Retention time (minutes)			
			N1	N2	N3	N4
65:35	5.0	10.0±0.3	19.9±0.7	26±1	52±3	123±7
	7.5	6.7±0.2	13.1±0.4	16.9±0.5	34±1	79±4
	10.0	4.92±0.07	10.±1	13±2	27±5	64±15
	12.5	3.89±0.01	7.741±0.003	9.99±0.01	19.94±0.04	47.00±0.06
70:30	5.0	10.5±0.1	16.7±0.3	20.0±0.4	34±1	71±3
	7.5	7.04±0.02	11.50±0.02	13.94±0.02	24.22±0.05	50.8±0.2
	10.0	5.29±0.01	8.5±0.1	10.3±0.2	17.7±0.4	37±1
	12.5	4.24±0.01	6.87±0.01	8.29±0.02	14.32±0.04	29.81±0.09
	15.0	3.53±0.01	5.62±0.03	6.77±0.04	11.56±0.09	23.8±0.2
	20.0	2.67±0.04	4.22±0.05	5.07±0.06	8.59±0.09	17.6±0.2
	25.0	2.115±0.002	3.30±0.01	3.94±0.01	6.64±0.02	13.50±0.05
	30.0	1.76±0.02	2.75±0.03	3.28±0.03	5.48±0.07	11.1±0.2

To be continued

Continued

Mobile phase composition (ACN : water)	Separation Voltage (kV)	Retention time (minutes)				
		Thiourea (EOF marker)	N1	N2	N3	N4
75:25	5.0	9.22±0.01	12.93±0.01	14.83±0.01	22.52±0.01	41.34±0.07
	7.5	6.14±0.01	8.58±0.03	9.82±0.05	14.8±0.1	27.1±0.3
	10.0	4.604±0.002	6.403±0.001	7.32±0.00	11.011±0.001	20.01±0.02
	12.5	3.69±0.01	5.13±0.01	5.85±0.01	8.78±0.01	15.89±0.01
80:20	5.0	8.98±0.06	11.32±0.08	12.40±0.09	16.6±0.2	26.3±0.3
	7.5	6.0±0.1	7.6±0.1	8.3±0.2	11.1±0.2	17.5±0.3
	10.0	4.461±0.003	5.604±0.001	6.123±0.002	8.154±0.004	12.86±0.02
	12.5	3.572±0.001	4.483±0.002	4.894±0.001	6.51±0.01	10.23±0.01

Errors are calculated from three replicate runs.

Table 4.2: Capacity factors and resolutions for the CEC separation of the N Series on the FPPM column under different conditions.

Mobile phase composition (ACN : water)	Voltage (kV)	Capacity Factor				Resolution		
		k_{N1}	k_{N2}	k_{N3}	k_{N4}	R(N1/N2)	R(N2/N3)	R(N3/N4)
65:35	5.0	0.99±0.02	1.57±0.03	4.2±0.1	11.2±0.4	12.8±0.8	33±2	40±3
	7.5	0.96±0.01	1.52±0.01	4.00±0.05	10.8±0.2	13.0±0.5	32±2	35±7
	10.0	1.0±0.2	1.7±0.4	4.4±1.1	12±3	13±2	32±5	38±4
	12.5	0.992±0.001	1.57±0.01	4.13±0.02	11.08±0.04	12.99±0.07	33±2	34±1
70:30	5.0	0.59±0.02	0.91±0.03	2.26±0.09	5.7±0.2	8.5±0.2	24.6±0.4	33±2
	7.5	0.63±0.01	0.98±0.01	2.44±0.02	6.21±0.05	10.2±0.2	27.2±0.5	34±2
	10.0	0.61±0.02	0.94±0.02	2.34±0.06	5.9±0.2	9.9±0.4	27.1±0.6	34±1
	12.5	0.625±0.003	0.95±0.01	2.38±0.01	6.03±0.03	9.3±0.3	25±1	34±2
	15.0	0.602±0.001	0.92±0.01	2.28±0.02	5.77±0.05	9.3±0.3	24.5±0.9	32±1
	20.0	0.58±0.01	0.90±0.01	2.22±0.02	5.60±0.05	8.4±0.2	22.6±0.4	31±1
	25.0	0.561±0.003	0.872±0.001	2.15±0.01	5.40±0.01	7.2±0.3	19.2±0.9	26±1
	30.0	0.56±0.01	0.86±0.02	2.11±0.06	5.3±0.2	6.9±0.4	18±2	24±2

To be continued

Continued

Mobile phase composition (ACN : water)	Voltage (kV)	Capacity Factor				Resolution		
		k_{N1}	k_{N2}	k_{N3}	k_{N4}	R(N1/N2)	R(N2/N3)	R(N3/N4)
75:25	5.0	0.401±0.002	0.612±0.001	1.441±0.003	3.48±0.01	6.40±0.08	18.5±0.6	24±1
	7.5	0.404±0.001	0.60±0.01	1.42±0.02	3.41±0.04	7.18±0.04	20.4±0.2	23±3
	10.0	0.392±0.002	0.590±0.002	1.390±0.001	3.352±0.001	7.00±0.03	19.5±0.4	21±2
	12.5	0.392±0.004	0.581±0.003	1.382±0.001	3.304±0.002	6.73±0.09	18.6±0.4	23.3±0.3
80:20	5.0	0.261±0.003	0.384±0.001	0.85±0.01	1.92±0.01	4.42±0.06	13.7±0.2	19±2
	7.5	0.25±0.01	0.37±0.01	0.83±0.01	1.89±0.03	4.6±0.2	14.3±0.3	20±1
	10.0	0.262±0.001	0.371±0.004	0.830±0.002	1.892±0.001	4.80±0.06	14.2±0.2	16±3
	12.5	0.250±0.001	0.371±0.006	0.825±0.008	1.864±0.002	4.65±0.08	13.5±0.3	18.3±0.7

Errors are calculated from three replicate runs.

The separation efficiency, in theoretical plates per metre (N), was calculated for each analyte (N1, N2, N3, N4) using the full baseline width equation. These values were converted to plate height, H (*i.e.* N^{-1}), and plotted against mobile phase linear velocity (determined from EOF marker migration times at each voltage) to prepare van Deemter curves (Figure 4.4). The minimum plate height was found to be between 0.47 mm/s (7.5 kV) and 0.78 mm/s (12.5 kV).
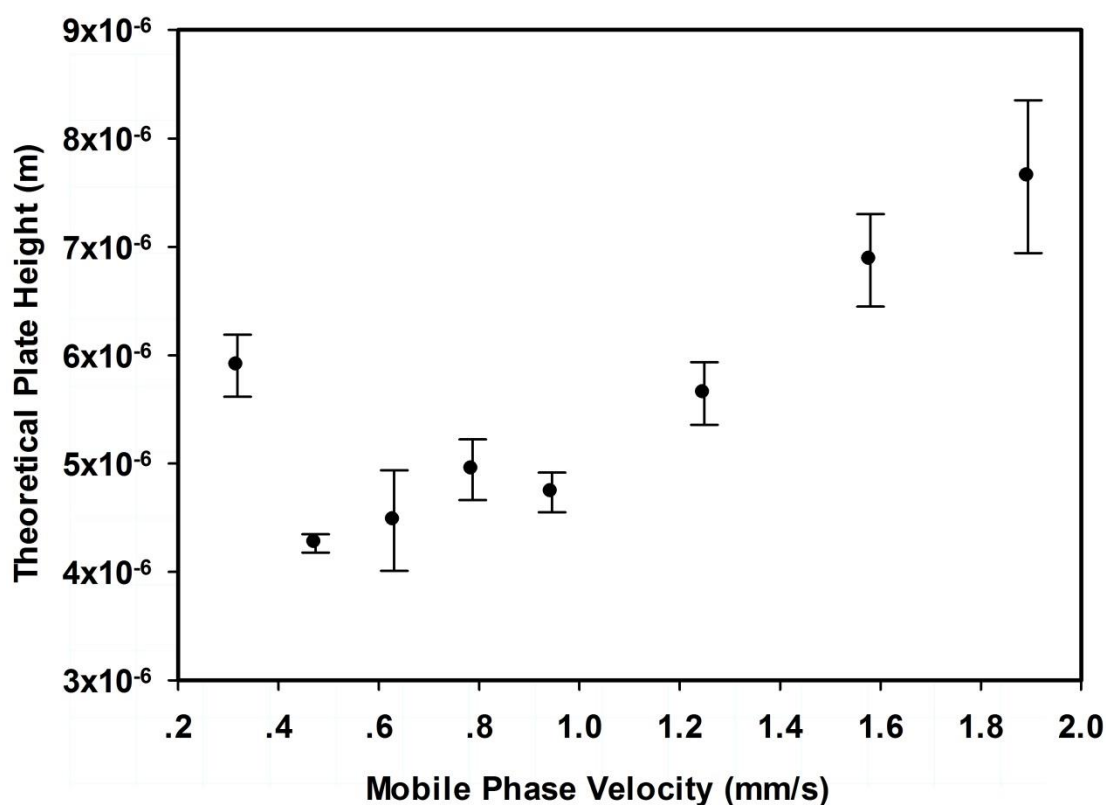
Figure 4.4: van Deemter curve for the elution of N1 over the voltage range 5–30 kV with a mobile phase 70 : 30 (ACN : water). Errors are calculated from three replicate runs.

4.2.2 – Mobile Phase Investigation

The mobile phase buffer composition was explored over the separation voltage range 5 -12.5 kV, which encompasses the optimal voltage range as determined above. The capacity factor

(k), a measure of the partitioning of the analyte between the mobile and stationary phases, was calculated for each analyte (N1-N4) over the above voltage range in the mobile phases described in the Chapter 2 Experimental Section and included in Table 4.2. As expected, the capacity factor is mainly determined by the mobile phase composition. For N1, the least retained analyte, k decreased from 0.96 to 0.25 for the mobile phase compositions 65:35 (ACN : water) to 80:20 (ACN : water), respectively, while for N4 it decreased from 10.8 to 1.9 over the same solvent range.

Peak resolutions, displayed in Table 4.2, show the corresponding increase with capacity factors expected from Equation 4.1.

$$R_{1/2} = \frac{\sqrt{N}}{4} \left(\frac{\alpha_{1/2}-1}{\alpha_{1/2}}\right)\left(\frac{k_2}{1+k_2}\right)$$

Equation 4.1

$R_{1/2}$: The resolution between peaks 1 and 2

$\alpha_{1/2}$: The selectivity factor between peaks 1 and 2

k_2: The capacity factor of the slower peak, 2

The dependence of $R_{1/2}$ on k stems from the ability of a column to retain components 1 and 2 selectively. The selectivity factor, $\alpha_{1/2}$, is therefore defined in terms of k (Equation 4.2). For the solvent compositions of 65-80% ACN/water (v/v) in this study, the surface adsorbed layer has a constant composition as it has been saturated by the mobile phase.[184] Under these conditions, a plot of *ln*k *versus* ACN volume composition is expected to be linear. The 3-D plot in Figure 4.5 shows the dependence of *ln*k on the mobile phase composition for each of

the four compounds of the N Series of analytes. The R^2 value of the linear regression is no less than 0.999 for any analyte over the composition range tested. For any mobile phase composition in this linear range, the capacity factors of each analyte can be used to calculate the selectivity factor for an analyte series. As the analytes in this series differ only by the number of $-CF_2-$ "perfluoromethylene" units in the fluorous tag, a plot of *ln*k *versus* number of $-CF_2-$ groups should also be linear. The selectivity factor for a single $-CF_2-$ unit, the "perfluoromethylene selectivity" α_{-CF_2-}, is therefore attainable from the slope of this line (as the natural logarithm). This approach is common for the determination of the so-called "methylene" selectivity for chains differing by $-CH_2-$ units in reversed-phase LC or CEC, [185,186] but it stands to reason that the analogous value should be a good standard for comparing the selectivity of a column for fluorous analytes. A high value for α_{-CF_2-} thus demonstrates strong fluorous-fluorous interaction as judged by the enhanced selectivity between analytes with differing per-fluorinated chain lengths.

$$\alpha_{1/2} = \frac{k_2}{k_1} \qquad\qquad \text{Equation 4.2}$$

k_1, k_2 are capacity factors of peaks 1 and 2, with peak 2 being the later eluted
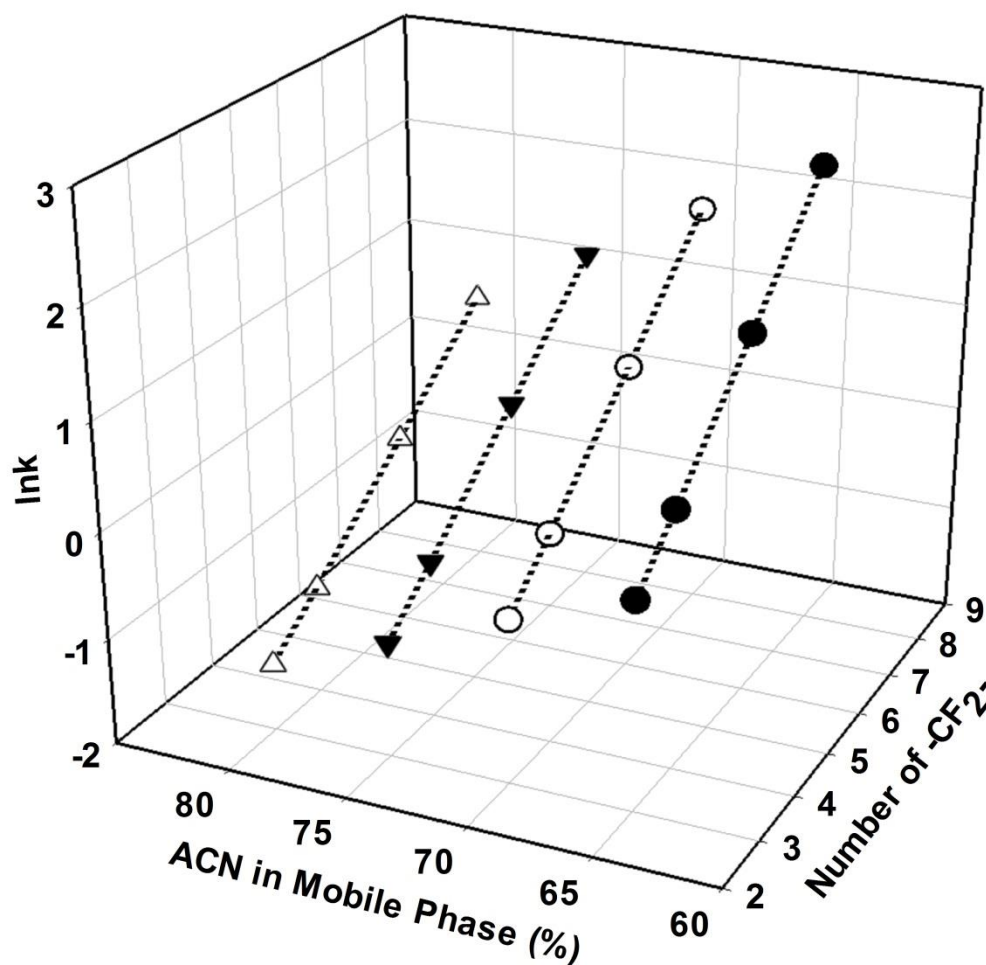
Figure 4.5: Natural logarithm of the capacity factor (*ln*k) for the retention of the N Series on the FPPM column over different ACN percentage in the mobile phase. The slopes of the lines shown on the plot give the perfluoromethylene selectivity, α_{-CF_2-}. Separation voltage is set to 7.5 kV.

Figure 4.5 shows the linear plots of *ln*k *versus* $-CF_2-$ number at four different mobile phase compositions, the R^2 value in the linear regression of each plot being ≥ 0.999. The perfluoromethylene selectivities calculated from the slope of each of these plots appear in Table 4.3, ranging from 1.49-1.63.

Table 4.3: Linear trend line equations of lnk across different numbers of $-CF_2-$ units in the fluorous tag of the N- and P Series of analytes, and Gibbs free energy changes for transferring one $-CF_2-$ unit from the mobile phase to the stationary phase.

	Mobile phase composition (ACN : water)	α_{-CF_2-}	$\Delta G^{\circ}_{-CF_2-}$ (J/mol)
	65:35	1.626±0.007	-1200±10
	70:30	1.579±0.006	-1130±9
N Series on FPPM Column	75:25	1.537±0.006	-1060±9
	80:20	1.493±0.005	-994±8
N Series on FPPM Column	75:25	1.539±0.005	-1070±7
P Series on FPPM Column	75:25	1.533±0.006	-1060±9
N Series on non-FPPM	75:25	1.1434±0.0007	-332±2
P Series on non-FPPM	75:25	1.1366±0.0007	-317±2

Thermodynamically, if α_{-CF_2-} describes the selectivity of the column for a $-CF_2-$ unit, the Gibbs free energy change for the transfer of a $-CF_2-$ unit from the mobile phase to the stationary phase is given by Equation 4.3.[184-186]

$$-RT ln\alpha_{-CF_2-} = \Delta G^{\circ}_{-CF_2-} \qquad \text{Equation 4.3}$$

These $\Delta G^{\circ}_{-CF_2-}$ values were calculated for each mobile phase composition for the N Series and appear alongside the corresponding α_{-CF_2-} values in Table 4.3. In each case, the negative $\Delta G^{\circ}_{-CF_2-}$ value indicates a thermodynamically favourable transfer of $-CF_2-$ to the stationary phase. As expected, an increase in ACN content of the mobile phase leads to more

positive (less negative) $\Delta G^{\circ}_{-CF_2-}$ values, for instance from -1200 J/mol in 65:35 (ACN : water) to -994 J/mol in 80:20 (ACN : water), as it becomes more thermodynamically difficult to get the analyte in the mobile phase to transfer to the stationary phase.

4.2.3 – FPPM Column *versus* Non-FPPM Column

Using a monomer equivalent in structure to FBA but which contains no fluorine, a non-FPPM column was fabricated using the same protocol to allow comparison of the selectivity toward per-fluorinated analytes between fluorous and non-fluorous stationary phases.

To aid in the evaluation of the two column types, another group of fluorous analytes was employed having equivalent structure to the N Series but having a phenyl group replacing the nitro moiety, which we call the P Series. Due to the limited solubility of the P Series in the ACN and water mobile phase system, a 75:25 (ACN : water) composition was used to prepare all N- and P Series samples for these experiments. Likewise, 75:25 (ACN : water) was used as the mobile phase in separations involving the P Series.

Peak resolutions from both fluorous and non-fluorous PPM columns are presented in Table 4.4. Under the same conditions (mobile phase composition 75:25 (ACN : water), applied potential 7.5 kV), resolutions provided by the FPPM column were consistently much higher than those from the non-FPPM. This advantage results from the selective fluorous-fluorous interaction between the fluorous tags in the analytes and the fluorous moieties in the stationary phase. This difference in selectivity is emphasized when both N- and P Series analytes are chromatographed (A, B, Figure 4.6). From these electrochromatograms, it is

103

clear that peaks for the fluorous analytes are more spread out for the FPPM column owing to the selectivity of the fluorous interactions with the stationary phase. More importantly, the elution order of the eight analytes strongly supports the fundamental difference in separation mechanism between the two columns. The non-FPPM column, operating by a reversed-phase mechanism, relies primarily on hydrophobic selectivity. Between the N and P Series, the only difference is the replacement of the more polar nitro moiety in the former with a phenyl group. Within each series, compounds only differ by the addition of $-CF_2-$ groups in the per-fluorinated tag. These small additions make the analyte slightly more hydrophobic, *e.g.*, the retention of N4 is longer than that of N1, whose fluorous tag is shorter. However, because the effect of the nitro and phenyl groups on the hydrophobicity of each series far outweighs the effect of the short per-fluorinated linker on the non-FPPM column, the entire N Series elutes before any of the P Series analytes. This outcome is markedly different than for the FPPM column. The fluorous column has some reversed-phase character, and thus N Series analytes elute earlier than their P Series analogues. Indeed, per-fluorinated stationary phases have seen use as strictly reversed-phase columns.[24,43] However, the fluorous interactions dominate this column's selectivity, causing the resolution between N- and P Series analogues to be greatly reduced and the resolution between members of the same series to be greatly improved. In other words, the added $-(CF_2)_n-$ linker in the per-fluorinated tag effected a much greater difference in retention time than the change in hydrophobicity arising from the replacement of a nitro group with a phenyl group. In fact, the difference in selectivity between the FPPM and non-FPPM is so significant that, as shown in Figure 4.6, while the non-FPPM column elutes all the N Series before any of the P Series, the FPPM separation has each N/P

analogue pair (*e.g.* N1/P1) eluting before the next N/P analogue pair having a slightly longer

fluorous tag (except that N2 elutes just before P1 as N1 and N2 differ by only one –CF$_2$–

group).
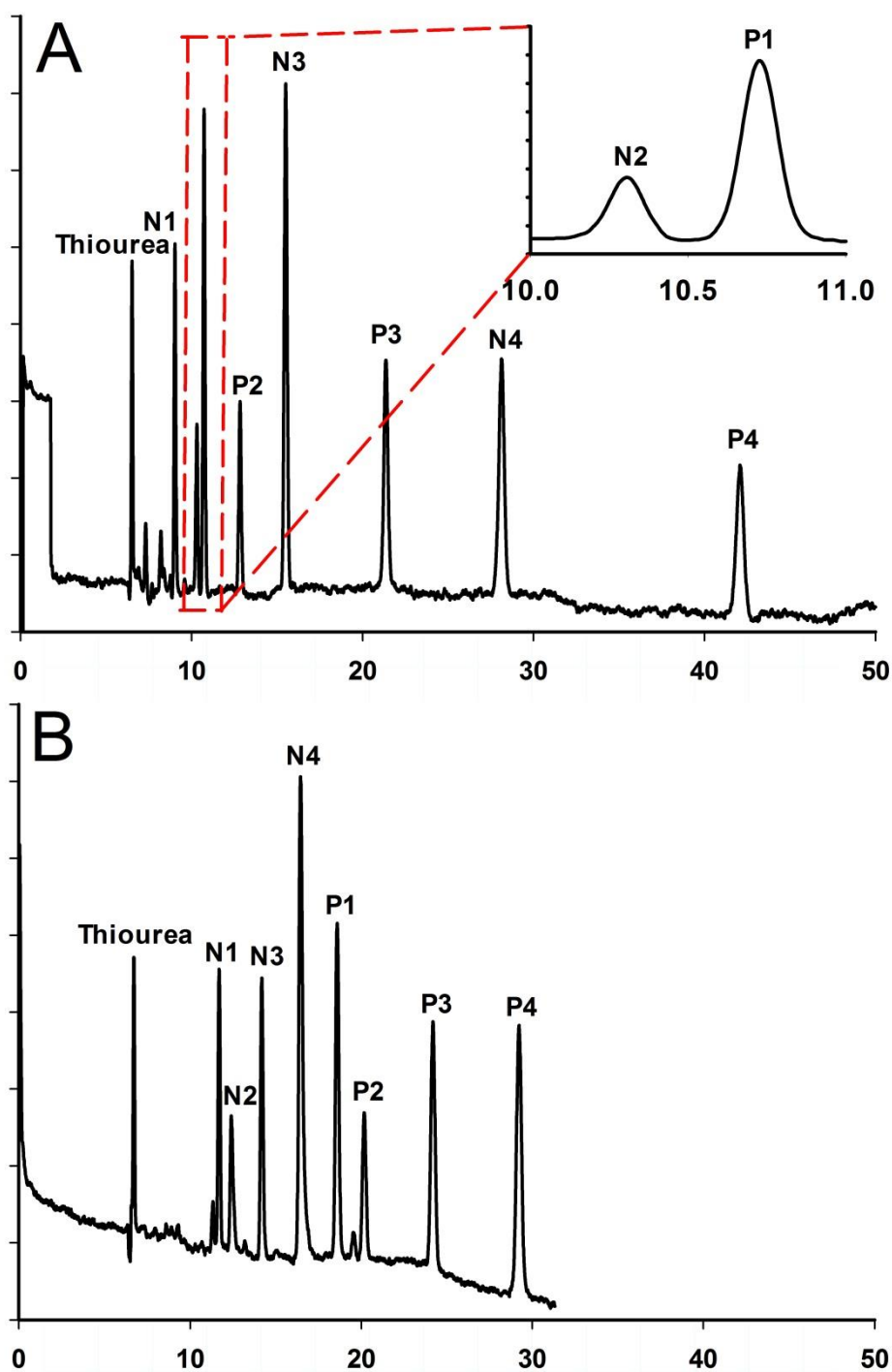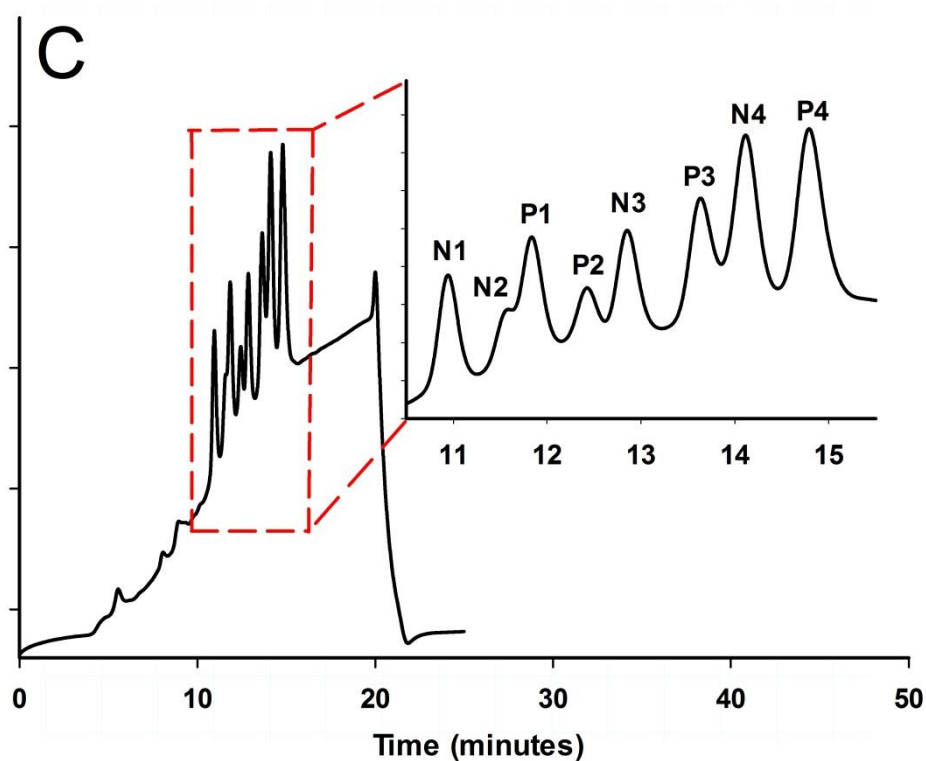
Figure 4.6: Elution order of N- and P Series analytes under different conditions showing column selectivity. A and B are the CEC electrochromatograms of the N and P Series analytes on the FPPM and non-FPPM columns, respectively (7.5 kV separation voltage, mobile phase 75:25 (ACN : water), 0.097 mg/mL analyte concentration, 0.010 mg/mL thiourea concentration, samples in 75:25 (ACN : water)). C is a nano-HPLC chromatogram showing the gradient elution (shown in Figure 2.7) of the N and P Series analytes on a similar FPPM column.

Table 4.4: Resolutions for the CEC separation of the N- and P Series on the FPPM and non-FPPM columns under different conditions.

Mobile phase composition (ACN : water)	Separation voltages (kV)	Resolution					
		R(N1/N2)	R(N2/N3)	R(N3/N4)	R(P1/P2)	R(P2/P3)	R(P3/P4)
FPPM column							
75:25	7.5	6.25±0.22	19.41±0.78	27.09±0.48	8.44±0.22	22.87±0.78	30.7±1.1
80:20	30.0	2.69±0.03	7.12±0.18	9.57±0.29			
75:25	7.5	2.55±0.03	5.89±0.16	6.84±0.28	4.04±0.06	9.01±0.15	9.57±0.15
Non-FPPM column							
	12.5	1.59±0.04	3.56±0.13	3.79±0.12			
80:20	15.0	1.50±0.02	3.36±0.05	3.41±0.37			
	20.0	1.33±0.11	2.96±0.25	3.04±0.41			

Errors are calculated from three replicate runs.

Graphically, the difference in retention mechanism can be best seen in Figure 4.7, which shows the linear regression of lnk $versus$ the number of perfluoromethylene units for the N and P Series analytes on the fluorous and non-fluorous PPM columns. Recall that the slope of this plot allows the calculation of α_{-CF_2-}, which appears in Table 4.3 for each case. In Figure 4.7, the slopes of the lines for plots representing the fluorous column are steeper, indicating a greater fluorous selectivity, as expected. Comparing the difference between plots of the N and P Series in the Y-axis, however, it is apparent that the lines are much closer together for the fluorous column than the non-fluorous column. The slopes for the N and P Series on the same column are almost the same, indicating that the contribution of the fluorous interaction of the analytes with the column relative to all other interactions is similar between the N and P Series (this would not be the case if the analyte series were very different). Consider, however, that extrapolating these plots to the Y-axis gives an indication of the capacity factor (k) of the same molecule having no fluorous tag. Comparing the Y-intercepts of the N and P Series lines, therefore, gives the selectivity of the column for the phenyl group over the nitro group, the analyte being otherwise equal and without fluorous affinity. For the non-FPPM column, the selectivity factor for the P Series over the N Series, calculated from the Y-intercepts of the plots in Figure 4.7, is 2.42. For the FPPM column, the analogous selectivity factor is 1.70, indicating that the reversed-phase character of the fluorous column is much poorer than that of the non-FPPM column. Thus, while the FPPM column can be used to separate non-fluorous analytes, it is expected that a more conventional reversed-phase column would provide greater selectivity for compounds that are separated primarily by hydrophobic interactions.
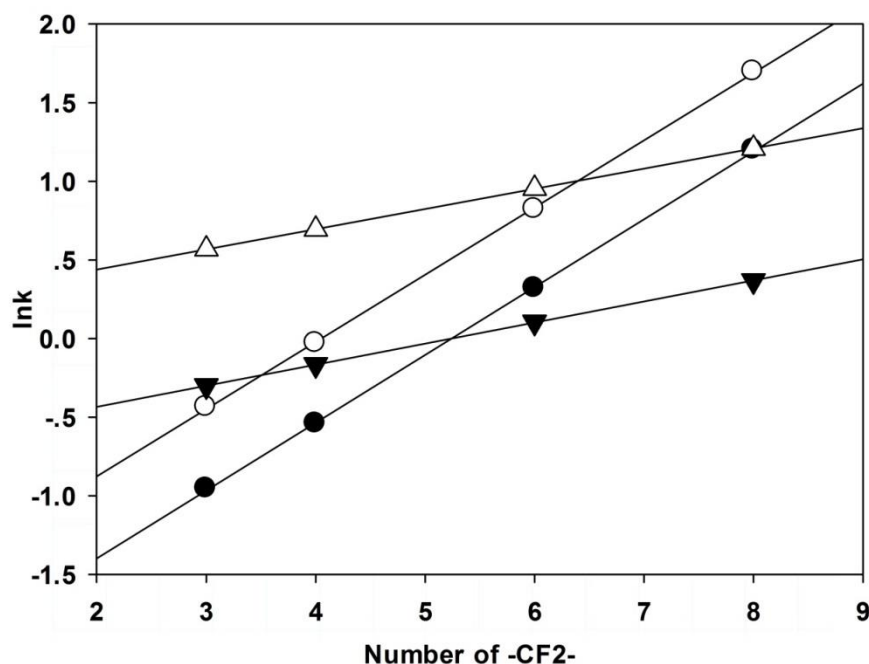
Figure 4.7: Natural logarithm of the capacity factor (*ln*k) *versus* number of $-CF_2-$ units in the fluorous tag for the N- (solid symbols ▼, ●) and P- (open symbols Δ, ○) series separation on the FPPM (circles) and non-FPPM (triangles) columns. Separation voltage was set to 7.5 kV. Mobile phase was 75:25 (ACN : water).

For the sake of completeness, and to allow a more universal comparison, the Gibbs free energy change for the transfer of a perfluoromethylene unit from the mobile phase to the stationary phase ($\Delta G^{\circ}_{-CF_2-}$) was calculated and is shown in Table 4.3 alongside the α_{-CF_2-} values for both the N and P Series analytes on both the FPPM and non-FPPM columns. Again, the negative free energy change indicates a favourable transfer to the stationary phase under the conditions in Figure 4.7, and the similar values between N and P Series analytes shows that the value sufficiently isolates the effect of the perfluoromethylene units on the free energy change. Furthermore, the much more negative $\Delta G^{\circ}_{-CF_2-}$ for the fluorous analytes on

109

the fluorous column shows the strength of the fluorous-fluorous interactions on these columns relative to columns that contain no per-fluorinated groups.

The elution order in the CEC separation of the N- and P Series analytes matched that for their nano-LC separation on a similar column.[81] In that study, however, the resolution of N2 and P1 was incomplete (C, Figure 4.6), despite the use of a solvent gradient. To be fair, the length of the LC column was only 10 cm compared to the 20 cm effective column length in the current study, although doubling the column length in the LC case would still not allow complete resolution of N2 and P1 as resolution is expected to improve only by the square root of column length. Given the inherently better plate numbers of CEC arising from the plug shape of electro-kinetically driven flow, these two peaks are fully resolved under the standard conditions (7.5 kV, 75:25 (ACN : water), Table 4.4, A, Figure 4.6), where R(N2/P1) was 1.90 ± 0.05. Going to 70:30 (ACN : water) (Figure 4.8), R(N2/P1) improves to 3.17 ± 0.12. This result further demonstrates the power of CEC for high-efficiency separations, allowing high resolution of peaks in less time while maintaining selectivity.
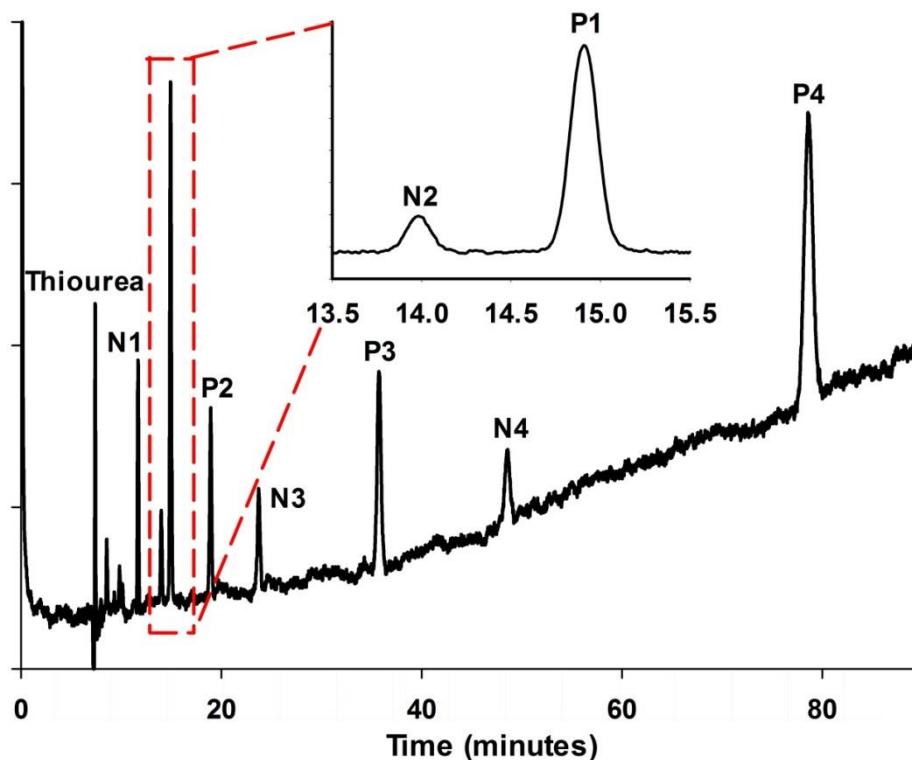
Figure 4.8: N- and P Series analytes separated by CEC on the FPPM column under separation voltage 7.5 kV, mobile phase 70:30 (ACN : water) showing improved resolution between N2 and P1. N Series concentration is 0.060 mg/mL, P Series is 0.060 mg/mL, and thiourea is 0.007 mg/mL in buffer 70:30 (ACN : water).

4.2.4 – Analysis Time

The goal of a chromatographic separation is to separate all the analytes in a mixture in as little time as possible while maintaining a minimum resolution between any two peaks of 1.5. Analysis time can most effectively be shortened by increasing voltage, which increases mobile phase velocity, or by increasing the organic component of the mobile phase, which decreases capacity factor. At 30 kV, the voltage limit for the instrument, and mobile phase composition 80:20 (ACN : water), the practical upper limit that ensures analyte solubility, the N Series was separated by CEC on the FPPM column as shown in Figure 4.9. Under these conditions, all

analytes were completely eluted in 5 minutes, with the lowest resolution being R(N1/N2) = 2.69 ±0.03 (Table 4.4). Despite the small difference in per-fluorinated tag length, the fluorous interactions are sufficient to fully resolve this entire series of peaks at the operational limit of analysis time.
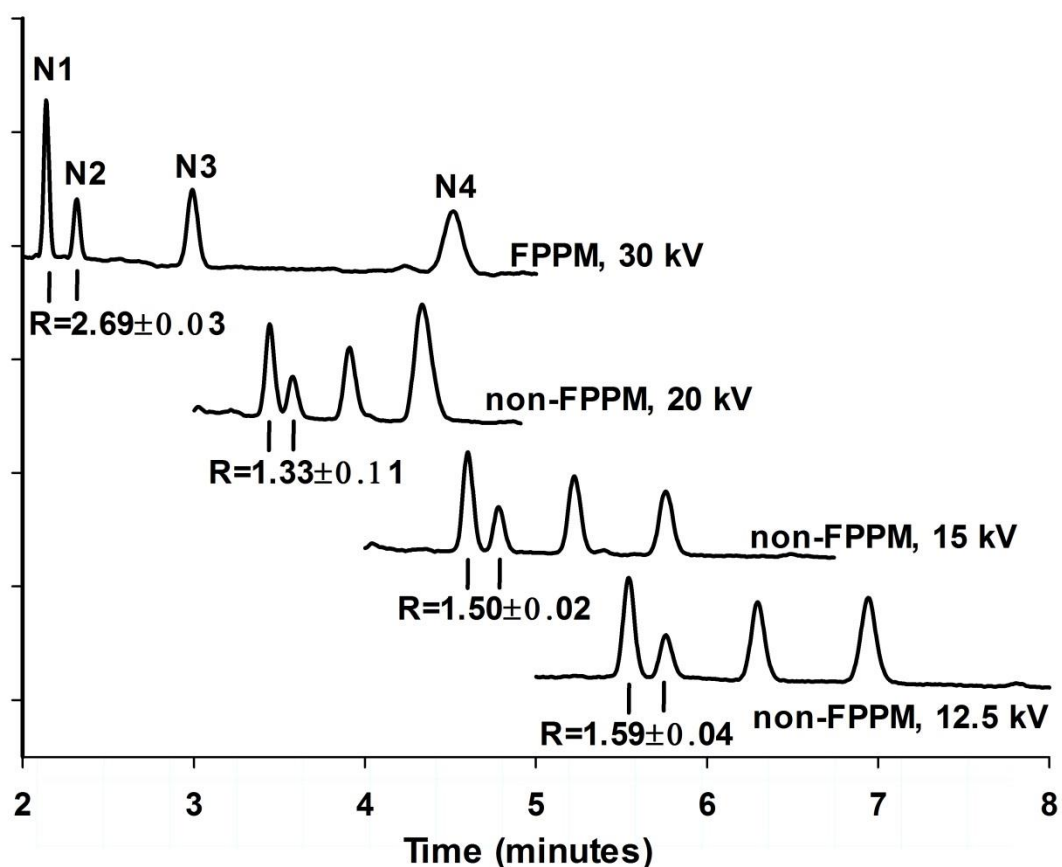
Figure 4.9: Electrochromatograms for the CEC separation of the N Series on a FPPM column and a non-FPPM column in buffer 80:20 (ACN : water). Errors are calculated from three replicate runs.

In nano-LC mode, as determined in an earlier study,[81] optimized conditions that allowed full resolution of all N Series peaks required 15 minutes from the beginning of the solvent gradient.

Despite the aid of gradient elution, the inherently poorer column efficiency of hydrodynamic flow separations caused the time for full resolution to increase in that case. Furthermore, a dead time of about 12 minutes from injection to the beginning of the gradient and 6 minutes of re-equilibration time afterward caused the total analysis time to be >33 minutes, markedly longer than that for the same separation on a similar column in CEC mode.

For the non-FPPM column in CEC mode, the inferior selectivity toward fluorous analytes led to a poorer resolution between any two analytes compared to that for the FPPM. This meant that at the operational limit of the analysis as described above (30 kV; 80:20 (ACN : water)), peaks N1 and N2 were not resolved. To achieve the necessary resolution R(N1/N2) ≥ 1.5), an applied potential of 15 kV (Table 4.4, Figure 4.9) was required. Under these conditions, all analytes completely eluted within 6 minutes, significantly longer than with the FPPM column and with N1/N2 barely resolved.

4.3 – Conclusion

The CEC separation of fluorous analytes based on fluorous-fluorous interaction was reported for the first time in this chapter. Two sets of analytes, one having a nitro group (N Series) and one having a phenyl group (P Series), both functionalized with a per-fluorinated chain of varying length, were employed to characterize the fluorous PPM column. Under optimized conditions, the column efficiency (calculated for the N1 peak) was as high as 234,000 plates/m, and complete resolution (>1.5) was obtained for analytes differing only by a single perfluoromethylene unit (*i.e.* N1 and N2) under all conditions tested.

An equivalent non-FPPM column was fabricated to compare with the FPPM column and to illustrate the effects of fluorous-fluorous interactions on the separation of the fluorous analytes. Perfluoromethylene selectivity, α_{-CF_2-}, and subsequently Gibbs free energy change for the transfer of a –CF_2– unit from mobile to stationary phase, $\Delta G^{\circ}_{-CF_2-}$, were used to evaluate the fluorous interaction of the columns, showing that the FPPM column had significantly greater selectivity for the –CF_2– unit than the non-FPPM column. Furthermore, with the improved peak resolution of the FPPM column, complete separation was attainable in less time than with the non-FPPM column.

Comparing separations from similar FPPM columns in HPLC and CEC modes, the inherent column efficiency advantages of CEC over LC lead to much greater resolutions in CEC despite the lack of a mobile phase gradient. With this improved resolution, combined with instrumental factors including injection time and equilibration time, CEC analysis was possible in much less time than for nano-LC (5 minutes in CEC analysis, 33 minutes in nano-LC analysis).

The work in this chapter successfully demonstrated that the FPPM stationary phase presented allows separation based on fluorous-fluorous interaction that provides significantly enhanced selectivity for analytes containing per-fluorinated groups. One can take advantage of the excellent selectivity for per-fluorinated compounds by separating such analytes from non-fluorinated compounds in a complicated mixture, or by purposely tagging target analytes with per-fluorinated tags prior to analysis. This approach would be particularly useful in proteomics studies whereby target proteins or peptides can be tagged and more easily

separated from other compounds in the mix. These benefits make the presented approach, combining the high resolution of CEC with the unconventional selectivity of fluorous-fluorous interactions, a promising alternative for the analysis of fluorine-containing compounds.

Chapter 5 – Qualitative and Thermodynamically Quantitative Study of the Fluorous and Hydrophobic Interaction with PPM Stationary Phases

5.1 – Introduction

The term "like dissolves like" was frequently and ambiguously used to describe the origin of hydrophobic interaction or reversed-phase retention.[26,28,44,187-193] The pursuit for the mechanism of the reversed-phase LC retention, the most widely used method for analysis and purification, has continued the last two decades and is still active now.[184-186,194-196] Two major mechanisms have been proposed: adsorption mechanism and partitioning mechanism. The question remains as to whether the analytes partition or adsorb when transferring from mobile phase to stationary phase.

In the adsorption mechanism, both mobile phase and the analytes only dwell on the "tips" or/and the "stem" of the stationary phase functional chains (Figure 5.1). Alternatively, the analytes will dwell in the mobile phase and the cavities formed within the stationary phase functional moieties in the partitioning mechanism (Figure 5.2). Another view of the partitioning mechanism is that a thin layer of solution (different from the bulk mobile phase) is present on the surface of the stationary phase as shown in Figure 5.2. This thin layer provides the cavities to accommodate analytes. Nevertheless, it is difficult to determine the exact location of analyte in practice.[197]
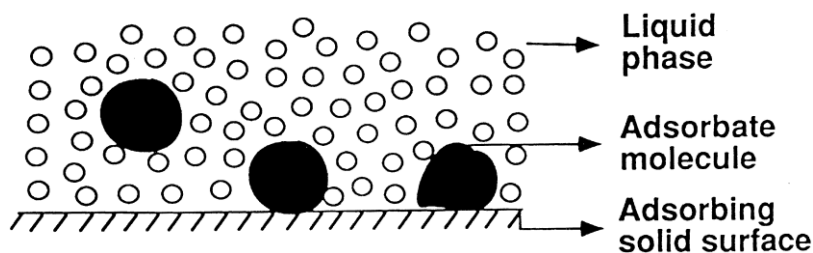
Figure 5.1: Illustration of adsorption mechanism.[198,199]
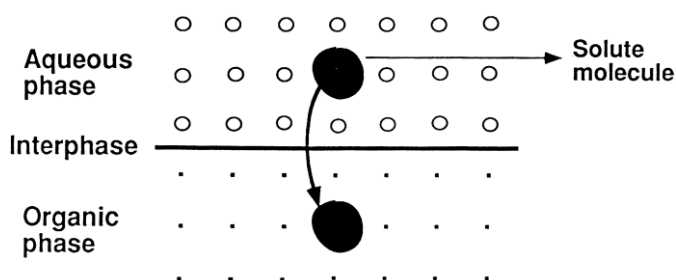
Figure 5.2: Illustration of partitioning mechanism. This figure is reproduced from references.[199,200]

To establish the mechanism, one needs to determine if an analyte is located in the interfacial region (adsorption) or in the "central region" (partition) of the stationary phase. The "central region" refers to the functional moieties, *e.g.* C_{18} side chain, in bonded silica microspheres rather than the micro-pores. Ideally, the spatial distribution of the analyte is the most convincing evidence for the mechanism type. Unfortunately, no experimental approaches have been able to provide detailed information on the analyte distribution. Instead, researchers have relied upon computational simulation.[199] Figure 5.3 clearly shows the spatial distribution of analytes in the mobile phase with different water and methanol ratio. Rafferty and coworkers found that there is a combination of the partitioning mechanism and adsorption mechanism for n-butane retention on an octadecylsilane grafted (ODS) silica microsphere stationary phase.[200] It was also found that the relatively polar mobile phase, *e.g.*

methanol and ACN, will induce collapse of the n-alkyl chains. Alternatively, in the less polar mobile phase, *e.g.* THF, the CBP causes the chains to bend and extend. Generally, the adsorption mechanism is more likely to be dominant for the retention of small and polar analytes in C_{18} reversed-phase LC.[201] Whereas the partition mechanism is more appropriate to describe the behavior of non-polar analytes.[198-200] It was also found that the analyte locations are highly dependent on the local solubility.[110,111,116]

It is difficult to clearly attribute the reversed-phase retention process to either partitioning or adsorption.[202] Thermodynamically there is no apparent distinction between the partition and adsorption mechanisms. Furthermore the physicochemical principles of these two apparently disparate processes are fundamentally identical and both are derived from lattice models.[200,201,203,204]

As a result, no partitioning or adsorption is specified in this chapter's discussion. Instead, a much simplified theory based upon both the solvophobic theory (considering solvent-solvent, solute-solvent, and solute-stationary phase interaction), and the lattice theory (considering cavity-formation related thermodynamics) is going to be used to quantitatively thermodynamically analyze the difference between hydrophobic interaction and fluorous interaction. [194,197,205-207]
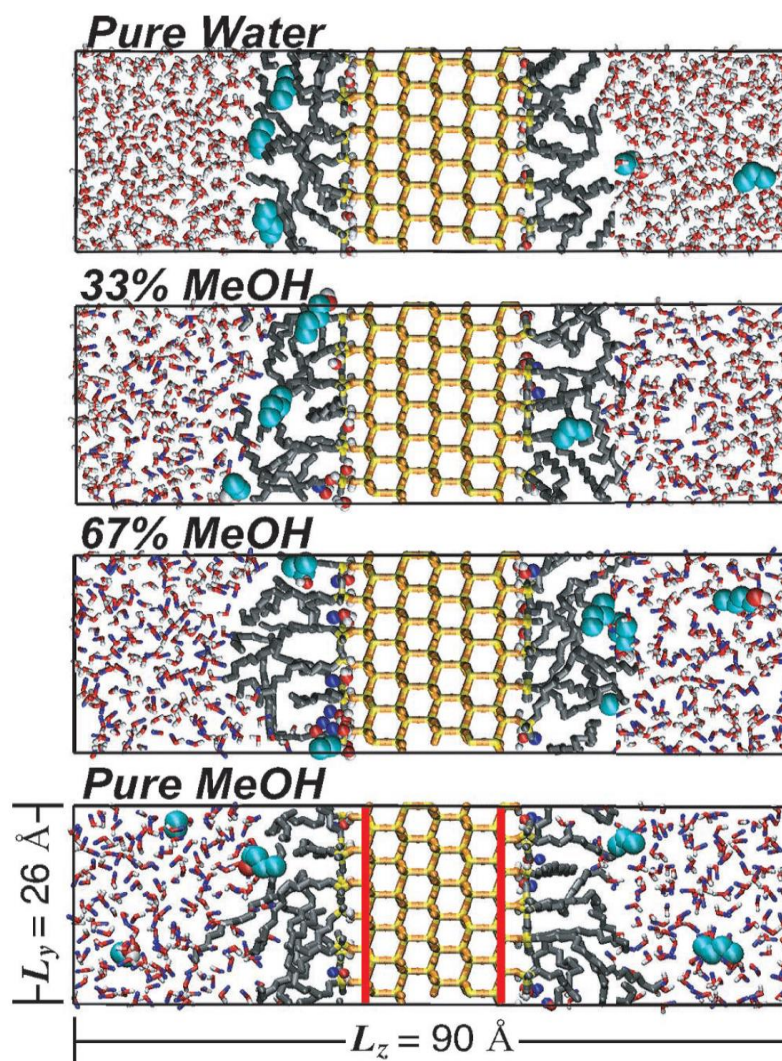
Figure 5.3: Simulation results of four different solvent component ratios (water and methanol). Shown from top to bottom are pure water, 33:67 (methanol : water), 67:33 (methanol : water), and pure methanol. The silica substrate and grafted alkyl chains are shown as large tubes with oxygen in orange, silica in yellow, and CHx groups in gray. Methanol and water are shown with oxygen in red, hydrogen in white, and methyl groups in blue. Solvent molecules are depicted as small tubes except for those molecules involved in hydrogen bonding with the substrate, which are shown as small spheres for emphasis. Solutes are shown as large spheres with CHx groups, oxygen, and hydrogen in cyan, red, and white, respectively. The simulation boxes are shown in the z-y plane. Vertical red lines in the bottom snap shot indicate the positions along the long axis defined. This figure is reproduced from reference.[200]

The hard dipole shell theory concerning the origin of fluorous interaction is proposed in Section 1.2. In this chapter, fluorous interaction theory is explored based upon the CEC data obtained from PPM stationary phases with different fluorous fractions. The selectivity and thermodynamics associated with fluorous/hydrophobic interactions are examined as well. Furthermore, a novel classification method "hypothetical water percentage" (HWP) is proposed for the first time to quantitatively characterize the hydrophobicity/fluorophilicity of a stationary phase.

5.2 – Results and Discussion

5.2.1 – Methylene Selectivity and Perfluoromethylene Selectivity

In chromatographic studies the selectivity factor, $\alpha_{1/2}$, is defined in terms of capacity factor (k, a measure of the adjusted retention time of an analyte on a stationary phase) to compare the interaction difference of two analytes on a stationary phase (Equation 4.2).

The methylene ($-CH_2-$) group is a typical chemical constituent of hydrophobic analytes. An increase in the alkyl moiety length on the analytes enhances the hydrophobic interaction with the stationary phase and corresponding k of the analyte. It follows that the lnk is proportional to the number of $-CH_2-$ units in the alkyl moiety. When plotting the lnk *versus* the $-CH_2-$ number in their alkyl moiety, a linear trend should be observed.[82,184,186] The so-called methylene selectivity α_{-CH_2-} for substituents differing by $-CH_2-$ units is therefore obtained from the slope of the trend line (Equation 5.1) where a steeper trend line indicates that the stationary phase is more sensitive to a $-CH_2-$ unit change.

$$ln\alpha_{-CH_2-} = ln\left(\frac{k_{i+1}}{k_i}\right) = \frac{ln\,k_2 - ln k_1}{1} = \text{slope of trend line of } lnk \text{ } versus - CH_2 - \text{number}$$

Equation 5.1

The same method can be applied to calculate perfluoromethylene ($-CF_2-$) selectivity α_{-CF_2-} to evaluate the strength of the fluorous interaction between fluorous analytes and a stationary phase.

Similarly, this method also works for a stationary phase, *i.e.* changing the $-CH_2-$ content or $-CF_2-$ content in the stationary phase will also change the interactions with the analytes and corresponding selectivity values. Methylene selectivity and perfluoromethylene selectivity can be used to evaluate the specific interaction between analytes (containing $-CH_2-$ and/or $-CF_2-$) and stationary phase (containing $-CH_2-$ and/or $-CF_2-$).The PPM-based stationary phases were employed in all chromatographic trials. PPM enables the chemistry of the monolith to be tailored through the choice of monomer and cross-linker. A hydrophobic stationary phase can be fabricated using a hydrophobic monomer (*e.g.* BA) and hydrophobic cross-linker (*e.g.* BDDA). An analogous fluorous monolith can be prepared by replacing BA and/or BDDA ($-CH_2-$ unit) with fluorous monomer (*e.g.* FBA and/or TFBDA, $-CF_2-$ unit) to render a stationary phase with more fluorous character. To evaluate both the hydrophobic - and fluorous character of stationary phases, a series of stationary phases with different ($-CH_2-/-CF_2-$) ratio were fabricated (Figure 5.4). The impact of the $-CF_2-$ fraction was evaluated using two groups of fluorous analytes (N Series and P Series, with different $-CF_2-$ unit number) and a homologous Phenyl Alkane Series (with different $-CH_2-$ unit number). The *ln*k of N Series and P Series *versus* $-CF_2-$ unit number and the *ln*k

of Phenyl Alkane Series *versus* $-CH_2-$ unit number are plotted in Figure 5.5. Both α_{-CH_2-} and α_{-CF_2-} are calculated using Equation 4.2 and Equation 5.1 (*i.e.* the slopes of the trend lines in Figure 5.5) and are shown in Table 5.2. The N Series and P Series exhibit steeper slopes on the more fluorinated stationary phases (top and middle, Figure 5.5), which demonstrates that more fluorous stationary phases provide higher α_{-CF_2-}. Conversely, the Phenyl Alkane Series exhibits steeper slopes on stationary phases prepared with greater hydrophobic content (*i.e.* less fluorous, bottom, Figure 5.5, which indicates that more hydrophobic stationary phases can provide a higher α_{-CH_2-}. Stated in another way, fluorous stationary phases are more sensitive to $-CF_2-$ unit number in analytes containing fluorous moieties. In particular, the α_{-CF_2-} increases from 1.11 on the stationary phase prepared with (0)FM+(4)M (*i.e.* 100% hydrophobic monomer, BA), to 1.49 on the stationary phase prepared with (4)FM+(0)M (*i.e.* 100% fluorous monomer, FBA). Conversely, α_{-CH_2-} exhibits the opposite trend where it decreases from 1.21 on (0)FM+(4)M to 1.13 on (4)FM+(0)M. Interestingly, for the same stationary phase, the α_{-CF_2-} values calculated from for the N Series and P Series are virtually identical ((3)FM+(1)M,1.43 *versus* 1.42, value from N Series *versus* value from P Series). This observation points to the fluorous selectivity being primarily dependent upon fluorous interaction rather than hydrophobic/secondary interactions for similar molecules.[80,81]
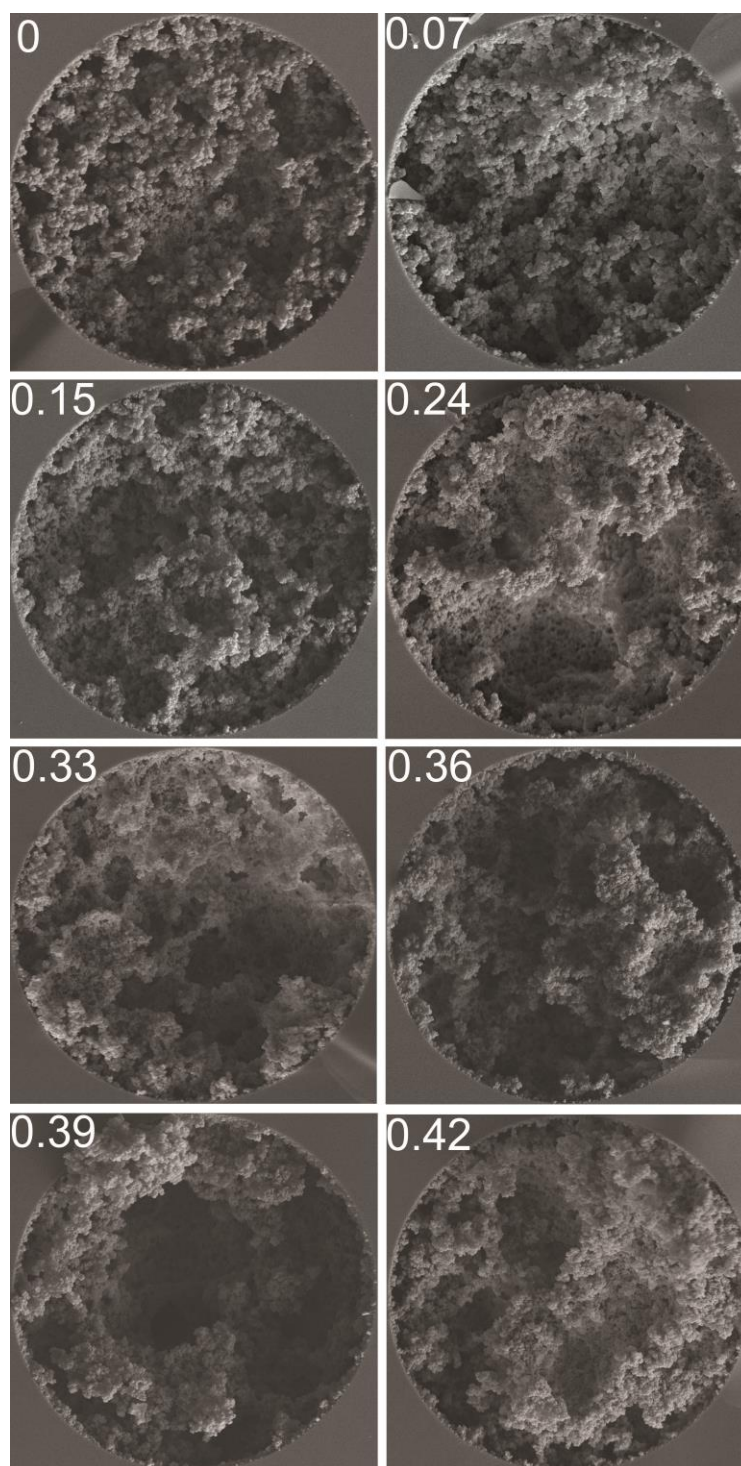
Figure 5.4: SEM images of PPM with different $-CF_2-$ fractions. The $-CF_2-$ fractions are shown in top left of each SEM images and can be calculated through Equation 5.2

$$-CF_2- \text{ fraction} = \frac{\text{molar amount of } -CF_2-}{\text{molar amount of } -CF_2- + \text{ molar amount of } -CH_2-} \qquad \text{Equation 5.2}$$
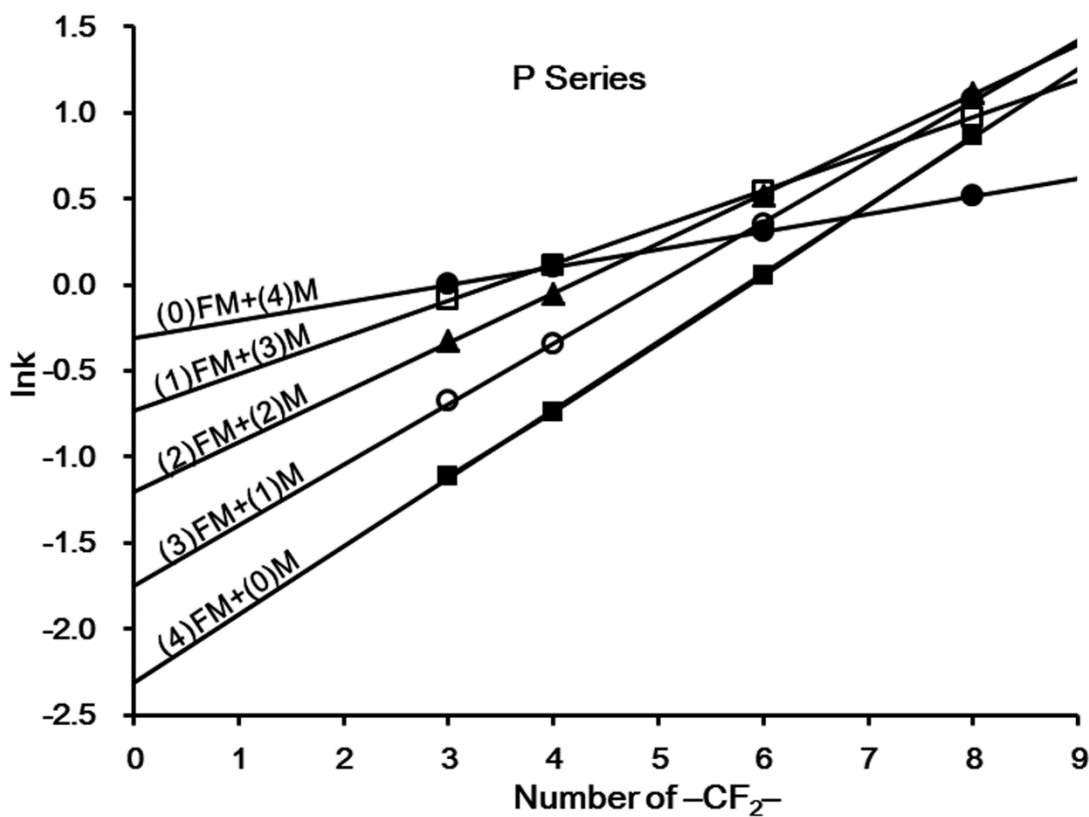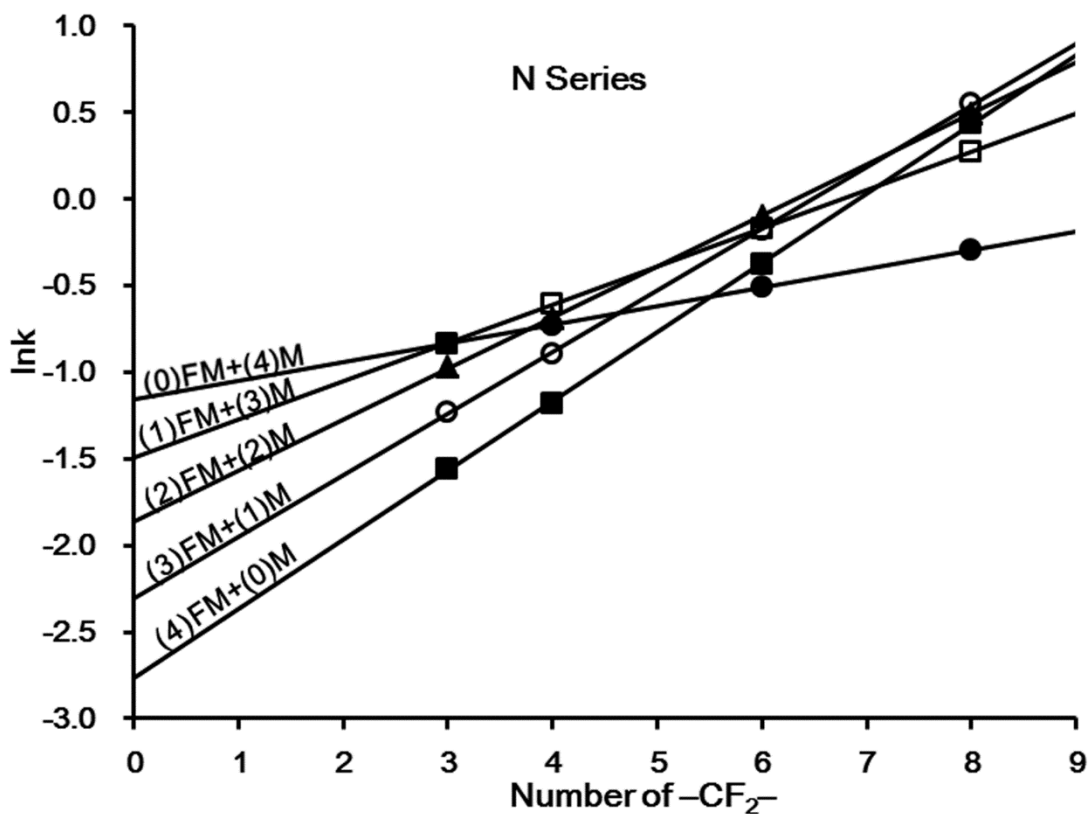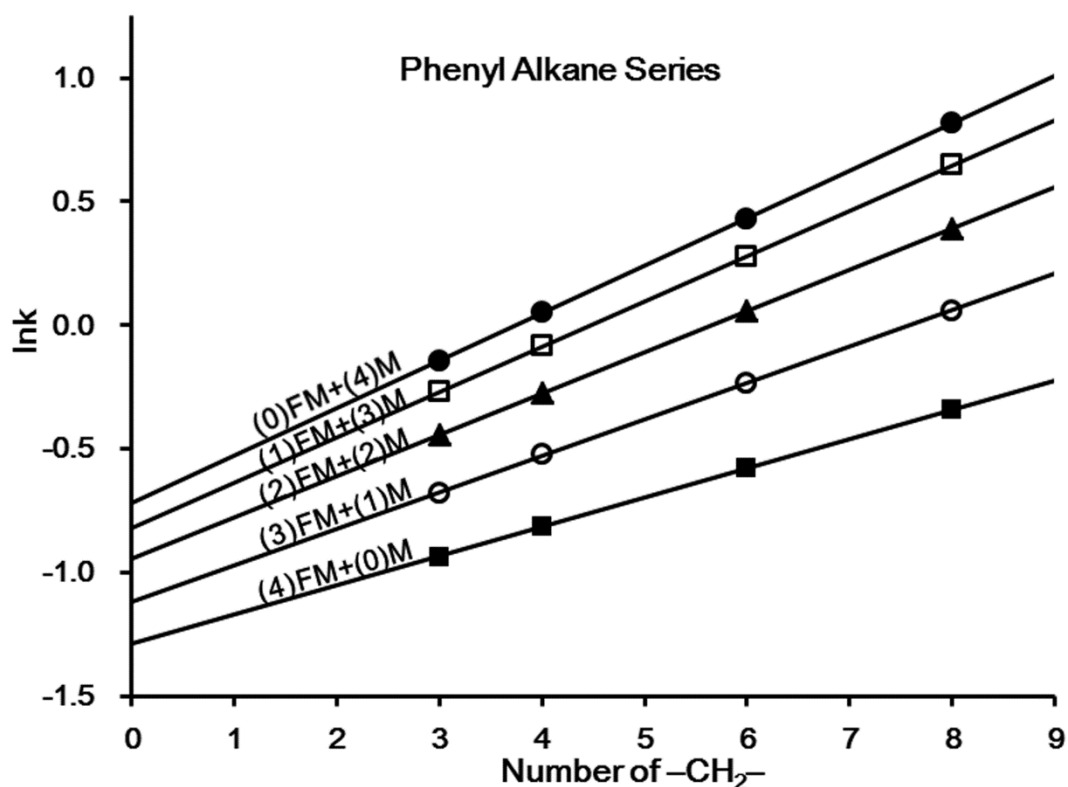
Figure 5.5: Natural logarithm of the capacity factor (*ln*k) *versus* number of –CF$_2$– units in the fluorous moiety for the N Series (top), P Series (middle), and *ln*k *versus* number of –CH$_2$– units in the alkane moiety for the Phenyl Alkane Series (bottom) separated on five columns with different –CF$_2$– fraction in stationary phase. FM+(4)M, (1)FM+(3)M, (2)FM+(2)M, (3)FM+(1)M are (4)FM+(0)M are the columns made of 0:4, 1:3, 2:2, 3:1, and 4:0 fluorous monomer : hydrophobic monomer (FBA : BA; volume ratio) respectively. Cross-linker is hydrophobic one (BDDA) for this group of stationary phase. Mobile phase was 80:20 (ACN : water).

Table 5.1: Perfluoromethylene selectivities, methylene selectivities, and Gibbs free energy changes for transferring one –CF_2– or –CH_2– unit from the mobile phase to five stationary phases with different –CF_2– fraction

Column	–CF_2– Fraction in Stationary Phase	N Series		P Series		Phenyl Alkane Series	
		α_{-CF_2-}	$\Delta G^{\circ}_{-CF_2-}$ (J/mol)	α_{-CF_2-}	$\Delta G^{\circ}_{-CF_2-}$ (J/mol)	α_{-CH_2-}	$\Delta G^{\circ}_{-CH_2-}$ (J/mol)
(0)FM+(4)M	0	1.11	-267.7±1.5	1.11	-255.4±1.9	1.21	-475.9±1.1
(1)FM+(3)M	0.08	1.24	-538.3±1.9	1.24	-527.8±0.4	1.20	-455.0±0.3
(2)FM+(2)M	0.16	1.34	-729.6±0.8	1.34	-716.3±0.8	1.18	-414.0±0.5
(3)FM+(1)M	0.24	1.43	-883.8±0.3	1.42	-873.0±0.1	1.16	-364.7±0.1
(4)FM+(0)M	0.33	1.49	-991.6±0.5	1.49	-981.3±1.2	1.13	-293.5±0.0

Mobile phase was 80:20 (ACN : water). Errors are calculated from three replicate trials.

Extending the trend lines to the y-axis, a lnk value for the fluorous analytes without a fluorous moiety, and a value for the Phenyl Alkane Series without the alkyl chain (*i.e.* benzene) can be calculated. This extrapolation is validated by the addition of benzene to the Phenyl Alkane Series analytes and checking for linearity. A plot of the lnk *versus* the number of $-CH_2-$ units in the alkyl moiety number in the sample containing benzene and six phenyl alkanes is shown in Figure 5.6. The trend line R^2 is 0.9994, shows that the lnk value for benzene (*i.e.* number of $-CH_2- = 0$) is accurately predicted. It was found that the y-intercept values decrease for stationary phases with increased fluorous character. The value of lnk can be used to gauge the strength of the interaction with the stationary phase while keeping the other parameters constant (*i.e.* mobile phase, applied potential, temperature, etc.). Stronger interactions with stationary phases having more $-CH_2-$ content can be attributed to the $-CH_2-$ instantaneous or induced dipole interaction being larger than $-CF_2-$ interactions resulting from weaker (reduced) $-CF_2-$ instantaneous or induced dipole interactions.

The addition of $-CF_2-$ or $-CH_2-$ units to a compound's structure significantly changes the compounds retention characteristics. As shown in Figure 5.5, one $-CF_2-$ unit attached to both the N and P Series analytes produces a more dramatic effect on retention for more fluorous stationary phases compared to hydrophobic stationary phases. Adding $-CF_2-$ units will render analytes with more fluorous character and produce enhanced affinity on the stationary phase with more fluorous character. It is important to note that increases in fluorous content for the stationary phase enhance selectivity for fluorous analytes as well.
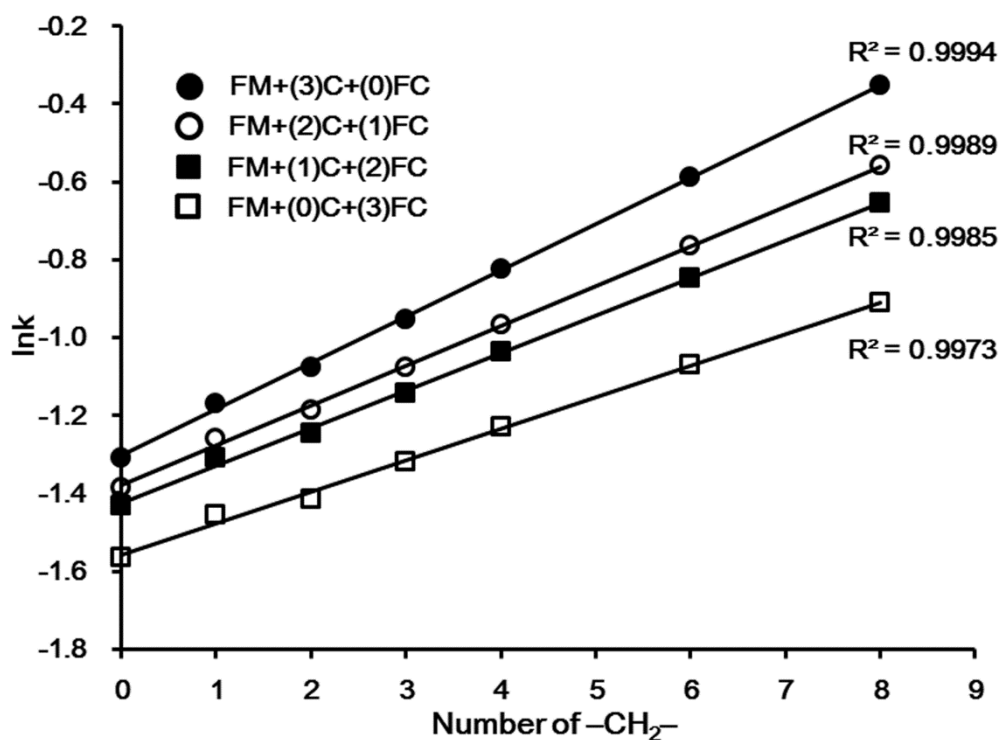
Figure 5.6: Natural logarithm of the capacity factor (*ln*k) *versus* number of –CH$_2$– units in the alkane chain for the benzene and Phenyl Alkane Series separated on stationary phase FM+(3)C+(0)FC, FM+(2)C+(1)FC, FM+(1)C+(2)FC, and FM+(0)C+(3)FC. Stationary phase FM+(3)C+(0)FC is the same as (4)FM+(0)M. Mobile phase was 80:20 (ACN : water). Phenyl Alkane Series includes toluene, ethyl benzene, n-propyl benzene, n-butyl benzene, n-hexyl benzene, and n-octyl benzene. Errors were obtained from three replicate trials and too small to be observed.

Furthermore increased fluorous content for the analytes increases the retention on both hydrophobic and fluorous stationary phases. Interestingly, the plots of different stationary phase compositions with the N Series and P Series (Top and Middle, Figure 5.5) have intersection points while the plot of the phenyl alkanes do not. This is attributed to the relative strengths of the hydrophobic and fluorous interactions. When the stationary phase has high fluorous content (*e.g.* (4)FM+(0)M), and an analyte has relatively small number of

$-CF_2-$ units (*e.g.* 4 (N Series) and 6 (P Series)) the *ln*k observed is less than that for a (0)FM +(4)M column. Eventually the fluorous interaction is large enough that retention on a fluorous phase surpasses the retention of that analyte on a reversed-phase (0)FM +(4)M column. Conversely no intersection points are observed for the Phenyl Alkane Series and the *ln*k values all increase similarly with each of the column compositions. An additional $-CH_2-$ unit attached to the Phenyl Alkane Series enhances the interaction more significantly for a more hydrophobic stationary phase compared to a fluorous stationary phase. The relatively large hydrophobic interaction exceeds any interactions resulting from the increased fluorous content of the stationary phase which results in a decrease in methylene selectivity (Bottom, Figure 5.5). The retention time of each series in electrochromatograms (Figure 5.7) makes the comparison more obvious.
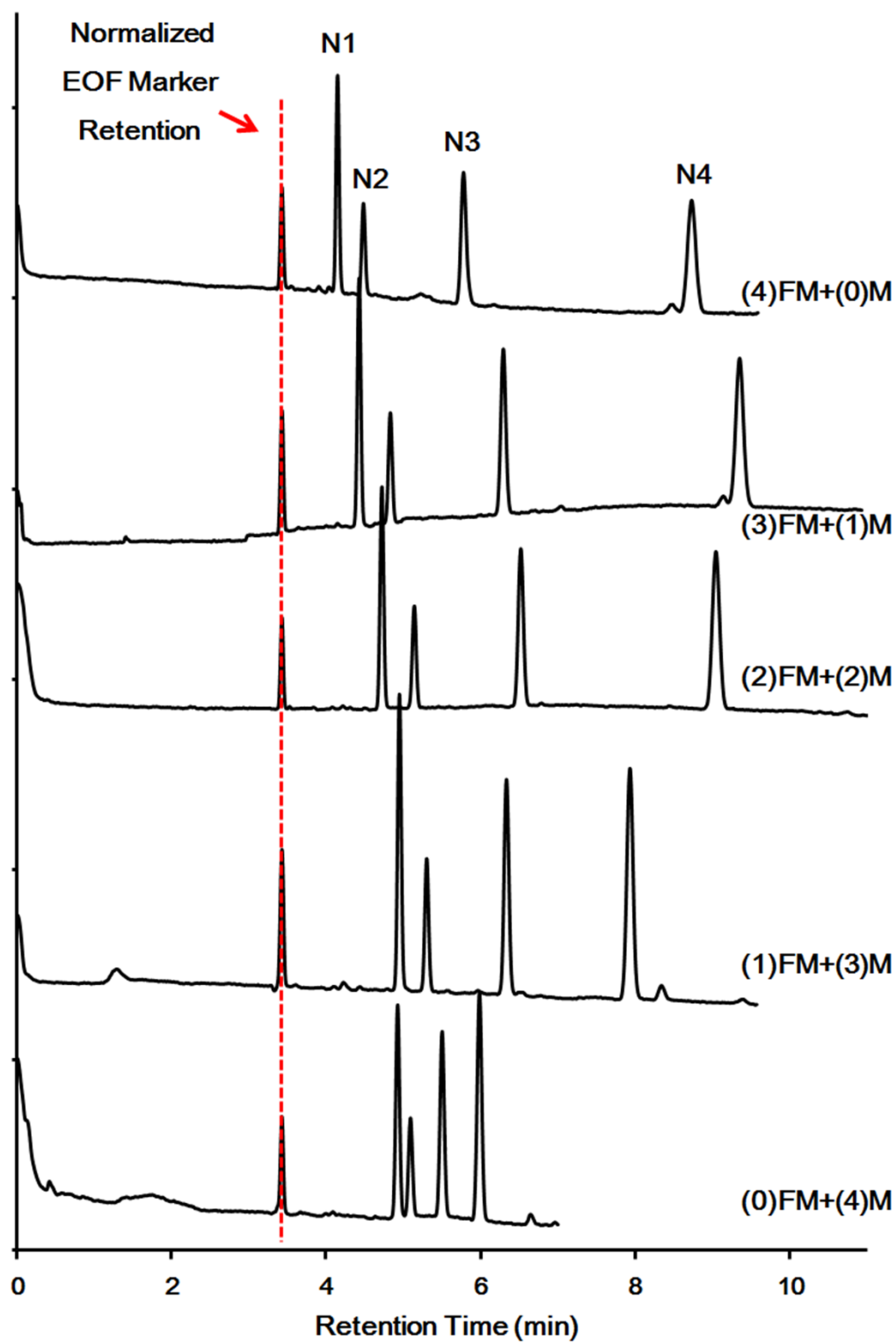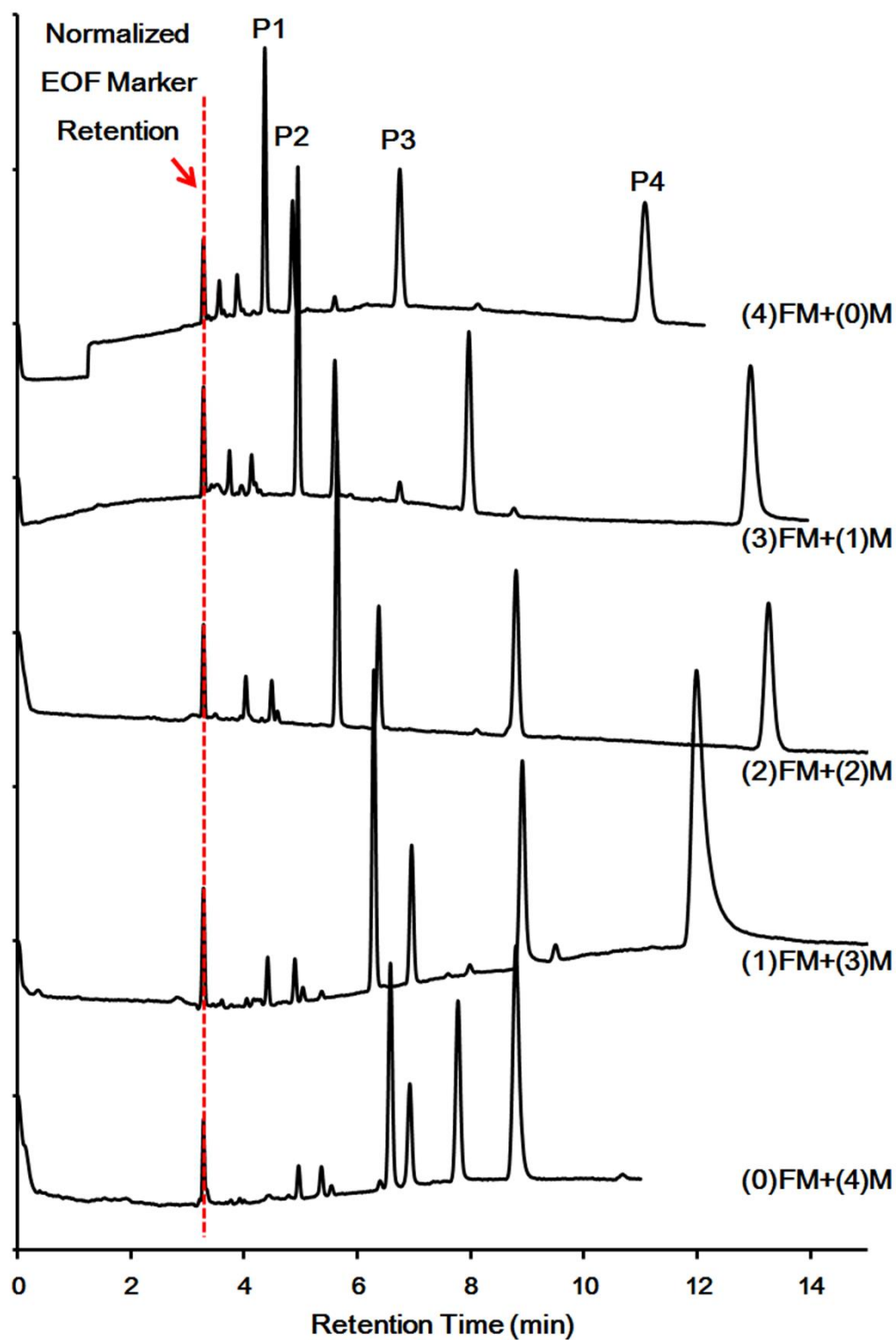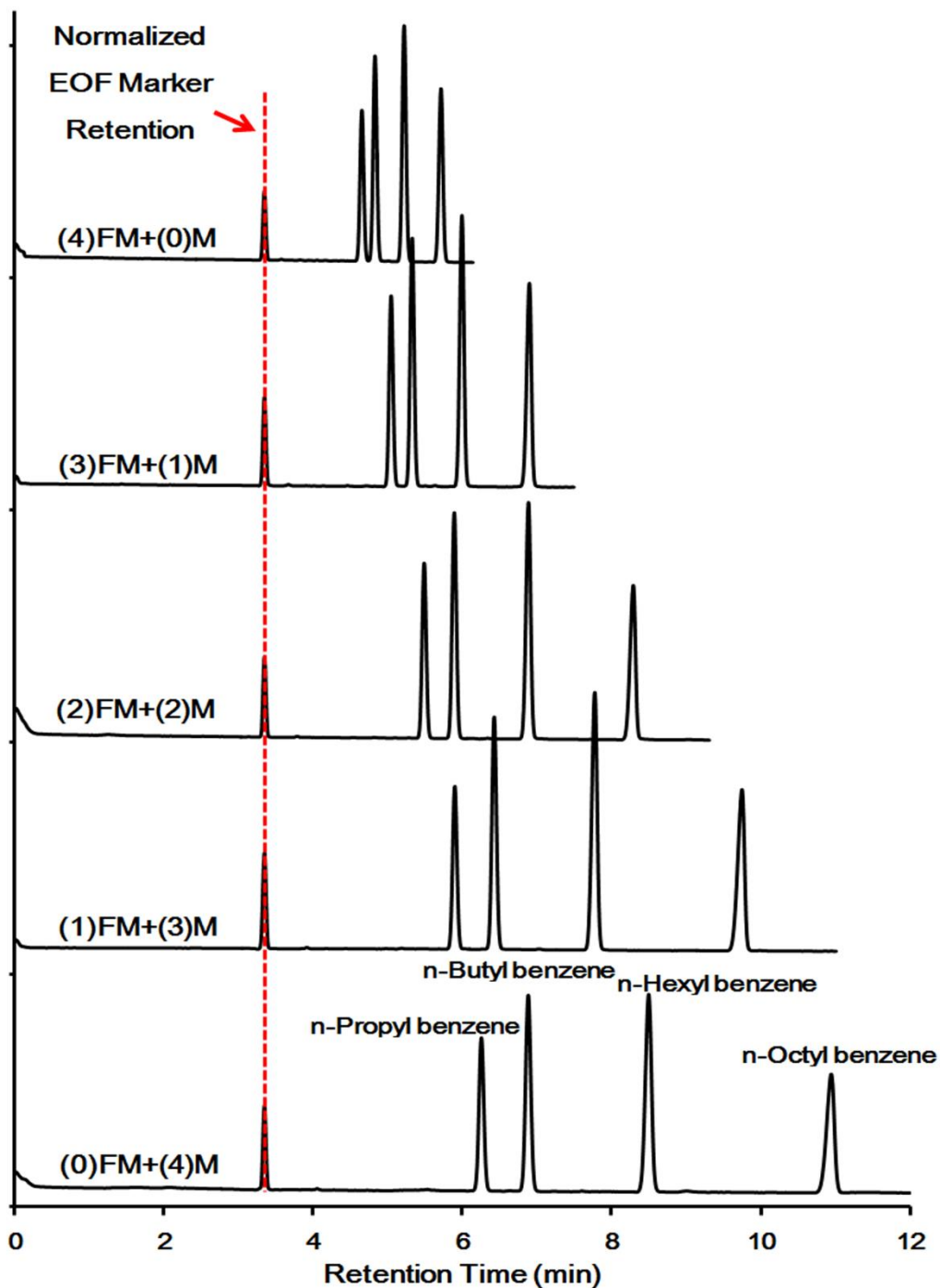
Figure 5.7: Unified electrochromatogram for N Series (top), P Series (middle), and Phenyl Alkane Series (bottom) separated on five columns with different –CF$_2$– fractions in stationary phase. FM+(4)M, (1)FM+(3)M, (2)FM+(2)M, (3)FM+(1)M are (4)FM+(0)M are the columns made of 0:4, 1:3, 2:2, 3:1, and 4:0 fluorous monomer : hydrophobic monomer (FBA : BA; volume ratio) respectively. Cross-linker is hydrophobic one (BDDA) for this group of stationary phase. Mobile phase was 80:20 (ACN : water).

5.2.2 – Thermodynamic Comparison between Fluorous Interaction and Hydrophobic Interaction

The Gibbs free energy change for transferring a –CH$_2$– unit from the mobile phase to the stationary phase ($\Delta G^{\circ}_{-CH_2-}$) can be calculated through Equation 4.3.[184,186]

A negative $\Delta G^{\circ}_{-CH_2-}$ value indicates that transferring a –CH$_2$– unit from the mobile phase to stationary phase is thermodynamically favorable (spontaneous). Similarly, the equation can be also applied to calculate $\Delta G^{\circ}_{-CF_2-}$. The $\Delta G^{\circ}_{-CH_2-}$ and $\Delta G^{\circ}_{-CF_2-}$ were calculated for five stationary phases with different fluorous fraction (–CF$_2$–fraction) and are shown in Table 5.1

With increasing –CF$_2$– fraction in the stationary phase, transferring one –CF$_2$– from the mobile phase to the stationary phase becomes thermodynamically more favorable. For example, the $\Delta G^{\circ}_{-CF_2-}$ for N Series is -267.7 J/mol on stationary phase (0)FM+(4)M which contains no –CF$_2$–. The $\Delta G^{\circ}_{-CF_2-}$ for N Series becomes -991.6 $\pm$ 0.5 J/mol for (4)FM+(0)M in which –CF$_2$– fraction is 0.33. The $\Delta G^{\circ}_{-CF_2-}$ calculated for the P Series and N Series are very similar for each stationary phase formulation tested, which can be attributed to the relatively small difference between the two different substituents (*i.e.* –NO$_2$ and phenyl) relative to the total size of the analytes in question.

Alternatively, comparing the $\Delta G^{\circ}_{-CF_2-}$, an opposite trend of $\Delta G^{\circ}_{-CH_2-}$ is observed. Increasing the –CF$_2$– fraction in the stationary phase makes transferring one –CH$_2$– from mobile phase to stationary phase become thermodynamically less favorable. When looking at the two

monomeric extremes (*i.e.* (0)FM+(4)M and (4)FM+(0)M), the $\Delta G^{\circ}_{-CH_2-}$ calculated from the

Phenyl Alkane Series changes from -475.9 J/mol in to -293.5 J/mol respectively.

Upon closer observation, transferring one $-CF_2-$ unit from the mobile phase to the stationary

phase becomes more favorable (more negative) with the increasing $-CF_2-$ fraction in the

stationary phase. However, the resulting trend is not a linear relationship (Figure 5.8). The

non-linear relationship (observed for $\Delta G^{\circ}_{-CH_2-}$ as well), which is expected to decrease with

increasing $-CF_2-$ fraction in stationary phase, can be attributed to a neighbor effect and

functional group accessibility.
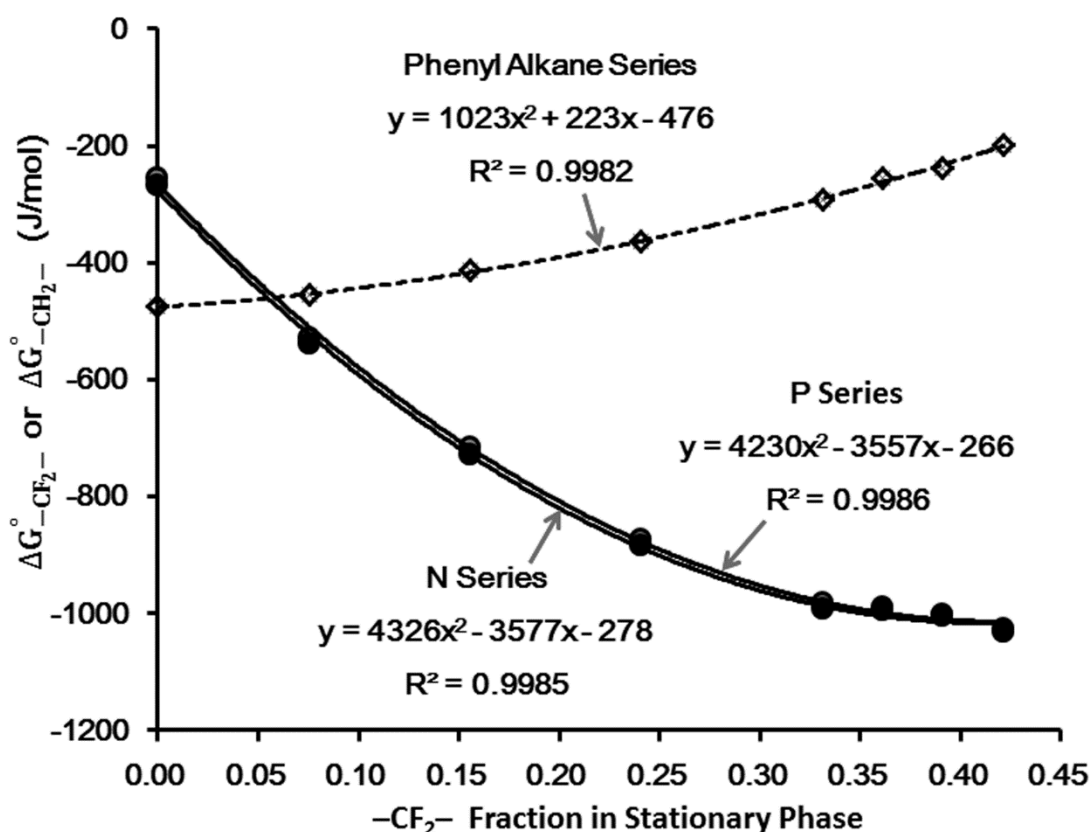
Figure 5.8: Gibbs free energy changes for transferring one $-CF_2-$ or $-CH_2-$ unit from the
mobile phase to stationary phases with different $-CF_2-$ fractions.

For a pure hydrophobic stationary phase containing only $-CH_2-$, a $-CF_2-$ will interact with a $-CH_2-$ unit through an instantaneous dipole – instantaneous dipole interaction. However, when $-CF_2-$ units are introduced, the $-CF_2-$ moieties in the analyte can preferentially form reduced instantaneous dipole – instantaneous dipole interactions between $-CF_2-$ (analyte) and a $-CF_2-$ (stationary phase).

There will be a series of weak interactions forming with neighboring $-CH_2-$ moieties. However, those weak interactions can be ignored. Because the neighbor $-CH_2-$s are shielded by the attached solvent, which form stronger interactions with $-CH_2-$ and the solvent is reluctant to displacement by $-CF_2-$ binding. At the same time, the instantaneous dipole – instantaneous dipole interaction is inversely proportional to sixth power of two instantaneous dipoles distance.[28] The longer distance between neighboring $-CH_2-$ and incoming $-CF_2-$ will further make the interaction with neighboring $-CH_2-$ groups negligible (*i.e.* weak neighbor effect, Panel A, Figure 5.9).

As the $-CF_2-$ fraction in the stationary phase is increased, the fluorous character of the phase is also increased. Simultaneously, there is a greater probability that adjacent $-CF_2-$ moieties can interact with the incoming $-CF_2-$ (strong neighbor effect, Panel A, Figure 5.9). It is possible that the extra neighbor $-CF_2-$ could cause a re-orientation of all three $-CF_2-$s (including itself) to make these a pair of reduced instantaneous dipole – instantaneous dipole interactions (strong neighbor effect, Panel A, Figure 5.9).
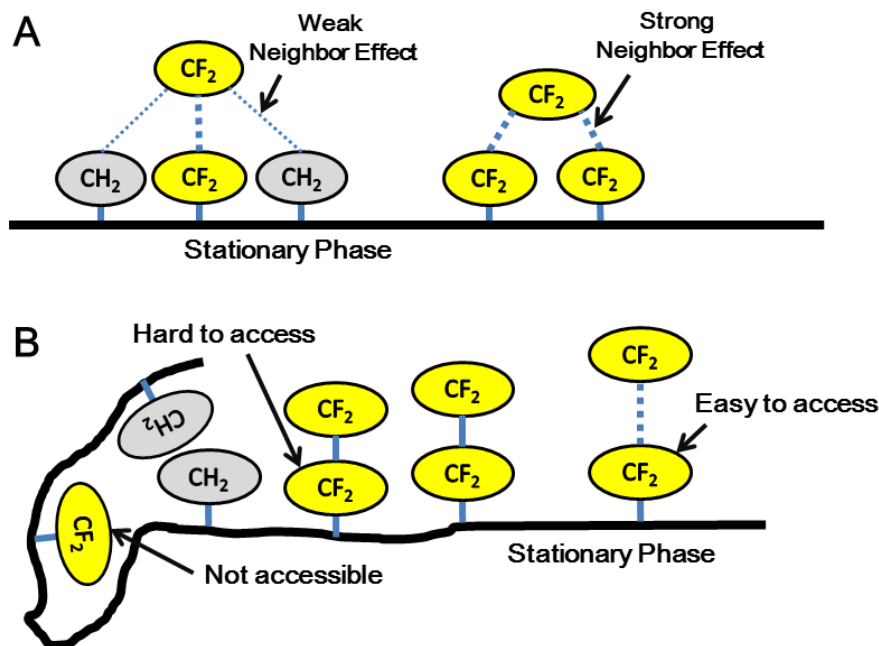
Figure 5.9: Illustration of neighbor effect (A) and spatial accessibility (B)

Due to the limitation of available materials, there is no way to synthesize a pure fluorous stationary phase. The value for $\Delta G^{\circ}_{-CF_2- \to -CF_2-}$ can only be obtained using extrapolated trend lines. An additional consideration of the non-linear relationship involving $\Delta G^{\circ}_{-CF_2-}$ and the $-CF_2-$ fraction in stationary phase is the accessibility of the $-CF_2-$ to interaction with the incoming analyte. As shown in Panel B, Figure 5.9, the location of the $-CF_2-$ group may be available for binding (*i.e.* at the surface) or buried within the monolith and not accessible. The three higher $-CF_2-$ fraction data points (0.36, 0.39, and 0.42) in Figure 5.8 were obtained by replacing the hydrophobic cross-linker (BDDA) with fluorous cross-linker (TFBDA). Shallower negatively sloped tangent lines were obtained for these three points compared to the five lower $-CF_2-$ fraction data points (0, 0.08, 0.16, 0.24, and 0.33) where only the fluorous monomer was utilized to increase the fluorous content. This may provide evidence that fluorous groups that are accessible have a greater influence on the fluorous character of

the monolith. The –CF$_2$– moieties in the cross-linker should be less accessible since it is likely that those –CF$_2$– moieties are sterically hindered. These two reasons, neighbor effect and accessibility, can be used to explain the non-linear relationship of $\Delta G^{\circ}_{-CH_2-}$ with –CF$_2$– fraction (–CH$_2$– fraction) as well.

In the above explanation, the composition of the mobile phase was not considered. However, the mobile phase plays an important differentiating role for the hydrophobic interaction and fluorous interaction, regardless of the retention mechanism employed (solvophobic and lattice).

Herein, we propose a simplified retention model to address the change in selectivity between a methylene unit (hydrophobic character) and a perfluoromethylene unit (fluorous character) on stationary phases with different fluorous content.

The interactions involving the mobile phase - analyte, mobile phase - stationary phase and mobile phase - mobile phase will be added to the following discussion for a more complete picture of the phase transfer process. In our simplified retention model, the process is disassembled into four individual steps (in terms of the Gibbs free energy changes) that take into account both the enthalpy and entropy involved in transferring a methylene or perfluoromethylene unit from the mobile phase to stationary phase. These include: isolation of the analyte from surrounding mobile phase (desolvation, $\Delta G^{\circ}_{desolvation(-CH_2- \text{ or } -CF_2-)- solvent}$ for –CH$_2$– or a –CF$_2$– respectively); isolation of the interaction site on the stationary phase from surrounding mobile phase

($\Delta G^{\circ}_{desolvation(-CH_2- \text{ or } -CF_2-)-solvent}$); combination of mobile phase

($\Delta G^{\circ}_{Combination \text{ solvent} - solvent}$); and combination of analyte and interaction site

($\Delta G^{\circ}_{Combination(-CH_2- \text{ or } -CF_2- \text{ in analyte}) -(-CH_2- \text{ or } -CF_2- \text{ in stationary phase})}$).

Processes indicated by panels A and B in Figure 5.10 have been determined experimentally.

ΔG° values associated with Panels C and D are not experimentally determinable. However the

ΔG° value in C can be predicted by extending the tangent line (x=0 to x=1, *i.e.* fraction of –

CF$_2$–) in Figure 5.8. The ΔG° value calculated for C can be validated by the experimental

value determined for B since they should be identical given the functional groups on the analyte

and stationary phase are simply reversed. Furthermore the validating of the extrapolation for C

allows us to predict the ΔG° value in the panel D process.

Four processes (shown in Figure 5.10,) are involved when transferring a –CH$_2$– or a –CF$_2$–

from the mobile phase to the stationary phase. In the four equations below, the unit prior to

the arrow sign represents the species in the mobile phase and the unit after the arrow sign is

the species within the stationary phase. For example, $\Delta G^{\circ}_{-CH_2- \rightarrow -CH_2-}$ is the Gibbs free

energy change associated with transferring a –CH$_2$– from the mobile phase to a –CH$_2$– in the

stationary phase.
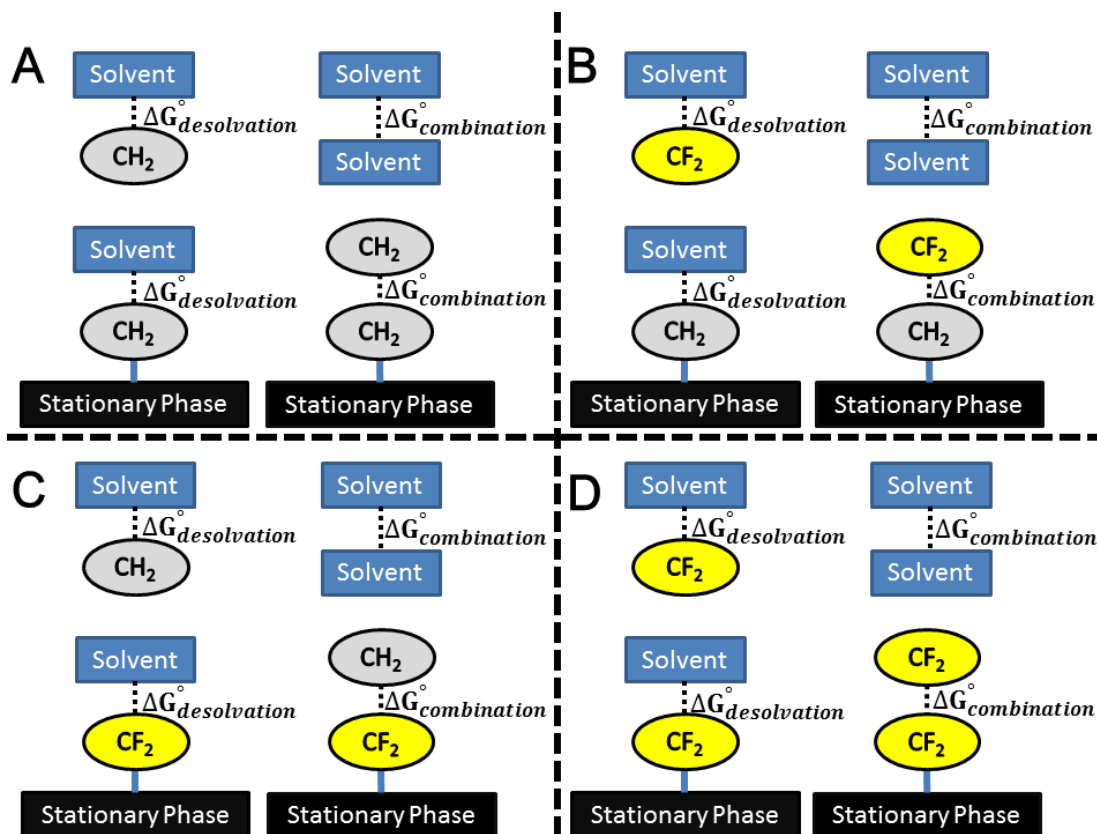
Figure 5.10: Four typical transfers. A: transferring a $-CH_2-$ from mobile phase to get close to a $-CH_2-$ in stationary to form an interaction between $-CH_2-$s. B: transferring a $-CF_2-$ from mobile phase to get close to a $-CH_2-$ in stationary to form an interaction between $-CF_2-$ and $-CH_2-$. C: transferring a $-CH_2-$ from mobile phase to get close to a $-CF_2-$ in stationary to form an interaction between $-CH_2-$ and $-CF_2-$. D: transferring a $-CF_2-$ from mobile phase to get close to a $-CF_2-$ in stationary to form an interaction between $-CF_2-$s.

For process A, Figure 5.10

$$\Delta G^{\circ}_{-CH_2- \rightarrow -CH_2-}$$

$$= 2\Delta G^{\circ}_{desolvation-CH_2--\,solvent} + \Delta G^{\circ}_{Combination\,solvent\,-\,solvent}$$

$$+ \Delta G^{\circ}_{Combination-CH_2---CH_2-}$$

Equation 5.3

For process B, Figure 5.10

$$\Delta G^{\circ}_{-CF_2- \rightarrow -CH_2-}$$

$$= \Delta G^{\circ}_{desolvation-CF_2- - \, solvent} + \Delta G^{\circ}_{desolvation-CH_2- - \, solvent}$$

$$+ \Delta G^{\circ}_{Combination \, solvent - solvent} + \Delta G^{\circ}_{Combination-CF_2- - -CH_2-}$$

Equation 5.4

For process C, Figure 5.10

$$\Delta G^{\circ}_{-CH_2- \rightarrow -CF_2-}$$

$$= \Delta G^{\circ}_{desolvation-CH_2- - \, solvent} + \Delta G^{\circ}_{desolvation-CF_2- - \, solvent}$$

$$+ \Delta G^{\circ}_{Combination \, solvent - solvent} + \Delta G^{\circ}_{Combination-CH_2- - -CF_2-}$$

Equation 5.5

For process D, Figure 5.10

$$\Delta G^{\circ}_{-CH_2- \rightarrow -CF_2-}$$

$$= 2\Delta G^{\circ}_{desolvation-CF_2- - \, solvent} + \Delta G^{\circ}_{Combination \, solvent - solvent}$$

$$+ \Delta G^{\circ}_{Combination-CF_2- - -CF_2-}$$

Equation 5.6

According to the discussion on the non-linear trend line for $\Delta G^{\circ}_{-CH_2-}$ and $\Delta G^{\circ}_{-CF_2-}$, the slope

of tangent line at the x=0 (fraction of $-CF_2-$ is 0) for each trend line can be used to evaluate

the $\Delta G^\circ_{-CF_2-}$ and $\Delta G^\circ_{-CH_2-}$. Differentiation of quadratic functions and the point-slope method were used to determine tangent lines for the N Series, P Series, and Phenyl Alkane Series (at x=0) as y = -3577 x - 278, y = -3557 x - 266, and y = 223 x - 476 respectively.

$\Delta G^\circ_{-CH_2- \rightarrow -CH_2-}$ is equal to -476 J/mol determined by the $\Delta G^\circ_{-CH_2-}$ of Phenyl Alkane Series in column (0)FM+(4)M. (no –CF$_2$–,Table 5.1) (Process A)

$\Delta G^\circ_{-CF_2- \rightarrow -CH_2-}$ is equal to -268 J/mol determined by the $\Delta G^\circ_{-CF_2-}$ of N Series in stationary phase (0)FM+(4)M, or equal to -255 J/mol determined by the $\Delta G^\circ_{-CF_2-}$ of P Series in stationary phase (0)FM+(4)M (Table 5.1). (Process B)

$\Delta G^\circ_{-CH_2- \rightarrow -CF_2-}$ = -253 J/mol calculated from the tangent line of the curve trend line of a Phenyl Alkane Series at point x = 0. This virtually identical to that of $\Delta G^\circ_{-CF_2- \rightarrow -CH_2-}$ determined experimentally for Process B which validates our extrapolation method. (Process C, calculated using P series)

$\Delta G^\circ_{-CF_2- \rightarrow -CF_2-}$ = to -3855 J/mol calculated from tangent line of curve trend line for the N Series at point x=1(–CF$_2$– fraction is 1). Whereas the value calculated for the P Series is similarly -3823 J/mol. (Process D, calculated using P series)

It was found that for both –CH$_2$– and –CF$_2$–, $\Delta G^\circ_{-CF_2- \rightarrow -CF_2-}$ (-3855 J/mol) and $\Delta G^\circ_{-CH_2- \rightarrow -CH_2-}$(-476 J/mol) are more negative than $\Delta G^\circ_{-CF_2- \rightarrow -CH_2-}$(-255 J/mol) and $\Delta G^\circ_{-CH_2- \rightarrow -CF_2-}$ (-253 J/mol), which means that, transferring –CH$_2$– and –CF$_2$– from mobile phase to the same corresponding stationary phase is thermodynamically favorable (*i.e.*

like dissolves like). The tremendous difference between $\Delta G^{\circ}_{-CF_2- \rightarrow -CF_2-}$ and

$\Delta G^{\circ}_{-CH_2- \rightarrow -CH_2-}(\Delta G^{\circ}_{-CF_2- \rightarrow -CF_2-} : \Delta G^{\circ}_{-CH_2- \rightarrow -CH_2-} \approx 8:1)$ can be used as solid evidence

to prove that the "hardness" or small polarizability of fluorous moieties. The interactions

involving the fluorous moiety (–CF$_2$–) are smaller than its hydrocarbon counterpart (–CH$_2$–).

The energy required for –CF$_2$– desolvation is less than that for –CH$_2$–. Therefore, less energy

of $\Delta G^{\circ}_{Combination\,solvent-solvent}$ is consumed, and a more negative $\Delta G^{\circ}_{-CF_2- \rightarrow -CF_2-}$ is

obtained.

5.2.3 – Mobile Phase Impact and Boundary between Hydrophobic Stationary Phase and Fluorous Stationary Phase

Previously the mobile phase used in all CEC trials was maintained at a constant composition.

In this section the mobile phase composition is varied to examine its impact on $\Delta G^{\circ}_{-CF_2-}$

and $\Delta G^{\circ}_{-CH_2-}$. The mobile phase composed of ACN and water is treated as a strong

permanent dipole to simplify the mobile phase impact discussion. The $\Delta G^{\circ}_{-CF_2-}$ and

$\Delta G^{\circ}_{-CH_2-}$ calculated for the N Series, P Series and Phenyl Alkane Series with four different

mobile phase compositions on three different stationary phases are shown in Table 5.2. For

each of the three stationary phases tested, both $\Delta G^{\circ}_{-CF_2-}$ and $\Delta G^{\circ}_{-CH_2-}$ become more

negative when the polar component (water) in the mobile phase is increased. For example,

$\Delta G^{\circ}_{-CF_2-}$ calculated with the N Series changes from -264 J/mol with 80:20 (ACN : water) to

-463 J/mol with 65:35 (ACN : water). Furthermore the $\Delta G^{\circ}_{-CH_2-}$ calculated for the Phenyl

Alkane Series changes from -472 J/mol with 80:20 (ACN : water) to -655 J/mol using 65:35

(ACN : water). The more negative $\Delta G^{\circ}_{-CF_2-}$ and $\Delta G^{\circ}_{-CH_2-}$ means a more

thermodynamically favorable transfer of both $-CF_2-$ unit and $-CH_2-$ unit to the stationary phase. Increasing the polar component in the mobile phase composition results in steeper trend lines in the plot of lnk *versus* number of $-CF_2-$ units in the fluorous moiety (Figure 5.8) for the N Series (top), P Series (middle) and lnk *versus* number of $-CH_2-$ units in the alkane moiety for the Phenyl Alkane Series (bottom).

Table 5.2: $\Delta \overset{\circ}{G}_{-CF_2-}$ calculated from N Series and P Series and $\Delta \overset{\circ}{G}_{-CH_2-}$ calculated from N Series and Phenyl Alkane Series in four different mobile phase components on three stationary phases. Errors are calculated from three replicate trials.

Stationary Phase	Mobile Phase Component (ACN : water)	$\Delta G^{\circ}_{-CF_2-}$ (J/mol)		$\Delta G^{\circ}_{-CH_2-}$ (J/mol)
		N Series	P Series	Benzene Alkane Series
M+C	80 : 20	-264.1 $\pm$ 0.1	-248.2 $\pm$ 0.6	-472.2 $\pm$ 0.2
	75 : 25	-332.1 $\pm$ 0.4	-317.3 $\pm$ 0.7	-534.4 $\pm$ 0.4
	70 : 30	-394.2 $\pm$ 1.2	-382.4 $\pm$ 0.6	-589.6 $\pm$ 1.5
	65 : 35	-462.7 $\pm$ 1.6	-448.6 $\pm$ 5.8	-655.3 $\pm$ 2.6
FM+C	80 : 20	-963.6 $\pm$ 1.1	-952.0 $\pm$ 4.6	-286.2 $\pm$ 0.7
	75 : 25	-1033.1 $\pm$ 3.9	-1027.0 $\pm$ 1.5	-349.9 $\pm$ 0.3
	70 : 30	-1102.4 $\pm$ 0.4	-1092.6 $\pm$ 3.0	-411.8 $\pm$ 6.4
	65 : 35	-1167.7 $\pm$ 2.6	-1153.6 $\pm$ 6.8	-468.6 $\pm$ 10.4
FM+FC	80 : 20	-1002.7 $\pm$ 0.9	-997.0 $\pm$ 2.7	-195.5 $\pm$ 0.7
	75 : 25	-1088.4 $\pm$ 1.8	-1082.9 $\pm$ 2.2	-257.8 $\pm$ 2.1
	70 : 30	-1148.6 $\pm$ 0.9	-1142.7 $\pm$ 5.6	-322.0 $\pm$ 0.2
	65 : 35	-1207.3 $\pm$ 1.1	-1203.5 $\pm$ 0.8	-383.7 $\pm$ 0.2

Linear ($R^2 > 0.99$) trend lines are obtained when plotting $\Delta G^{\circ}_{-CH_2-}$ and $\Delta G^{\circ}_{-CF_2-}$ against the polar component (water) concentration in the mobile phase, as shown in the insets in Figure 5.11 A, B and C. Considering that the $\Delta G^{\circ}_{-CF_2-}$ calculated from N Series and P Series have similar values and trends, only $\Delta G^{\circ}_{-CF_2-}$ calculated from P Series was used.

The mobile phase has a significant contribution to the transfer of $-CF_2-$ and $-CH_2-$ to the different stationary phases. Since the Gibbs free energy changes related to the combination of solvent and solvent are significantly negative, the overall sorption process is spontaneous. Breaking the dipole-dipole interaction between incoming $-CF_2-$ or $-CH_2-$ moiety and the stationary phase will consume part of the energy released by combination of solvent and solvent. As a result, the impact of the mobile phase composition can be used to classify the hydrophobic and fluorous stationary phases. A hydrophobic stationary phase is the stationary phase in which the $\Delta G^{\circ}_{-CH_2-}$ is higher than $\Delta G^{\circ}_{-CF_2-}$; while a fluorous stationary phase has a $\Delta G^{\circ}_{-CF_2-}$ higher than $\Delta G^{\circ}_{-CH_2-}$.

An interesting phenomenon was also observed for $\Delta G^{\circ}_{-CF_2-}$ and $\Delta G^{\circ}_{-CH_2-}$ with the different stationary phases. Each plot shows the same trend where increasing the polar component (*i.e.* H_2O) results in a more negative $\Delta G^{\circ}_{-CF_2-}$ and $\Delta G^{\circ}_{-CH_2-}$. However the rate at which $\Delta G^{\circ}_{-CF_2-}$ and $\Delta G^{\circ}_{-CH_2-}$ change is shown to be different. Regardless of the stationary phase composition, the slope of the trend line for $\Delta G^{\circ}_{-CF_2-}$ is always greater than the trend line for $\Delta G^{\circ}_{-CH_2-}$. The *ln*k for $-CF_2-$ is not as sensitive to the change of the permanent dipole (*i.e.* mobile phase polarity) moment as the $-CH_2-$. In other words, when increasing the mobile phase dipole moment (*i.e.* increased water content in mobile phase), the energy needed to

desolvate $-CF_2-$ ($\Delta G^{\circ}_{desolvation-CF_2--solvent}$) is increased. However, this is less than the energy needed to desolvate $-CH_2-$ ($\Delta G^{\circ}_{desolvation-CH_2--solvent}$). Overall, $\Delta G^{\circ}_{desolvation-CF_2--solvent}$ consumes less the energy that is released through the solvent-solvent interaction ($\Delta G^{\circ}_{combination\ solvent-solvent}$). Therefore, $\Delta G^{\circ}_{-CF_2-}$ changing rate is higher than $\Delta G^{\circ}_{-CH_2-}$ changing rate. One of the difficulties of mixed stationary phases is characterizing their hydrophobicity and fluorophilicity. We herein propose a new concept, hypothetical water percentage (HWP) to address this challenge.
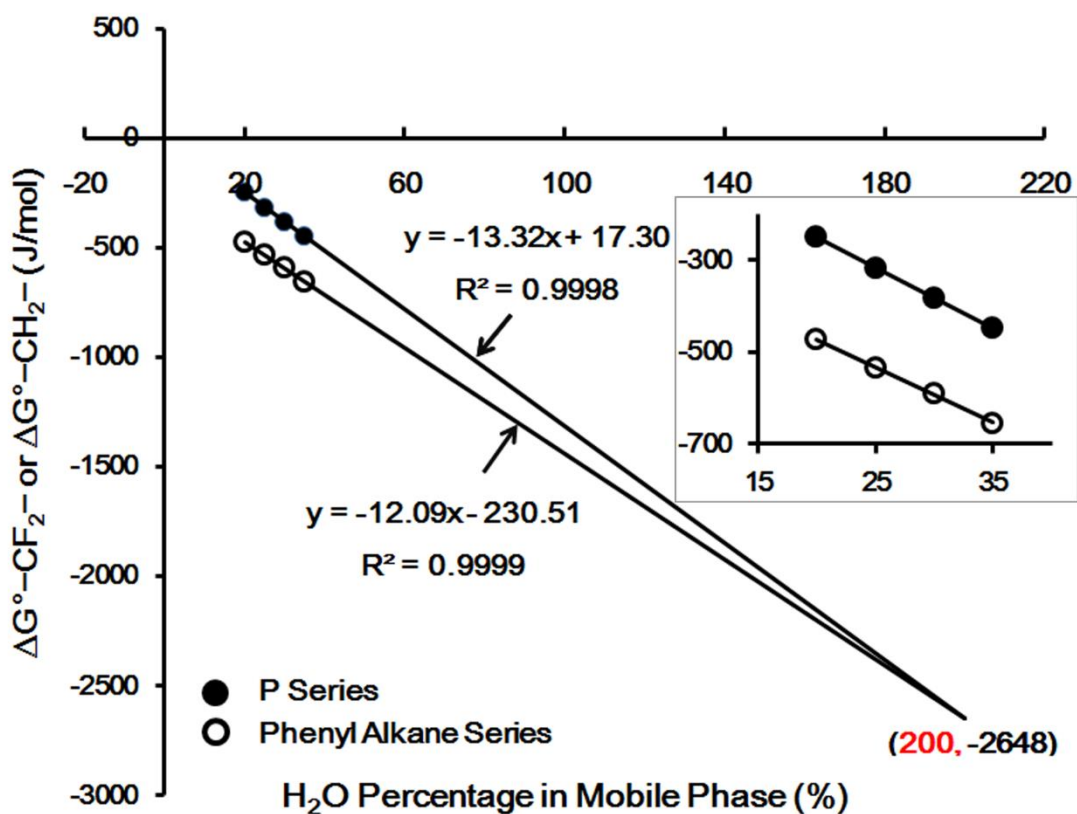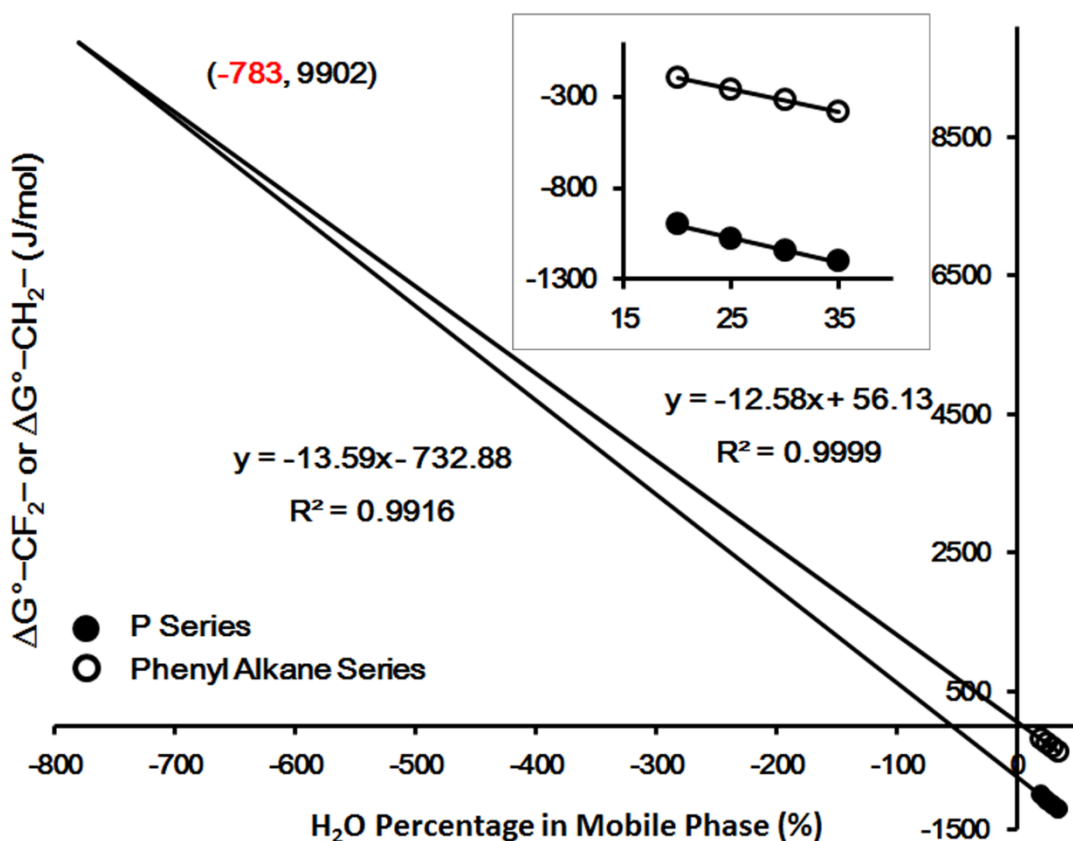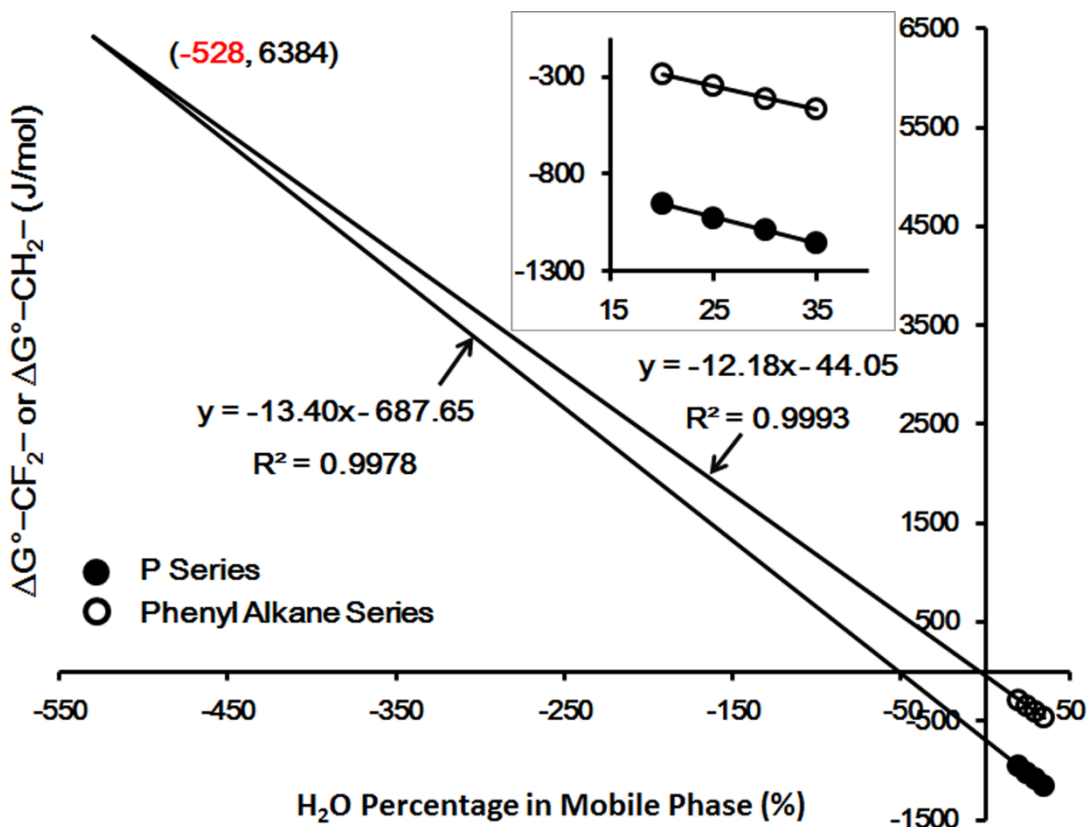
Figure 5.11: $\Delta \overset{\circ}{G}_{-CH_2-}$ and $\Delta \overset{\circ}{G}_{-CF_2-}$ *versus* H_2O percentage in mobile phase on stationary phase M+C (top), FM+C (middle), and FM+FC (bottom). M+C, FM+C, and FM+FC represent the stationary phase made of hydrophobic monomer (BA) + hydrophobic cross-linker (BDDA), stationary phase made of fluorous monomer (FBA) + hydrophobic cross-linker (BDDA), and stationary phase made of fluorous monomer (FBA) + fluorous cross-linker (TFBDA) respectively. Errors are calculated from three replicate trials.

Plotting the $\Delta G^{\circ}_{-CH_2-}$ and $\Delta G^{\circ}_{-CF_2-}$ and constructing trend lines in Figure 5.11 (top, middle, and bottom) results in two antiparallel lines. The coordinates of the intersections were determined by trend line equations as (200, -2648), (-528, 6384), and (-783, 9902) for stationary phase compositions M+C, FM+C, and FM+FC respectively. The x coordinates are water percentage in mobile phase, in which $\Delta G^{\circ}_{-CF_2-}$ and $\Delta G^{\circ}_{-CH_2-}$ will have the same value, *i.e.* transferring a –CF_2– unit or transferring a –CH_2– unit from mobile phase to stationary phase are thermodynamically the same. Although the values of 0-100 have a real physical meaning we may further extend this range of hypothetical water percentage (HWP) to classify fluorous stationary phase from hydrophobic stationary phase and to evaluate how "fluorous" or how "super hydrophobic" a fluorous stationary phase is. In detail, when HWP is higher than 100, this stationary phase is a hydrophobic stationary phase (*e.g.* M+C is hydrophobic stationary phase with a HWP 200). On the other hand, when HWP is less than 0, this stationary phase is deemed to be a fluorous stationary phase (e.g FM+C and FM+FC are fluorous stationary phase with HWPs of -528 and -783 respectively). In general, the more left the HWP is located in the coordinate system (more negative), the more fluorous the stationary phase is while the more right the HWP locates (more positive), the more hydrophobic the

147

stationary phase is. For the stationary phases with HWP from 0 to 100, which means the $\Delta G^{\circ}_{-CH_2-}$ and $\Delta G^{\circ}_{-CF_2-}$ on these stationary phases are close, can be treated as either hydrophobic or fluorous stationary phases. Adjusting the mobile phase component, *e.g.* adjusting water percentage from 0 to 100, $\Delta G^{\circ}_{-CH_2-}$ and $\Delta G^{\circ}_{-CF_2-}$ values could be made similar.

The HWP for a hydrophobic stationary phase is 200. Although a HWP mobile phase composition of either >100% or <0% is not a realistic value, the number nonetheless allows one to compare/characterize the stationary phase. It can be explained as increasing polar component in mobile phase (ACN and water system) to the scale equal to the permanent dipole moment that 200% water can provide. The permanent dipole moment has to be strong enough to make the following equation.

$$\left|\ \Delta G^{\circ}_{combination-CH_2---CH_2-}\ \right|\ -\ \left|\ \Delta G^{\circ}_{combination-CF_2---CH_2-}\ \right|\ =$$

$$\left|\Delta G^{\circ}_{desolvation-CH_2--solvent}\right| - \left|\Delta G^{\circ}_{desolvation-CF_2--solvent}\right|$$

Equation 5.7

The left side of the equation is the energy difference between $\Delta G^{\circ}_{combination-CH_2---CH_2-}$ (A, Figure 5.10, independent of solvent composition) and $\Delta G^{\circ}_{combination-CF_2---CH_2-}$(B, Figure 5.10, independent of solvent composition). Both $\Delta G^{\circ}_{combination-CH_2---CH_2-}$ and $\Delta G^{\circ}_{combination-CF_2---CH_2-}$ are negative (*i.e.* spontaneous), $|\Delta G^{\circ}_{combination-CH_2---CH_2-}| >$ $|\ \Delta G^{\circ}_{combination-CF_2---CH_2-}|$, since the $-CH_2---CH_2-$ has a more favourable dipole interaction .

The right side of equation is the energy difference between $\Delta G^{\circ}_{\text{desolvation}-CH_2-\ -\ \text{solvent}}$ (A, Figure 5.10, increases with increased solvent polarity) and $\Delta G^{\circ}_{\text{desolvation}-CF_2-\ -\ \text{solvent}}$ (B, Figure 5.10, increases with increased solvent polarity). However the rate of increase is lower than the rate of $\Delta G^{\circ}_{\text{desolvation}-CH_2-\ -\ \text{solvent}}$). In this case both $\Delta G^{\circ}_{\text{desolvation}-CH_2-\ -\ \text{solvent}}$ and $\Delta G^{\circ}_{\text{desolvation}-CF_2-\ -\ \text{solvent}}$ are positive, and $\mid \Delta G^{\circ}_{\text{desolvation}-CH_2-\ -\ \text{solvent}} \mid \ >$ $|\Delta G^{\circ}_{\text{desolvation}-CF_2-\ -\ \text{solvent}}|$, since more energy is required to break dipole-dipole interaction formed between stronger dipole moments, or instantaneous dipoles with higher polarizability.

Alternatively, HWP for a fluorous stationary phase is negative (HWFs for FM+C and FM+FC are -528 and -783 respectively), which means that increasing the polar component in the mobile phase is not making an equation like Equation 5.7. Because the difference between $|\Delta G^{\circ}_{\text{desolvation}-CH_2-\ -\ \text{solvent}}|$ (C, Figure 5.10) and $|\Delta G^{\circ}_{\text{desolvation}-CF_2-\ -\ \text{solvent}}|$ (D, Figure 5.10) increases with solvent dipole moment increasing, $\Delta G^{\circ}_{\text{desolvation}-CH_2-\ -\ \text{solvent}}$ (C, Figure 5.10) will consume more energy than that released by $\Delta G^{\circ}_{\text{combination solvent}\ -\ \text{solvent}}$. The total $\Delta G^{\circ}_{-CH_2-\ \rightarrow\ -CF_2-}$ can never reach the $\Delta G^{\circ}_{-CF_2-\ \rightarrow\ -CF_2-}$ with both less negative value and slower decreasing rate.

If reducing polar component in mobile phase (ACN and water system) to the scale equal to the dipole moment that -528% water for FM+C can provide (-783% water for FM+FC). Under these conditions where the dipole moment of the solvent is extremely low, the stationary phase (–CF$_2$– and –CH$_2$–) becomes relatively strong in comparison and will the energetics of which will dominate the –CF$_2$– and –CH$_2$– transfer process. Furthermore, under these conditions, transferring a –CF$_2$– unit or a –CH$_2$– unit from mobile phase to stationary

phase is no longer favourable. Instead, the opposite process becomes spontaneous as evidenced by a large positive value of $\Delta G^{\circ}_{-CH_2-}$ (6384 J/mol for FM+C, 9902 J/mol for FM+C, $\Delta G^{\circ}_{-CF_2-}$ equal to $\Delta G^{\circ}_{-CH_2-}$ at intersection) in fluorous stationary phase where the two trend lines meet. Such a boundary between the hydrophobic stationary phase and the fluorous stationary phase, therefore, can be set by their –CF$_2$– and –CH$_2$– selectivity which is dependent on the ACN/water mobile phase system. When the HWP is less than 0, the stationary phases can be placed in the fluorous domain. Alternatively, if the HWP is more than 100, the stationary phase belongs to the hydrophobic domain. Stationary phases with a HWP of 0 to 100 can be used to separate both hydrophobic analytes and fluorous analytes as their perfluoromethylene selectivity and methylene selectivity are very close (Figure 5.11).

5.3 – Conclusion

The origin of the fluorous interaction was examined in this chapter. It was found that the fluorous interaction is a kind of reduced (weaker) instantaneous or induced dipole interactions compared to hydrophobic interaction,

Quantitatively, it was found that hydrophobic stationary phases have better α_{-CH_2-}, while fluorous stationary phases have better α_{-CF_2-}. On PPM columns with 0 –CF$_2$– fraction, α_{-CH_2-} and α_{-CF_2-} are 1.21 and 1.11 respectively; on PPM column with 0.33 –CF$_2$– fraction, α_{-CH_2-} and α_{-CF_2-} are 1.13 and 1.49 respectively. This complies with the traditional expression "like dissolves like".

Thermodynamically, with the presence of mobile phase 80:20 (ACN : water), $\Delta G^{\circ}_{-CH_2- \rightarrow -CH_2-}$ (Gibbs free energy change of transferring a –CH$_2$– unit from mobile phase to pure hydrophobic stationary phase to form a methylene dipole – methylene dipole interaction) is -476 J/mol; similarly, $\Delta G^{\circ}_{-CF_2- \rightarrow -CF_2-}$ is -3855 J/mol; $\Delta G^{\circ}_{-CF_2- \rightarrow -CH_2-}$ and $\Delta G^{\circ}_{-CH_2- \rightarrow -CF_2-}$ have almost the same values (-255 J/mol, -253 J/mol respectively).

The large difference between $\Delta G^{\circ}_{-CF_2- \rightarrow -CF_2-}$ and $\Delta G^{\circ}_{-CH_2- \rightarrow -CH_2-}$ ($\approx$ 8:1) can be explained by the hardness of the fluorous moieties. The interactions involving fluorous moieties (–CF$_2$–) are smaller than their hydrocarbon counterpart (–CH$_2$–). The energy required for –CF$_2$– desolvation is less than that for –CH$_2$–. Therefore, less energy of $\Delta G^{\circ}_{Combination\,solvent - solvent}$ is consumed, *i.e.* more negative $\Delta G^{\circ}_{-CF_2- \rightarrow -CF_2-}$ is obtained.

A new concept, hypothetical water percentage (HWP) was proposed for the first time to quantitatively evaluate the hydrophobicity/fluorophilicity of a stationary phase. In detail, when HWP is higher than 100, this stationary phase is hydrophobic stationary phase. On the other hand, when HWP is lower than 0, this stationary phase is fluorous stationary phase. Stationary phases with HWP in the range from 0 to 100, can hardly be classified either way.

Chapter 6 – FPPM Column Liquid Chromatography – Mass Spectrometry

6.1 – Introduction

Due to the challenges discussed in section 1.7 – Overview of Proteomics, HPLC in tandem with MS is widely employed for qualitative and quantitative proteomics.

FPPM chromatography has demonstrated superior selectivity for analytes with perfluoroalkyl substituents (Chapter 3 - 5). In this chapter, fluorous PPM's are utilized as an alternative to hydrophobic interaction stationary phases to accomplish both chromatography and/or SPE. Fluorous chromatography coupled either directly with electrospray ionization (ESI) (on-line) or indirectly with matrix-assisted laser desorption/ionization (MALDI) (off-line) – mass spectrometry were used to separate and identify the fluorous tagged peptide/proteins from their non-tagged counterparts and matrix.

6.2 – Results and Discussion

6.2.1 – Fluorous LC – ESI – MS

As a step toward proving the utility of our FPPM in proteomic applications, we initially looked at a tagging experiment using a custom peptide (Custom Peptide I) to explore the efficacy of fluorous separations. Attaching a perfluoroalkyl chain to the custom peptide I by the reaction of N-[(3-perfluorohexyl)propyl] iodoacetamide ($C_{11}H_9F_{13}INO$) with the lone cysteine residue provides a handle for an affinity-based separation. In this way any tagged peptides can be

resolved from their non-fluorous counterparts. Unlike previous experiments where LC separation followed by UV detection could be used to determine resolution, the lack of a significant chromophore in the custom peptide meant that these tests required a change to an alternative detection method, mass spectrometry (LC-MS). Initial results showed (Figure 6.1) that there is indeed a significant separation between tagged and untagged peptides on the FPPM column. While the untagged peptide effectively elutes at the solvent front with little retention (immediately following the injection lag, at a solvent composition near 90% aqueous), the tagged analyte is more strongly retained and requires a significant change in organic modifier concentration to almost 90% ACN before it elutes from the FPPM stationary phase. This is the result that would be predicted by fluorous affinity interactions, lending further support to our assertion that fluorous monoliths can effectively be used as substrates in fluorous proteomic and other labeling applications.
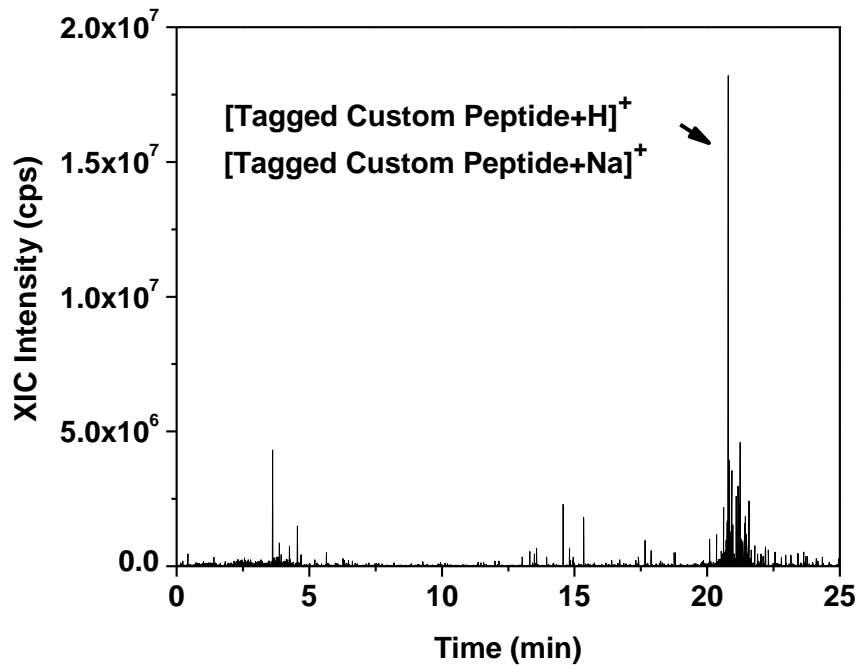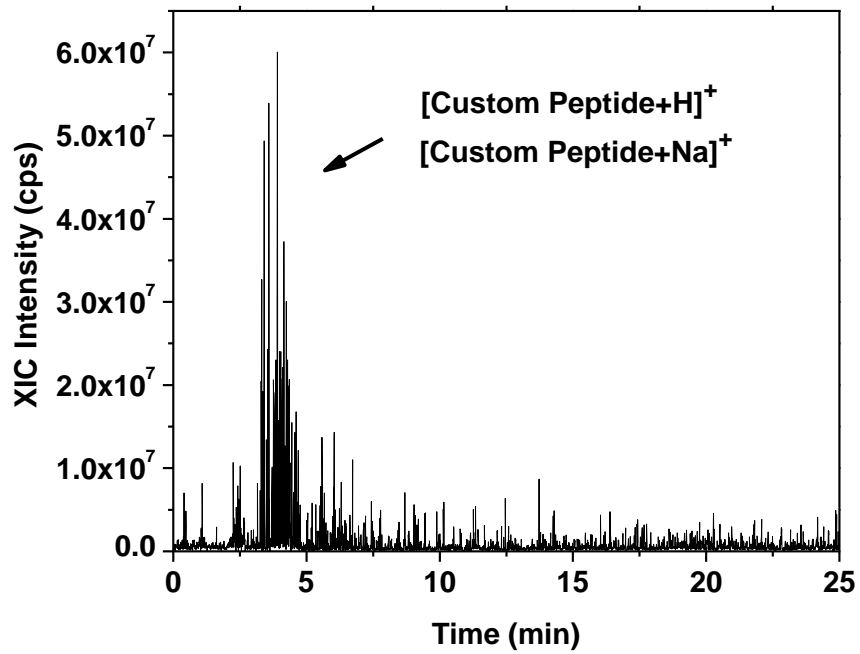
Figure 6.1: Extracted ion current (XIC) for custom peptide with both H$^+$ and Na$^+$ (top), as well as fluorous-tagged   custom peptide with both H$^+$ and Na$^+$ (bottom)

6.2.2 – Fluorous LC – MALDI – MS

Insulin, a more complex natural protein, was also fluorous tagged and separated in FPPM stationary phase. Then, the eluent was collected each minute and detected with the MALDI-MS setup as described in section 2.12 – Insulin Fluorous Tagging and 2.14 – MALDI-MS Operation.

It was found (Figure 6.2) that Chain B of insulin was eluted from the FPPM column from 15 to 17 minutes; the fluorous tagged Chain B was eluted out from 18 to 19 minutes; Chain A of insulin was eluted out the FPPM column from 19 to 21 minutes; while the fluorous tagged Chain A was eluted from 22 to 23 minutes. Both the fluorous tagged Chain A and Chain B are retained approximately 3 minutes longer than their non-fluorous counterparts due to the fluorous interaction between attached fluorous tags and fluorous stationary phase. The importance of the fluorous interaction in the insulin labeling mixture separation is not as strong as the importance in the fluorous tagged custom peptide I separation. The fluorous tagged custom peptide I was retained 15 minutes longer than the non-fluorous counterpart. This phenomenon is attributed to the increased number of secondary interactions associated with the larger molecular weight peptide.

Panel D

Chain B   16 minutes

Panel E

Chain B   17 minutes

Panel F

18 minutes

Chain B + Fluorous Tag
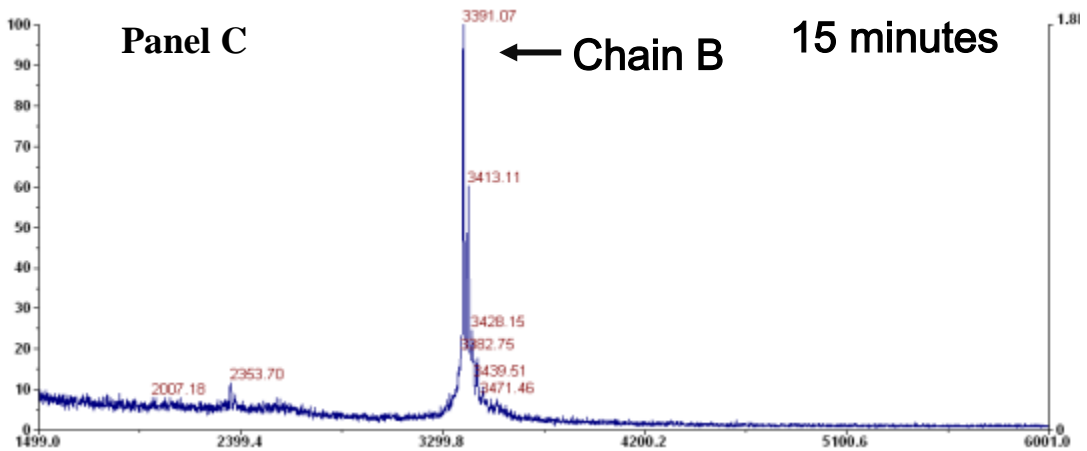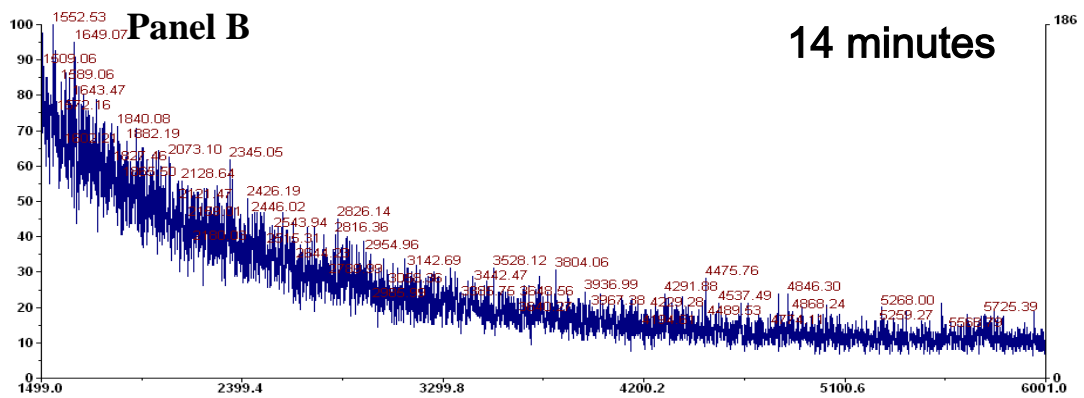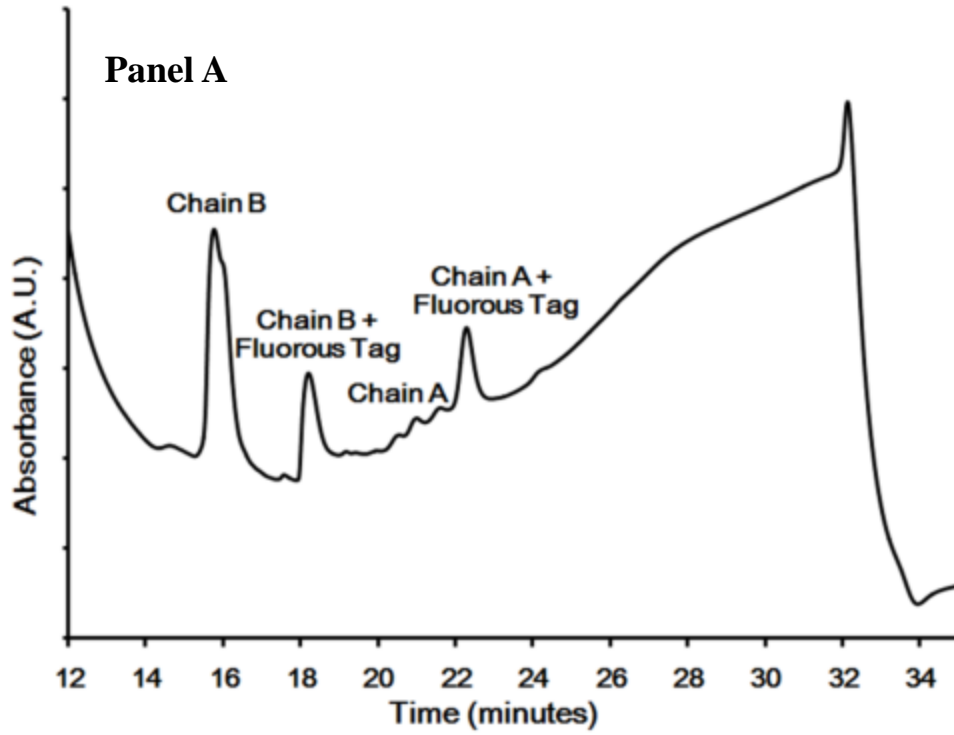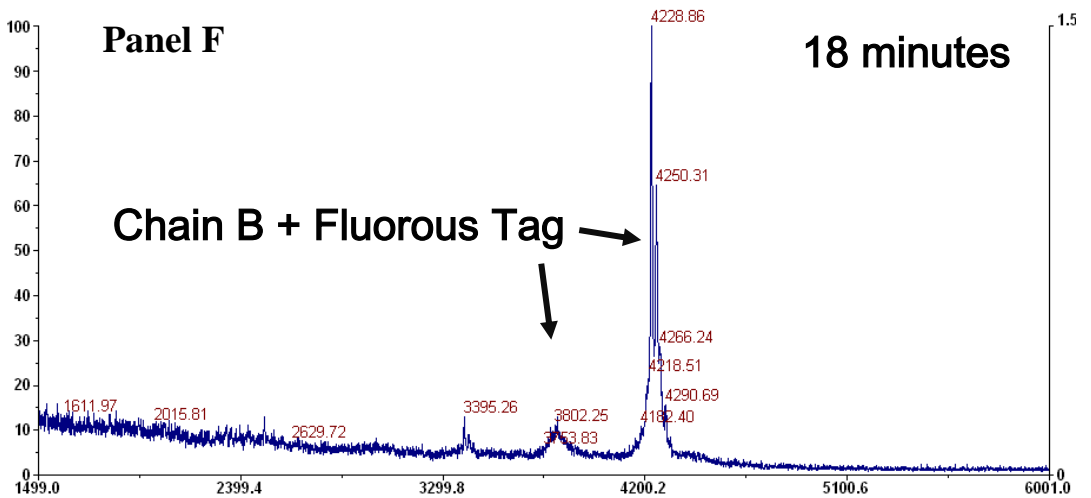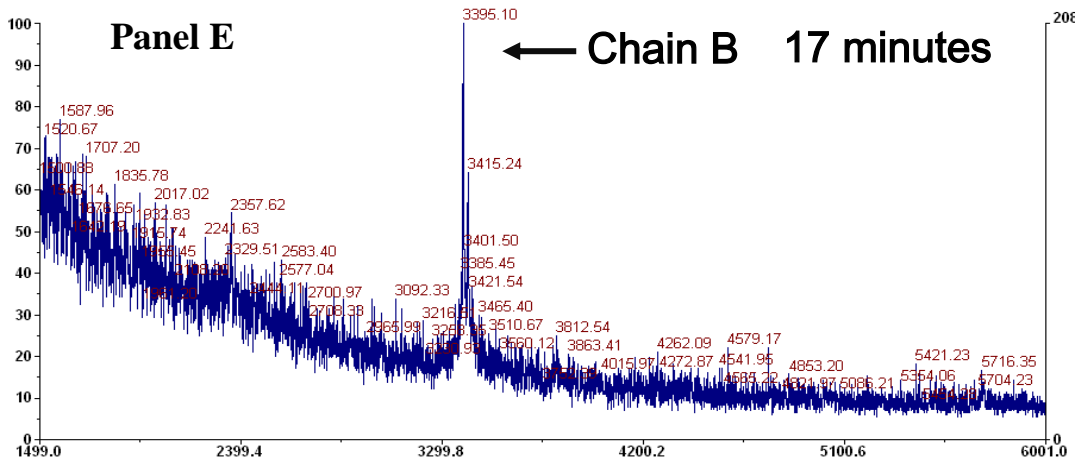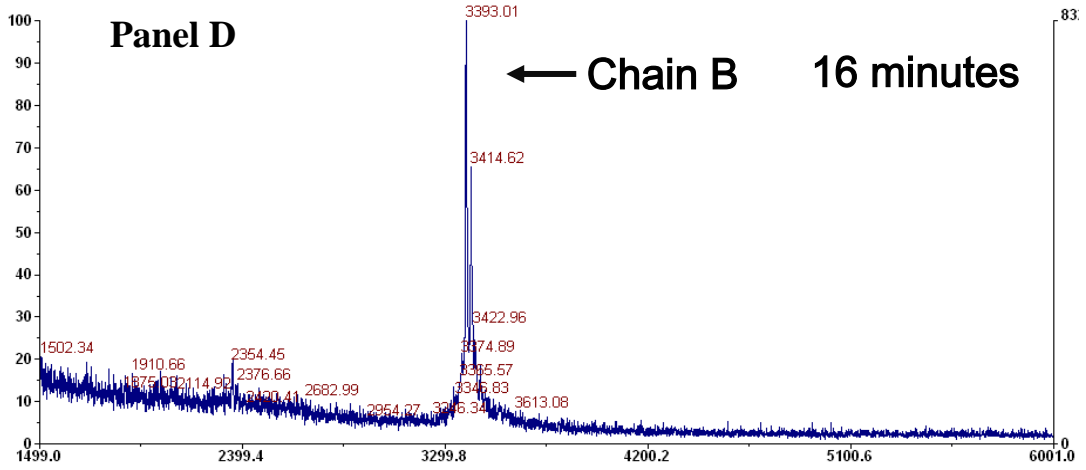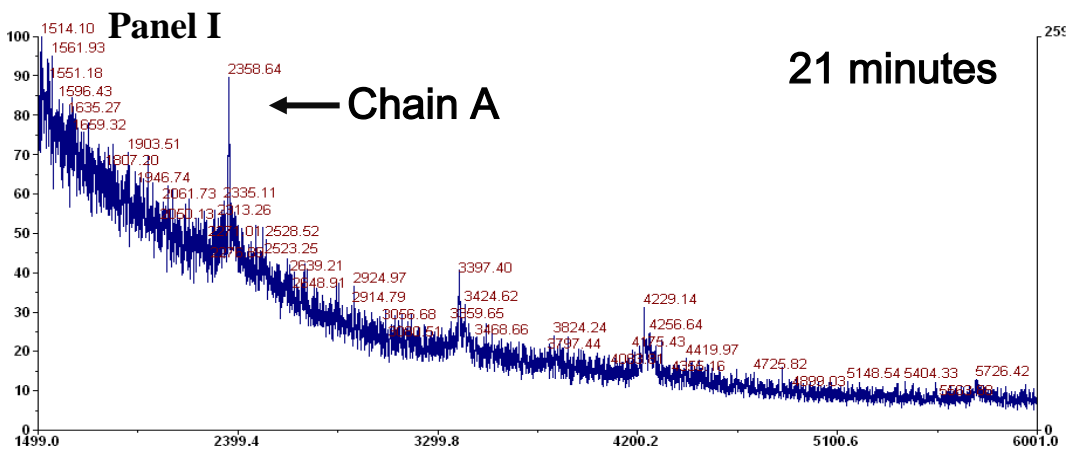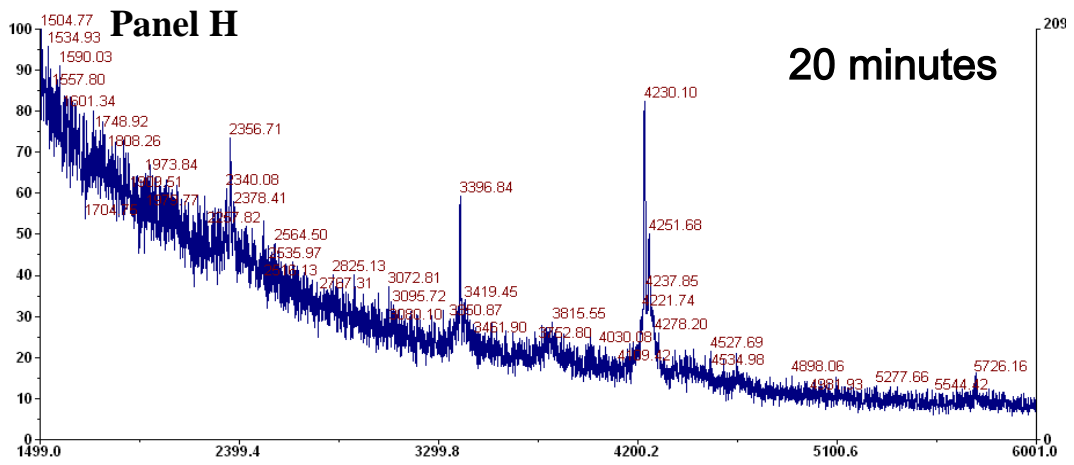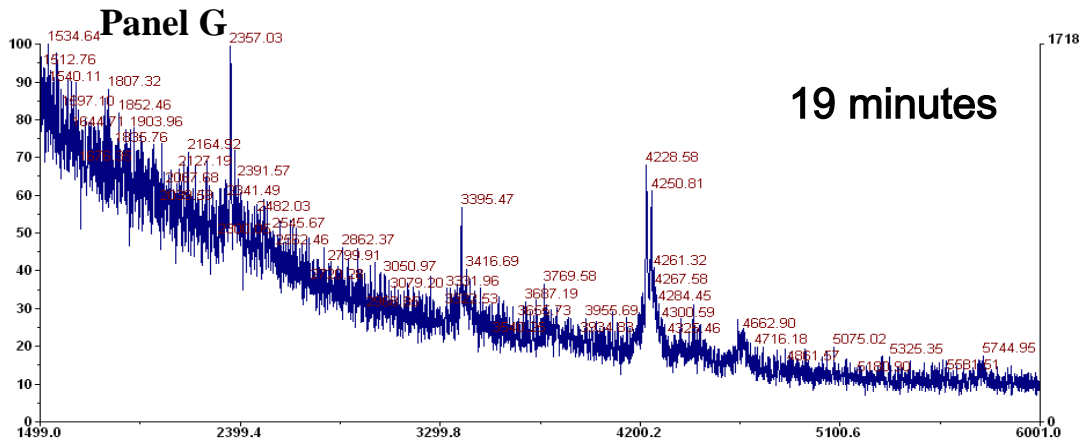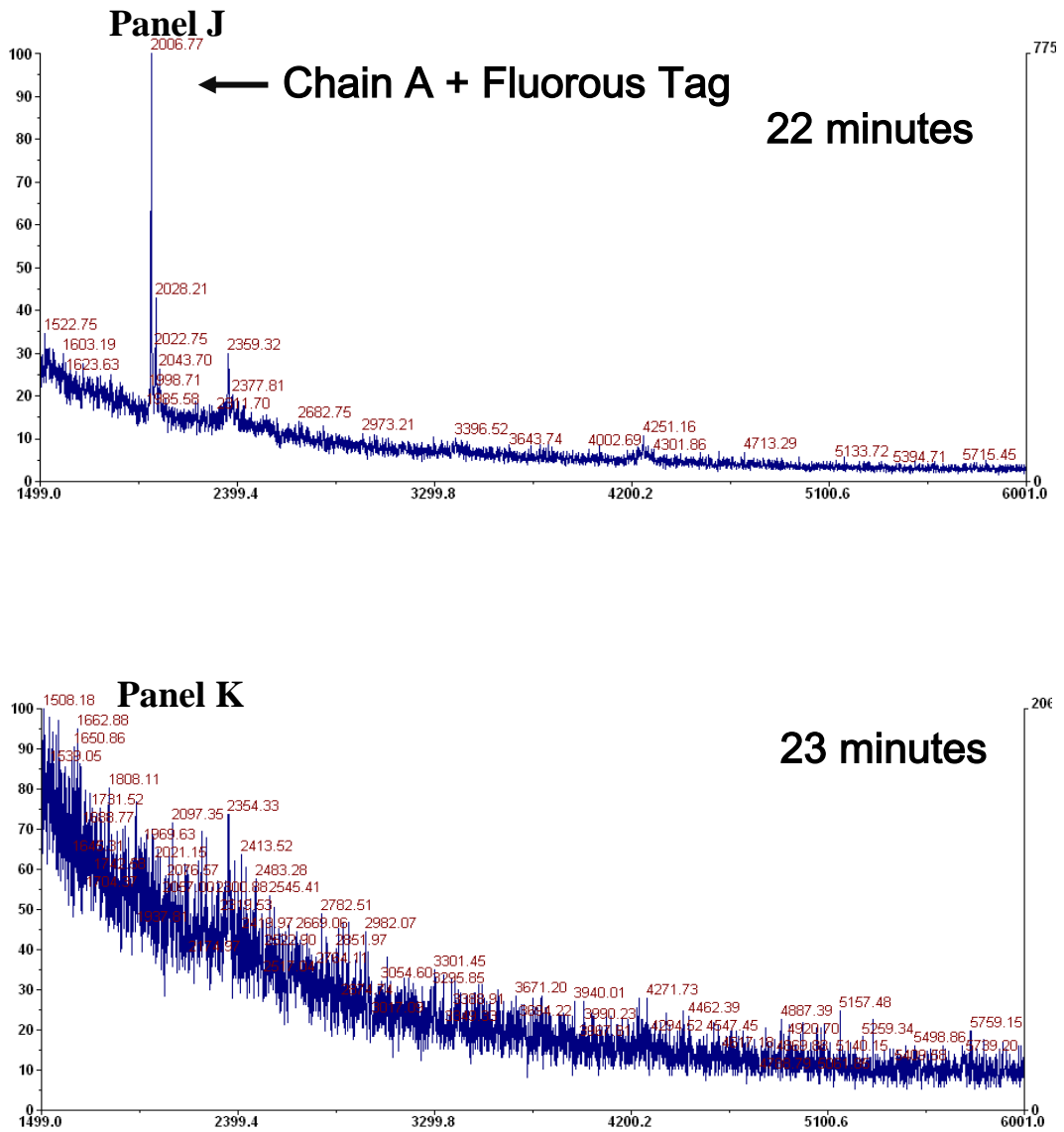
Figure 6.2: HPLC-UV analysis of fluorous tagged insulin (Panel A) and MALDI analysis of fractions collected during the separation of fluorous tagged insulin on a fluorous column (Panel B to Panel K). For example, the fraction 14 is collected at the end of fluorous column from 13.00 to 13.99 minutes.

6.3 – Conclusion

The FPPM columns can effectively be used to separate fluorous tagged custom peptide I and a more complex protein, insulin, from their non-fluorous counterparts. The importance of the fluorous affinity contribution decreases with increasing peptide/protein backbone

chain length or molecular weight. The fluorous selectivity can provide enough retention difference to resolve the more complex proteins. Further enhancements including optimization of stationary phase, mobile phase, and other experimental parameters could provide additional increases in separation efficiency.

Chapter 7 – Peptide Separation Using FPPM Photo-Patterned within Microchip Channels Combined with Laser Induced Fluorescence

7.1 – Introduction

Few reports on FSPE chips have appeared since fluorous chemistry was introduced in 1994, and formally established in 2002. Hu and coworkers reported a FSPE PDMS microchip for the purification of amino acids.[132] The fluorous reversed-phase silica gel beads (5 μm in diameter, dispersed in 100% methanol) were introduced into the microchannel through PDMS surface capillary force resulting from plasma oxidation treatment. Instant glue was used to fill the reservoirs at each end of the microchannel to retain stationary phase beads. A mixture of a fluorous peptide and non-fluorous peptides were electro-kinetically driven through FSPE channel. A solution of 80:20 (methanol : water) and 100% methanol served as the fluorophobic and fluorophilic eluents, respectively. The fractions collected containing fluorous peptide and non-fluorous peptides were detected by MALDI-MS (off-line). The microchip design that they employed would be difficult to automate and suffered from large pre- and post-column dead volume arising from the use of independent channels and reservoirs to retain the fluorous silica gel. We have attempted to address these two problems by incorporating a facile frit-less FPPM stationary phase in a glass-based microfluidic chip.

To our knowledge, there is no report of the use of a PPM microchip for proteomics, or the utilization of FPPM with selective fluorous-fluorous interaction. In our experience, the channel

clogging resulting from the PPM stationary phase is the biggest challenge encountered when transferring PPM methods from capillary-based to microchip-based channels. The origin of clogging is attributed to the formation of extraneous polymer during polymerization. In this chapter, the problem was addressed by adding a free radical quencher to control polymer formation. A FPPM SPE microchip was successfully fabricated for the first time (fabrication process is described in Section 2.4 – Microchip Channel-Based FPPM Column Fabrication). This microchip integrates the merits of both selective fluorous-fluorous interaction and μTAS technology, and enables target proteins/peptides to be tagged with fluorous tags followed by isolation from non-fluorous tagged proteins. Sample is manipulated by EOF during the loading and separation steps and the dead volume was minimized. On-line fluorescence detection was utilized to monitor the eluting species.

7.2 – Results and Discussion

7.2.1 – Unwanted Polymerization Initiated by UV Light Migrating under Photo-Masked Area

During photo-polymerization, light initiates a free radical based process to produce polymer. The advantages of this process result from the ability to produce polymer only in irradiated regions of a chip or capillary. Ideally, the initiating light would only illuminate regions directly under the window of the photo-mask. In this way, a sharp material cutoff would be produced with little material produced beyond the illumination window. In practice, polymer is formed well beyond the illumination window (upstream or downstream) in a capillary or

microchip (Figure 7.1). It is observed that the monolith density gradually tapers off as we go

further from the illumination window.
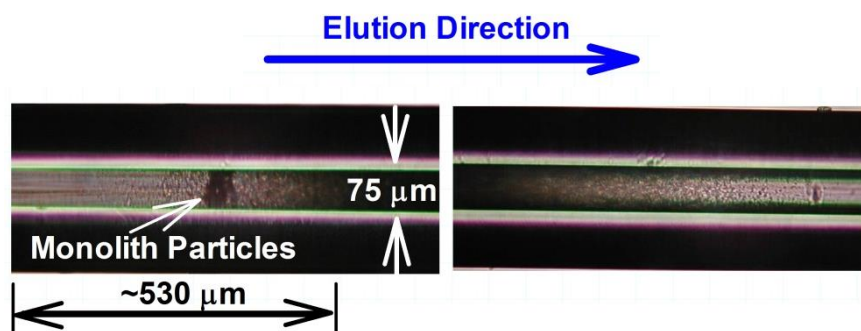
Figure 7.1: Microscope image of the pre-column and post-column regions of the FPPM column prepared in the microchip mimic capillaries without free radical quencher addition. A glass microchip was placed over the capillary when initiating the polymerization to mimic the channel in microchip while keeping capillary dimensions constant.

There are a number of probable causes for the gradual change of FPPM density (transparency). The primary reason is that UV light source is an area light source rather than spot light. The gradual change of FPPM density near the illumination window is attributed to the oblique illumination. In addition, light diffraction and free radical diffusion can also contribute to the formation of polymer beyond the photo-mask/illumination window.

The most significant difference between the capillary- and microchip-based FPPM fabrication is the distance that the initiating light travels vertically between the mask and the reflective medium (Figure 7.2). The distance between the mask and foil in the capillary case is equal to the capillary outer diameter, 375 μm (total of acrylate coating 14 μm × 2, fused silica 136 μm × 2 and capillary 75μm I.D.). Alternatively for the microchip, the distance is

equal to the microchip thickness, 2200 μm (top layer 1100 μm plus bottom layer 1100 μm).

The longer propagation distance combined with refraction will inevitably produce a longer

illumination region. This can be seen in Figure 7.2 where the regions on either side of the

illumination window (referred to as chromatographically pre-column or post-column) on

capillary (Figure 7.4) and microchip mimic (Figure 7.5). The PPM extends further from the

illumination mask for the microchip mimic (530 μm) compared to the capillary (155μm).
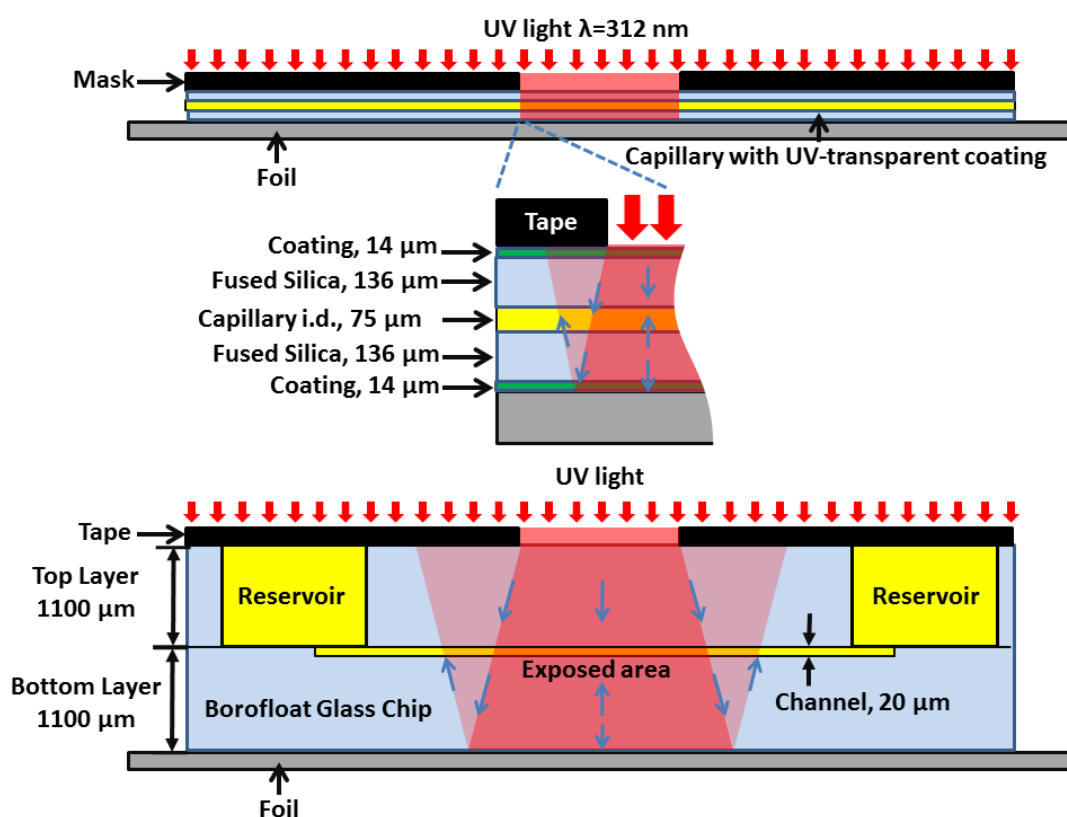
Figure 7.2: Migration of initiating UV light for *in situ* monolith preparation in capillary (top) and microchip mimic (bottom).

The monolith density gradually tapers off near the mask edge, which was found to cause

considerable clogging problems, where monolith not securely held to the microchip channel

wall, dislodges at the front end of the column. This extraneous polymer can cause increased

backpressure and clogging. For capillary-based systems, these problems can be minimized by physically removing the low density monolith by cleaving the capillary where the monolith density begins to decrease. However, this is not possible for a microchip format, because the channels (both upstream and downstream) of the chromatographic column are usually, connected to other functional units, like reservoirs. Furthermore, the cross sectional areas of the channels in microchips are typically much smaller than in capillaries. In the experiments described here, the cross sectional area ratio between capillary and microchip channel is around 4.55:1. The small cross sectional area in the microchip channel results in a much higher probability of clogging. In fact, in our hands, clogging rates of up to 100% occurred when using photo initiated FPPM, even when the illumination length was reduced to 1 cm. The additional backpressure resulting from the monolithic fragments at the leading edge of the monolith column cannot simply be overcome with pressure. Commercial microchips used in our trials were capable of withstanding 125,000 kPa beyond which leakage occurred and in some cases the excessive pressure resulted in chip fracture. The excessive back pressure necessitated an alternate route to minimize monolith clogging.

7.2.2 – Nitrobenzene as a Free Radical Quencher to Reduce Clogging

Initiation of a free radical polymerization requires the production of free radicals in the presence of an unsaturated molecule (monomer). Initiators are mainly responsible for "growing" polymer through a free radical transfer process, even though, strictly speaking, initiators are also responsible for termination by collision between free radical initiator and growing polymer radical. Alternatively, quenchers are a reactive species that terminates

polymer chain growth by inactivating either the free radical initiator or growing polymer chain. In this case, a free radical quencher can be added as a reagent to minimize polymer produced in regions with lower light intensity (*i.e.* at the leading and trailing edges of a monolithic column). Several different quenchers were examined and nitrobenzene was chosen due to quenching characteristics and solubility in the polymerization mixture. Nitrobenzene can react with any free radicals including the growing polymer chains in the polymerization system to form the intermediates (shown in Scheme 7.1 top). The intermediates have four types of resonances (shown in Scheme 7.1 bottom), which increase their life and chance to be quenched.[208,209]

Intermediate

Intermediate resonance
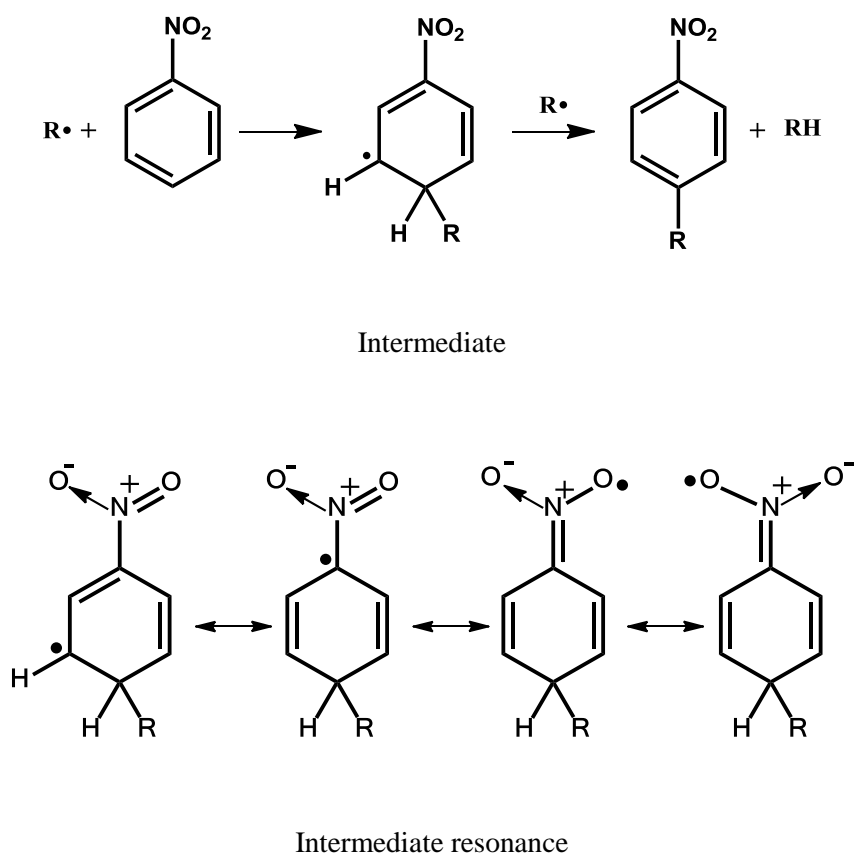
Scheme 7.1: Scheme for the free radical quenching by nitrobenzene. This figure is reproduced from reference.[209]

The amount of quencher should be carefully controlled as too much will limit polymer synthesis resulting in low density polymer, which will ultimately compromise separation efficiency, while too little will result in extraneous polymer formation and clogging.

Molecular weight distributions of polymers can be tailored through controlling the amount of photo initiator. In this case, we used a free radical quencher (nitrobenzene) and BME to control the polymer morphology.

Figure 7.3 shows plots of the pressure required to flow a mixture of 50:50 (ACN : water) through a 10 cm monolithic column prepared with different initiator/quencher ratios within a capillary and microchip mimic. A microchip mimic (comprised of a capillary illuminated through a microfluidic chip) was utilized to enable the direct comparison of backpressure. The capillary with no quencher added shows the highest flow-induced backpressure (densest monolith). As the ratio of nitrobenzene to BME is increased, the monolith density decreases. Commensurately, the flow-induced backpressure drops to approximately 50% of the value with no quencher added. A similar trend was observed for the chip-covered capillary. However, the capillary monolith density is consistently less due to reduced illumination intensity afforded by attenuation from the microchip.
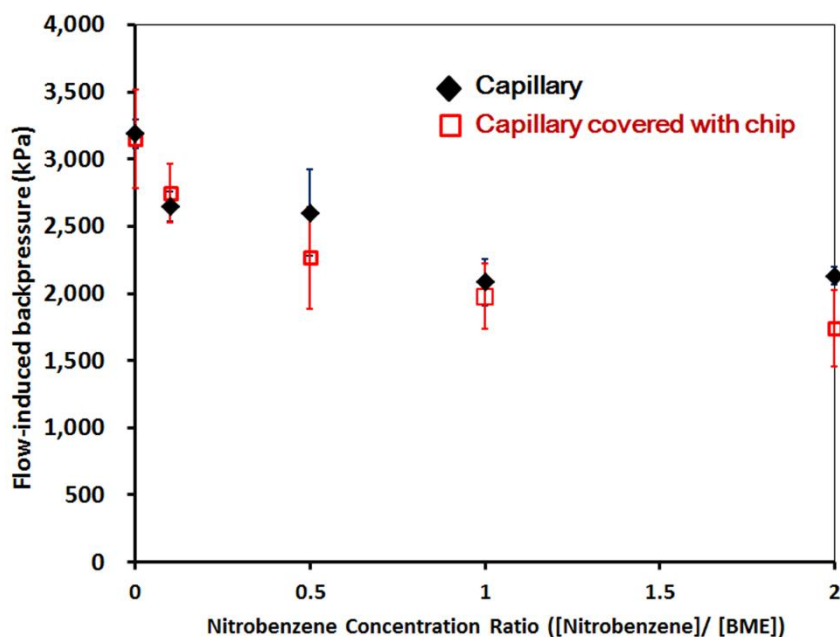
Figure 7.3: Flow-induced backpressure for columns prepared with different quencher /initiator (nitrobenzene/BME) ratios. Column length is 10 cm, flow rate is 0.4 μL/min, 50:50 (ACN : water). Each data point is the average of the results for three replicate columns.

7.2.3 – Optimal Concentration of Free Radical Quencher

The free radical quencher (nitrobenzene) was added to both capillary and microchip mimic and polymerization carried out. No clogging was observed for any of the capillary examples (Figure 7.4) polymerized with or without quencher. Conversely, utilizing a nitrobenzene : BME ratio of 0:1 or 2:1   resulted in the microchip mimic clogging (Figure 7.5). These two clogging events presumably originate from different causes. In the case of the 0:1 ratio, UV stray/refracted/reflected light produced significant extraneous polymer outside the illumination window. In fact, extraneous polymer formed a considerable distance beyond the illumination mask edge in either channel direction ≈ 530 μm. Once the capillary was flushed, the low density monolith particulate on the pre-column side is flushed onto the column

effectively clogging it and monolith particulate on the post-column side is flushed away. For the 2:1 ratio, the UV stray/refracted/reflected light will illuminate the same region of the capillary. However, the density and length of the resulting monolith is significantly reduced from the addition of an excessive amount of quencher. As a result, some regions of the intensely illuminated capillary do not fully polymerize and significant monolith particulate is produced instead. This is evidenced by a shorter resulting monolith and similar increased clogging characteristics.
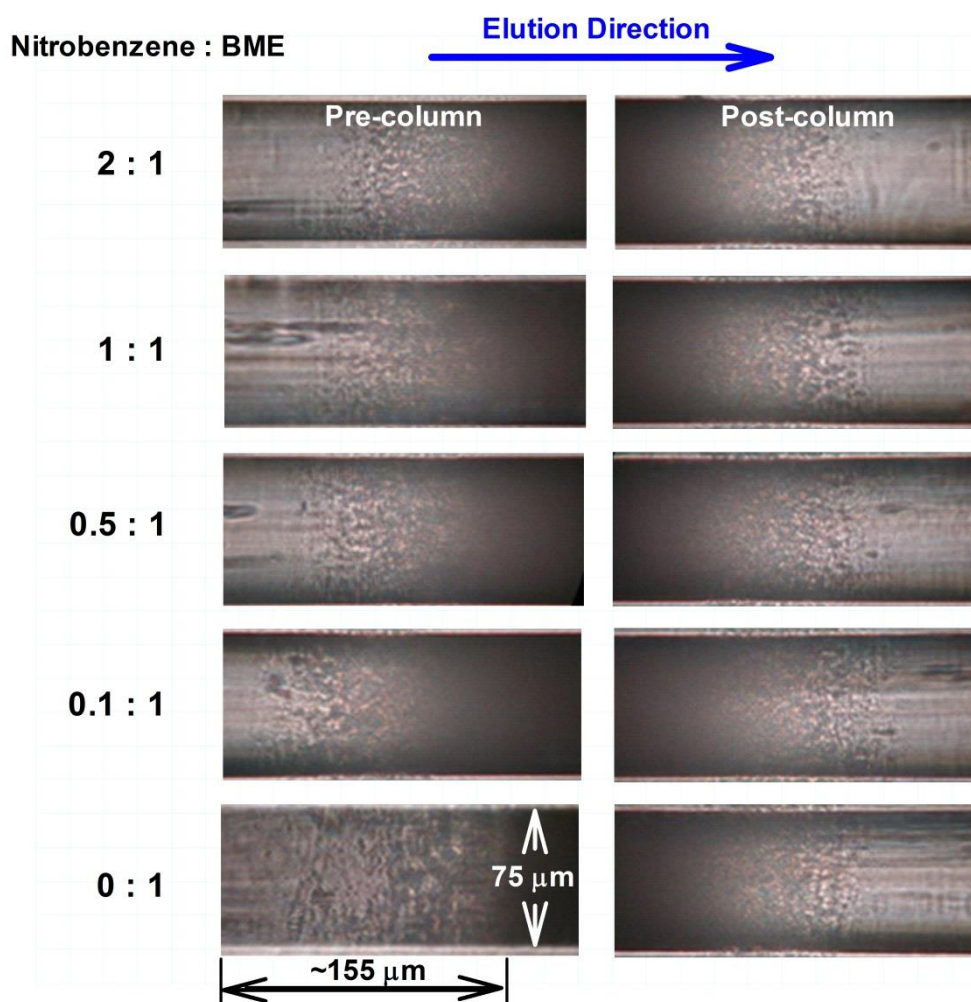
Figure 7.4: Microscope images of the pre-column and post-column regions of the FPPM column prepared in the capillary.
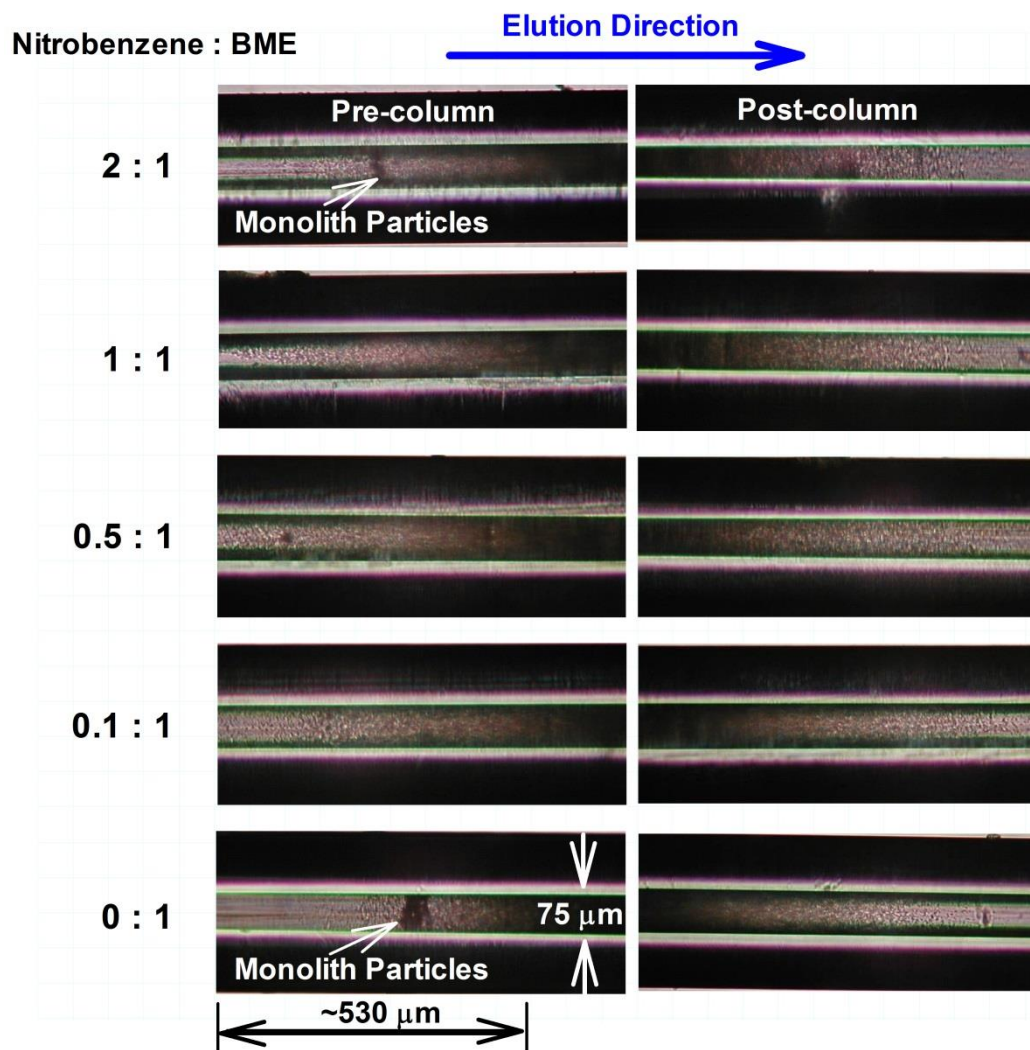
Figure 7.5: Microscope images of the pre-column and post-column regions of the FPPM column prepared in the microchip mimic capillaries. A glass microchip was placed over the capillary when initiating the polymerization to mimic the channel in a microchip while keeping capillary dimensions constant.

In the area farther from the interface, free radicals produced by BME, and growing polymer chains were quenched more efficiently since there is more quencher added. The more efficient quenching gives smaller debris, which can pass through the FPPM. According to the above speculation, there is an effective range for quencher and initiator ratio, at which clogging is minimized. At intermediate quencher : initiator values of 0.1:1 to 1:1 monoliths

that possessed adequate permeability and robustness were produced and no clogging events due to monolith formation were observed. A middle value 0.5:1 (nitrobenzene : BME) was chosen to fabricate the FPPM stationary phase chips for CEC separation based on the fluorous-fluorous interaction.

7.2.4 – CEC Separation with *In situ* Polymerized FPPM Column

CEC is a hybrid of the high performance liquid chromatography and capillary electrophoresis. In a microchip-based CEC separation, there are two main steps involving plug formation/sample injection followed by separation. These steps are performed by the application of voltages to specific reservoirs on the chip to induce EOF. The voltage program utilized for the analysis of the fluorous and fluorescently tagged products is shown in Table 7.1. Sample loading was performed for 30 seconds to ensure the cross region of the chip had been sufficiently filled. During loading the labeling products within the sample (R2) were driven by the positive potential gradient between R2 and R3 and flowed through the cross. Voltages of 180 V and 350 V were applied to R1 and R4 respectively to "pinch" the sample during loading to limit band broadening as much as possible. Then, the separation step involved the application of a 300 V separation voltage between reservoirs R1 and R4, and push back voltages (275 V to R2 and R3) to prevent sample leakage into the separation channel.

Fluorescent microscope images of the cross injector region are shown in Figure 7.6. At approximately 12 seconds, the sample front reaches the cross. An additional 18 seconds was

used to produce a stable injection plug within the cross. At the 30 second mark, the sample portion in the cross region was driven onto the 1 cm FPPM column and remaining sample retreated slowly back to either reservoir R2 or R3. The fluorescent detector was positioned immediately downstream of the FPPM and in the centre of the channel to minimize post column band broadening as much as possible.

Table 7.1: Optimized voltages applied to each reservoir during sample loading/injection and electrochromatographic separation

Reservoir	Applied voltage (V)	
	Sample loading step (0-30 s)	Separation step (30-300 s)
R1	180	300
R2	350	275
R3	Ground	275
R4	260	Ground

Figure 7.6: Fluorescent images of the cross injector region during injection and separation. All images were taken on a Nikon Eclipse Ti microscope, with 635/670 nm filter cube set.

If each step of the fluorous and fluorescently tagged process were quantitative, we would expect to see an individual peak for the single tagged product. Instead, we expect to see a

172

mixture of products, the concentration of which is dependent upon the labeling efficiencies (The Custom Peptide II tagging process is shown in Section 2.10). The tagged product mixture includes custom peptide (CP), fluorous tagged custom peptide (CP-F), mono fluorescently tagged custom peptide (CP-Cy5), doubly fluorescently tagged custom peptide (CP-2Cy5), fluorous/mono fluorescently tagged custom peptide (F-CP-Cy5), and fluorous/doubly fluorescently tagged custom peptide (F-CP-2Cy5). The presence of the various labeling products was determined by MALDI-MS. However, the relative concentrations of the species could not be determined due to the semi-quantitative limitations of MALDI-MS (Figure 7.7). The electrochromatogram of a sample containing the fluorescently tagged mixture separated in a chip that possesed a 1 cm FPPM is shown in Figure 7.8 top. The chip used an isocratic solvent mixture of 80:20 (ACN : water), buffered to a pH of 7. Three principal species are observed including hydrolyzed Cy5 and two labeling products which included the custom peptide tagged by both one and two Cy5 fluorescent moieties. The migration rate of an analyte in a CEC separation involves both the amount of analyte retention on the stationary phase and the electrophoretic mobility of the analyte.
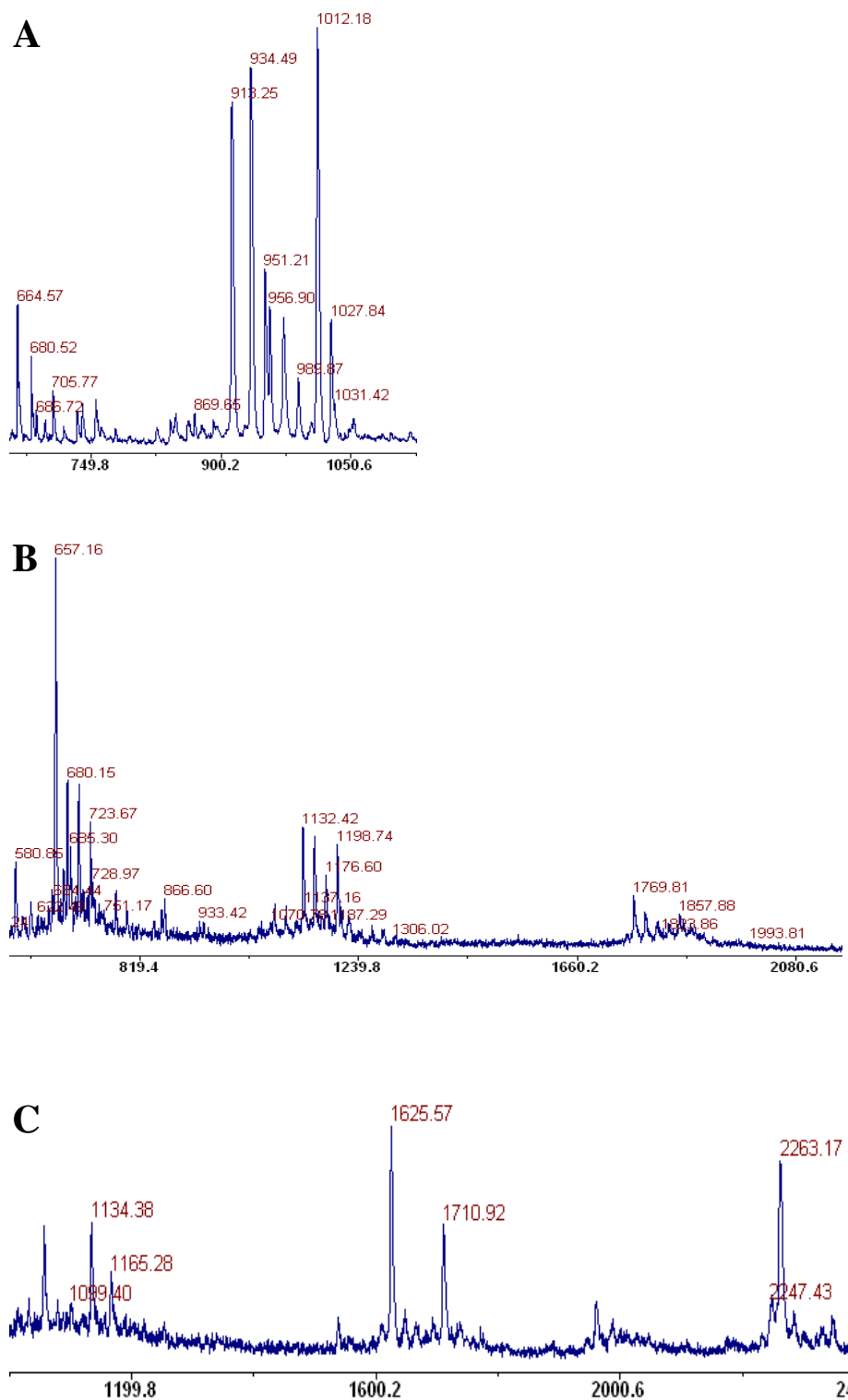
Figure 7.7: Matrix-assisted laser desorption/ionization (MALDI) spectra of fluorous tagged custom peptide (Panel A), fluorescently tagged custom peptide (Panel B), and fluorous and fluorescently tagged custom peptide (Panel C).

Peaks (Panel A) with m/z values of 913.25, 934.49, 951.21 are corresponding to protonated, sodiated and potassiated CP-F cations respectively. When tagging with the fluorescent moieties, several Cy5 derivatives are possible, since the cations neutralizing the negative sulfonic acid group can be H^+, Na^+, or K^+, yielding 9 possibilities when one Cy5 tagged on fluorous tagged peptide (3 possibilities (H^+, Na^+, and K^+ choices to attaching on fluorous tagged peptide) $\times$ 3 possibilities (H^+, Na^+, and K^+ choices neutralizing negative sulfonic acid group in the Cy5 tag)). When the second Cy5 is tagged, at least 27 possibilities will theoretically show on the spectrum (9 fluorous/one fluorescently tagged possibilities $\times$ 3 possibilities (H^+, Na^+, and K^+ choices neutralizing negative sulfonic acid group in the second Cy5 tag). Due to the resolution limitation of MALDI-TOF-MS we used and the hard determination/controlling on specific cations to attach peptides, only broad peaks were detected on fluorous and fluorescently tagged result mass spectra (Panel B, Panel C). All possibilities of the molecular weight to charge ratio (m/z) of fluorescently tagged custom peptide, and fluorous and fluorescently tagged custom peptide II are shown in Table 7.2.

Table 7.1: Possibilities of the molecular weight to charge ratio (m/z) of fluorous tagged, fluorescently tagged, and fluorous/fluorescently tagged custom peptide II

Custom peptide II	After singly fluorescently tagged	After doubly fluorescently tagged	After fluorous tagged	After singly fluorescently tagged	After doubly fluorescently tagged
CP+H+ 495.6	Cy5+H+ 1134.4	Cy5+H+ 1773.2	CP+F+H+ 912.7	Cy5+H+ 1551.5	Cy5+H+ 2190.3
		Cy5+Na+ 1795.2			Cy5+Na+ 2212.3
		Cy5+K+ 1811.2			Cy5+K+ 2228.3
	Cy5+Na+ 1156.4	Cy5+H+ 1795.2		Cy5+Na+ 1573.5	Cy5+H+ 2212.3
		Cy5+Na+ 1817.2			Cy5+Na+ 2234.3
		Cy5+K+ 1833.2			Cy5+K+ 2250.3
	Cy5+K+ 1172.4	Cy5+H+ 1811.2		Cy5+K+ 1589.5	Cy5+H+ 2228.3
		Cy5+Na+ 1833.2			Cy5+Na+ 2250.3
		Cy5+K+ 1849.2			Cy5+K+ 2266.3
CP+Na+ 517.6	Cy5+H+ 1156.4	Cy5+H+ 1795.2	CP+F+Na+ 934.7	Cy5+H+ 1573.5	Cy5+H+ 2212.3
		Cy5+Na+ 1817.2			Cy5+Na+ 2234.3
		Cy5+K+ 1833.2			Cy5+K+ 2250.3
	Cy5+Na+ 1178.4	Cy5+H+ 1817.2		Cy5+Na+ 1595.5	Cy5+H+ 2234.3
		Cy5+Na+ 1839.2			Cy5+Na+ 2256.3
		Cy5+K+ 1855.2			Cy5+K+ 2272.3
	Cy5+K+ 1194.4	Cy5+H+ 1869.2		Cy5+K+ 1611.5	Cy5+H+ 2286.3
		Cy5+Na+ 1855.2			Cy5+Na+ 2272.3
		Cy5+K+ 1871.2			Cy5+K+ 2288.3
CP+K+ 533.6	Cy5+H+ 1172.4	Cy5+H+ 1811.2	CP+F+K+ 950.7	Cy5+H+ 1589.5	Cy5+H+ 2228.3
		Cy5+Na+ 1833.2			Cy5+Na+ 2250.3
		Cy5+K+ 1849.2			Cy5+K+ 2266.3
	Cy5+Na+ 1194.4	Cy5+H+ 1833.2		Cy5+Na+ 1611.5	Cy5+H+ 2250.3
		Cy5+Na+ 1855.2			Cy5+Na+ 2272.3
		Cy5+K+ 1871.2			Cy5+K+ 2288.3
	Cy5+K+ 1210.4	Cy5+H+ 1849.2		Cy5+K+ 1627.5	Cy5+H+ 2266.3
		Cy5+Na+ 1871.2			Cy5+Na+ 2288.3
		Cy5+K+ 1887.2			Cy5+K+ 2304.3
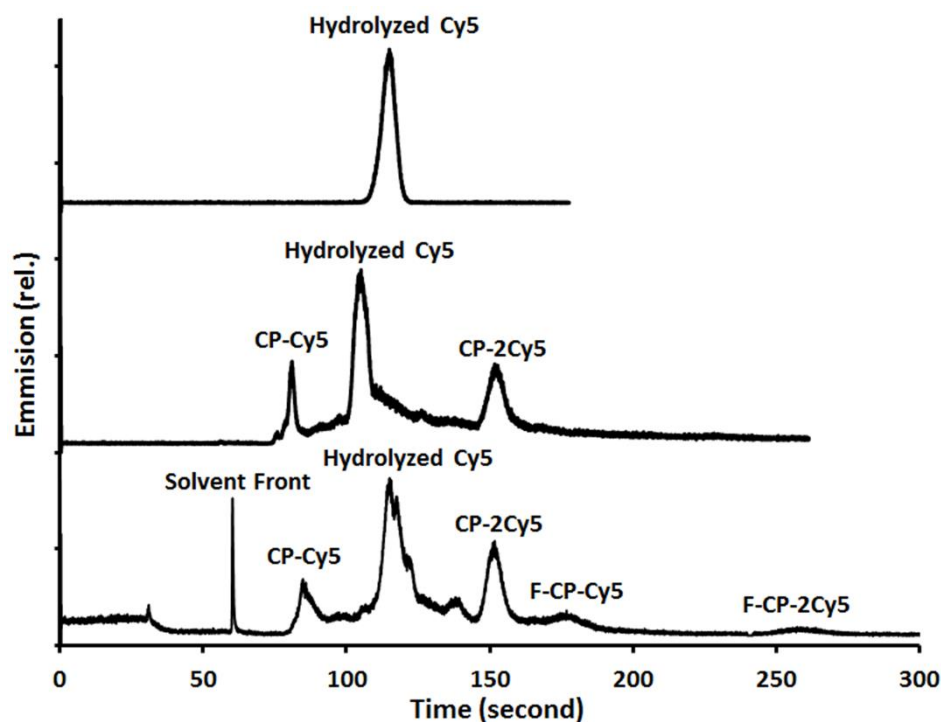
Figure 7.8: Electrochromatographic separation of Cy5 (top), the fluorescent (middle), and the fluorous and fluorescently tagged custom peptide (bottom).

In the 80:20 (ACN : water) buffer (pH 7), the hydrolyzed Cy5 (minus the -*N*-hydroxysuccinimide group) will possess two negative charges due to deprotonated carboxylic acid and sulfonic acid moieties.[210] Its electrochromatogram is shown in Figure 7.8 top. The charges states for CP-Cy5, CP-2Cy5, F-CP-Cy5, and F-CP-2Cy5 are rationalized to be 1⁻, 3⁻, 1⁻, and 3⁻ respectively using pKa values of the amino acid side chains and functional groups present on the Cy5 labels. The relatively high elutropic strength of the mobile phase (*i.e.* 80% ACN) and lack of fluorous character resulted in the species eluting primarily in order of charge (*i.e.* CP-Cy5, hydrolyzed Cy5, and CP-2Cy5) shown in Figure 7.8 middle. The electropherogram of the fluorous and fluorescently tagged species is shown in Figure 7.8 bottom. The increased migration time of the fluorous tagged species is due to the fluorous

interaction between the fluorous tag and the FPPM stationary phase. For comparison purposes, the same sample was run on a commercial CEC system with a significantly longer column (20 cm FPPM) and the electrochromatogram is shown in Figure 7.9. The integrated peak area ratio between CP-Cy5 and CP-2Cy5 is ~0.63, which is the same as the integrated area ratio calculated from the electrochromatogram in Figure 7.8. Similarly, the integrated area ratio between FCP-Cy5 and F-CP-2Cy5 is ~1.80, which is the same as the integrated area ratio calculated from the electrochromatogram in Figure 7.8 as well. Along with the MALDI spectra, the reproducibility of integrated peak area ratios further confirm the identification of the species in the fluorous and fluorescently tagged mixture. When comparing the analysis time required for the microchip and commercial CEC instrument, it was found that there is an order of magnitude reduction in analysis time (approximately 4.5 min *versus* 50 min respectively for the last analyte, *i.e.* F-CP-2Cy5).
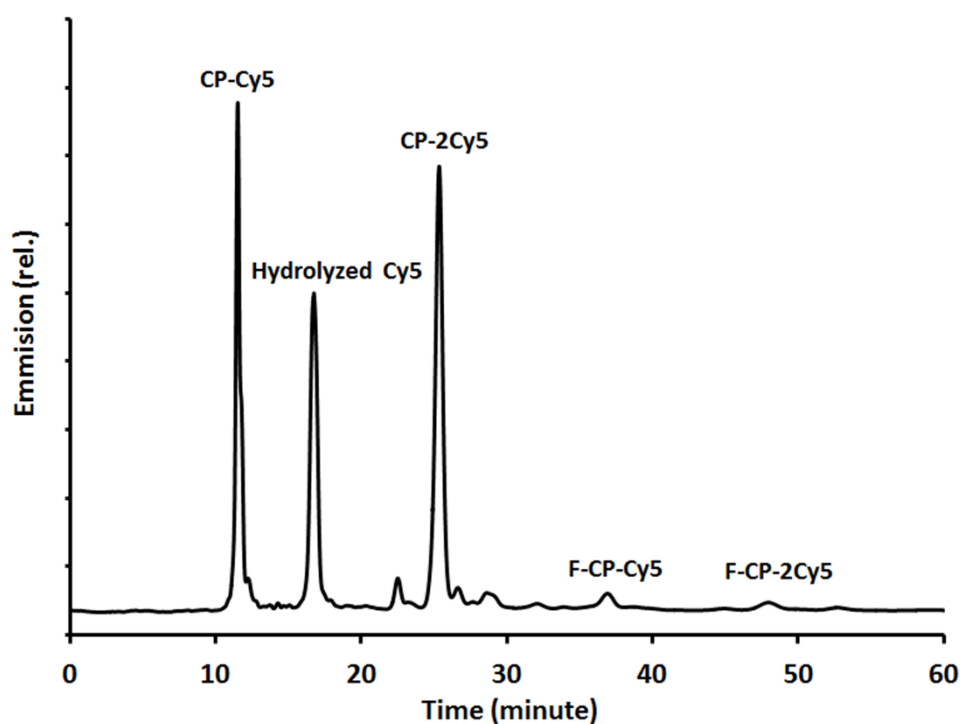
Figure 7.9: Electrochromatographic separation of the fluorous and fluorescently tagged custom peptide on a commercial CEC system. Mobile phase is 80:20 (ACN : water) with total sodium phosphate concentration of 1.6 mmol/L. The samples were loaded by electro-kinetic injection using 8.0 kV for 5 seconds. Separation voltage was 7.5 kV.

7.3 – Conclusion

To our knowledge, this is the first report on the fabrication a microchip utilizing a FPPM stationary phase. This microchip has the merits of both selective fluorous-fluorous interaction and µTAS technology. Nitrobenzene was used as a free radical quencher to control the small polymer particulate that resulted from extraneous polymerization. The use of the quencher (nitrobenzene): initiator (BME) in molar ratios ranging from 0.1:1 to 1:1 eliminated any clogging concerns. The optimized polymerization conditions were used to fabricate a CEC chip to determine and separate the labeling products of a custom peptide. A custom peptide with free N terminus, lysine unit, and a cysteine unit was fluorous and fluorescently tagged to prepare the analytes. Cysteine reacted with N-[(3-perfluorohexyl)propyl]iodoacetamide to attach fluorous moiety for enhanced retention on a FPPM stationary phase. While the free N terminus and lysine side chain reacted with Cy5-*N*-Hydroxysuccinimide mono-functional ester to tag the custom peptide for fluorescent detection purposes. The fluorous and fluorescently tagged custom peptide was electrokinetically loaded and resolved.

179

Chapter 8 – Conclusions and Outlook

In this Ph.D thesis project, a fluorous porous polymer monolith (FPPM) - based solid-phase extraction (SPE) stationary phase was successfully fabricated in both capillary-based columns and microchip format, and employed to separate fluorous analytes, hydrocarbon analytes, and proteomic samples. This project involves the combination of a number of materials and devices, and as a result was carried out in a number of sub-projects.

Firstly, a series of FPPM preparation parameters including fluorous monolith density, initiating UV wavelength, and initiator (BME) usage were optimized. Capillary columns were examined using flow-induced backpressure measurements, scanning electron microscopy (SEM) morphology analysis, and high performance liquid chromatography (HPLC) separation data of custom fluorous analytes N Series with per-fluorinated chains of varying length (mixture of N1, N2, N3, and N4) and P Series (mixture of P1, P2, P3, and P4). It was found that a 30% (volume percentage) mixture of polymerizable material (1H,1H-heptafluorobutyl acrylate (FBA) and 1, 3-butanediol diacrylate (BDDA) in volumetric ratio of 7:3) relative to the porogenic solvent (60:20:20, (ACN : water : ethanol)) produces the best HPLC resolution results for N Series and P Series. The optimal FPPM exhibits the greatest degree of reproducibility as well as the superior resolving power compared to their non-fluorous counterparts (replaced FBA with butyl acrylate (BA) while keeping the rest of experimental parameter constant). It was also found that longer initiating UV wavelength (365 nm) makes a finer PPM skeleton resulting better performance on separating the N Series and P Series.

The analysis of a complex mixture containing both N Series and P Series further expanded upon these results. The optimized FPPM column can resolve the components in a manner that was otherwise not possible with its non-fluorous counterpart. The presence of secondary effects in addition to the fluorous interaction was also observed for these optimized columns (similar to those noted for fluorous silica gels). Despite the secondary effects, no adverse effect on the performance of the porous polymer monoliths (PPM) was noted. Analyte specificity was shown to primarily be a function of the choice of fluorous tag, with the secondary effects causing slight deviations from ideal fluorous behavior (less polar analytes retained slightly longer than their more polar counterparts). These effects are suggested to have positive implications for the analysis of complex mixtures though, with the differentiation of components with different polarities but identical tagging potentially providing useful information in more complicated separations with multiple dimensions.

Following, the capillary electrochromatography (CEC) of fluorous analytes on FPPM stationary phase based on fluorous-fluorous interaction was realized for the first time. The experimental conditions including separation voltages and mobile phase composition were optimized. Under the optimal conditions, the FPPM column efficiency (calculated for the N1 peak) was as high as 234,000 plates/metre, and complete resolution (>1.5) was obtained for analytes differing only by a single perfluoromethylene unit (*i.e.* N1 and N2) under all conditions tested. An equivalent non-FPPM column was fabricated to compare with the FPPM column and to illustrate the effects of fluorous-fluorous interactions on the separation of the fluorous analytes. Perfluoromethylene selectivity, α_{-CF_2-}, and subsequently Gibbs

free energy change for the transfer of a –CF$_2$– unit from mobile to stationary phase, $\Delta G^\circ_{-CF_2-}$, were used to evaluate the fluorous interaction of the columns, showing that the FPPM column had significantly greater selectivity for the –CF$_2$– unit than the non-FPPM column. Furthermore, the inherent column efficiency advantages of CEC over LC lead to much greater resolutions in CEC despite the lack of a mobile phase gradient. With this improved resolution, combined with instrumental factors including injection time and equilibration time, CEC analysis was possible in much less time than for LC (5 minutes in CEC analysis, 33 minutes in LC analysis).

The long lasting question on the origin of fluorous interaction was also explored and experimentally examined based on CEC data. The selective fluorous interaction is a kind of reduced instantaneous or induced dipole interactions compared to hydrophobic interaction. Herein, the ambiguous term "like dissolves like" can be used to the express the unique super hydrophobic character of fluorous phase. The interactions of fluorinated molecule - fluorinated molecule, and fluorinated molecule - non-fluorinated molecule are weaker than interactions of non-fluorinated molecules. Therefore, fluorinated molecule cannot break the interaction of non-fluorinated molecules, which prevent miscibility of fluorinated phase with other phases (organic phases and aqueous phases).

A comparison on separation of the hydrophobic analytes (–CH$_2$–) and the fluorous analytes (–CF$_2$–) on both the hydrophobic stationary phases (–CH$_2$–) and the fluorous stationary phases (–CF$_2$–) was conducted. It was found that, quantitatively, hydrophobic stationary phases have better α_{-CH_2-}, while fluorous stationary phases have better α_{-CF_2-}. On a PPM

column without $-CF_2-$ fraction, α_{-CH_2-} and α_{-CF_2-} are 1.21 and 1.11 respectively. While, on PPM column with 0.33 $-CF_2-$ fraction, α_{-CH_2-} and α_{-CF_2-} are 1.13 and 1.49 respectively. Thermodynamically, with the presence of mobile phase 80:20 (ACN : water), $\Delta G^{\circ}_{-CH_2- \rightarrow -CH_2-}$ (Gibbs free energy change of transferring a $-CH_2-$ unit from mobile phase to "pure" hydrophobic stationary phase to form a methylene dipole – methylene dipole interaction) is -476 J/mol. Similarly, $\Delta G^{\circ}_{-CF_2- \rightarrow -CF_2-}$ is -3855 J/mol. $\Delta G^{\circ}_{-CF_2- \rightarrow -CH_2-}$ and $\Delta G^{\circ}_{-CH_2- \rightarrow -CF_2-}$ have almost the same values (-255 J/mol, -253 J/mol respectively). The big difference between $\Delta G^{\circ}_{-CF_2- \rightarrow -CF_2-}$ and $\Delta G^{\circ}_{-CH_2- \rightarrow -CH_2-}$ ($\approx$ 8:1) can be explained by the origin of the fluorous interaction, a kind of reduced (weaker) instantaneous or induced dipole interactions compared to hydrophobic interaction. The interactions involving fluorous moieties ($-CF_2-$) are smaller than its hydrocarbon counterpart ($-CH_2-$). The energy required for $-CF_2-$ desolvation is less than the one for $-CH_2-$. Therefore, less energy of $\Delta G^{\circ}_{Combination\ solvent - solvent}$ is consumed, *i.e.* more negative $\Delta G^{\circ}_{-CF_2- \rightarrow -CF_2-}$ was obtained consequently.

A new concept, hypothetical water percentage (HWP) was proposed for the first time to quantitatively evaluate the hydrophobicity/fluorophilicity of a stationary phase. In detail, when HWP is higher than 100, this stationary phase is a hydrophobic stationary phase. On the other hand, when HWP is less than 0, this stationary phase is classified as a fluorous stationary phase. Stationary phases with HWP in the range from 0 to 100 can hardly be classified either way. These stationary phases can be used to separate both hydrophobic analytes and fluorous analytes.

Fluorous tagged peptide and protein were also effectively separated from their non-fluorous counterparts on the FPPM SPE stationary phase and detected both on-line with electrospray ionization - mass spectrometry (ESI-MS) and off-line with matrix-assisted laser desorption/ionization - mass spectrometry (MALDI-MS). It was found that the weight of fluorous interaction effect on retention decreases with the increasing peptide/protein backbone chain length or molecular weight. However the fluorous selectivity can still provide enough differentiated retention ability to resolve the complex proteomic sample mixtures at least up to the size of insulin (up to 5800 Da).

Finally, the optimized FPPM SPE stationary phase with the fluorous selectivity was transplanted from capillary-based columns to microchip format. To our knowledge, this is the first report on fabrication a microchip with photo-patterned FPPM stationary phase. This microchip exhibits the merits of both selective fluorous interaction and micro total analysis systems (µTAS). Nitrobenzene was used as free radical quencher to control the small polymer debris that resulted from unwanted UV light initiated polymerization. Optimized conditions using the quencher (nitrobenzene): initiator (BME) molar ratio range from 0.1:1 to 1:1 that resulted in no clogging. A fluorescence detector was used immediately downstream of the FPPM stationary phase to minimize post column dead volume. A custom peptide (CP) was fluorous (F-) and fluorescently (-Cy5) tagged and electrically loaded onto the CEC separation chip and a separation successfully accomplished.

As to outlook of this project, several aspects are suggested as a follow up. Firstly, there is a need to further explore the origin of the fluorous interaction to provide guidance for the

design of fluorous stationary phases, and optimal separation conditions. A further study to understand the FPPM polymerization mechanism and morphology control is necessary to accomplish better performance for the separation of much more complicated organic- and proteomic samples. At the same time, more functionalities (*e.g.* micro-reactors, micro-pumps, micro-values, and etc.) can be added to the FPPM SPE microchip to realize an on-chip reaction, sample loading and other automated operations. PPM-based emitters developed in our group can also be used as an electrospray ionization (ESI) interface to a mass spectrometer (MS) to realize on-line detection. Some of the ideas have already been put into practice in our group, for example using digital microfluidics (DMF) technology to manipulate samples to accomplish more complicated multi-step operations.

References

(1)   Horvath, I. T.; Rabai, J. *Science* **1994**, *266*, 72.

(2)   Curran, D. P.; Luo, Z. *J. Am. Chem. Soc.* **1999**, *121*, 9069.

(3)   Curran, D. P.; Hadida, S.; He, M. *J. Org. Chem.* **1997**, *62*, 6714.

(4)   Gladysz, J. A.; Curran, D. P. *Tetrahedron* **2002**, *58*, 3823.

(5)   Horvath, I. T.; Kiss, G.; Cook, R. A.; Bond, J. E.; Stevens, P. A.; Rabai, J.; Mozeleski, E. J. *J. Am. Chem. Soc.* **1998**, *120*, 3133.

(6)   Banks, R. E.; Smart, B. E.; Tatlow, J. C. *Organofluorine Chemistry Principles and Commercial Applications*; Plenum Press: New York, 1994.

(7)   Gladysz, J. A.; Curran, D. P.; Horvath, I. T. *Handbook of Fluorous Chemistry*; WILEY-VCH, 2004.

(8)   Zhang, W. *J. Fluorine Chem.* **2008**, *129*, 910.

(9)   Israelachvili, J. N. *Contemp. Phys.* **1974**, *15*, 159.

(10)   Kotz, J. C.; JR., P. T. *Chemsitry & Chemical Reactivity*; Fourth ed.; Emily Barrosse: Orlando, Florida, US, 1999.

(11)   Oss, C. J. V.; Absolom, D. R.; Neumann, A. W. *Colloid & Polymer Science* **1980**, *258*, 424.

(12)   Pauling, L. *J. Am. Chem. Soc.* **1932**, *54*, 3570.

(13)   Allen, L. C. *J. Am. Chem. Soc.* **1989**, *111*, 9003.

(14)   Lemal, D. M. *J. Org. Chem.* **2004**, *69*, 1.

(15)   Allred, A. L. *Journal of Inorganic and Nuclear Chemistry* **1961**, *17*, 215.

(16)   O'Hagan, D. *Chem. Soc. Rev.* **2008**, *37*, 308.

(17)   Wilberg, K. B.; Rablen, P. R. *J. Am. Chem. Soc.* **1993**, *115*, 614.

(18)   Peters, D. *The Journal of Chemical Physics* **1963**, *38*, 561.

	Reference
(19)	McMillen, D. F.; Golden, D. M. *Annu. Rev. Phys. Chem.* **1982**, *33*, 493.
(20)	Vincent, J.-M. *J. Fluorine Chem.* **2008**, *129*, 903.
(21)	Grosse, A. V.; Cady, G. H. *Industrial and Engineering Chemistry* **1947**, *39*, 367.
(22)	Scott, R. L. *J. Am. Chem. Soc.* **1948**, *70*, 4090.
(23)	Freed, B. K.; Biesecker, J.; Middleton, W. J. *J. Fluorine Chem.* **1990**, *48*, 63.
(24)	Billiet, H. A. H.; Schoenmakers, P. J.; de Galan, L. *J. Chromatogr.* **1981**, *218*, 443.
(25)	Ubeda, M. A.; Dembinski, R. *J. Chem. Educ.* **2006**, *83*, 84.
(26)	Marchand, D. H.; Croes, K.; Dolan, J. W.; Snyder, L. R.; Henry, R. A.; Kallury, K. M. R.; Waite, S.; Carr, P. W. *J. Chromatogr. A* **2005**, *1062*, 65.
(27)	Biffinger, J. C.; Kim, H. W.; DiMagno, S. G. *ChemBioChem* **2004**, *5*, 622.
(28)	Reichardt, C. *Solvents and solvent effects in organic chemistry*; WILEY-VCH, 2003.
(29)	Scatchard, G. *Chemical Reviews* **1931**, *8*, 321.
(30)	George, S. *Chemical Reviews* **1949**, *44*, 7.
(31)	Hildebrand *Proceedings of the National Academy of Sciences* **1979**, *76*, 6040.
(32)	Hansen, C. M. *Eur. Polym. J.* **2008**, *44*, 2741.
(33)	Rohrschneider, L. *Anal. Chem.* **1973**, *45*.
(34)	Snyder, L. R. *J. Chromatogr.* **1974**, *92*, 223.
(35)	Brady, J. E.; Carr, P. W. *Anal. Chem.* **1982**, *54*, 1751.
(36)	Hayama, T.; Sakaguchi, Y.; Yoshida, H.; Itoyama, M.; Todoroki, K.; Yamaguchi, M.; Nohta, H. *Rapid Commun. Mass Spectrom* **2010**, *24*, 2868.
(37)	Majors, R. E. *LC GC North America* **2008**, *26*.
(38)	Snyder, L. R.; Kirkland, J. J. *Introduction to Modern Liquid Chromatography*; A Wiley-Interscience Publication, 1979.

Reference

(39)   Euerbya, M. R.; McKeowna, A. P.; Peterssonb, P. *J. Sep. Sci.* **2003**, *25*, 295.

(40)   Nakamura, H.; Linclau, B.; Curran, D. P. *J. Am. Chem. Soc.* **2001**, *123*, 10119.

(41)   Horvath, I. T. *Acc. Chem. Res.* **1998**, *31*, 641.

(42)   Rebek, J. J. *Tetrahedron* **1979**, *35*, 723.

(43)   Berendsen, G. E.; Pikaart, K. A.; de Galan, L.; Olieman, C. *Anal. Chem.* **1980**, *52*, 1990.

(44)   Curran, D. P.; Lee, Z. *Green Chem.* **2001**, *3*, G3.

(45)   Horvath, I. T.; Rabai, J.; Patent, U. S., Ed. United States, 1995.

(46)   Zhang, W.; Curran, D. P. *Tetrahedron* **2006**, *62*, 11837.

(47)   *The essence of chromatography*; Poole, C. F., Ed.; Elsevier, 2003.

(48)   Leonard, M. *J. Chromatogr. B* **1997**, *699*, 3.

(49)   Rezeli, M.; Kilara, F.; Hjerten, S. *J. Chromatogr. A* **2006**, *1109*, 100.

(50)   Svec, F. *J. Chromatogr. A* **2010**, *1217*, 902.

(51)   http://www.sigmaaldrich.com;   http://www.silicycle.com; http://www.chem.agilent.com; January 19, 2011 ed. 2011.

(52)   Sander, L. C.; Pursch, M.; Wise, S. A. *Anal. Chem.* **1999**, *71*, 4821.

(53)   Tanaka, H.; Kamada, M.; Nyudo, M.; Ohira, M. *J. Chromatogr. A* **1997**, *762*, 89.

(54)   Sander, L. C.; Wise, S. A. *Anal. Chem.* **1984**, *56*, 504.

(55)   Sander, L. C.; Wise, S. A. *Anal. Chem.* **1995**, *67*, 3284.

(56)   Lork, K. D.; Unger, K. K.; Kinkel, J. N. *J. Chromatogr.* **1986**, *352*, 199.

(57)   Engelhardt, H.; Orth, P. *J. Liq. Chromatogr. Relat. Technol.* **1987**, *10*, 1999.

(58)   Sudo, Y. *J. Chromatogr. A* **1996**, *737*, 139.

(59)   Pesek, J. J.; Matyska, M. T.; Yu, R. J. *J. Chromatogr. A* **2002**, *947*, 195.

(60)   Potter, O. G.; Hilder, E. F. *J. Sep. Sci.* **2008**, *31*, 1881.

(61)   Ross, W. D.; Jefferson, R. T. *J. Chromatogr. Sci.* **1970**, *8*, 386.

(62)   Lynn, T. R.; Rushnec, D. R.; Cooper, A. R. *J. Chromatogr. Sci.* **1974**, *12*, 76.

(63)   Schnecko, H.; Bieber, O. *Chromatographia* **1971**, *4*, 109.

(64)   Yu, C.; Svec, F.; Fréchet, J. M. J. *Electrophoresis* **2000**, *21*, 120.

(65)   Tanaka, N.; Ebata, T.; Hashizume, K.; Hosoya, K.; Araki, M. *J. Chromatogr. A* **1989**, *475*, 195.

(66)   Svec, F.; Frechet, J. M. J. *Anal. Chem.* **1992**, *64*, 820.

(67)   Gibson, G. T. T.; Koerner, T. B.; Xie, R.; Shah, K.; de Korompay, N.; Oleschuk, R. D. *J. Colloid Interface Sci.* **2008**, *320*, 82.

(68)   http://www.micralyne.com/microfluidic-chips/; January 19, 2011 ed.

(69)   Lloyd, L. L. *J. Chromatogr.* **1991**, *544*, 201.

(70)   Xie, R.; Oleschuk, R. D. *Electrophoresis* **2005**, *26*, 4225.

(71)   Nevejans, F.; Verzele, M. *J. Chromatogr. A* **1987**, *406*, 325.

(72)   Gowanlock, D.; Bailey, R.; Cantwell, F. F. *J. Chromatogr. A* **1996**, *726*, 1.

(73)   Jingyi, L.; Cantwell, F. F. *J. Chromatogr. A* **1996**, *726*, 37.

(74)   Jingyi, L.; Litwinson, L. M.; Cantwell, F. F. *J. Chromatogr. A* **1996**, *726*, 25.

(75)   Hjerten, S.; Liao, J.; Zhang, R. *J. Chromatogr.* **1989**, *473*, 273.

(76)   Tennikova, T. B.; Bleha, M.; Švec, F.; Almazova, T. V.; Belenkii, B. G. *J. Chromatogr. A* **1991**, *555*, 97.

(77)   Frey, D. D.; Schweinheim, E.; Horvath, C. *Biotechnology Progress* **1993**, *9*, 273.

(78)   Hjerten, S. *Ind. Eng. Chem. Res* **1999**, *38*, 1205.

(79)   Yurtsever, A.; Saracoglu, B.; Tuncel, A. *Electrophoresis* **2009**, *30*, 589.

(80)   Daley, A. B.; Oleschuk, R. D. *J. Chromatogr. A* **2009**, *1216*, 772.

(81)   Daley, A. B.; Xu, Z.; Oleschuk, R. D. *Anal. Chem.* **2011**, *83*, 1688.

(82)   Xu, Z.; Gibson, G. T. T.; Oleschuk., R. D. *Analyst* **2013**, *138*, 611.

(83)   Hutchison, J.; Ledwith, A. *Polymer* **1973**, *14*, 405.

(84)   Lewis, F. D.; Lauterbach, R. T.; Heine, H. G.; Hartmann, W.; Rudolph, H. *J. Am. Chem. Soc.* **1974**, *97*, 1519.

(85)   Kuhlmann, R.; Schnabel, W. *Polymer* **1977**, *18*, 1163.

(86)   Fouassier, J. P.; Ruhlmann, D.; Zahouily, K. *Polymer* **1992**, *33*, 3569.

(87)   Beebe, D. J.; Moore, J. S.; Bauer, J. M.; Yu, Q.; Liu, R. H.; Devadoss, C.; Jo, B.-H. *Nature* **2000**, *404*, 588.

(88)   Smith, R. M.; Garside, D. R. *J. Chromatogr. A* **1987**, *407*, 19.

(89)   Morra, M.; Occhiello, E.; Marola, R.; Garbassi, F.; Humphrey, P.; Johnson, D. *J. Colloid Interface Sci.* **1990**, *137*, 11.

(90)   Petro, M.; Svec, F.; Fréchet, J. M. J. *Biotechnol. Bioeng.* **1996**, *49*, 355.

(91)   Xie, S.; Svec, F.; Fréchet, J. M. J. *Biotechnol. Bioeng.* **1999**, *62*, 30.

(92)   Tong, S.; Zhou, X.; Zhou, C.; Li, Y.; Li, W.; Zhou, W.; Jia, Q. *Analyst* **2013**, *138*, 1549.

(93)   Nischang, I. *J. Chromatogr. A* **2013**, *1287*, 39.

(94)   Matsugi, M.; Curran, D. P. *Org. Lett.* **2004**, *6*, 2717.

(95)   Manz, A.; Graber, N.; Widmer, H. M. *Sens. Actuators, B* **1990**, *1*, 244.

(96)   Manz, A.; Miyahara, Y.; Miura, J.; Watanabe, Y.; Miyagi, H.; Sato, K. *Sens. Actuators, B* **1990**, *1*, 249.

(97)   Linden, W. E. v. d. *Trends Anal. Chem.* **1987**, *6*, 37.

(98)   Terry, S. C.; Jerman, J. H.; Angell, J. *IEEE Trans. Electron Devices* **1979**, *ED-26*, 1880.

	Reference
(99)	Jacobson, S. C.; Moore, A. W.; Ramrey, J. M. *Anal. Chem.* **1995**, *67*, 2059.
(100)	Lazar, I. M.; Ramsey, R. S.; Ramsey, J. M. *Anal. Chem.* **2001**, *73*, 1733.
(101)	Reyes, D. R.; Iossifidis, D.; Auroux, P.-A.; Manz, A. *Anal. Chem.* **2002**, *74*, 2623.
(102)	Auroux, P.-A.; Iossifidis, D.; Reyes, D. R.; Manz, A. *Anal. Chem.* **2002**, *74*, 2637.
(103)	Dittrich, P. S.; Tachikawa, K.; Manz, A. *Anal. Chem.* **2006**, *78*, 3887.
(104)	Vilkner, T.; Janasek, D.; Manz, A. *Anal. Chem.* **2004**, *76*, 3373.
(105)	West, J.; Becker, M.; Tombrink, S.; Manz, A. *Anal. Chem.* **2008**, *80*, 4403.
(106)	Kirby, B. J.; Hasselbrink Jr., E. F. *Electrophoresis* **2004**, *25*, 203.
(107)	Dodge, A.; Brunet, E.; Chen, S.; Goulpeau, J.; Labas, V.; Vinhb, J.; Tabelinga, P. *Analyst* **2006**, *131*, 1122.
(108)	Jacobson, S. C.; Hergenroder, R.; Koutny, L. B.; Ramsey, J. M. *Anal. Chem.* **1994**, *66*, 1114.
(109)	Woolley, A. T.; Mathies, R. A. *Proc. Natl. Acad. Sci. U. S. A.* **1994**, *91*, 11348.
(110)	Duffy, D. C.; McDonald, J. C.; Schueller, O. J. A.; Whitesides, G. M. *Anal. Chem.* **1998**, *70*, 4974.
(111)	Skelley, A. M.; Scherer, J. R.; Aubrey, A. D.; Grover, W. H.; Ivester, R. H. C.; Ehrenfreund, P.; Grunthaner, F. J.; Bada, J. L.; Mathies, R. A. *Proc. Natl. Acad. Sci. U. S. A.* **2005**, *102*, 1041.
(112)	Ko, Y.-J.; Maeng, J.-H.; Ahn, Y.; Hwang, S. Y.; Cho, N.-G.; Lee, S.-H. *Electrophoresis* **2008**, *29*, 3466.
(113)	McKnight, T. E.; Culbertson, C. T.; Jacobson, S. C.; Ramsey, J. M. *Anal. Chem.* **2001**, *73*, 4045.
(114)	Liu, R. H.; Yu, Q.; Beebe, D. J. *Journal of Microelectromechanical Systems* **2002**, *11*, 45.
(115)	Yu, C.; Mutlu, S.; Selvaganapathy, P.; Mastrangelo, C. H.; Svec, F.; Fréchet, J. M. J. *Anal. Chem.* **2003**, *75*, 1958.

Reference

(116)   Rathore, A. S. *Electrophoresis* **2002**, *23*, 3827.

(117)   Inoue, I.; Wakamoto, Y.; Moriguchi, H.; Okano, K.; Yasuda, K. *Lab Chip* **2001**, *1*, 50.

(118)   Takayama, S.; Ostuni, E.; Qian, X. P.; McDonald, J. C.; Jiang, X. Y.; LeDuc, P.; Wu, M. H.; Ingber, D. E.; Whitesides, G. M. *Adv. Mater.* **2001**, *13*, 570.

(119)   Tanase, M.; Felton, E. J.; Gray, D. S.; Hultgren, A.; Chen, C. S.; Reich, D. H. *Lab Chip* **2005**, *5*, 598.

(120)   Munro, N. J.; Huang, Z. L.; Finegold, D. N.; Landers, J. P. *Anal. Chem.* **2000**, *72*, 2765.

(121)   Oki, A.; Adachi, S.; Takamura, Y.; Ishihara, K.; Ogawa, H.; Ito, Y.; Ichiki, T.; Horiike, Y. *Electrophoresis* **2001**, *22*, 341.

(122)   Zuborova, M.; Masar, M.; Kaniansky, D.; Johnck, M.; Stanislaski, B. *Electrophoresis* **2002**, *23*, 774.

(123)   Moorthy, J.; Mensing, G. A.; Kim, D.; Mohanty, S.; Eddington, D. T.; Tepp, W. H.; Johnson, E. A.; Beebe, D. J. *Electrophoresis* **2004**, *25*, 1705.

(124)   Campbell, L. C.; Wilkinson, M. J.; Manz, A.; Camilleri, P.; Humphreys, C. J. *Lab Chip* **2004**, *4*, 225.

(125)   Footz, T.; Somerville, M. J.; Tomaszewski, R.; Elyas, B.; Backhouse, C. J. *Analyst* **2004**, *129*, 25.

(126)   Nge, P. N.; Pagaduan, J. V.; Yu, M.; Woolley, A. T. *J. Chromatogr. A* **2012**, *1261*, 129.

(127)   Reichmuth, D. S.; Shepodd, T. J.; Kirby, B. J. *Anal. Chem.* **2005**, *77*, 2997.

(128)   Emrich, C. A.; Medintz, I. L.; Chu, W. K.; Mathies, R. A. *Anal. Chem.* **2007**, *79*, 7360.

(129)   Belloy, E.; Pawlowski, A.-G.; Sayah, A.; Gijs, M. A. M. *Journal of Microelectromechanical System* **2002**, *11*, 521

(130)   Hierlemann, A. B.; Hagleitner, O.; Baltes, H. C. *Proceedings of IEEE* **2003**, *91*, 839

Reference

(131)   Arora, A.; Simone, G.; Salieb-Beugelaar, G. B.; Kim, J. T.; Manz, A. *Anal. Chem.* **2010**, *82*, 4830.

(132)   Hu, G.; Lee, J. S. H.; Li, D. *J. Colloid Interface Sci.* **2006**, *301*, 697.

(133)   Yu, C.; Davey, M. H.; Svec, F.; Frechet, J. M. J. *Anal. Chem.* **2001**, *73*, 5088.

(134)   Oleschuk, R. D.; Shultz-Lockyear, L. L.; Ning, Y.; Harrison, D. J. *Anal. Chem.* **2000**, *72*, 585.

(135)   Fortier, M.-H.; Bonneil, E.; Goodley, P.; Thibault, P. *Anal. Chem.* **2005**, *77*, 1631.

(136)   Sato, K.; Tokeshi, M.; Kimura, H.; Kitamori, T. *Anal. Chem.* **2001**, *73*, 1213.

(137)   Wang, P.-C.; DeVoe, D. L.; Lee, C. S. *Electrophoresis* **2001**, *22*, 3857.

(138)   Lion, N.; Gobry, V.; Jensen, H.; Rossier, J. S.; Girault, H. *Electrophoresis* **2002**, *23*, 3583.

(139)   James, P. *Q. Rev. Biophys.* **1997**, *30*, 279.

(140)   Whitford, D. *Proteins structure and function*; John Wiley & Sons Ltd, 2005.

(141)   Means, G. E.; Feeney, R. *J. Food Biochem.* **1998**, *22*, 399~425.

(142)   Rabilloud, T. *Proteomics* **2002**, *2*, 3.

(143)   Ro, K. W.; Nayak, R.; Knapp, D. R. *Electrophoresis* **2006**, *27*, 3547.

(144)   Bousse, L.; Mouradian, S.; Minalla, A.; Yee, H.; Williams, K.; Dubrow, R. *Anal. Chem.* **2001**, *73*, 1207.

(145)   Macounova, K.; Cabrera, C. R.; Yager, P. *Anal. Chem.* **2001**, *73*, 1627.

(146)   Brittain, S. M.; Ficarro, S. B.; Brock, A.; Peters, E. C. *Nat. Biotechnol.* **2005**, *23*, 463.

(147)   Wallman, L.; Ekström, S.; Marko-Varga, G.; Laurell, T.; Nilsson, J. *Electrophoresis* **2004**, *25*, 3778.

(148)   Dandapani, S. *QSAR Comb. Sci.* **2006**, *25*, 681.

(149)   Pesek, J. J.; Matyska, M. T.; Prajapati, K. V. *J. Sep. Sci.* **2010**, *33*, 2908.

Reference

(150)   Go, E. P.; Uritboonthai, W.; Apon, J. V.; Trauger, S. A.; Nordstrom, A.; O'Maille, G.; Brittain, S. M.; Peters, E. C.; Siuzdak, G. *J. Proteome Res.* **2007**, *6*, 1492.

(151)   Filippov, D. V.; Zoelen, D. J. v.; Oldfield, S. P.; Marel, G. A. v. d.; Overkleeft, H. S.; Drijfhout, J. W.; Booma, J. H. v. *Tetrahedron Lett.* **2002**, *43*, 7809.

(152)   Xiao, N.; Yu, Y. B. *J. Fluorine Chem.* **2010**, *131*, 439.

(153)   Eeltink, S.; Hilder, E. F.; Geiser, L.; Svec, F.; Frechet, J. M. J.; Rozing, G. P.; Schoenmakers, P. J.; Kok, W. T. *J. Sep. Sci.* **2007**, *30*, 407.

(154)   Ou, J.; Gibson, G. T. T.; Oleschuk, R. D. *J. Chromatogr. A* **2010**, *1217*, 3628.

(155)   Peters, E. C.; Petro, M.; Svec, F.; Frechet, J. M. J. *Anal. Chem.* **1997**, *69*, 3646.

(156)   Upchurch Scientifc, Instructions for use NanoPort™ Assemblies.

(157)   http://psec.uchicago.edu/glass/borofloat_33_e.pdf; Vol. 2013.

(158)   Cleland, W. W. *Biochemistry* **1964**, *3*, 480.

(159)   Lukesh, J. C.; Palte, M. J.; Raines, R. T. *J. Am. Chem. Soc.* **2012**, *134*, 4057.

(160)   Su, S.; Gibson, G. T. T.; Mugo, S. M.; Marecak, D. M.; Oleschuk, R. D. *Anal. Chem.* **2009**, *81*, 7281.

(161)   Koerner, T.; Turck, K.; Brown, L.; Oleschuk, R. D. *Anal. Chem.* **2004**, *76*, 6456.

(162)   Lee, S. S. H.; Douma, M.; Koerner, T.; Oleschuk, R. D. *Rapid Commun. Mass Spectrom.* **2005**, *19*, 2671.

(163)   Bedair, M.; Oleschuk, R. D. *Analyst* **2006**, *131*, 1316.

(164)   Bedair, M. F.; Oleschuk, R. D. *Anal. Chem.* **2006**, *78*, 1130.

(165)   Dai, Y.; Whittal, R. M.; Li, L. *Anal. Chem.* **1999**, *71*, 1087.

(166)   Leinweber, F. C.; Tallarek, U. *J. Chromatogr. A* **2003**, *1006*, 207.

(167)   Nischang, I.; Svec, F.; Fréchet, J. M. J. *Anal. Chem.* **2009**, *81*, 7390.

(168)   Bakry, R.; Stoggl, W. M.; Hochleitner, E. O.; Stecher, G.; Huck, C. W.; Bonn, G. K. *J. Chromatogr. A* **2006**, *1132*, 183.

(169)   Svec, F.; Frechet, J. M. *J. Chem. Mater.* **1995**, 707.

(170)   Guiochon, G. *J. Chromatogr. A* **2007**, *1168*, 101.

(171)   Yamamoto, F. M.; Rokushika, S. *J. Chromatogr. A* **2000**, *898*, 141.

(172)   Turowski, M.; Morimoto, T.; Kimata, K.; Monde, H.; Ikegami, T.; Hosoya, K.; Tanaka, N. *J. Chromatogr. A* **2001**, *911*, 177.

(173)   Poole, C. F.; Ahmed, H.; Kiridena, W.; DeKay, C.; Koziol, W. W. *Chromatographia* **2007**, *65*, 127.

(174)   Sakaguchi, Y.; Yoshida, H.; Todoroki, K.; Nohta, H.; Yamaguchi, M. *Anal. Chem.* **2009**, *81*, 5039.

(175)   Mathies, R. A.; Huang, X. C. *Nature* **1992**, *359*, 167.

(176)   Gusev, I.; Huang, X.; Horvath, C. *J. Chromatogr. A* **1999**, *855*, 273.

(177)   Ericson, C.; Holm, J.; Ericson, T.; Hjertén, S. *Anal. Chem.* **2000**, *72*, 81.

(178)   Landers, J. P. *Capillary and Microchip Electrophoresis and Associated Microtechniques*; Third Edtion ed.; CRC Press: Boca Raton, 2008.

(179)   Waguespack, B. L.; Hodges, S. A.; Bush, M. E.; Sondergeld, L. J.; Bushey, M. M. *J. Chromatogr. A* **2005**, *1078*, 171.

(180)   Choodum, A.; Smith, N. W.; Thavarungkul, P.; Kanatharana, P. *J. Sep. Sci.* **2011**, *34*, 2264.

(181)   Palonen, S.; Jussila, M.; Porras, S. P.; Hyotylainen, T.; Riekkola, M.-L. *J. Chromatogr. A* **2001**, *916*, 89.

(182)   Wang, Y.; Lin, Q.; Mukherjee, T. *Lab Chip* **2004**, *4*, 625.

(183)   Harris, D. C. *Quantitative Chemical Analysis*; Seventh ed.; W.H. Freeman and Company: New York, 2007.

(184)   Marchetti, N.; Caciolli, L.; Laganà, A.; Gasparrini, F.; Pasti, L.; Dondi, F.; Cavazzini, A. *Anal. Chem.* **2012**, *84*, 7138.

(185)   Johnson, B. P.; Khaledi, M. G.; Dorsey, J. G. *J. Chromatogr.* **1987**, *384*, 221.

(186)   Bhagwat, V.; Bereznitski, Y.; Buszewski, B.; Jaroniec, M. *J. Liq. Chromatogr. Relat. Technol.* **1998**, *21*, 923.

(187)   Marchand, D. H.; Croes, K.; Dolan, J. W.; Snyder, L. R. *J. Chromatogr. A* **2005**, *1062*, 57.

(188)   Wilson, N. S.; Gilroy, J.; Dolan, J. W.; Snyder, L. R. *J. Chromatogr. A* **2004**, *1026*, 91.

(189)   Gilroy, J. J.; Dolan, J. W.; Carr, P. W.; Snyder, L. R. *J. Chromatogr. A* **2004**, *1026*, 77.

(190)   Gilroy, J. J.; Dolan, J. W.; Snyder, L. R. *J. Chromatogr. A* **2003**, *1000*, 757.

(191)   Wilson, N. S.; Dolan, J. W.; Snyder, L. R.; Carr, P. W.; Sander, L. C. *J. Chromatogr. A* **2002**, *961*, 217.

(192)   Wilson, N. S.; Nelson, M. D.; Dolan, J. W.; Snyder, L. R.; Carr, P. W. *J. Chromatogr. A* **2002**, *961*, 195.

(193)   Wilson, N. S.; Nelson, M. D.; Dolan, J. W.; Snyder, L. R.; Wolcott, R. G.; Carr, P. W. *J. Chromatogr. A* **2002**, *961*, 171.

(194)   Shibukawa, M.; Takazawa, Y.; Saitoh, K. *Anal. Chem.* **2007**, *79*, 6279.

(195)   Sentell, K. B.; Dorsey, J. G. *J. Chromatogr.* **1989**, *4610*, 193.

(196)   Gritti, F.; Guiochon, G. *J. Chromatogr. A* **2005**, *1099*, 1.

(197)   Rafferty, J. L.; Zhang, L.; Siepmann, J. I.; Schure, M. R. *Anal. Chem.* **2007**, *79*, 6551.

(198)   Tijssen, R.; Schoenmakers, P. J.; Böhmer, M. R.; Koopal, L. K.; Billiet, H. A. H. *J. Chromatogr. A* **1993**, *656*, 135.

(199)   Vailaya, A.; Horvath, C. *J. Chromatogr. A* **1998**, *829*, 1.

(200)   Rafferty, J. L.; Siepmann, J. I.; Schure, M. R. *Advances in Chromatography* **2010**, *48*, 1.

(201)   Mansfield, E. R.; Mansfield, D. S.; Patterson, J. E.; Knotts, T. A. *J. Phys. Chem.* **2012**, *116*, 8456.

(202)   Poole, C. F.; Poole, S. K. *J. Chromatogr. A* **2009**, *1216*, 1530.

(203)   Dill, K. A. *J. Phys. Chem.* **1987**, *91*, 1980.

(204)   Dill, K. A.; Naghizadeh, J.; Marqusee, J. A. *Annu. Rev. Phys. Chem.* **1988**, *39*, 425.

(205)   Martire, D. E.; Boehm, R. E. *J. Phys. Chem.* **1983**, *87*, 1045.

(206)   Horvath, C.; Lin, H.-J. *J. Chromatogr. A* **1976**, *126*, 401.

(207)   Horvath, C.; Melander, W.; Molnar, I. *J. Chromatogr.* **1976**, *125*, 129.

(208)   Fieser, L. F.; Clapp, R. C.; Daudt, W. H. *J. Am. Chem. Soc.* **1942**, *64*, 2052.

(209)   Price, C. C.; Durham, D. A. *J. Am. Chem. Soc.* **1943**, *65*, 757.

(210)   Dempsey, G. T.; Bates, M.; Kowtoniuk, W. E.; Liu, D. R.; Tsien, R. Y.; Zhuang, X. *J. Am. Chem. Soc.* **2009**, *131*, 18192.
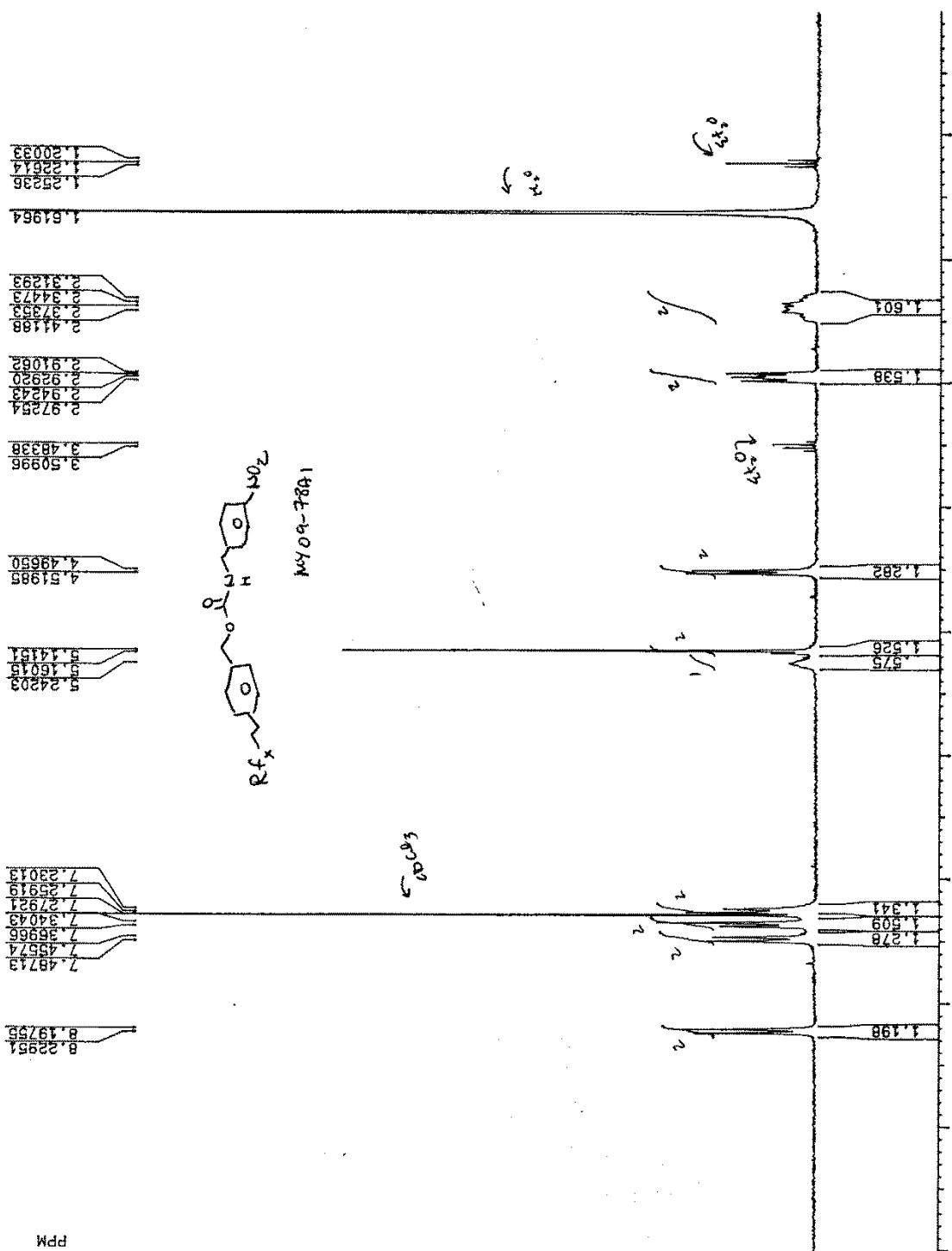
Appendices
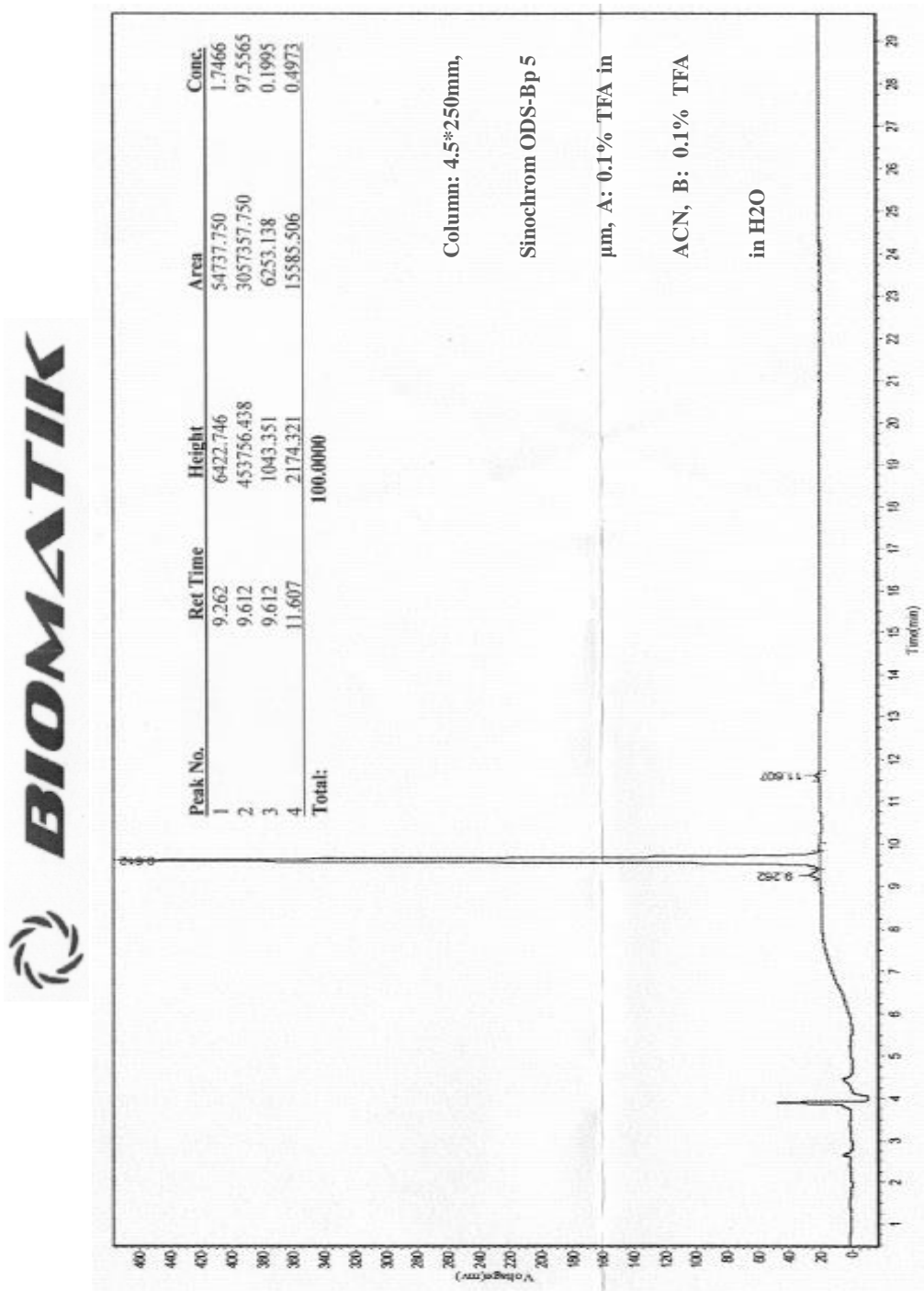
Appendix Figure 1: Liquid chromatogram of Custom peptide II (Alanine-Serine-Lysine-Serine-Cystaine, provided by Biomatik, Cambridge, ON, Canada)
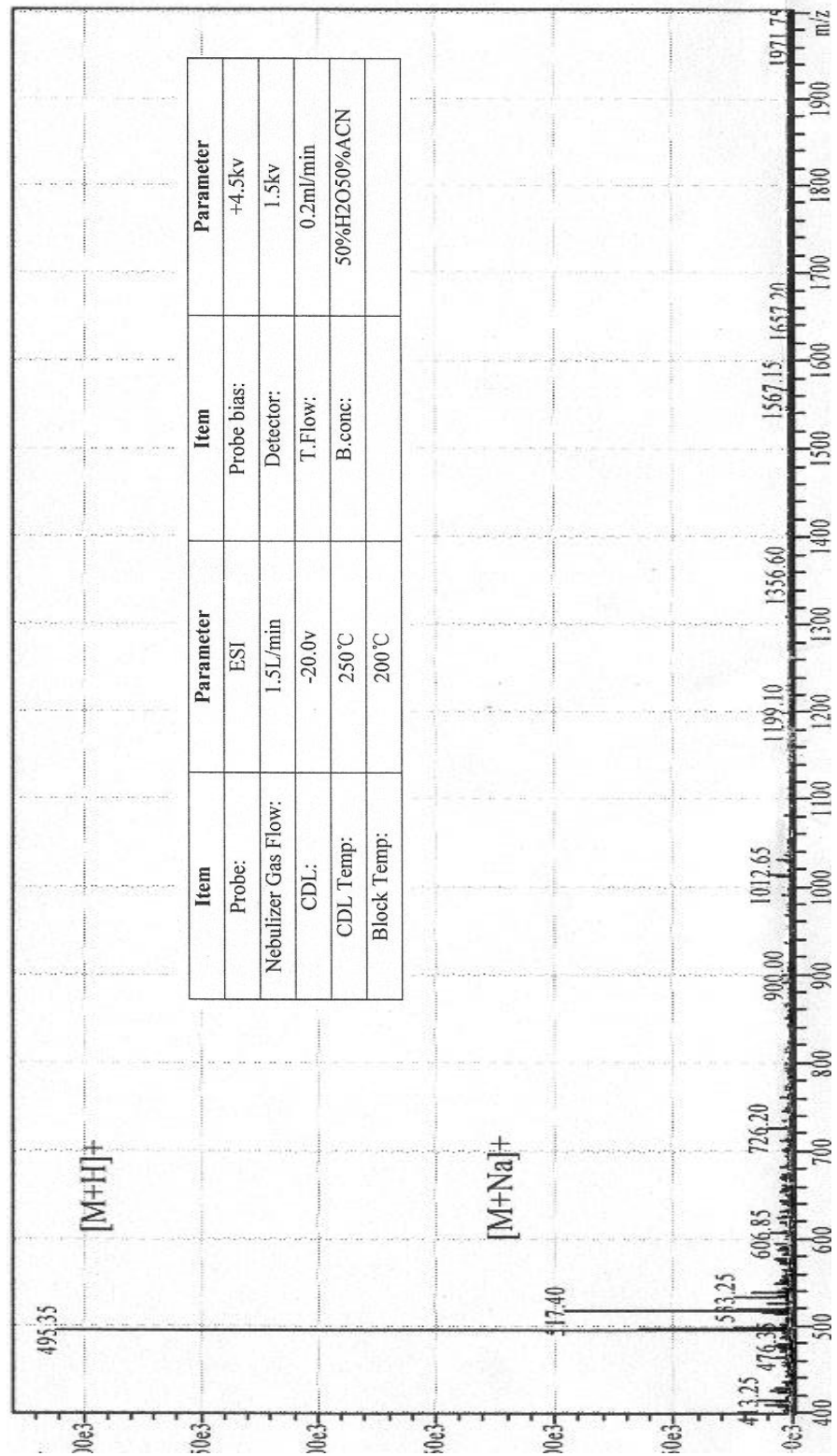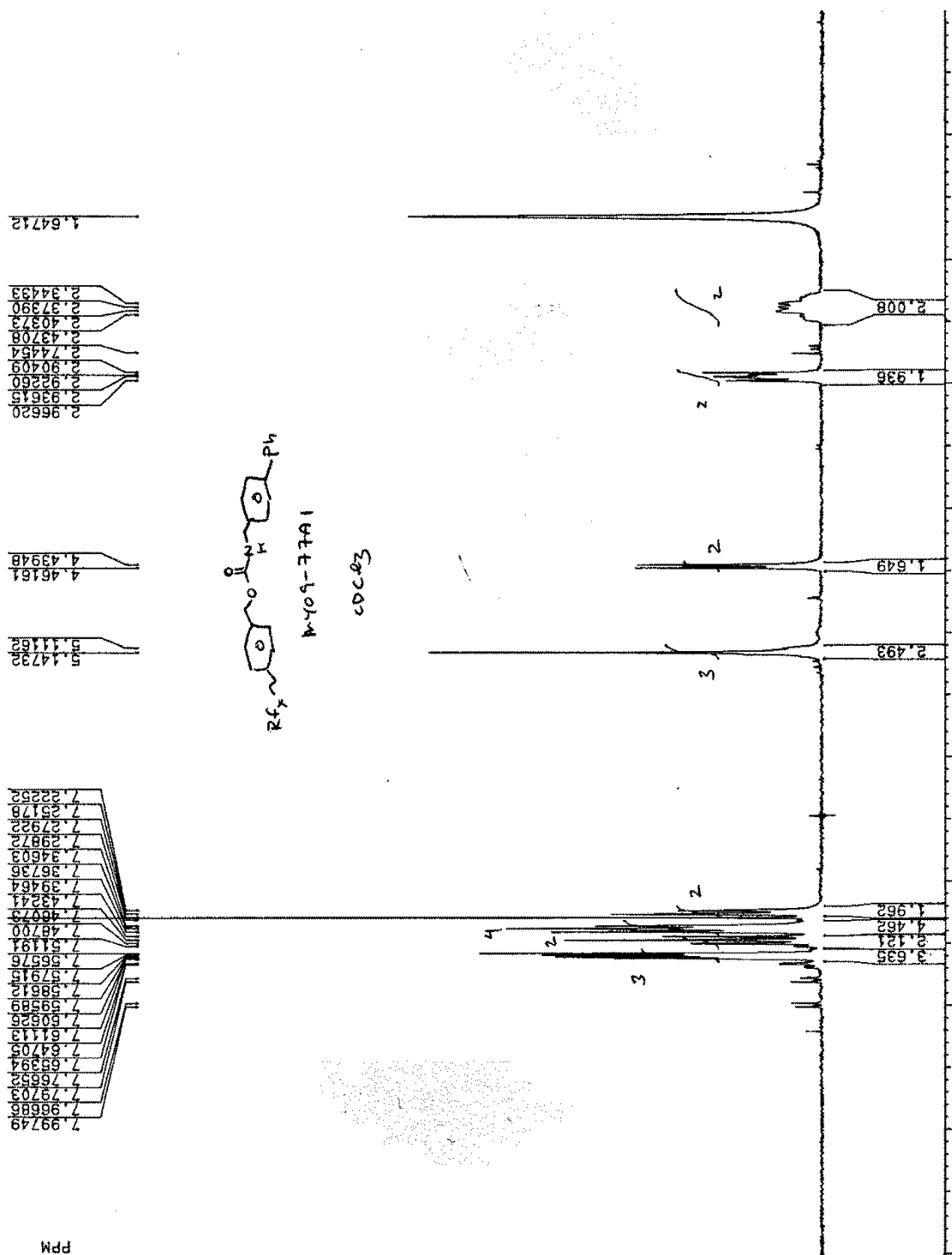
Appendix Figure 2: Mass spectrum of Custom peptide II (Alanine-Serine-Lysine-Serine-Cystaine, provided by Biomatik, Cambridge, ON, Canada)
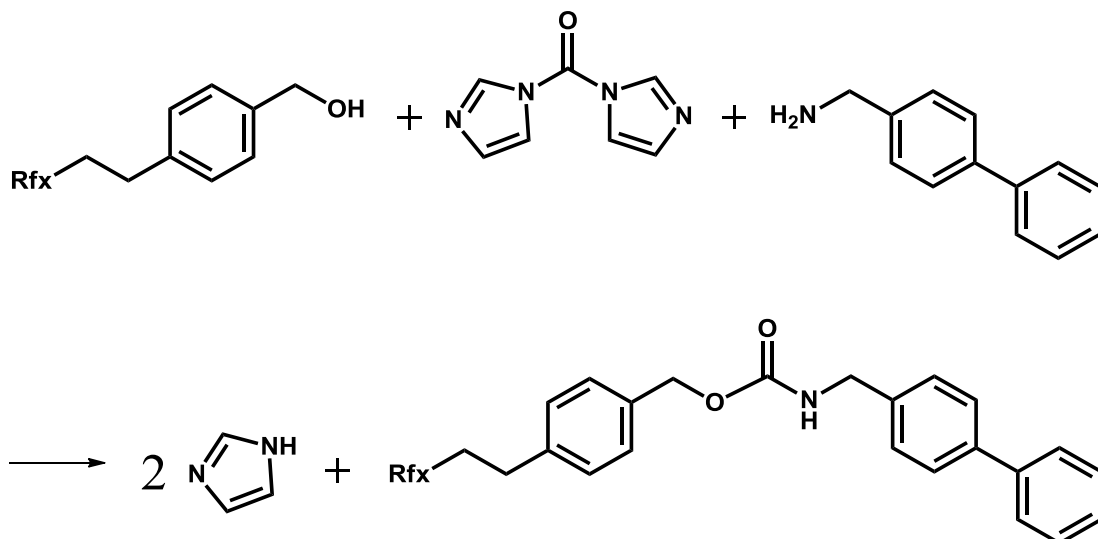
Appendix Figure 3: NMR spectrum of *N*-f-Cbz-4-nitrobenzylamine mixture (N Series, provided by Fluorous Technologies, Pittsburgh, PA, USA)

Appendix Figure 4: NMR spectrum of *N*-f-Cbz-4-phenylbenzylamine mixture (P Series, provided by Fluorous Technologies, Pittsburgh, PA, USA)

Appendix Scheme 1: Synthesis protocol of *N*-f-Cbz-4-phenylbenzylamine mixture (P Series,

provided by Fluorous Technologies, Pittsburgh, PA, USA)